TAMPEREEN TEKNILLINEN YLIOPISTO
TAMPERE UNIVERSITY OF TECHNOLOGY

Kati Stranius

Photochemistry of Self-Assembled Donor-Acceptor Architectures for Photoactive Supramolecular Devices

Julkaisu 1269 • Publication 1269

Tampere 2014

Tampereen teknillinen yliopisto. Julkaisu 1269
Tampere University of Technology. Publication 1269

Kati Stranius

Photochemistry of Self-Assembled Donor-Acceptor Architectures for Photoactive Supramolecular Devices

Thesis for the degree of Doctor of Philosophy to be presented with due permission for public examination and criticism in Konetalo Building, Auditorium K1702, at Tampere University of Technology, on the 26th of November 2014, at 12 noon.

Tampereen teknillinen yliopisto - Tampere University of Technology
Tampere 2014

ISBN 978-952-15-3412-6 (printed)
ISBN 978-952-15-3424-9 (PDF)
ISSN 1459-2045

ABSTRACT

Supramolecular donor-acceptor assemblies were prepared and studied with spectroscopic methods. The two main objectives of this work were: (i) fundamental study of photoinduced energy and electron transfer processes in self-assembled supramolecular donor-acceptor complexes in solutions and (ii) self-assembly and photophysical characterization of donor-acceptor films on titanium dioxide (TiO_2) surface. The study of these systems aims to develop more complex architectures for artificial photosynthesis and understand factors that affect efficiency of the photoinduced energy and electron transfer processes in natural and artificial photosynthesis. This knowledge can be used for building photoactive molecular devices such as organic solar cells.

The singlet excited state energy transfer in dyads formed *via* axial metal–ligand coordination of free-base porphyrin to metal (Mg, Ru) complexes of pthalocyanine was observed. The position of imidazole linker group on one of the *meso*-aryl groups of the free-base porphyrin was used to tune the rates of energy transfer. The two-point binding provides better control over complex geometry and it was implemented utilizing metal-ligand and crown-ether coordination in zinc chlorin–fullerene supramolecular dyads. This approach allowed to increase the binding efficiency and achieve a well-defined mutual orientation between the moieties. The electron transfer rate was found to depend on the donor-acceptor distance as well as the mutual orientation of the entities and could be manipulated by changing positions of binding groups.

The donor-acceptor layers were assembled on TiO_2 using two methods. First, a layer of covalently linked porphyrin-pthalocyanine dyads was formed on TiO_2 *via* supramolecular approach. Then, a new method was developed to construct donor-acceptor two-layer films using separate porphyrin and fullerene molecules. In both cases, photo-excitation of donor molecules resulted in charge-separation (CS) inside the organic layer and sequential electron transfer towards the TiO_2. Furthermore, the charge recombination (CR) process was found to be slower than for systems sensitized with single chromophores.

PREFACE

First of all, I would like to thank my supervisor, Prof. Nikolai Tkachenko for his undaunted guidance and patience throughout the years. His help has been always available when I have needed it. Together with Prof. Helge Lemmetyinen, I would like to thank them for giving me the opportunity to work in this research group equipped with state of the art instruments and teams which truly work together.

Dr. Alexander Efimov I would like to thank for the compounds which were synthesized in his lab and his help with real chemistry. I appreciate Dr. Vladimir Chuckharev's help with all the practical matters in the lab. My warmest thanks go also to all the co-authors of the papers in Prof. Francis D'Souza's and Dr. Juho Helaja's groups.

I am grateful to all the people of the chemistry lab for the nice working atmosphere and help in all kinds of practical and technical matters. Especially, I want to thank my team members, Hanna Hakola and Kirsi Virkki, for peer support and my roommate, Dr. Tiia-Maaria Ketola, for lively companionship.

Finally, I thank my family for their constant interest and support during the life. Especially I want to thank my mother, Pirjo who has always been there for me. My friends in KWP Ry, I thank for the multidisciplinary peer support and for all the fun to counterbalance the work. Last but certainly not the least, I want to thank Heikki for the encouragement and being on my side.

This work was carried out at the Department of Chemistry and Bioengineering in Tampere University of Technology during years 2010-2014. The Academy of Finland and The National Doctoral Programme in Nanoscience (NGS-NANO) are gratefully acknowledged for funding.

Tampere, September 2014

Kati Stranius

TABLE OF CONTENTS

LIST OF PUBLICATIONS

The Thesis is based on the work contained in the following papers, which will hereafter be referred to by their Romain numerals:

I **Excitation transfer in metal-ligand coordinated free-base porphyrin-magnesium phthalocyanine and free-base porphyrin-magnesium naphthalocyanine dyads**
Kati Stranius, Rachel Jacobs, Eranda Maligaspe, Helge Lemmetyinen, Nikolai V. Tkachenko, Melvin E. Zandler and Francis D'Souza
Journal of Porphyrins and Phthalocyanines **2010**, *14*, 948–961.

II **Syntheses and Excitation Transfer Studies of Near-Orthogonal Free-Base Porphyrin-Ruthenium Phthalocyanine Dyads and Pentad**
Rachel Jacobs, Kati Stranius, Eranda Maligaspe, Helge Lemmetyinen, Nikolai V. Tkachenko, Melvin E. Zandler and Francis D'Souza
Inorganic chemistry **2012**, *51*, 3656–3665.

III **Sequential Photoinduced Energy and Electron Transfer Directed Improved Performance of the Supramolecular Solar Cell of a Zinc Porphyrin-Zinc Phthalocyanine Conjugate Modified TiO_2 Surface**
Chandra B. KC, Kati Stranius, Preston D'Souza, Navaneetha K. Subbaiyan, Helge Lemmetyinen, Nikolai V. Tkachenko and Francis D'Souza
The Journal of Physical Chemistry C **2013**, *117*, 763–773.

IV **Effect of Mutual Position of Electron Donor and Acceptor on Photoinduced Electron Transfer in Supramolecular Chlorophyll-Fullerene Dyads**
Kati Stranius, Vladimir Iashin, Taru Nikkonen, Mikko Muuronen, Juho Helaja and Nikolai Tkachenko
The Journal of Physical Chemistry A **2014**, *118*, 1420–1429

V **Self-assembled donor-acceptor two-layer film on TiO_2**
Kati Stranius, Lijo George, Alexander Efimov, Tero-Petri Ruoko, Juuso Pohjola and Nikolai V. Tkachenko
Langmuir **2014**, submitted

Author´s contribution
Kati Stranius carried out all spectroscopy measurements including ultrafast time-resolved spectroscopy and data analysis. She developed methods for SAM deposition and prepared the samples for spectroscopic studies in all publications and performed electrochemical measurements for publication IV. She wrote the manuscript drafts for publications IV and V and participated in writing the other manuscripts.

LIST OF ABBREVIATIONS AND SYMBOLS

A	Acceptor
CCD	Charge-coupled device
CF	Carboxy fullerene
CR	Charge recombination
CS	Charge separation, charge-separated
Chl	Chlorophyll
D	Donor
DCB	O-dichlorobenzene
DFT	Density functional theory
DPV	Differential pulse voltammetry
DSSC	Dye-sensitized solar cells
E_{ox}	Oxidation potential
E_{red}	Reduction potential
E_{CS}	Energy of charge-separated state
ET	Energy transfer
$\Delta G^{\dagger}$	Activation energy
ΔG_S	Coulombic energy
ΔG_{CS}	Free-energy of charge separation

HOMO	Highest occupied molecular orbital
H_2P	Free-base porphyrin
ISC	Intersystem crossing
J_F	Overlap integral
K	Equilibrium constant, binding constant
k	Rate constant
LUMO	Lowest unoccupied molecular orbital
MgNc	Magnesium napthalocyanine
MgPc	Magnesium pthalocyanine
NLC	Non-linear crystal
Nd:YAG	Neodymium-doped yttrium aluminium garnet, Nd:$Y_3Al_5O_{12}$
OPA	Optical parametric amplifier
PhCN	Benzonitrile
R_0	Förster radius
R_{C-C}	Center-to-center distance
R_{E-E}	Edge-to-edge distance
Ru(CO)Pc	Ruthenium carbonyl pthalocyanine
SAM	Self-assembled monolayer
SHG	Second harmonic generator
TiO_2	Titanium dioxide
WCG	White continuum generator
ZnO	Zinc oxide
ZnP	Zinc porphyrin

β	Damping factor
λ	Reorganization energy
ν_d	Sum frequency
ν_g	Gate pulse
ν_{em}	Maximum emission frequency
τ_{CR}	Charge recombination time constants
τ_{CS}	Charge transfer time constants
τ_{ET}	Energy transfer time constant
κ^2	Orientation factor
τ_{SI}	Fluorecence decay time constants

1. INTRODUCTION

Congratulations to the Earth for the new record!

We set a new milestone level, 400 pm, for atmospheric carbon dioxide (CO_2) during spring 2014.[1] CO_2 is one of the most harmful greenhouse gases, and it's concentration in our atmosphere has been increasing at an accelerating rate since the industrial revolution. Greenhouse gases are transparent to the visible light coming from Sun, but prevent infrared light to escape from the Earth by absorbing it. Thus, they cause the global warming and climate change. The world's energy consumption is still expected to increase in the coming years. Therefore, it is extremely important to find and develop new energy sources to meet the growing demand and to replace the fossil fuels responsible for atmospheric CO_2. This carbon-neutral energy should be produced using renewable energy sources safely and with competitive costs. The ultimate renewable energy source is the Sun, which emits in one hour more energy onto the Earth's surface than is needed to cover out annual worldwide consumption.[2] Thus, solar energy technologies are the most promising solutions for sustainable energy production.

In natural photosynthesis, sunlight is converted extremely efficiently into chemical energy. The energy capture and photon energy conversion into electric potential is done by supramolecularly organized light harvesting complexes capable of unidirectional excitation transfer towards reaction center. Mimicking this natural phenomenon with the help of synthetic molecular architectures capable of collecting, translating and accumulating sunlight is desirable for developing efficient and affordable solar energy converting systems. Furthermore, this knowledge is also useful for developing other photoactive molecular devices such as sensors, switches and memories.[3–6]

The simplest synthetic molecular architectures mimicking the natural complexes are molecules consisting of a donor (D) and an acceptor (A) chromophores which are capable of energy and/or charge transfer. The supramolecular assembly of these

complexes makes it possible to build complicated architectures with less effort and to produce structures that cannot be built by covalent chemistry.[3,7–9] Studying the complexes in solution gives important information on the dependence of the energy and electron transfer rate and efficiency on the donor-acceptor distance and orientation, the free energy of the reactions and electronic coupling. For actual solar energy converting devices, the donor-acceptor complexes should be assembled on a semiconductor surface in such way that they maintain their properties and are able to transfer an electron across the organic-semiconductor interface. The self-assembled monolayer (SAM) technique is a highly promising method for constructing such molecular architectures on metal and semiconductor surfaces.[10–12]

In this Thesis, the photochemistry of self-assembled donor-acceptor architectures consisting of porphyrin, pthalocyanine, chlorin and fullerene derivatives were investigated. The energy and electron transfer reactions in these systems take place in the femto- and picosecond time domain. Thus ultrafast optical spectroscopy was used to resolve these fast reactions in self-assembled supramolecular donor-acceptor dyads in solutions [I, II, IV] and donor-acceptor SAMs on TiO_2 [III, V].

Self-assembly *via* metal-ligand axial coordination is one of the successful approaches developed to study donor-acceptor dyads.[9,13,14] However, using this approach to couple energy donor and acceptor compounds to mimic energy transfer processes has not been studied much.[15] In papers [I] and [II], supramolecular porphyrin-pthalocyanine and -napthalocyanine complexes were constructed using self-assembly *via* metal-ligand axial coordination. Although, fullerenes and porphyrins are mostly used to study photoinduced electron transfer in donor-acceptor dyads, the studies utilizing nature's own choice, chlorophyll, are rare.[16,17] In paper [IV], chlorin-fullerene complexes were assembled using two-point binding *via* metal-ligand and crow-ether coordination. The attachment position of the metal coordinating ligand was changed in these complexes in order to study the effect of distance and mutual orientation of the donor and the acceptor on the photochemistry of the supramolecular assemblies.

The usage of donor-acceptor assemblies to build organic solar cells to probe the possible charge transfer inside the organic layer has not been explored much.[18–21] In paper [III], monolayers of covalently linked free-base and zinc porphyrin–zinc phthalocyanine dyads were self-assembled on TiO_2 surface *via* a metal-ligand axial coordination approach. The photochemistry of these SAMs was studied to reveal the mechanism of photocurrent generation in the supramolecular solar cell.

A new method for constructing the ordered donor-acceptor layers on TiO_2 was proposed and tested in paper [V]. The donor and acceptor molecules were self-assembled one after another on the surface using anchoring groups with different lengths. The fullerene acceptor monolayer was first self-assembled close to the surface *via* shorter linker and the porphyrin layer was assembled on top of that *via* a longer linker capable to penetrate between fullerenes. The formation and functionality of this two-layer film was confirmed with spectroscopic methods.

2. BACKGROUND

2.1 Energy transfer

In photosynthesis, light-harvesting molecules absorb solar energy and transfer it to reaction centers. Absorption of a photon raises the molecule to an excited singlet state where the energy hops to the nearby molecule *via* an energy transfer (ET) mechanism. Solar energy capture is efficient because the rate of the energy transfer is much faster than the rates of alternative relaxation pathways of the singlet excited state. The energy transfer in light-harvesting systems occurs either *via* Dexter's (exchange) mechanism or Förster's (dipole-dipole or Coulombic) mechanism depending on their structures. These are non-radiative mechanisms *i.e.* they do not involve emission of the donor to be absorbed by the acceptor but rely on the interaction between the donor and acceptor molecules. The important difference between these two mechanisms is that the exchange is a short-range (less than 10 Å) interaction and that dipole-dipole interaction is possible also in a long-range (80-100 Å).[22,23]

2.1.1 Förster Energy Transfer

Energy transfer *via* the Förster mechanism is efficient if the emission spectrum of the donor molecule overlaps significantly with the absorption spectrum of the acceptor (Figure 1) *i.e.* $\Delta E(D^* \longrightarrow D) = \Delta E(A \longrightarrow A^*)$. These transitions are in resonance and the energy transfer arises from long-range dipole-dipole interaction. Thus the donor and acceptor can be spatially separated by relatively large distances.[22–24]

The energy transfer rate constant from donor to acceptor, k_F, is given by

$$k_F = \frac{1}{\tau_D}\left(\frac{R_0}{R_{C-C}}\right)^6 \tag{1}$$

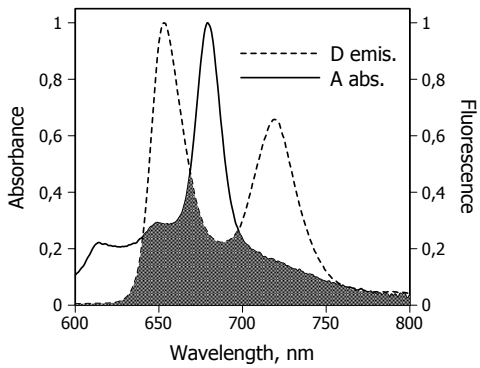

Fig. 1. *The spectral overlap area for free-base porphyrin donor and magnesium phthalocyanine acceptor.*

where τ_D is the fluorescence lifetime of the donor in the absence of the acceptor, R_{C-C} is the center-to-center distance between the donor and acceptor and R_0 is the Förster radius *i.e.* the distance at which half of the donor molecules decay by energy transfer and half decay by the usual radiative and non-radiative mechanisms.[22–24] The Förster radius R_0 is calculated according to

$$R_0 = A \left(\frac{\kappa^2 \, \Phi_D \, J}{\eta^4} \right)^{1/6} \tag{2}$$

where A is the numerical constant, η is the solvent refractive index, κ^2 is the orientation factor, Φ_D is the fluorescence quantum yield of the isolated donor and J is the overlap integral determined by the emission of the donor and absorption of the acceptor and it is given by

$$J_F = \int F_D(\lambda) \, \varepsilon_A(\lambda) \, \lambda^4 d\lambda \tag{3}$$

where $F_D(\lambda)$ is the fluorescence intensity of the donor with total intensity normalized to unity, $\varepsilon_A(\lambda)$ is the molar extinction coefficient of the acceptor expressed in units of $M^{-1}cm^{-1}$ and λ in nanometers.

The orientation factor, κ^2, describes the relative orientation in space of the transition moments of the donor and acceptor

$$\kappa^2 = [\cos\nu - 3 \cos\alpha \cos\beta]^2 \tag{4}$$

where α and β are the angles made by the transition dipoles of the donor and acceptor entities with the line joining the centers of the transitions and ν is the angle between the two transition dipoles.[22–25] The k_F values, calculated by using parameters described in the above equations can be used to estimate the energy transfer rates between two molecules, for example the light-harvesting molecules.

2.1.2 Dexter Energy Transfer

The Dexter mechanism is based on the intermolecular orbital overlap of the donor and acceptor and is thus only possible at short distances. The mechanism is based on double-electron exchange. In the initial state, the excited donor has an electron in the LUMO and after the exchange the acceptor has an electron in the LUMO.[22,23,26]

The rate of electron exchange depends on the interaction between the electron clouds in the donor and acceptor. The electronic wave function at a sufficiently large distance from the the nuclei decreases exponentially with distance and the rate constant for the energy transfer following the exchange mechanism is given by

$$k_D = K J \exp\left(-\frac{2R_{C-C}}{L}\right) \tag{5}$$

where K is related to orbital overlap, J is normalized spectral overlap (similar to Equation 1) and R_{C-C} is the donor-acceptor center-to-center separation relative to their Van der Waals radii L.[25] In contrast to the inverse sixth power distance dependence for the Förster mechanism, the distance dependence is exponential in the case of the Dexter mechanism. This means that within assemblies with the donor-acceptor distance less than 1 nm, the Dexter-type coupling is likely, whereas for large, spatially separated subunits the longer-range Förster-type energy transfer is predominant.

2.2 Electron transfer

In the reaction center, one component becomes electronically excited by transferred energy and initiates the electron transfer process in which an electron is transferred from an electron donating species (D) to an electron accepting species (A). The free energy of this charge separation can be calculated by

$$-\Delta G_{CS} \;=\; \Delta E_{0-0} - e(E_{ox} - E_{red}) + \Delta G_S \tag{6}$$

where ΔG_{CS} is the free energy of the charge separation, E_{0-0} is the energy of the lowest excited state of the chromophore and E_{ox} and E_{red} are the first oxidation potential of the donor and first reduction potential of the acceptor, respectively. The Coulombic energy of the CS state is calculated by $\Delta G_S = -e^2/(4\,\pi\,\varepsilon_0\,\varepsilon_R\,R_{C-C})$ and ε_0 and ε_R refer to the vacuum permittivity and dielectric constant of the solvent and R_{C-C} is the center-to-center distance between the donor and acceptor which are assumed to be spherical.[22]

2.2.1 Marcus electron transfer theory

Classical Marcus electron transfer theory represents the multidimensional potential energy surfaces of the reactants (DA) and the products (D^+A^-) by using two identical but displaced parabolas vs. the reaction coordinate q corresponding to the changing geometries of the system (Figure 2). The electron transfer reaction takes place at the transition state, where the reactant and product parabolas intersect *i.e.* at the point where the reactants and products have the same configuration of nuclear coordinates.[3,27,28]

The activation energy for the electron transfer reaction, $\Delta G^{\dagger}$, can be calculated by

$$\Delta G^{\dagger} \;=\; \frac{(\Delta G_{CS} + \lambda)^2}{4\lambda} \tag{7}$$

where ΔG_{CS} and λ are the free energy of charge separation and the total reorganization energy defined as the change in free-energy upon the shift in reaction coordinates from the reactant to product, respectively. The total reorganization energy is composed of the solvent reorganization λ_s and internal reorganization λ_i components. Within dielectric continuum model of a solvent and considering the donor and acceptor to be spheres with radii r_D and r_A and with center-to-center distance R_{C-C}, the λ_s is given by

$$\lambda_s \;=\; \frac{e^2}{4\pi\varepsilon_0}\left(\frac{1}{2r_D} + \frac{1}{2r_A} + \frac{1}{R_{C-C}}\right)\left(\frac{1}{\varepsilon_{op}} - \frac{1}{\varepsilon_S}\right) \tag{8}$$

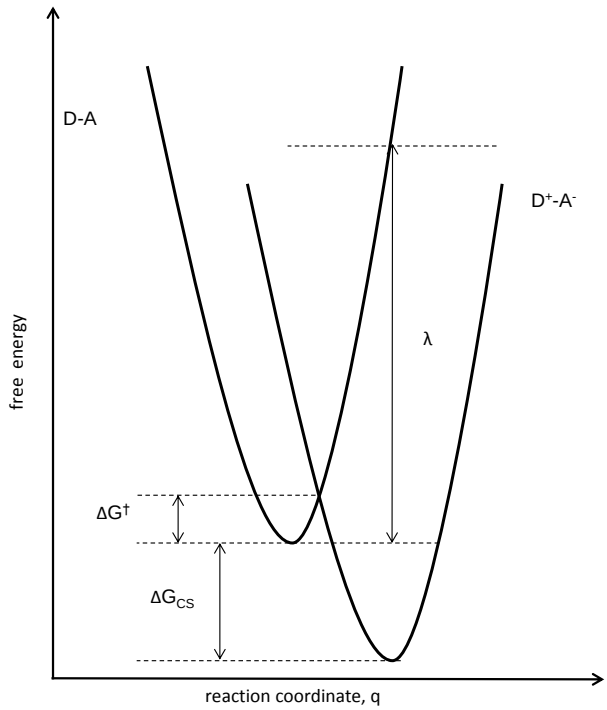

Fig. 2. *Representation of the potential energy curves of the complexes DA and D^+A^- by parabolas characteristic of harmonic oscillators. The plots also represent the activation energy, $\Delta G^\dagger$, the free-energy of charge separation, ΔG_{CS}, and the reorganization energy, λ.*

where ε_{op} is the optical and ε_S is the statistic dielectric constant of the medium.

The rate constant for the electron transfer, k_{ET} is given by

$$k_{ET} = \kappa_{el} \upsilon_n \exp\left(\frac{-\Delta G^\dagger}{k_B T}\right) \tag{9}$$

where κ_{el} is the electronic transition coefficient, υ_n is the frequency of passage through transition state and $k_B T$ is the thermal energy.

Some interesting conclusions can be made based on the theory. First, Equation 7 reveals that the maximum rate is achieved when $\lambda = -\Delta G$. When $\lambda > -\Delta G$, the electron transfer rate increases as the reaction becomes more exergonic. This is called the normal region. However, the electron transfer rate will slow down when the free energy of the reaction becomes very large *i.e.* $\lambda < -\Delta G$ and thus this region is called

inverted.[3,27,28] In addition, the $\Delta G^{\dagger}$ in the exponential term of Equation 9 indicates that the electron transfer rate depends on the dielectric properties of medium. For example, decreasing solvent polarity ε_S in Equation 8, decreases the reorganization energy and thus increases k_{ET}. However, a certain point the inverted region is reached and k_{ET} starts to decrease again.

In the frame of the semi-classical electron transfer theory the treatment of solvent remains classical, but the vibrations are treated using quantum mechanics. Consequently, the electron transfer rate depends on the electronic coupling between the product and reactant states which is affected by the donor-acceptor orientation and nature of the bridge.[3,27] The magnitude of electron coupling decreases exponentially as a function of distance and the dependence of the electron transfer rate constant on the donor-acceptor distance is described by the relation

$$k_{ET} \propto exp(-\beta\, r) \tag{10}$$

where r is the donor-acceptor distance and β is the damping factor depending primary on the nature of the bridge molecule.[3,29–31]

2.3 Donor-acceptor compounds

In natural photosynthesis, the light-harvesting assemblies capture sunlight and transfers the energy to the reaction center. At reaction center, the excited state energy is used to generate the charge separated state. This process contains a cascade of very efficient energy and electron transfer events between well-arranged supramolecular assemblies of chlorophylls acting as donors and acceptors. However, since the natural photosynthetic system is extremely complex, much simpler models are needed for studying and reproducing these events in artificial photosynthetic systems.[5,32]

Donor-acceptor systems combining two or more chromophores are used as artificial models which mimic the natural photosynthetic assemblies. For building efficient artificial solar energy converting systems, the donor-acceptor systems must meet certain requirements. First, the light-harvesting systems must efficiently absorb the light *i.e.* chromophores should have strong and extensive absorption in the visible region to utilize the most of the solar light. In addition, the excitation must be

transferred efficiently from one chromophore to another and eventually to the reaction center. This requires well-matched energy levels of the energy donors and acceptors. Secondly, in order to achieve the charge separation, the excited electron donor must transfer the electron to the electron acceptor. An important factor is the preferential matching of electrochemical properties for the occurance of exothermic electron transfer. Furthermore, the arrangement of donors and acceptors in the system is important since the distance and orientation influences the efficiency of both the energy and the electron transfer.[5–7,33]

2.3.1 Chromophores

Chlorophylls play key roles in primary phtosynthetic events, *i.e.* in light harvesting, energy transfer and charge separation, occurring in natural photosystems.[32] Although nature has evolved chlorophyll to show excellence in the multitasking roles, the complicated purification of chlorophylls, instability of unmodified chlorophyll being exposured to light and limited amount of synthetic modification methods developed so far have limited its use in artificial systems.[17,34–39] Thus, its analogues, porphyrins, pthalocyanines and naphthalocyanines, are widely used in artificial photosynthetic systems.[40] However, despite the difficulties in synthesis of chlorophyll and its stability, the asymmetry of chlorophyll has its advantages over easily accessible symmetric porphyrines and phthalocyanines. The asymmetry of chlorophylls enables formation of precise supramolecular assemblies *e.g.* derivation of chlorins for face-selective ligation[16] and high order helix formation.[41]

Chlorins and porphyrins are large heterocyclic aromatic rings (Figure 3). Chlorins consist of three pyrroles and one pyrroline rings and porphyrins consist of four pyrrole rings. The chlorophylls are characterized by the presence of a fifth ring, isocyclic ring E. In phthalocyanines the pyrrole units are extended to isoindoles, which are joined *via* aza bridges instead of methynes as in porphyrins.[32,40,42] Molecules having two imine hydrogens inside the macrocycles are called free-base structures and the metallized structures are metallochlorins and -porphyrins.

The large aromatic macrocycle is responsible for both the absorption and the redox chemistry of these compounds. These properties can be modified by the choice of metal center and peripheral substituents.[32,40,42] The absorption spectra of zinc phthalocyanine, zinc chlorophyll and zinc porphyrin used in the study are presented in

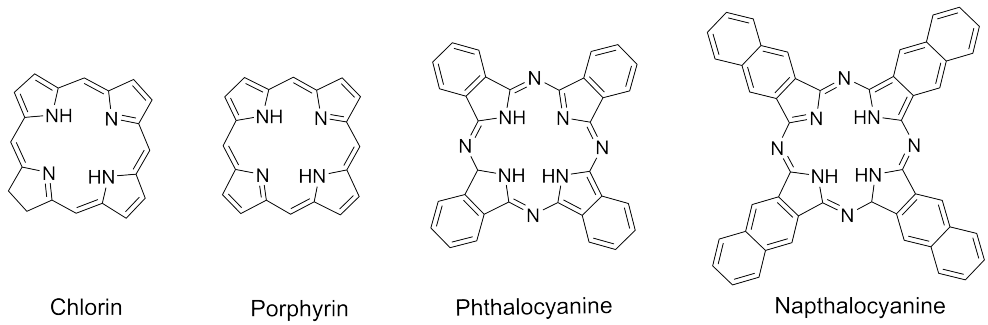

Fig. 3. *General structure for the light-harvesting dyes used in this Thesis.*

Figure 4. All of the chromophores show strong absorption in the visible region and thus they are commonly used as light-harvesting compounds. These chromophores can act also as either electron donors or acceptors depending on the environment, *i.e.* on the chromophores they are coupled to.

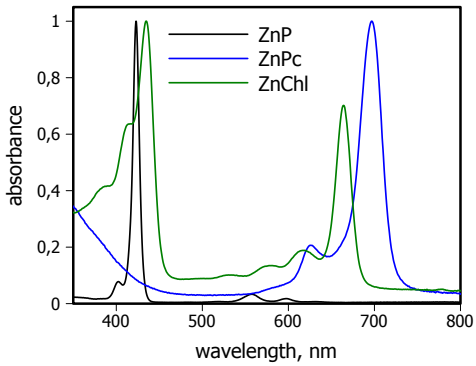

Fig. 4. *Absorption spectra of zinc phthalocyanine (ZnPc) [III], zinc chlorophyll (ZnChl) [IV] and zinc porphyrin (ZnP) [V] used in the study.*

Fullerenes are spherical molecules that consist of carbon atoms only. The most stable fullerene is C_{60} consisting of 12 pentagons and 20 hexagons (Figure 5). Due to its spherical shape, fullerene has unique chemical and physical properties. The high electron affinity, up to 6 electrons, and small reorganization energy in electron transfer processes has made C_{60} the most commonly used acceptor in artificial donor-acceptor systems. In addition, the unique anion absorption band of the fullerene in near-IR makes identification of C_{60}^{-} reliable and detection of electron transfer dynamics accurate.[43–45]

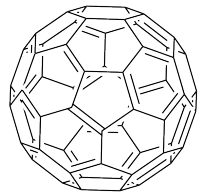

Fig. 5. *Structure of fullerene C_{60}.*

2.4 Supramolecular assembly

The different strategies developed to-date to construct the donor-acceptor molecules to mimic the natural energy and electron transfer processes include covalent linking the donor and acceptor chromophores,[6,8,11,46,47] arranging the chromophores in polymer[48] or dendrimer molecular framework,[49] or self-assembly approaches.[7–9,13,44,50]

Self-assembled supramolecular complexes are held together by weak and reversible noncovalent interactions between molecules which offer significant advantages over the traditionally used covalently linked ones for construction of complex multicomponent structures. One practical advantage is the possibility to prepare a series of donor and acceptor molecules with the same connecting groups and generate a large number of different donor-acceptor complexes solely by mixing different combinations of molecules.[13,14,51–53] However, since the interactions are weak and associated with multiple equilibrium processes, controlling the distance and orientation between the donor and acceptor moieties is difficult using a single binding site. Thus, employing additional binding sites (multi-point binding) for construction of supramolecular assemblies helps to achieve structural rigidity by decreasing the free rotation between molecules.[17,54–58]

2.4.1 Supramolecular binding modes

Supramolecular systems are composed of donor and acceptor molecules that are functionalized so that the entities are able to bind reversibly in solution. The basic supramolecular interactions include hydrogen bonding, halogen bonding, ionic interactions, π-interaction and van der Waals interaction.[59] Typically the modes of binding for the chromophores mentioned above have been metal-ligand or crown-ether coordination or ion pairing, hydrogen bonding or $\pi - \pi$-stacking.[7–9,13,44]

Self-assembly *via* metal-ligand axial coordination is simple yet successful approach.[9,13,14] Metallated porphyrins and chlorins accept ligands such as pyridine or imidazole nitrogens eagerly. Due to the rigid coordination geometries of metals, these systems produce well-defined and controllable structures. The binding constants (K) of metal-ligand coordinated systems are often large, approaching, in some cases, the stabilities observed for the covalent systems.[9,60] The strategy involving pyridine functionalized C_{60} coordinated to metallated porphyrin/phthalocyanine has been very popular for constructing systems capable for efficient electron donor-acceptor systems,[7–9,13] but studies with metal chlorin complexes are rare.[16,17] In addition, only a few studies have been conducted utilizing this method to couple energy donor and acceptor compounds to mimic energy transfer processes.[15]

Another widely used method for supramolecular assembling is based on crown-ether binding of cation ions such as alkyl ammonium salts (Na^+, K^+, Rb^+, Cs^+, Ca^{2+} and $NH_4{}^+$) or alike. Several studies where a crown-ether and an alkyl ammonium are attached to the electron donor or acceptor have been published.[8,51,55–58,61] An advantage of the crown-ether–cation binding is that it is effective in polar solvents and thus allows to construct supramolecular assemblies in polar environment.

Self-assembly processes involving more than one interaction through separate ligands are called multi-point self-assembly or multiple interaction self-assembly.[60] While a single point binding results in dyads with a substantial degree of conformational flexibility, multi-point binding leads to formation of more rigid complexes with better defined distance and orientation between the donor and acceptor entities.[17,54–57,62] This is an important advantage of the multi-point binding, since the mutual orientation and distance of the functional units in the donor-acceptor system affect the energy and electron transfer rates. In many studies axial metal-ligand and crown-ether coordination are combined to achieve two-point binding between porphyrin and fullerene.[55–57,62] Also few studies employing metal-ligand coordination and hydrogen bonding to construct these type of dyads have been reported.[17,54]

2.4.2 Determination of binding constant

The binding constant (equilibrium constant) is used to describe how tight the supramolecular binding is. The reaction scheme for a reversible complex formation between molecules A and B is

$$A + B \overset{K}{\rightleftharpoons} AB \tag{11}$$

where K is the equilibrium constant. The total concentrations of A and B are constants and are denoted as A_0 and B_0. The concentrations of molecules in equilibrium are represented by the relations

$$\begin{cases} [A] = A_0 - [AB] \\ [B] = B_0 - [AB] \\ [AB] = K\,[A]\,[B] \end{cases} \tag{12}$$

where concentrations of reactants A and B and product AB are denoted as $[A]$, $[B]$ and $[AB]$, respectively.

The general solution for the equilibrium equation is then

$$\begin{aligned} [AB] = {} & K(A_0 - [AB])(B_0 - [AB]) \\ = {} & \frac{K(A_0+B_0)+1-\sqrt{(K^2(A_0-B_0)^2+2K(A_0+B_0)+1}}{2K} \end{aligned} \tag{13}$$

However, a simpler solution can be obtained if the concentration of one of the compounds is much higher than the other, $A_0 \gg B_0$. Then, $A_0 - [AB] \simeq A_0$ and

$$[AB] = B_0 \frac{KA_0}{1+KA_0} \tag{14}$$

To obtain the equilibrium constant K, absorption and fluorescence titration methods can be used. According to the Beer-Lambert law,[63] the absorbance of the complex is

$$Abs(AB) = \varepsilon_{AB} l [AB] \tag{15}$$

where ε_{AB} is the molar absorbance of the complex and l is the path length of the sample.

Substituting the complex concentration from Equation 14 into Equation 15 and rearranging gives

$$\frac{B_0}{Abs(AB)} = \frac{1}{\varepsilon_{AB} l} + \left(\frac{1}{\varepsilon_{AB} l K}\right)\left(\frac{1}{A_0}\right) \tag{16}$$

Plotting the $\frac{1}{Abs(AB)}$ vs. $\frac{1}{A_0}$ gives $\frac{1}{\varepsilon_{AB} l}$ from intercept and K can be then calculated from the slope. This is known as Benesi-Hildebrand analysis.[64] For the case, where also A absorbs in the region of measurement, $Abs = Abs(AB) + Abs(A)$ and thus $\frac{Abs}{A_0 - A}$ is plotted vs. $\frac{1}{A_0}$.

The stern-Volmer plot is used to determine K from emission quenching measurements where A completely quenches emission of B. The emission intensity ratio is given by

$$\frac{I_0}{I} = \frac{B_0}{B_0 - [AB]} \tag{17}$$

where I_0 and I are the emission intensities without and with the quencher.[23]

Substituting the complex concentration from Equation 14 to Equation 17 and rearranging gives

$$\frac{I_0}{I} = 1 + K A_0 \tag{18}$$

The binding constant can be evaluated by plotting the $\frac{I_0}{I}$ vs. A_0, which ´then gives the K from the slope.

2.4.3 Determination of stoichiometry

To determine the stoichiometry using absorption or emission spectroscopy, Job's method (continuous variation method)[22] or molar ratio methods[65] can be used. In Job's method, the sum of the total concentrations of the donor and acceptor is kept constant, but the molar fraction of the chromophores is changed. The complex concentration is calculated from measured absorption or emission values and plotted versus the molar fraction. The stoichiometry $\left(\frac{[A]}{[A]+[B]}\right)$ of the complex can be extracted from the maximum of the Job's plot which for example is at 0.5 for the 1:1 complex. In the molar ratio method, the concentration of the acceptor is usually kept constant and a variable amount of the donor agent is added and absorbance is plotted versus the molar ratio of donor. A break in the slope of the curve occurs at the molar ratio corresponding to the stoichiometry of the complex.

2.5 Self-assembled donor-acceptor layers

Dye-sensitized semiconductor surfaces capable of photoinduced electron transfer across the interface have special interest for applications in photovoltaic devices such as hybrid solar cells.[66–69] The generation of electrostatic potential between the organic layer and the electrode surface modified by a single chromophore layer requires the light absorption by the chromophore and electron transfer across the interface in a direction determined by the energy states of the semiconductor and the chromophore. However, replacing the dye layer with the ordered donor-acceptor layer and having the primary charge separation inside the donor-acceptor film could have some advantages over the direct electron transfer in single chromophore films. The multistep electron transfer results in a longer charge separation distances and thus can reduce the probability and the rate of the charge recombination. In addition, the close contact of the donor and acceptor moieties can promote the fast and efficient intermolecular charge separation. Thus the total efficiency of the photocurrent generation is expected to increase. The self-assembled monolayer (SAM) method is promising to construct of such molecular architectures on metal and semiconductor surface.[11,19]

2.5.1 Self-assembled monolayer method

Self-assembled monolayers (SAM) are formed by the binding of an active group of molecule on a metal or semiconductor surface, which is a spontaneous chemical reaction leading to stable, ordered and close-packed structures.[10,60] Semiconductors such as titanium dioxide (TiO_2) and zinc oxide (ZnO) are widely used as an electrode in artificial light-harvesting application. The light harvesting efficiency (absorption) of a single monolayer is low. Therefore, porous films of nanometer size semiconductor particles or nanorods are used to increase the effective surface area in solar cell applications.[66–69]

There are a number of active groups which can bind to specific metal, metal oxide and semiconductor surfaces. Among them, carboxyl groups are commonly used for anchoring chromophores on some metal oxide surfaces of practical importance. Several binding mechanisms for carboxyl anchors on TiO_2 or ZnO have been reported, including a simple adsorption by electrostatic attraction and hydrogen bonding, or chemical bond formation of ester-like linkage, bridging and chelating (Figure 6). Many factors

affect binding mechanism such as the reaction temperature, solvent, pH, co-anchoring groups and steric effects, and the surface properties of TiO_2 nanoparticles.[70–72] However, the main binding modes reported for chromophores in dye-sensitized solar cells (DSSC) are a chelating and/or a bridging of the carboxylate on the TiO_2 surface.[73–76]

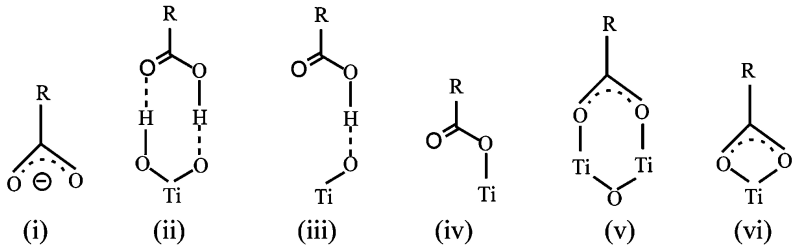

Fig. 6. *Different binding modes of carboxyl group on a metal oxide surface: (i) electrostatic attraction, (ii) double H-bonding , (iii) single H-bonding, (iv) ester-like linkage, (v) bridge, and (vi) chelating.*[70]

Although SAM method is promising to construct molecular architectures on semiconductor surfaces, the majority of studies have been aimed at attaching layer of single chromophore on surfaces.[9,67,68,77] Very few studies have attempted to implement this approach to self-assemble the donor-acceptor films on the surfaces.[18–21] Potentially the donor-acceptor complexes can be attached to the semiconductor surface either from the donor or acceptor side, so that the direction of electron transfer can be changed. One problem of the immobilization of covalently linked dyads is the tilted arrangement and thus formation of loosely packed structures and poor vectorial electron flow.

3. MATERIALS AND METHODS

Photoinduced processes in different supramolecular donor-acceptor complexes, porphyrin-phthalocyanine [I, II, III], chlorin-fullerene [IV] and porphyrin-fullerene [V], were studied in this Thesis.

Optical spectroscopy was used to examine the interaction between light and matter. Steady-state spectroscopy was used to monitor the complex and SAM formation as well as to determine the optical properties of them. Time-resolved measurements were utilized to identify the transient states and find out the characteristic timescales of the photoinduced processes. The different time scales of these processes require different measurement setups. Time-resolved absorption in the femtosecond timescale was measured with a pump-probe setup, whereas a flash-photolysis setup was used when time resolution in the microsecond timescale was needed. Time-resolved fluorescence in the femtosecond timescale was measured with the up-conversion method. The differential pulse voltametry was carried out to determine the HOMO and LUMO energy levels of the studied molecules.

3.1 Compounds

Porphyrin-phtalocyanine complexes consisting of free-base porphyrin (**H_2PIm**) as donor and metal phtalocyanine (**MgPc**, **Ru(CO)Pc**) or naphthalocyanine (**MgNc**) as acceptor were used for mimicking the natural excitation transfer process in solutions [I, II]. The structures of porphyrins and phtalocyanine/naphthalocyanine are presented in Figure 7 and 8, respectively. Self-assembled dyads were formed *via* metal-ligand coordination of the imidazole entity at the *ortho*-, *meta*- and *para*-positions of one of the *meso*-aryl groups of porphyrin to either magnesium phthalocyanine, magnesium naphthalocyanine or ruthenium carbonyl phthalocyanine. For formation of pentad, porphyrin functionalized with four entities of *para*-imidazole substituen

($\mathbf{H_2P_p(Im)_4}$**:**$\mathbf{(Ru(CO)Pc)_4}$) was used to coordinate up to four ruthenium carbonyl phthalocyanines.

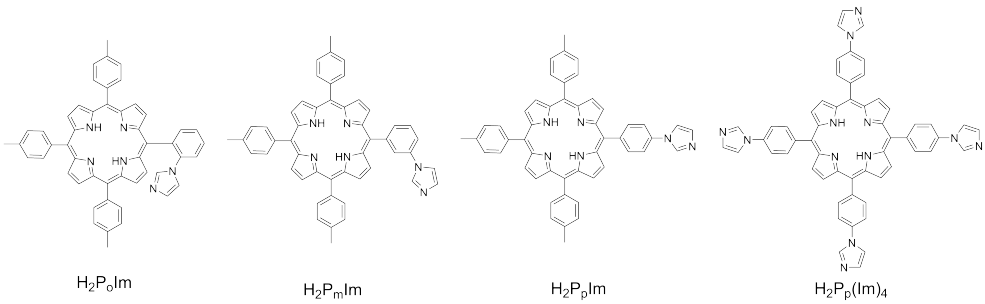

Fig. 7. *Molecular structures of free-base porphyrins,* ***H_2P_oIm****,* ***H_2P_mIm****,* ***H_2P_pIm*** *and* ***$H_2P_p(Im)_4$****.*

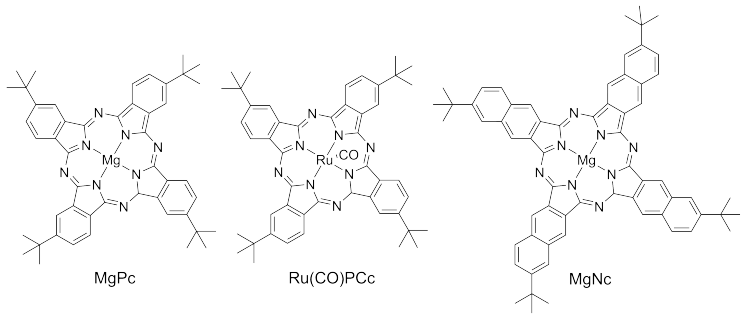

Fig. 8. *Molecular structures of pthalocyanines* ***MgPc*** *and* ***Ru(CO)Pc*** *and naphthalocyanine* ***MgNc****.*

Covalently linked poprhyrin-phthalocyanine dyads and triad were studied in solutions and supramolecular films. The macrocycles in the dyads, free-base porphyrin-zinc pthalocyanine (**H_2P–ZnPc**) and zinc porphyrin-zinc pthalocyanine (**ZnP–ZnPc**) and in the triad **ZnPc–ZnP–ZnPc** were connected using amide bond (Figure 9). The dyads and triad were immobilized *via* metal-ligand coordination on TiO_2 nanoparticle thin film surface modified with axial coordinating ligand, 4-carboxyphenylimidazole [III].

Supramolecular chlorin-fullerene dyads were formed *via* two-point binding to study the influence of mutual position of chlorin (Chl) electron donor and fullerene (C_{60}) electron acceptor on the photoinduced electron transfer [IV]. The chiral zinc chlorin had crown-ether moiety attached to either 13^4 or 17^4 positions (Figure 10). The fullerene was equipped with alkyl aminium ion and pyrrolidine (3-pyridine, 4-pyridine or furan) entities (Figure 11). The synthesis yielded a 1:1 mixture of R- and S-

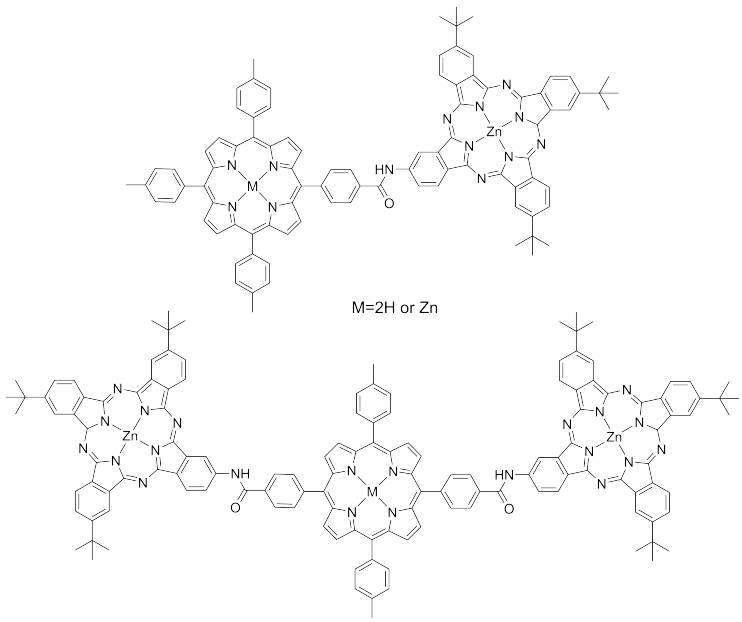

Fig. 9. *Molecular structures of porphyrin-pthalocyanine dyad* ***MP–ZnPc*** *and triad* ***ZnPc–ZnP–ZnPc****.*

enantiomers which were not separated. The two-point binding was achieved by the axial coordination of the pyrrolidine entity to the zinc center of chlorin and the complexation of the aminium ion with crown-ether. The coordination of the chiral chlorin to each fullerene enantiomer resulted in different donor-acceptor distances and geometries.

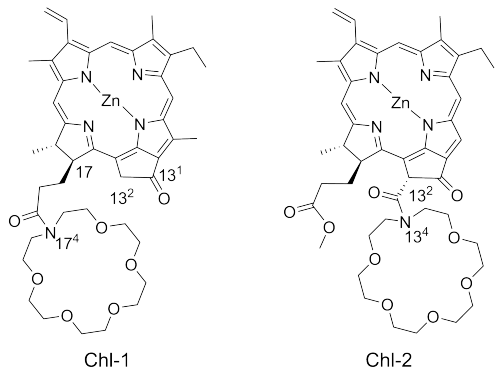

Fig. 10. *Molecular structures of zinc-chlorin-aza-[18]crown-6 molecules,* ***Chl-1*** *and* ***Chl-2****.*

The self-assembled monolayer technique was employed to fabricate a two-layer

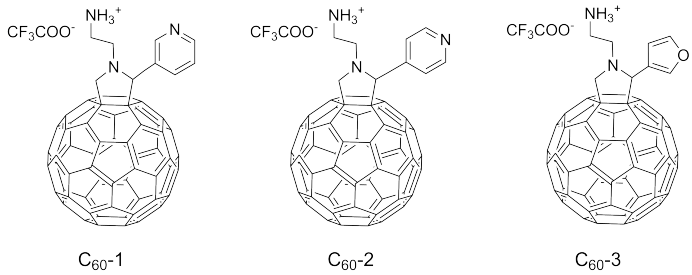

Fig. 11. *Molecular structures of pyrrolidino-[60]fullerenes,* ***C_{60}-1****,* ***C_{60}-2*** *and* ***C_{60}-3****.*

film of porphyrin donor and fullerene acceptor on surface of TiO_2 [V]. Fullerene and porphyrin derivatives were equipped with a carboxyl linker which enabled the anchoring on the TiO_2 surface. The acceptor, fullerene (**CF**), had a short linker which placed it close to the surface. The donor, porphyrin, had longer linker which could penetrate between the fullerenes and keep the porphyrin on top of the fullerenes (Figure 12).

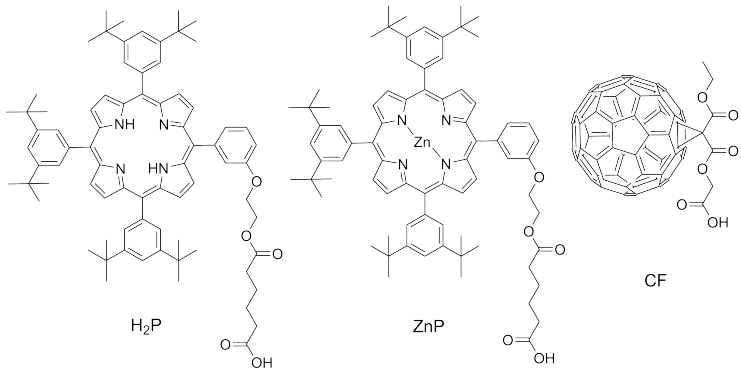

Fig. 12. *Molecular structures of carboxy-substituted porphyrins* ***H_2P****,* ***ZnP*** *and fullerene* ***CF*** *derivatives.*

3.2 Film preparation

The film samples under study [III, V] were prepared using the self-assembled monolayer (SAM) method on nanoporous TiO_2 thin films. Self-assembled monolayers are molecular assemblies formed by the adsorption of an active anchoring group on a solid substrate.[10] SAMs are formed by simply immersing a substrate into an organic solution of the molecules with a group capable of anchoring to the surface. The driving

force for spontaneous formation of the SAMs includes chemical bond formation of the anchoring group with the surface and intermolecular interactions. In this Thesis, SAMs were prepared from molecules containing carboxyl as TiO_2 anchoring group.

3.2.1 TiO_2 nanoparticle deposition

The absorption of SAM on flat surfaces was too low for transient absorption measurements. Thus nanostructured semiconductor thin films with high specific surface area were used as substrates.

TiO_2 nanoparticle (Solaronix:Ti-Nanoxide-T) thin films with a layer thickness of 2 μm were formed on glass substrates by using standard doctor blade technique.[78–81] The substrates were framed with Scotch tape creating 1 $\times$ 3 cm channels. 30 μl of Solaronix:Ti-Nanoxide-T paste was dropped in the channel with a pipette and spread evenly with a glass rod (pasteur pipette). The resulting films were dried in air for one hour while the tape was removed after 5 minutes of drying. After that, the samples were heated for 10 minutes at 120, 250, 330, 450 and 520 °C, respectively, and cooled in air. The uniform thickness of the films was verified by measuring the absorption spectra from the films before SAM deposition.

3.2.2 SAM preparation

The immobilization of the compounds on TiO_2 films was done by immersing the films in the solutions of corresponding compounds (Figure 13). Prior to the immobilization, the TiO_2 films were heated at 150°C for 30 minutes to remove moisture and cooled quickly in air to under 80°C. The solvent, compound concentration and immersion time were adjusted individually for each compound. The layer formation was controlled by measuring the film absorption after different immersion times. After deposition, the samples were washed by dipping them into pure solvent to remove the physisorbed molecules. Washing time was also controlled by absorption measurements. Details of the SAM parameters are given in papers III and V.

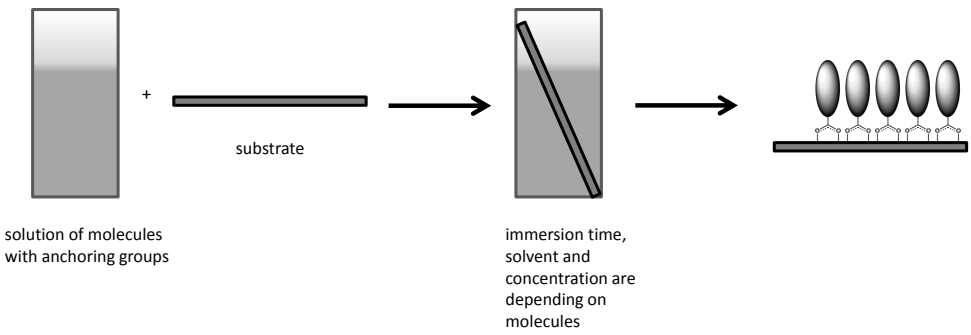

Fig. 13. *Self-assembled monolayers are formed by simply immersing a substrate into a solution of the molecule with anchoring group.*[10]

3.3 Spectroscopy

3.3.1 Steady-state absorption and emission

Steady-state absorption and emission spectroscopy were used to determine the wavelengths where the studied molecules and supramolecules absorb and emit light. Binding constants for self-assembled supramolecular complexes were determined from absorption and emission spectral changes during titration [I, II, IV]. Absorption spectra were also used for selecting the excitation wavelength for fluorescence and time-resolved absorption measurements so that the particular chromophore was selectively excited. In addition, immersion and washing times for self-assembled monolayer deposition were determined from absorption measurements [V].

Fluorescence spectra were used to study the interactions between chromophores in supramolecular dyads. A selective excitation of acceptor molecules was used and efficient emission quenching by the donor molecules indicating energy or electron transfer between the chromophores was observed. Furthermore, fluorescence spectra were used for selecting the monitoring wavelength for time-resolved fluorescence measurements so that the fluorescence decay of a specific chromophore could be followed.

3.3.2 Pump-probe

Time-resolved transient absorption spectra in the femtosecond timescale were measured by using the pump-probe method (Figure 14). In this Thesis, two separate setups were used, which had different characteristics (Table 1), but the same operational principles. The excitation source, a Ti:Sapphire laser system, generates femtosecond pulses at 800 nm. The laser output is split in two parts used for generating pump and probe beams. The pump beam is delivered to an optical parametric amplifier (OPA) or a second harmonic generator (SHG) to produce the excitation pulses at the desired wavelength. The second beam is passed through a white continuum generator (WCG, water cuvette or sapphire for Setups 1 and 2, respectively) to produce the probe beam for detecting the absorbance changes in a wide spectral region. The probe beam is split in two parts, reference and signal, which are both focused on the sample. The pump beam is passed through a delay line, which is a moving right angle reflector and thus its position changes the optical path length of the pump beam relative to the probe beam. The pump pulse is then focused on the same spot in the sample as the signal beam. After the sample, the reference and signal beams arrive at a photo-detector coupled with a monochromator. The photo-detector records both the reference and signal spectra and from those the absorption change induced by the excitation is obtained. Depending on the position of the delay line, the pump pulse arrives at the sample at a certain time before the probe pulse and the transient absorption spectra of the sample at different time delays after excitation are measured.

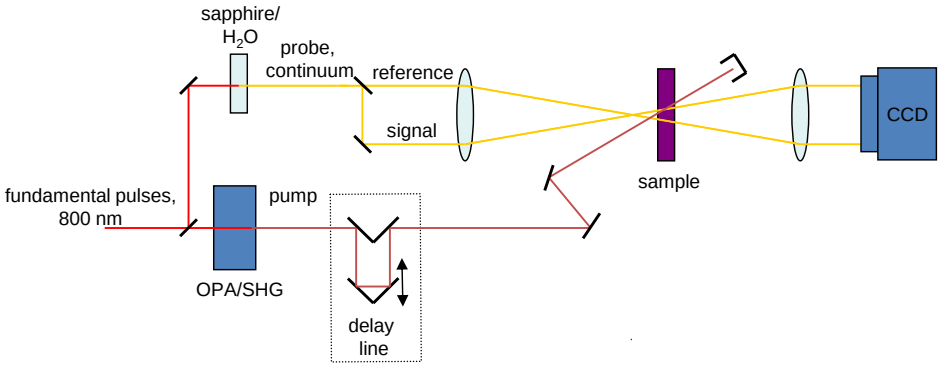

Fig. 14. *Simplified scheme of the pump-probe setup. OPA is a optical parametric amplifier and SHG is a second harmonic generator.*[82]

Table 1. *Characteristics of the pump-probe setups.*

	Setup 1	Setup 2
Laser	Ti:Sapphire	Libra F
Repetition rate	10 Hz	1 kHz
Pulse energy	0.5 mJ	1 mJ
Pulse duration	100 fs	100 fs
ΔA_{min}	10^{-3}	10^{-5}
Delay line length	1.2 ns	6 ns

The main difference between Setup 1 and Setup 2 is the laser repetition rate, which is 100 times faster in Setup 2 than in Setup 1. Consequently, the sensitivity of Setup 2 is 100 times better, which makes possible to study low absorbing samples such as films more accurately. Also the delay line is longer in Setup 2. The pump-probe measurements for papers [I]–[IV] were done with Setup 1 and Setup 2 was used in paper [V].

To avoid photodegration of the samples during the measurements, solution samples were measured in rotating 1 mm cuvette. For solid samples, the assembly consisting of two plates was used. One plate was the sample with the sensitisized TiO_2 film and another was a glass window. The inner volume was sealed and filled with nitrogen so that the sample surface was inside and the measurements could be conducted in an oxygen-free atmosphere.

The transient states and lifetimes of the photoinduced reactions can be identified from the detected changes in absorption. The raw data obtained from the measurements are the differential transient spectra at different delay times. The array of transient absorption spectra can be converted to the array of transient absorption decay curve in range of wavelengths and fitted globally with a multi-exponential or other model to get the decay time constant and component spectra associated with them.

3.3.3 Flash-photolysis

The flash-photolysis method was used to study transient absorption in the millisecond timescale [V]. The method is similar to the pump-probe method, but a continuous light is used for the monitoring and the transient absorption at only one wavelength

can be monitored at a time. The scheme of the flash-photolysis setup used in this Thesis is presented in Figure 15. The measurements were performed with excitation pulses from a Nd:YAG laser at 532 nm (5 ns, 5-15 mJ per pulse). The monitoring light was obtained from a tungsten halogen light source. The signal was detected by a silicon photoreceiver coupled with a monochromator and recorded by a digitizing oscilloscope. The Luzchem laser flash system (mLFP-111) was used to control the experiments.

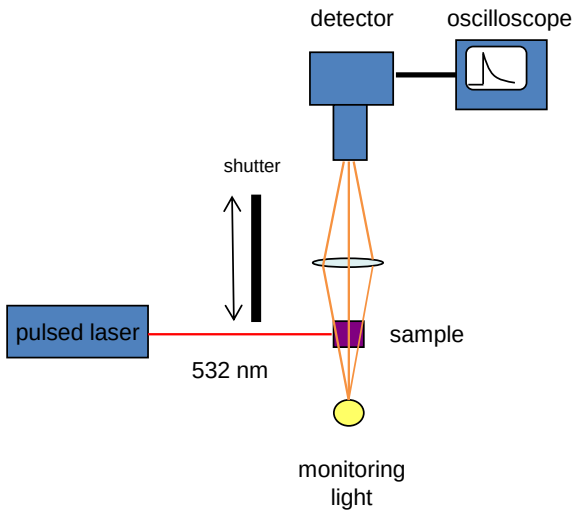

Fig. 15. *The flash photolysis system used in the study.*[82]

3.3.4 Up-conversion

The up-conversion method for time-resolved fluorescence measurements was used to detect the fast emission decays with a femtosecond time resolution [I,II, IV]. In the up-conversion instrument (Figure 16) the second-harmonic of the fundamental pulses generated by a Ti:Sapphire laser at 800 nm was used to excite the sample. Emission from the sample was focused on a nonlinear crystal (NLC) together with the gate pulses, which were the laser fundamentals passed through a delay line and determining the delay time of the gate relative to the excitation pulse. The emission at the sum frequency (ν_d) of the gate pulse (ν_g) and the selected emission maximum (ν_{em}) of the sample, *i.e.* $\nu_d = \nu_g + \nu_{em}$, was measured. The method is called up-conversion because the signal is not detected at the frequency of sample (ν_{em}), but at a frequency

shifted up by the gate pulse (ν_g). The emission decay curve of the sample was detected by scanning the delay line.

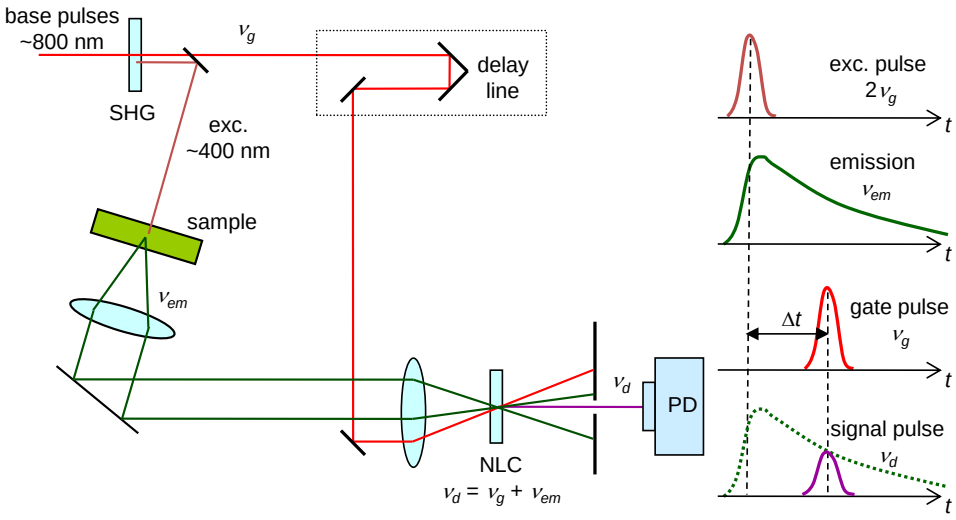

Fig. 16. *Simplified scheme of the up-conversion setup for fluorescence decay measurements. SHG is a second harmonic generator and NLC is a non-linear crystal.*[82]

3.3.5 Data fitting models

In the data analysis procedure the decay curves, obtained from the pump-probe, flash-photolysis or up-conversion measurements, are fitted globally using, for example, sum of exponentials as the model decay:

$$\Delta A(\lambda,t) = \sum_{i=1}^{N} a_i(\lambda)\exp(-\frac{t}{\tau_i}) \tag{19}$$

where a_i are the amplitudes and τ_i are the lifetimes of the components. In a simple case, the number of components needed for a reasonable fitting of the data give the number of transient species in the reaction. The transient states which have lifetime longer than the used delay line are included in the component with inaccurate long lived lifetime. The amount of components was determined based on the improving fit quality *i.e.* the mean square deviation, σ^2, of the fit. The quality was considered improved, if σ^2 improved by more than 10% after adding the exponentials one by one.

Multiexponential global data fitting was used to analyze the time-resolved absorption and emission spectra in solution. However, in film samples, the population of the excited states may decrease non-exponentially due to the inhomogeneity of the local environments of individual molecules in the film.

The distributed decay model was used for film samples when the transitions between the states did not follow the exponential law [V]. This model assumes that the total decay is the sum of the exponential decays with a specific distribution of energy. The probability to find a molecule in reactant state decreases exponentially with time $p(t) = e^{-k_{et}t}$, assuming that at $t = 0$ the system is in the reactant state *i.e.* $p(0) = 1$. For a macroscopically large number of molecules the population of the product state is the sum of the probabilities $p(t)$. The decay of the reactant state is given by an integral over all possible values of x

$$p_r(t) = \frac{1}{\sqrt{\pi}\Delta E} \int_{-X}^{+X} \exp\left(-\frac{x^2}{\Delta E^2}\right) \exp\left(-\frac{t}{\tau_0} e^{\frac{ax}{k_B T}}\right) dx \tag{20}$$

where x is the deviation of the the energy from an average non-distributed value, ΔE is the distribution width and $a = -\frac{\Delta G + \lambda}{2\lambda}$ is a factor determining how sensitive the decay profile to the energy distribution is and it depends on the free energy of the reaction, ΔG, and reorganization energy, λ.[83,84]

3.4 Differential pulse voltammetry

Differential pulse voltammetry (DPV) [IV] and cyclic voltammetry [I,II] were used to measure the oxidation, E_{ox}, and reduction potentials, E_{red}, of donors and acceptors separately. A potentiostat and a three-electrode cell configuration were employed. A platinum wire sealed in glass or platinum button was used as working electrode. A Ag/AgCl wire was used as a reference electrode and a graphite rod as a counter electrode. Measurements were done in 0.1 M tetrabutylammonium chloride in o-dichlorobenzene (DCB, dried and stored under molecular sieves) as supporting electrolyte. The samples were purged prior to measurements using argon or nitrogen gas. After measuring the background, the sample dissolved in supporting electrolyte was added to the electrochemical cell. The concentration of all the measured samples in the cell were $\sim$0.5 mM. Finally, an internal reference ferrocene in DCB was added

to the cell and measurements were repeated to scale the measured potential against vacuum level. All the measurements were carried out towards the positive and negative potential.

4. RESULTS AND DISCUSSION

This chapter summarizes the most important results and findings of the studies presented in detail in the papers [I]–[V]. The self-assembly approach was used to construct donor-acceptor architectures in order to study of the influence of the structure on the photophysics of the assemblies. First, the self-assembly of supramolecular donor-accceptor structures and their photoinduced properties in solutions are discussed. Secondly, the preparation of donor-acceptor self-assembled monolayers (SAMs) on a TiO_2 nanoporous surface is introduced and their photophysics is described.

4.1 Supramolecular dyads in solution

The self-assembly of supramolecular donor-acceptor complexes was studied in solutions. The complexes were formed *via* one-point metal-ligand axial coordination or two-point metal-ligand and crown-ether coordination. Effective donor fluorescence quenching after selective excitation of donor indicated electronic interaction between chromophores and these photoinduced processes were studied using the time-resolved absorption and emission spectroscopy.

4.1.1 Supramolecular dyad formation

The binding constant for the formation of supramolecular complex describes how stable the supramolecular binding is. To obtain the binding constants, K, from absorption or emission data, the Benesi-Hildebrand plot or the Stern-Volmer plot were used, respectively. To determine the stoichiometry with absorption or emission spectroscopy, Job's method or molar ratio methods were used. In addition, the structures of the supramolecular dyads were obtained from computational studies done at Wichita State University ([I, II]) and University of Helsinki ([IV]).

Poprhyrin-phthalocyanine assemblies via axial coordination

The dyads were self-assembled by using free-base porphyrins functionalized with phenylimidazole capable to react with the central metal of phthalocyanine or naphthalocyanine. The axial coordination of free-base poprhyrin, **H_2PIm**, to pthalocyanine or napthalocyanine compounds, **MgPc**, **MgNc** and **Ru(CO)Pc**, was studied in non-coordinating non-polar solvents, DCB or toluene. The binding strengths for **H_2PIm**:**MgPc** and **H_2PIm**:**MgNc** complexes were studied by measuring the absorption spectral changes occurring on the addition of **H_2PIm** to the solution of **MgPc** or **MgNc**. The binding constants were obtained from the data by using Benesi-Hildebrand analysis and the obtained values were in the range $10^2 - 10^3$ M^{-1}. Compared to earlier published measurements for **H_2PIm**:**ZnPc** complexes,[51] the magnitudes of the *K* values were smaller and suggested weaker binding for **H_2PIm**:**MgPc** complexes. The molar ratio method, which was used to determine the stoichiometry of the complexes, confirmed 1:1 dyad formation between the donor and acceptor molecules (Figure 17). The CO group in **Ru(CO)Pc** resulted in stronger ligation due to the π-acceptor carbonyl ligand at one of the two axial Ru(II) coordination sites and led certainly to 1:1 complex formation with **H_2PIm**.

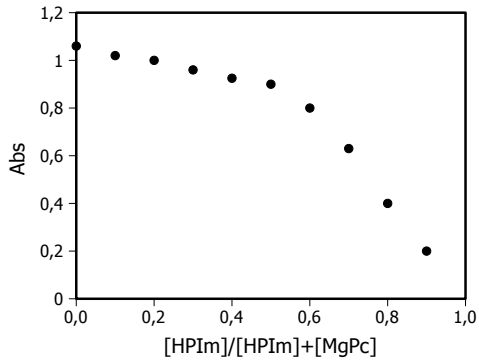

Fig. 17. *The molar ratio plot to determine the supramolecular stoichiometry for* ***H_2P_pIm:MgPc*** *complex [I].*

The structures of supramolecular dyads were calculated to visualize the different donor-acceptor distances and orientations due to different imidazole substitutions. The geometry of all porphyrin-pthalocyanine dyads were similar despite of different central metals or macrocycle structures. The two macrocyclic rings of the dyads revealed closer distance and skipped coplanar configuration for the *ortho* derivatives,

and relatively longer distance and larger angle between macrocycles for the *meta* and *para* substituted derivatives (Figure 18). Generally, the donor-acceptor center-to-center distance (R_{C-C}) varied as: *ortho* < *meta* < *para* for complexes with imidazole substituted porphyrins (Table 2).

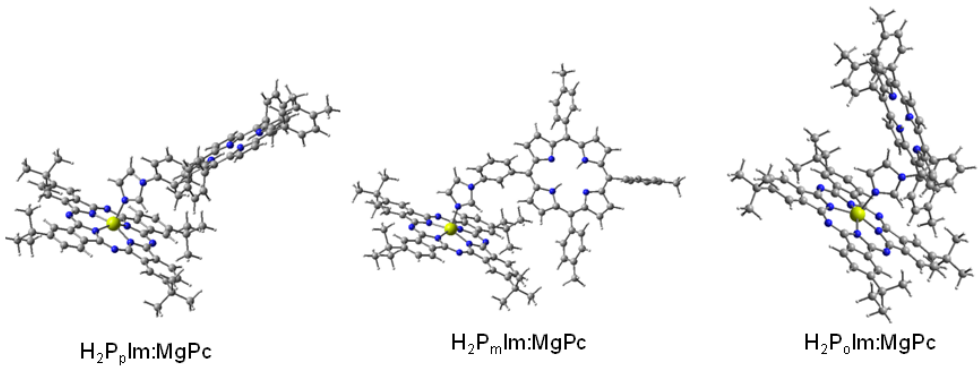

Fig. 18. *B4LYP/3-21G(*) optimized structures of the dyad formed* via *axial coordination of* ***H_2PIm*** *(***p**ara,**m**eta *or* **o**rtho *derivatives) to* ***MgPc*** *[I].*

For pentad formation, **$H_2P_p(Im)_4$:(Ru(CO)Pc)$_4$**, all of the meso positions of free-base porphyrin were functiolized with phenylimidazole at *para* position. All the four coordinated **Ru(CO)Pc** entities oriented at approx. 50° angle to the plane of the porphyrin ring. The donor-acceptor distance (R_{C-C}) was 13.2 Å, which is close to the same value for the **H_2P_pIm**:**Ru(CO)Pc** complex.

Stable supramolecular dyads and even pentads could be formed using the metal-ligand binding approach. The stability of these supramolecular dyads was found to depend on the central metal indicated by the highest binding constant for ruthenium based dyads and lower binding constant for magnesium based dyads compared to previously reported zinc analog. Furthermore, the binding efficiency depended on the position of the imidazole linker which affected the steric accessibility. The *para*-substitution provided less steric restrictions for complex formation and binding constants for **H_2P_pIm** containing dyads were higher than for others. The *ortho*-position of the imidazole group was sterically the least accessible and thus the binding constant was smallest for **H_2P_oIm** containing dyds. The substitution of the imidazole entity at different positions resulted in dyads of different orientations and donor-acceptor distances.

Chlorin-fullerene dyads via two-point binding

Two zinc chlorins equipped with crown-ether moiety at different positions and three pyrrolidine functiolized fullerenes armed with alkyl aminium were used for two-point self-assembly of supramolecular dyads. The two-point binding was achieved by axial coordination of pyrroldine (pyridine or furan) moiety to Zn and simultaneously alkyl aminium coordination to crown-ether. Titration experiments were carried out by adding concentrated solution of $\mathbf{C_{60}}$ to solution of **Chl** in DCB and the fluorescence quenching of **Chl** was used to evaluate the strength of the complex formation. However, the linear dependence in Stern-Volmer plot is only observed when the concentration of one of the compounds is much higher than the other. Therefore, since the fullerene concentration was as high as the chlorin concentration, the complex concentration was calculated from the Equation 13 and plotted versus $\mathbf{C_{60}}$ concentration. The obtained binding constants for different combination of $\mathbf{C_{60}}$ and **Chl** were in the range $10^3 - 10^5$ M^{-1} and indicated enhanced binding strength due to two-point binding compared to dyads assembled *via* one-point binding. To determine the stoichiometry of formed complexes, the absorption titration data was used and Job's plot in Figure 19 indicates the formation of 1:1 complex.

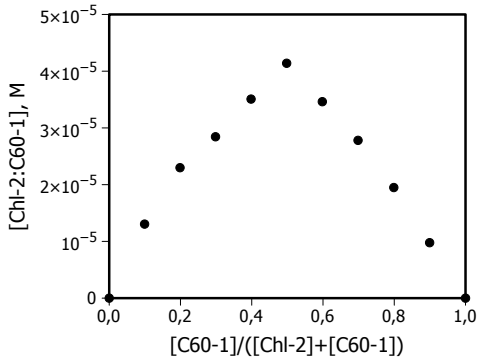

Fig. 19. *Job's plot to determine the supramolecular stoichiometry for* ***Chl-2*:*C_{60}-1*** *complex [IV].*

The self-assembled **Chl**:$\mathbf{C_{60}}$ complexes had different DA distances and orientations for R- and S-enantiomers of different fullerenes coordinating to the chiral crown-ether functionalized chlorin. The computational studies of dyads showed enantiospecific binding and global minimum structures for the fullerene enantiomers. This means that the diastereomeric chlorins have the ability to discriminate between different enan-

tiomers of fullerene derivatives and thus favor complexation with only one enantiomer. Furthermore, for the formed enantiospecific complexes, the DA distances varied as: *meta*-pyridine < furan < *para*-pyridine functionalized fullerenes with both chlorins (Figure 20).

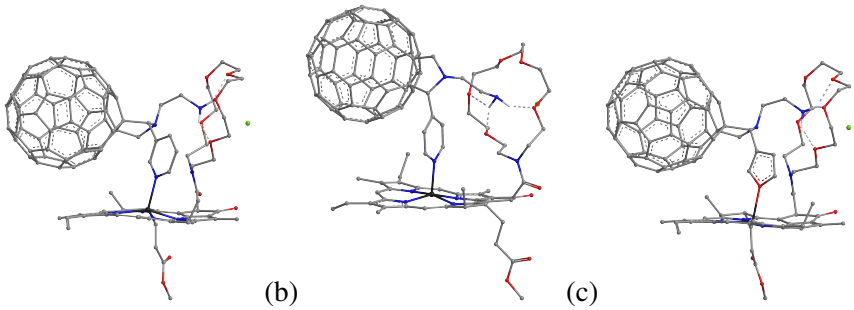

Fig. 20. *Optimized structures at DFT level in solution, with TPSS-D3/def2-TZVP//def2-SVP, of the (a)* ***Chl-2*****:C_{60}-1***, (b)* ***Chl-2*****:C_{60}-2** *and (c)* ***Chl-2*****:C_{60}-3** *dyads formed* via *two-point binding.*

Consequently, at high concentrations needed for transient absorption measurements, it was presumed that the lower energy complex was formed predominantly and studied complexes were monoenantiomeric. Moreover, since the high stability of these complexes and the crown-ether coordination, the complexes were formed in both nonpolar DCB and polar PhCN.

4.1.2 Photoinduced energy and electron transfer

The fluorescence quenching studies for the free-base porphyrin-phthalocyanine or -napthalocyanine assemblies demonstrated efficient fluorescence quenching of **H_2PIm** on addition of either **MgPc**, **MgNc** or **Ru(CO)Pc**, indicating that energy and/or electron transfer takes place between the chromophores. Since fluorescence of the **H_2PIm** energy donor overlaps with the Q-band absorption of the studied pthalocyanine and napthalocyanine acceptors, at least Förster type energy transfer from the excited donor to acceptor was expected to occur in the dyads and pentad.

The energy of the CS state was estimated from DPV measurements. The lowest energy charge-separated states (E_{CS}) for dyads were slightly lower than the lowest singlet excited state energies (1.89 eV for **H_2PIm**, 1.78 eV for **MgPc**, 1.58 eV for **MgNc** and 1.85 eV for **Ru(CO)Pc**) if the Coulombic interaction was neglected (Table 2). The

lowest energy CS state was in all cases H_2PIm^-:Pc^+, which means that the electron transfer would occur from the pthalocyanine electron donor to porphyrin acceptor. However, the calculated free-energies of charge-separation using Equation 6 revealed the CS to be endothermic in nonpolar toluene and close to zero or only slightly exothermic in polar PhCN.

Table 2. *Computed center-to-center distances (R_{C-C}), calculated CS state energies (E_{CS}) and free-energies for CS state formation (ΔG_{CS}) for studied supramolecular dyads in nonpolar toluene and polar PhCN.*

Complex	R_{C-C}, Å	E_{CS}, eV	ΔG_{CS}^{Tol}, eV	ΔG_{CS}^{PhCN}, eV
H_2P_oIm:MgPc	7.7	1.73	-0.73	-0.02
H_2P_mIm:MgPc	11.0	1.73	-0.50	0.00
H_2P_pIm:MgPc	13.1	1.73	-0.41	0.01
H_2P_oIm:MgNc	8.3	1.41	-0.56	0.11
H_2P_mIm:MgNc	12.1	1.41	-0.33	0.13
H_2P_pIm:MgNc	13.1	1.41	-0.29	0.13
H_2P_oIm:Ru(CO)Pc	8*	1.74	-0.64	0.04
H_2P_mIm:Ru(CO)Pc	11*	1.79	-0.48	0.01
H_2P_pIm:Ru(CO)Pc	12*	1.80	-0.45	0.00
Chl-1:C_{60}-1	8.9	1.25	0.44	0.54
Chl-1:C_{60}-2	10.9	1.25	0.47	0.55
Chl-1:C_{60}-3	8.9	1.25	0.44	0.54
Chl-2:C_{60}-1	8.6	1.27	0.41	0.52
Chl-2:C_{60}-2	9.6	1.27	0.43	0.52
Chl-2:C_{60}-3	8.8	1.27	0.42	0.52

* Exact values were not provided, but values were mentioned to range between 8-12 Å and varied as: *ortho* < *meta* < *para* imidazole-substituted porphyrins.

The transient absorption measurements with the pump-probe method for the porphyrin-phthalocyanine or -napthalocyanine assemblies were carried out with excitation at 420 nm which allowed a predominant excitation of the porphyrin chromophore. The selective excitation of the energy donor moiety resulted in efficient excitation transfer from **H_2PIm** to **MgPc** or **MgNc** in non-coordinating toluene, but no experimental evidence of the electron transfer was obtained which could be predicted based on the calculated free-energies summarized in Table 2. The free-energies for electron transfer in polar solvent such as PhCN were generally slightly exothermic. However, the magnesium-imidazole coordination was not stable in polar media and thus meas-

urements were done only in non-polar toluene. In addition, the degradation of **MgPc** and **MgNc** during up-conversion measurements was unreasonably high. Therefore those results were not reliable and were left out of discussion.

As has been mentioned, the ruthenium-imidazole coordination was stronger and the pump-probe measurements for **H_2PIm**:**Ru(CO)Pc** complexes could be done also in PhCN. The transient absorption component spectra of **H_2P_mIm**:**Ru(CO)Pc** complexes in toluene and PhCN are shown in Figure 21. In both solvents the time-resolved spectra right after the excitation (at 0 ps) showed bleaching of the ground state absorption due to the instant formation of the singlet excited state of excited porphyrin. After fast relaxation of the singlet excited state (18 ps and 14 ps components in toluene and PhCN, respectively), the state with lifetime slower than the longest time delay for the instrument (> 2 ns, Setup 1) is formed. However, the longest decay components had considerably different features indicating that excited **H_2P_mIm** returns to the ground state through different intermediates in nonpolar and polar solvent. In toluene, the longest component (>2 ns) had characteristic features of the **Ru(CO)Pc** excited state at 585 and 645 nm and triplet state at 720–730 nm but no sings of porphyrin transient state. Therefore, the 18 ps component was attributed to the energy transfer from porphyrin to pthalocyanine. However, the 18 ps component showed also features of the **Ru(CO)Pc** triplet state at 720–730 nm and revealed that the singlet excited state of **Ru(CO)Pc** was instantly converted to triplet state through intersystem crossing (ISC) before returning to the ground state. Whereas for the dyad in polar PhCN, the longest living component showed features of the ground state bleaching of both chromophores and the **Ru(CO)Pc** cation band at 690–780 nm. Therefore, the 14 ps component was attributed to charge transfer form **Ru(CO)Pc** to **H_2P_mIm**. The other two complexes with **H_2P_pIm** and **H_2P_oIm** revealed similar transitions that with **H_2P_mIm**. The result for pentad, **H_2P_p(Im)$_4$:(Ru(CO)Pc)$_4$**, differed from those of the dyads since no charge transfer reactions was observed in PhCN. This was attributed to different orientation factors promoting the competing ISC process.

The fluorescence decays measured with the up-conversion method showed the relaxation of porphyrin singlet excited state with essentially the same time constants that the energy transfer. Therefore, since the energy transfer was the time limiting step in all cases, the time constants for ISC or CS could not be determined. The measured energy transfer time constants and fluorescence decay time constants are listed in Table 3.

The chlorin-fullerene complexes had better energetics to favor charge-transfer than the

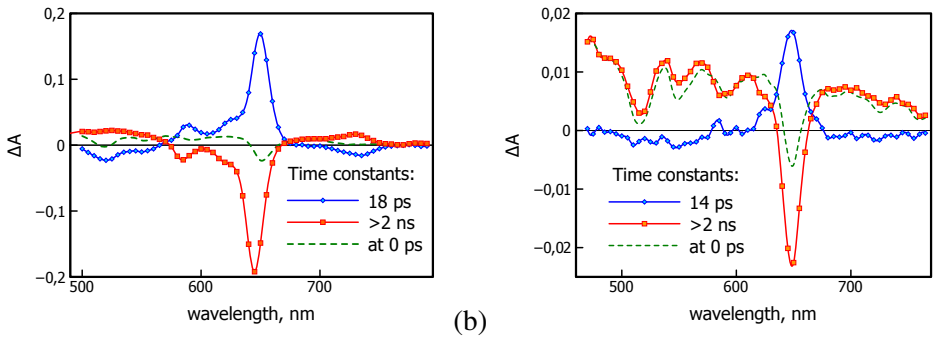

Fig. 21. *Transient absorption component and time resolved (at zero delay) spectra of* ***H_2P_mIm:Ru(CO)Pc*** *in a) toluene and b) benzonitrile [II].*

Table 3. *Time constants for the energy transfer (τ_{ET}) and the fluorecence decay time constants (τ_{SI}) in porphyrin-pthalocyanine and -napthalocyanine complexes obtained from pump-probe and up-conversion measurements, respectively.*

Complex	τ_{ET}^{Tol}, ps	τ_{ET}^{PhCN}, ps	τ_{SI}^{Tol}, ps	τ_{SI}^{PhCN}, ps
H_2P_oIm:MgPc	2.9			
H_2P_mIm:MgPc	11			
H_2P_pIm:MgPc	18		n/a	
H_2P_oIm:MgNc	0.2			
H_2P_mIm:MgNc	15			
H_2P_pIm:MgNc	13			
H_2P_oIm:Ru(CO)Pc	6	8	8	9
H_2P_mIm:Ru(CO)Pc	18	14	16	15
H_2P_pIm:Ru(CO)Pc	30	28	32	28
$H_2P_p(Im)_4$:$(Ru(CO)Pc)_4$	10	26	12	10

porphyrin-pthalocyanine or -napthalocyanine complexes. The estimated free-energies for CS indicate that the electron transfer from chlorin to fullerene was clearly exothermic both in nonpolar and polar solvents (Table 2). The pump-probe measurements of the dyads showed two intermediates with time constants in ps timescale and one long-lived time constant with the time constant much longer than the measurement scale (Setup 1). Figure 22 presents the transient absorption component spectra for **Chl-2**:**C_{60}-1** dyad. The fastest component (5 ps) was attributed to the formation of the CS state based on the bleaching of the ground state absorption of chlorin and increasing absorbance at 1040 nm, which is characteristic for fullerene anion. The

second component had spectrum typical for the CS state with chlorin cation band around 750 nm and fullerene anion band at 1040 nm and it was attributed to the charge recombination.[34,37,85] The longest living component was attributed to nonbonded chlorins. The singlet state lifetime obtained from the emission decay measurements with up-conversion method was somewhat shorter than the fast time constant obtained from the pump-probe measurement. That indicated that the accuracy of the pump-probe measurements was insufficient to identify all transitions, for example the energy transfer or exciplex, prior to the formation of the CS state. All the studied chlorin-fullerene dyads showed similar spectral features in nonpolar DCB and polar PhCN.

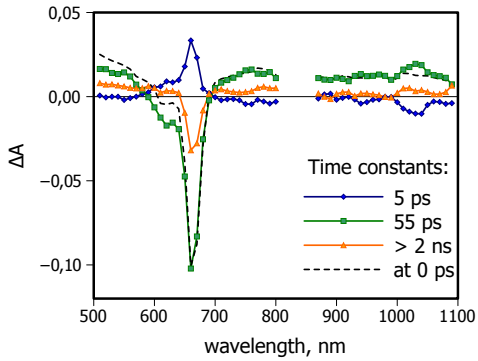

Fig. 22. *Transient absorption component and time resolved (at zero delay) spectra of* ***Chl-2:C_{60}-1*** *in DCB [IV].*

The experimentally measured kinetic results agreed well with the free-energy calculations suggesting inefficient CS in nonpolar media. The excitation of the **H_2PIm** entity in porphyrin-pthalocyanine and -napthalocyanine dyads resulted in efficient energy transfer to pthalocyanine and napthalocyanine in non-polar toluene. In addition, the calculations were suggesting slightly possible CS in polar media, which was confirmed with the **Ru(CO)Pc** containing dyads revealing charge transfer from the **Ru(CO)Pc** to **H_2PIm** in polar benzonitrile. Furthermore, due to the high electron affinity of the **C_{60}**, the electron transfer from chlorin to fullerene was observed in both non-polar DCB and polar PhCN as expected.

4.1.3 Effect of distance and orientation on kinetics of photoinduced processes

The effect of donor-acceptor distance and orientation on the kinetics of the photoinduced energy and electron transfer in supramolecular complexes was studied by changing the position of metal coordinating moieties in free-base porphyrin of **H_2PIm**:**MPc** complexes and in fullerene of **Chl**:**C_{60}** complexes. The substitution of the imidazole entity at the *ortho*, *meta* or *para* positions of one of the meso-aryl groups of free-base porphyrin and fullere with the 3-pyridine, 4-pyridine or 3-furan resulted in formation of the dyads with different geometries and rates of the photoinduced processes.

Effect of distance and orientation on energy transfer

The measured time constants of the energy transfer (Table 3) for **H_2PIm**:**MgPc** dyads increased in the sequence *ortho<meta<para* which was in line with the increase of the calculated distance between the donor and acceptor. Also for the **H_2PIm**:**MgNc** and **H_2PIm**:**Ru(CO)Pc** dyads, the distances and time constants of the energy transfer were in agreement. However, although the donor-acceptor distance for pentad **$H_2P_p(Im)_4$:$(Ru(CO)Pc)_4$** was almost same as for dyad **H_2P_pIm**:**Ru(CO)Pc**, the time constants of the energy transfer was slightly faster for the pentad. The higher number of acceptor entities increased the total rate of the energy transfer.

In addition, the rate of the energy transfer depended on the position of imidazole linker on the **H_2PIm**. Transient absorption curves at 680 nm, which corresponded to the Q-band absorption of the phthalocyanine and showed the degree of the band bleaching are presented in Figure 23. There were two reasons for the Q-band bleaching: the direct photoexcitation of **MgPc** and the energy transfer from **H_2PIm** to **MgPc**. The relative contribution of the slower component due to energy transfer was found to be in agreement with determined binding constants for dyad formation i.e. the **H_2P_mIm**:**MgPc** dyad had the highest relative amount of **MgPc** which is excited *via* energy transfer and the highest binding constant. Although the energy transfer was fastest and donor-acceptor distance was shorter for **H_2P_oIm**:**MgPc** dyad, the contribution of the slower component was lowest. The lowest binding constant and thus the lowest amount of pthalocyanines that received excitation *via* energy transfer were a consequence of the sterically least accessible position of the imidazole group in **H_2PIm** for coordination to **MgPc**.

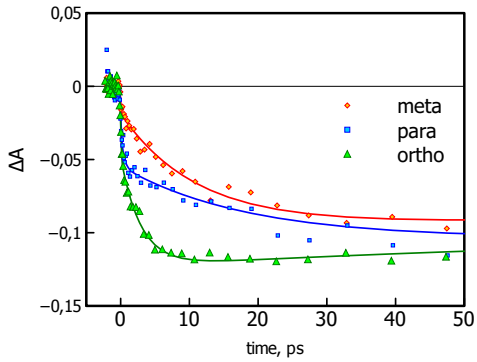

Fig. 23. *Transient absorption curves of* ***H_2PIm:MgPc*** *dyads at 680 nm [I].*

Effect of distance and orientation on electron transfer

According to the semi-classical Marcus electron transfer theory (see Chapter 2.2.1), the rate of electron transfer depends on the electronic coupling between the donor and acceptor, the nature of the bridge and the dielectric constant of the medium. The electronic coupling decreases exponentially and the distance dependence follows the exponential law given by Equation 10. The CS state lifetimes obtained from pump-probe measurements for **Chl-C_{60}** complexes (Table 4) were found to correlate with the donor-acceptor edge-to-edge distances (see paper IV) with the damping factor roughly 0.44 $Å^{-1}$. In addition, the rate of electron transfer was found to be four times shorter in polar PhCN than in nonpolar DCB. This was expected, since at higher solvent polarity the energy of CS state is slower (Table 2) and the reorganization energy is higher (Equation 8) and the net effect is a shorter lifetime of the CS state.

The CS state lifetime for the covalently linked zinc phytochlorin-fullerene dyad was reported to be 21 ps in PhCN,[34] which is longer than observed lifetimes in PhCN for supramolecular dyads used in this study, whereas the edge-to-edge distance was shorter. Structures of the studied **Chl**:**C_{60}** dyads are presented in Figure 20, where it can be seen that the fullerenes were located on the top of the chlorin macrocycle. However, in covalently linked dyad, the fullerene was close to the edge of chlorin macrocycle. Thus the center-to-center distance was found to correlate better with lifetimes between dyads with different mutual orientations of the donor and acceptor entities. This was attributed to a stronger electronic coupling between entities with the same edge-to-edge distance but shorter center-to-center distance.

Table 4. *The fluorescence decay time constants (τ_{SI}) and the charge transfer and charge recombination time constants (τ_{CS} and τ_{CR}) for chlorin-fullerene complexes obtained from up-conversion and pump-probe measurements, respectively.*

Complex	τ_{SI}^{DCB}, ps	τ_{CS}^{DCB}, ps	τ_{CR}^{DCB}, ps	τ_{CR}^{PhCN}, ps
Chl-1:$\mathbf{C_{60}}$**-1**	2.0	1.7	63	14
Chl-1:$\mathbf{C_{60}}$**-2**	2.5	0.3	76	
Chl-1:$\mathbf{C_{60}}$**-3**	3.1			
Chl-2:$\mathbf{C_{60}}$**-1**	1.6	5	55	15
Chl-2:$\mathbf{C_{60}}$**-2**	2.2	7	187	60
Chl-2:$\mathbf{C_{60}}$**-3**	4.4			

The kinetics of the energy and electron transfer processes revealed that the time constants for the processes depended on the structure of the complexes. The rate of energy transfer was affected by the position of the imidazole linker on the free-base porphyrin entity. Also the pyrrolidine linker affected the efficiency of electron transfer in chlorin-fullerene dyads. Due to supramolecular assembly, the different complexes were easy to study by only changing the linker or its position but keeping otherwise the donor and acceptor units untouched and solely to mix different combinations.

4.2 Donor-acceptor systems on TiO_2 surface

The self-assembled monolayer (SAM) technique was used to build donor-acceptor layers on a TiO_2 nanoparticle thin film. The prepared TiO_2 films are known to have mesoporous structure with the much greater pore size than the size of dye molecules which makes possible to deposit dye SAMs and provides samples with sufficiently high specific surface area for effective light collection and spectroscopy studies.[78] The covalently linked porphyrin-phthalocyanine dyad was immobilized on the surface with two step self-assembly [III]. In the first step, the TiO_2 surface was functionalized with the phenylimidazole SAM. After that, the dyad layer was immobilized *via* axial coordination of zinc porphyrin of the dyad to imidazole.

An alternative approach was developed for deposition of the donor-acceptor two-layer films [V]. The porphyrin-fullerene two-layer films were constructed by using compounds with anchoring groups of different length. First, the fullerene with shorter

linker formed the primary SAM and after that porphyrin, with a longer linker able to penetrate between the fullerenes, formed the porphyrin layer on top of it. The photoinduced electron transfer at these organic-semiconductor interfaces were studied with time-resolved absorption spectroscopy.

4.2.1 Deposition of SAMs

Covalently linked **H_2P–ZnPc** and **ZnP–ZnPc** dyads (Figure 9) were immobilized *via* metal-ligand coordination to 4-carboxyphenylimidazole functionalized TiO_2 nanoparticle film. The SAM preparation was done according to an earlier published method for similar structures.[86] The control experiments confirmed that the coordination through **ZnP** is stronger than through the **ZnPc** entity of the dyad and thus, the **ZnP–ZnPc** dyad is coordinated predominantly through the porphyrin side (Figure 24).

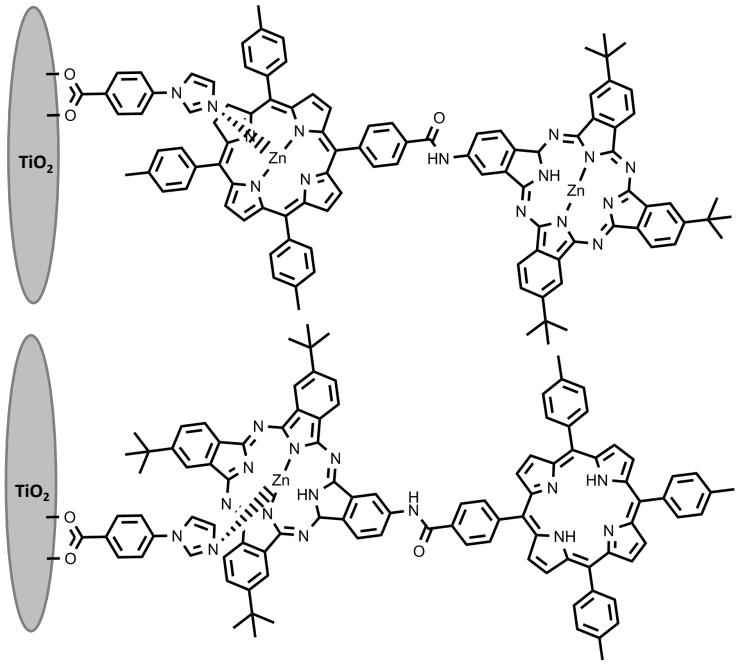

Fig. 24. *Schematic structure of* ***ZnP–ZnPc*** *and* ***H_2P–ZnPc*** *dyads on TiO_2.*

A new layer-by-layer assembly method for deposition of layered donor-acceptor films was proposed and implemented by assembling a TiO_2 **| CF | P** structure. The method was based on using two separate molecules with different linker lengths allowing the two-layer assembly in two steps (Figure 25). In the first step, **CF** with short linker

formed a monolayer close to the TiO_2 surface. After that the porphyrin, **H_2P** or **ZnP**, was immobilized on the surface *via* a long linker which could penetrate between **CF** moieties in the primary SAM and attach to TiO_2 so that the porphyrin layer is formed atop of the fullerene layer. The monolayer formation and washing procedure to remove the physisorpted molecules were studied to ensure the successful carboxyl anchoring to TiO_2. Also the stability of the secondary porphyrin layer was tested with washing test to ensure that the porphyrin was able to penetrate between fullerenes (see paper [V] for details). The absorption spectra of prepared TiO_2 | **CF**, TiO_2 | **ZnP** and TiO_2 | **CF** | **ZnP** samples are presented in Figure 26.

The specific surface areas of TiO_2 nanoporous films are expected to be the same for all the samples. Therefore relative absorption intensities of the samples can be compared to get an estimation of relative densities of the molecular layers on TiO_2 surfaces. The surface densities of porphyrin and fullerene molecules in single layer SAMs were roughly the same and in the case of two-layer SAM the ratio is **C_{60}:P** $\approx$ 3:2. The lower absorption indicating lower density of porphyrins in two-layer film was attributed to less dense poprhyrin layer on top of the fullerene compared to the porphyrin layer formed directly on TiO_2 surface.

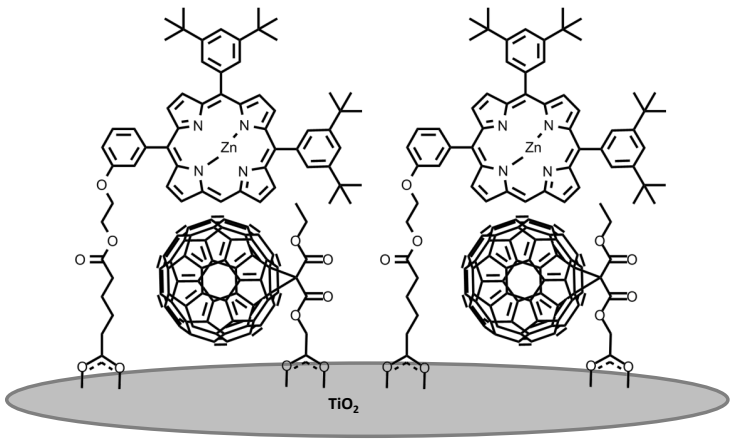

Fig. 25. *Schematic structure of* ***CF | ZnP*** *two-layer film assembled on TiO_2.*

The new method has some advantages compared to the supramolecular approach used to deposit the dyad layer. First, it can be used to easily construct ordered donor-acceptor structures with different combinations of donors and acceptors. In addition, the structure of two-layer films is expected to be defined better than for the directly assembled dyads.

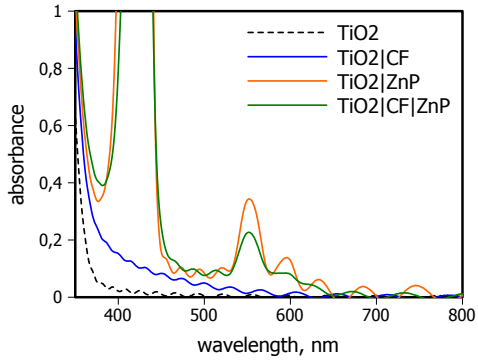

Fig. 26. *Absorption spectra of TiO_2 | **CF**, TiO_2 | **ZnP** and TiO_2 | **CF** | **ZnP** samples [V].*

4.2.2 Electron transfer in TiO_2–dyad monolayer films

The **H_2P–ZnPc** and **ZnP–ZnPc** dyad SAMs were used to build supramolecular donor-acceptor solar cells [III]. The photoelectrochemical studies for these cells revealed improved performance of the **ZnP–ZnPc** cell compared to either **ZnP**, **ZnPc**, **H_2P–ZnPc** or **ZnPc–ZnP–ZnPc** cells. The poor performance of **ZnPc–ZnP–ZnPc** was attributed to poor adsorption of the triad molecule on TiO_2 due to steric restrictions. The transient absorption measurements with the pump-probe method were used to investigate the difference in cell performances with different sensitizers.

The selective excitation of the **ZnP** chromophore of **ZnP–ZnPc** revealed sequential energy and electron transfer processes towards TiO_2. The transient absorption component spectra and time-resolved transient absorption spectra at a few delay times are presented in Figure 27. The time-resolved spectra showed that within 1 ps after excitation, the bleaching of **ZnPc** at 690 nm increases and the porphyrin Q-band at 540 nm partially recovers, indicating that the energy is transferred from **ZnP** to **ZnPc**. At the same time, characteristic features for pthalocyanine cation were appearing including the broad band around 850 nm, a decrease in absorption in the 600-660 nm range and formation of band around 500 nm. These changes were completed within 3 ps delay time. With this delay time the porphyrin Q-band was still bleached indicating the charge separation between **ZnPc** and **ZnP**. However, at longer delay times, the porphyrin Q-band recovered but the pthalocyanine cation spectrum remained the same revealing that ZnP^- donated an electron to TiO_2. Hence, the first component in Figure 27a was attributed to the energy transfer to **ZnPc** with the time constant of 0.2 ps. The energy transfer from **ZnP** to **ZnPc** was found to be faster than that for the

same dyad in solution (see paper III), which meant that in SAM the distance between neighboring molecules was short enough for intermolecular energy transfer. The excited **ZnPc** relaxed through the charge transfer within 2 ps producing ZnP^{-}–$ZnPc^{+}$ state. Since the CS state formation was not observed in solution, the charge transfer process was also assigned to be intermolecular in SAM. This was attributed to a shorter overall donor-acceptor distance in array of tightly packed **ZnP–ZnPc** dyads. The next step in the sequence was the electron transfer from ZnP^{-} to TiO_2 with 30 ps time constant. The charge recombination was found to be slower than the longest time delay for the instrument (> 2 ns, Setup 1).

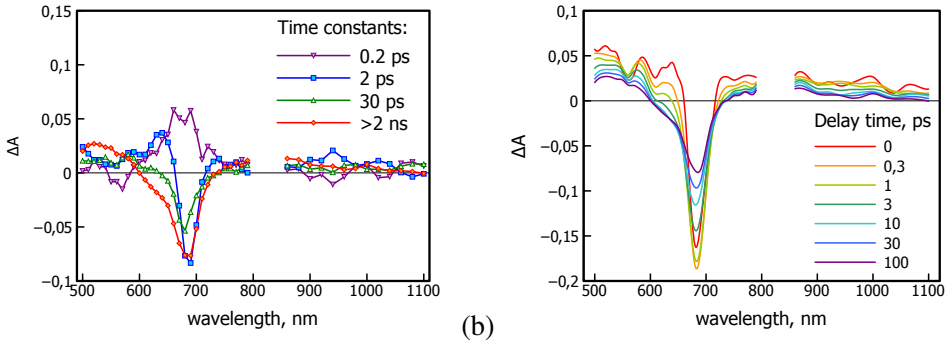

(a) (b)

Fig. 27. *(a) Transient absorption component spectra and (b) time-resolved transient absorption spectra for TiO_2 | **ZnP–ZnPc** [III].*

The time-resolved spectra for **H_2P–ZnPc** are shown in Figure 28b. The main difference in the spectra compared to **ZnP–ZnPc** spectra was that the porphyrin Q-band was recovered simultaneously with enhanced bleaching of the **ZnPc** Q-band and reshaping of the spectrum of pthalocyanine. This revealed that porphyrin participitates in the reaction by energy transfer only and that there was no primary charge separation inside the organic layer. The components in Figure 28a were assigned to energy transfer from **H_2P** to **ZnPc** (0.8 ps) and further to electron injection from the excited **ZnPc** to TiO_2 (4.5 ps). The charge recombination was found to take place with two time constants showed in Figure 28a with 90 ps and over 2 ns components.

As a result of these multiple photochemical events, the charge recombination process was slowed down in both dyad cells compared to cells sensitized with single chromophores. The final charge recombination in both **ZnP–ZnPc** and **H_2P–ZnPc** films took place between the pthalocyanine and TiO_2. However, because of the different alignments, in former case the **ZnPc** and TiO_2 was separated by the layer of **ZnP**. Thus

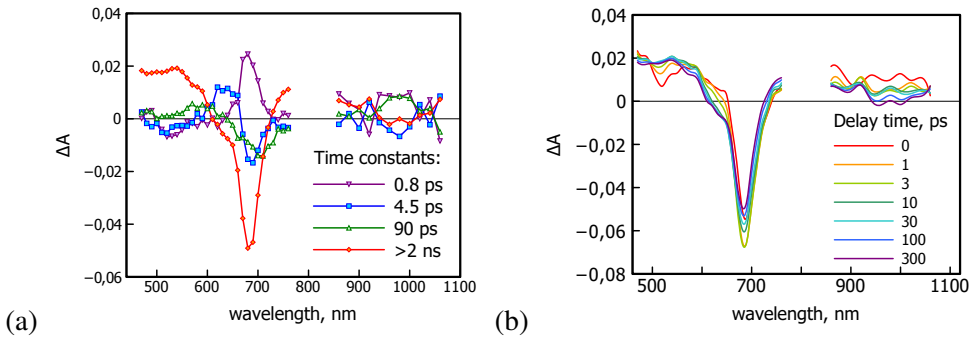

Fig. 28. *(a) Transient absorption component spectra and (b) time-resolved transient absorption spectra for TiO_2 | **H_2P–ZnPc** [III].*

longer CR distance made the charge recombination slower and caused the enhanced performance of the **ZnP–ZnPc** cell.

4.2.3 Electron transfer in TiO_2–donor-acceptor two-layer films

The formation of **CF | ZnP** two-layer film on TiO_2 was confirmed and the kinetics of photoinduced processes were studied using transient absorption measurements. The transient absorption component spectra of TiO_2 | **ZnP** sample are shown Figure 29. The two shorter-lived components (4 and 30 ps) have quite similar spectra showing dips at 605 and 660 nm, which were characteristic for the singlet excited state of **ZnP**. Thus they both were attributed to the relaxation of the **ZnP** singlet excited state. Also the shape of the two following components were rather similar showing the porphyrin cation band in the 650-700 nm region indicating electron injection from **ZnP** to TiO_2 as was expected based on the previously published studies.[80,81,87] However, the electron injection was relatively slow for used **ZnP** compared to earlier results, which was explained by a longer linker of **ZnP** and thus larger distance between the sensitizer and TiO_2.

The **CF | ZnP** two-layer formation was proved by the formation of the fullerene anion band at 1050 nm after the selective excitation of **ZnP**. The transient absorption data for TiO_2 | **CF | ZnP** sample was fitted using a combination of exponential and distributed decay models (see Section 3.3.5). The transient absorption component spectra and time-resolved transient absorption spectra at a few delay times are presented in Figure 30. The time-resolved spectra at long delay time showed the spectrum which

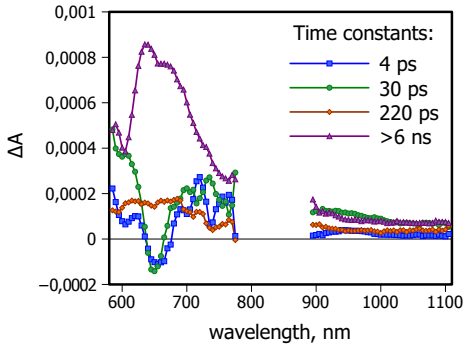

Fig. 29. *Transient absorption component spectra for TiO_2 | **ZnP** [V].*

was almost identical to ZnP^+ band in the case of TiO_2 | **ZnP** sample. However, the formation process of ZnP^+ is different in these two films. The spectrum at 20 ps time delay showed band at 1040 nm which is characteristic for C_{60}^-, but also the ZnP^+ band and was since attributed to the intermolecular CS state. The fullerene anion band is already seen in shorter time delays as well as sort of combination of porphyrin cation and singlet excited state features. This was assigned to different types of porphyrin-fullerene arrangements in the film which led to that the intermolecular CS proceed with different time constants. Alternatively, the features of the first spectrum could arise from intermolecular porphyrin-fullerene exciplex, which was reported previously to form in few hundreds of femtosecond in face-to-face porphyrin-fullerene dyads.[88] Hence, the fastest component (5 ps) in Figure 30a showing a minor relaxation of the singlet excited state of **ZnP** was attributed to the relaxation of remaining part of the singlet excited state. The two following distributed decay components had quite similar spectrum in visible part but differed in the near IR part of the spectrum. The 230 ps component showed both ZnP^+ and C_{60}^- band and it was assigned to the decay of intermolecular CS state. The last component resembled spectrum for ZnP^+ only without any indication of C_{60}^- band and it was assigned for ZnP^+ and electron in TiO_2. Thus decay of intermolecular CS state was a result from two competing processes, the electron injection to TiO_2 and intermolecular charge recombination.

The final state of photoinduced processes for both TiO_2 | **ZnP** and TiO_2 | **CF** | **ZnP** samples was the same, ZnP^+. However, the lifetimes of this state were longer than the delay line of pump-probe instrument (Setup 2) and thus flash-photolysis instrument was used to measure transient absorption of the samples in the millisecond time scale.

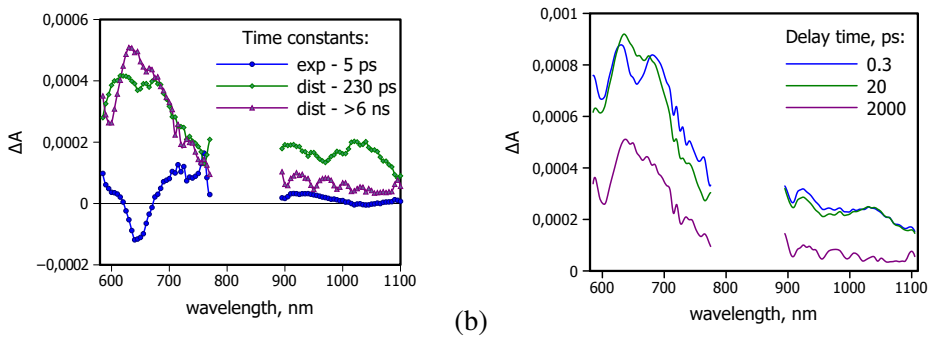

(a) (b)

Fig. 30. *(a) Transient absorption component spectra and (b) time-resolved transient absorption spectra for TiO_2 | **CF** | **ZnP** [V].*

The spectrum of the distributed decay component obtained from the flash-photolysis measurement corresponds well to that of the longest-lived component obtained from the pump-probe measurements (Figure 31) and the flash-photolysis measurements confirmed that the long-lived ZnP^+ is formed in both cases. The obtained lifetime for ZnP^+ were 6 and 23 ms for TiO_2 | **ZnP** and TiO_2 | **CF** | **ZnP**, respectively. The four times longer CR time constant was attributed to the longer distance between **ZnP** and TiO_2 for TiO_2 | **CF** | **ZnP** sample than for TiO_2 | **ZnP**. The relatively long linker and attachment of this linker in *meta* position of one of the meso-aryl groups of porphyrin gives freedom for bending and decreases the distance between porphyrin and TiO_2.[80] In two-layer samples, the primary fullerene layer led to ordered structure where there was no freedom for **ZnP** to bend.

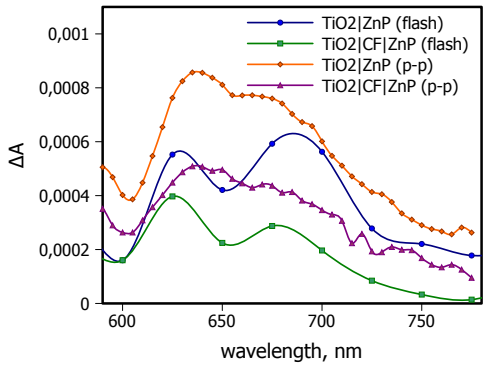

Fig. 31. *Spectra of the longest-living components obtained from the pump-probe and flash-photolysis measurements for TiO_2 | **ZnP** and TiO_2 | **CF** | **ZnP**. [V].*

The primary electron transfer inside the donor-acceptor two-layer film was fast. However, the electron injection to TiO_2 in two-layer film was slower and less efficient than for **ZnP** film because the driving force for the charge separation was lower for TiO_2 | C_{60}^- pair than for TiO_2 | ZnP^{1S}. For the same reason, the electron transfer from **ZnP** to TiO_2 in **ZnP–ZnPc** cell was also faster than from **CF** to TiO_2 from two-layer film. Although the comparison between these two donor-acceptor layers in TiO_2 is not straightforward since the layers have very different structures, it was clear that the more ordered structure and longer distance between the primary electron donor and TiO_2 slowed down the charge recombination process. The multistep photochemical events taking place in donor-acceptor films on TiO_2 mimicked the photochemical events in photosynthesis and resulted in slower charge recombination rates.

5. CONCLUSIONS

The following conclusions were reached based on the reported results:

1. Self-assembly *via* metal-ligand axial coordination enables building stable supramolecular porphyrin-pthalocyanine assemblies. Whereas, two-point binding of chlorin-fullerene dyads *via* metal-ligand and crown-ether coordination yields dyads with higher binding efficiency and well defined mutual orientation of the constituting molecular entities. The supramolecular assembly of donor-acceptor complexes makes it possible to build multicomponent arrays of units by a modular approach in such way that they could perform key functions of photosynthesis efficiently.

2. The photophysical properties of supramolecular assemblies can be easily tuned by changing the attachment position of the linker but keeping the donor and acceptor units otherwise untouched. This was done by changing the position of imidazole linking group on one of the meso-aryl groups of the free-base tetraphenylporphyrin donor entity and the series of metal pthalocyanine acceptor entities. The energy transfer efficiency in such donor-acceptor complexes was affected by the position of the linker group and the number of acceptor entities. Similarly, changing the pyrrolidine linker group of the fullerene entity and crown-ether position in chlorin entity affect the efficiency of electron transfer in chlorin-fullerene dyads.

3. As expected, the electron transfer rate depends on the donor-acceptor distance in chlorin-fullerene dyads. In addition, the mutual orientation of these entities was found to have a significant contribution to the rate. Though the edge-to-edge distance was the same, the favorable orientation *i.e.* the shorter center-to-center distance of entities leads to faster electron transfer and correlated better with lifetimes. This was attributed to a stronger electronic coupling between entities with shorter center-to-center distance.

4. A novel two-layer assembly method can be used to construct ordered donor-acceptor two-layer films on TiO_2. First, the fullerene acceptor monolayer is formed close to the surface *via* a short-linker and then the porphyrin donor layer is formed on top of that *via* a longer linker capable of penetrating between the fullerenes. This opens opportunity to construct advanced organic-semiconductor hybrids with control over the direction of the electron transfer in organic layer.

5. The sequential charge transfer was observed in two different donor-acceptor films constructed from covalently linked donor-acceptor dyads and prepared by donor-acceptor two-layer assembly on TiO_2. First, there was charge transfer between the organic donor and acceptor moieties, followed by charge injection from the acceptor to TiO_2. Due to spatial separation between the primary electron donor and TiO_2, the charge recombination process was significantly decelerated compared to single chromophore sensitized TiO_2. This has a potential to increase the efficiency of the dye-sensitized solar cells.

BIBLIOGRAPHY

[1] Pro Oxygen. Earth's CO_2 Home Page. `http://co2now.org/`, mar 2014. Accessed: 1.8.2014.

[2] The U.S. Department of Energy (DOE) Office of Basic Energy Sciences. Basic research needs for solar energy utilization, report on the basic energy sciences workshop on solar energy utilization. `http://science.energy.gov/~/media/bes/pdf/reports/files/seu_rpt.pdf`, apr 2005. Accessed: 1.8.2014.

[3] M. R. Wasielewski. Photoinduced electron transfer in supramolecular systems for artificial photosynthesis. *Chemical reviews*, 92(3):435–461, 1992.

[4] D. Gust, T. A. Moore, and A. L. Moore. Molecular mimicry of photosynthetic energy and electron transfer. *Accounts of Chemical Research*, 26(4):198–205, 1993.

[5] D. Gust, T. A. Moore, and A. L. Moore. Mimicking photosynthetic solar energy transduction. *Acc. Chem. Res.*, 34(1):40–48, 2001.

[6] D. Wröbel and A. Graja. Photoinduced electron transfer processes in fullerene-organic chromophore systems. *Coordination Chemistry Reviews*, 255(21-22):2555–2577, 2011.

[7] M. E. El-Khouly, O. Ito, P. M. Smith, and F. D'Souza. Intermolecular and supramolecular photoinduced electron transfer processes of fullerene-porphyrin/phthalocyanine systems. *Journal of Photochemistry and Photobiology C: Photochemistry Reviews*, 5(1):79–104, 2004.

[8] G. Bottari, G. de la Torre, D. M. Guldi, and T. Torres. Covalent and noncovalent phthalocyanine-carbon nanostructure systems: Synthesis, photoinduced

electron transfer, and application to molecular photovoltaics. *Chemical reviews*, 110(11):6768–6816, 2010.

[9] G. Bottari, O. Trukhina, M. Ince, and T. Torres. Towards artificial photosynthesis: Supramolecular, donor-acceptor, porphyrin- and phthalocyanine/carbon nanostructure ensembles. *Coordination Chemistry Reviews*, 256(21–22):2453–2477, 2012.

[10] A. Ulman. Formation and structure of self-assembled monolayers. *Chemical reviews*, 96(4):1533–1554, 1996.

[11] H. Imahori, Y. Mori, and Y. Matano. Nanostructured artificial photosynthesis. *Journal of Photochemistry and Photobiology C: Photochemistry Reviews*, 4(1):51–83, 2003.

[12] J. C. Love, L. A. Estroff, J. K. Kriebel, R. G. Nuzzo, and G. M Whitesides. Self-assembled monolayers of thiolates on metals as a form of nanotechnology. *Chemical Reviews*, 105:1103–1169, 2005.

[13] F. D'Souza and O. Ito. Photoinduced electron transfer in supramolecular systems of fullerenes functionalized with ligands capable of binding to zinc porphyrins and zinc phthalocyanines. *Coordination Chemistry Reviews*, 249(13–14):1410–1422, 2005.

[14] A. S. D. Sandanayaka, K. Ikeshita, Y. Araki, N. Kihara, Y. Furusho, T. Takata, and O. Ito. Photoinduced electron- and energy-transfer processes of [60]fullerene covalently bonded with one and two zinc porphyrin(s): effects of coordination of pyridine and diazabicyclooctane to Zn atom. *Journal of Materials Chemistry*, 15:2276–2287, 2005.

[15] E. Maligaspe, T. Kumpulainen, H. Lemmetyinen, N. V. Tkachenko, N. K Subbaiyan, M. E Zandler, and F. D'Souza. Ultrafast singlet-singlet energy transfer in self-assembled via metal-ligand axial coordination of free-base porphyrin-zinc phthalocyanine and free-base porphyrin-zinc naphthalocyanine dyads. *The Journal of Physical Chemistry A*, 114(1):268–277, 2010.

[16] J. S. Kavakka, S. Heikkinen, and J.Helaja. Zn pyropheophorbide a: A β-face selective nicotine receptor. *European Journal of Organic Chemistry*, 2008(29):4932–4937, 2008.

[17] J. S. Kavakka, S. Heikkinen, I. Kilpelainen, N. V. Tkachenko, and J. Helaja. Zn pyro-pheophorbide a-fulleronicotine dyad; supramolecular self assembled donor-acceptor system for photoinduced charge separation. *Chemical Communications*, 7(7):758–760, 2009.

[18] F. Fungo, L. Otero, C. D. Borsarelli, E. N. Durantini, J. J. Silber, and L. Sereno. Photocurrent generation in thin SnO_2 nanocrystalline semiconductor film electrodes from photoinduced charge-separation state in porphyrin-C_{60} dyad. *Journal of Physical Chemistry B*, 106(16):4070–4078, 2002.

[19] H. Imahori and S. Fukuzumi. Porphyrin- and fullerene-based molecular photovoltaic devices. *Advanced Functional Materials*, 14(6):525–536, 2004.

[20] H. Yamada, H. Imahori, Y. Nishimura, I. Yamazaki, T. K. Ahn, S. K. Kim, D. Kim, and S. Fukuzumi. Photovoltaic properties of self-assembled monolayers of porphyrins and porphyrin- fullerene dyads on ITO and gold surfaces. *Journal of the American Chemical Society*, 125(30):9129–9139, 2003.

[21] V. Chukharev, T. Vuorinen, A. Efimov, N. V. Tkachenko, M. Kimura, S. Fukuzumi, H. Imahori, and H. Lemmetyinen. Photoinduced electron transfer in self-assembled monolayers of porphyrin-fullerene dyads on ITO. *Langmuir*, 21:6385–6391, 2005.

[22] B. Valeur. *Molecular Fluorescence: Principles and Applications*. Wiley-VCH Verlag GmbH, 2001.

[23] J. R. Lakowicz. *Principles of Fluorescence Spectroscopy*. Springer, 2006.

[24] T. Förster. 10th spiers memorial lecture. Transfer mechanisms of electronic excitation. *Discussions of the Faraday Society*, 27:7–17, 1959.

[25] N. J. Turro. *Modern molecular photochemistry*. University Science Books, 1991.

[26] D. L. Dexter. A theory of sensitized luminescence in solids. *The Journal of Chemical Physics*, 21(5):836–850, 1953.

[27] Bolton J. R. and Archer M. D. *Basic Electron-Transfer Theory*. 1991.

[28] R. A. Marcus. Electron transfer reactions in chemistry. Theory and experiment. *Reviews of Modern Physics*, 65(3):599–10, 1993.

[29] H. Imahori, K. Tamaki, D. M. Guldi, C. Luo, M. Fujitsuka, O. Ito, Y. Sakata, and S. Fukuzumi. Modulating charge separation and charge recombination dynamics in porphyrin-fullerene linked dyads and triads: Marcus-normal versus inverted region. *Journal of the American Chemical Society*, 123(11):2607–2617, 2001.

[30] Y. K. Kang, I. V. Rubtsov, P. M. Iovine, J. Chen, and M. J. Therien. Distance dependence of electron transfer in rigid, cofacially compressed, π-stacked porphyrin-bridge-quinone systems. *Journal of the American Chemical Society*, 124(28):8275–8279, 2002.

[31] J. Wiberg, L. Guo, K. Pettersson, D. Nilsson, T. Ljungdahl, J. Mårtensson, and B. Albinsson. Charge recombination versus charge separation in donor-bridge-acceptor systems. *Journal of the American Chemical Society*, 129(1):155–163, 2007.

[32] B. Grimm, R. J. Porra, W. Rüdiger, and H. Scheer. *Chlorophylls and Bacteriochlorophylls : Biochemistry, Biophysics, Functions and Applications*. Dordrecht:Springer, 2006.

[33] M. G. Walter, A. B. Rudine, and C. C. Wamser. Porphyrins and phthalocyanines in solar photovoltaic cells. *Journal of Porphyrins and Phthalocyanines*, 14(09):759–792, 2010.

[34] N. V. Tkachenko, L. Rantala, A. Y. Tauber, J. Helaja, P. H. Hynninen, and H. Lemmetyinen. Photoinduced electron transfer in phytochlorin-[60]fullerene dyads. *Journal of the American Chemical Society*, 121(40):9378–9387, 1999.

[35] G. Zheng, T. J. Dougherty, R. K. Pandey, and R. K. Pandey. Novel chlorin-diene building block by enyne metathesis: synthesis of chlorin-fullerene dyads. *Chemical Communications*, 24(24):2469–2470, 1999.

[36] F.-P. Montforts and O. Kutzki. Simple synthesis of a chlorin-fullerene dyad with a novel ring-closure reaction. *Angewandte Chemie International Edition*, 39(3):599–601, 2000.

[37] S. Fukuzumi, K. Ohkubo, H. Imahori, J. Shao, Z. Ou, G. Zheng, Y. Chen, R. K. Pandey, M. Fujitsuka, O. Ito, and K. M. Kadish. Photochemical and electrochemical properties of zinc chlorin-C_{60} dyad as compared to corresponding free-base

chlorin-C_{60}, free-base porphyrin-C_{60}, and zinc porphyrin-C_{60} dyads. *Journal of the American Chemical Society*, 123(43):10676–10683, 2001.

[38] V. Vehmanen, N. V. Tkachenko, A. Y. Tauber, P. H. Hynninen, and H. Lemmetyinen. Ultrafast charge transfer in phytochlorin-[60]fullerene dyads: influence of the attachment position. *Chemical Physics Letters*, 345(3–4):213–218, 2001.

[39] V. Vehmanen, N. V. Tkachenko, A. Efimov, P. Damlin, A. Ivaska, and H. Lemmetyinen. The role of the exciplex state in photoinduced electron transfer of phytochlorin-[60]fullerene dyads. *The Journal of Physical Chemistry A*, 106(35):8029–8038, 2002.

[40] P.-C. Lo, X. Leng, and D. K. P. Ng. Hetero-arrays of porphyrins and phthalocyanines. *Coordination Chemistry Reviews*, 251(17–20):2334–2353, 2007.

[41] Y. Shinozaki, G. Richards, K. Ogawa, A. Yamano, K. Ohara, K. Yamaguchi, S. Kawano, K. Tanaka, Y. Araki, T. Wada, and J. Otsuki. Double helices of a pyridine-appended zinc chlorophyll derivative. *Journal of the American Chemical Society*, 135(14):5262–5265, 2013.

[42] K. M. Smith and J. E. Falk. *Porphyrins and metalloporphyrins*. Elsevier Amsterdam, 1975.

[43] H. Imahori and Y. Sakata. Fullerenes as novel acceptors in photosynthetic electron transfer. *European Journal of Organic Chemistry*, 1999(10):2445–2457, 1999.

[44] O. Ito and F. D'Souza. Recent advances in photoinduced electron transfer processes of fullerene-based molecular assemblies and nanocomposites. *Molecules*, 17(5):5816–5835, 2012.

[45] S. Kirner, M. Sekita, and D. M. Guldi. 25th anniversary article: 25 years of fullerene research in electron transfer chemistry. *Advanced Materials*, 26(10):1482–1493, 2014.

[46] Y. Araki and O. Ito. Factors controlling lifetimes of photoinduced charge-separated states of fullerene-donor molecular systems. *Journal of Photochemistry and Photobiology C: Photochemistry Reviews*, 9(3):93–110, 2008.

[47] D. M. Guldi, B. M. Illescas, C. M. Atienza, M. Wielopolski, and N. Martin. Fullerene for organic electronics. *Chemical Society Reviews*, 38:1587–1597, 2009.

[48] S. E Webber. Photon-harvesting polymers. *Chemical Reviews*, 90(8):1469–1482, 1990.

[49] J. M. J. Frächet. Dendrimers and other dendritic macromolecules: From building blocks to functional assemblies in nanoscience and nanotechnology. *Journal of Polymer Science Part A: Polymer Chemistry*, 41(23):3713–3725, 2003.

[50] M. Li, S. Ishihara, Q. Ji, M. Akada, J. P. Hill, and K. Ariga. Paradigm shift from self-assembly to commanded assembly of functional materials: Recent examples in porphyrin/fullerene supramolecular systems. *Science and Technology of Advanced Materials*, 13(5), 2012.

[51] E. Maligaspe, N. V. Tkachenko, N. K. Subbaiyan, R. Chitta, M. E. Zandler, H. Lemmetyinen, and F. D'Souza. Photosynthetic antenna-reaction center mimicry: Sequential energy- and electron transfer in a self-assembled supramolecular triad composed of boron dipyrrin, zinc porphyrin and fullerene. *The Journal of Physical Chemistry A*, 113(30):8478–8489, 2009.

[52] M. E. El-Khouly, D. K. Ju, K.-Y. Kay, F. D'Souza, and S. Fukuzumi. Supramolecular tetrad of subphthalocyanine-triphenylamine-zinc porphyrin coordinated to fullerene as an "antenna-reaction-center" mimic: Formation of a long-lived charge-separated state in nonpolar solvent. *Chemistry – A European Journal*, 16(21):6193–6202, 2010.

[53] F. D'Souza, E. Maligaspe, A. S. D. Sandanayaka, N. K. Subbaiyan, P. A. Karr, T. Hasobe, and O. Ito. Photochemical charge separation in supramolecular phthalocyanine-multifullerene conjugates assembled by crown ether-alkyl ammonium cation interactions. *The Journal of Physical Chemistry A*, 114(41):10951–10959, 2010.

[54] F. D'Souza, G. R Deviprasad, M. E Zandler, M. E El-Khouly, M. Fujitsuka, and O. Ito. Photoinduced electron transfer in "two-point" bound supramolecular triads composed of N,N-dimethylaminophenyl-fullerene-pyridine coordinated to zinc porphyrin. *Journal of Physical Chemistry A*, 107(24):4801–4807, 2003.

[55] F. D'Souza, R. Chitta, S. Gadde, M. E. Zandler, A. S. D. Sandanayaka, Y. Araki, and O. Ito. Supramolecular porphyrin-fullerene via "two-point" binding strategy: Axial-coordination and cation-crown ether complexation. *Chemical Communications*, pages 1279–1281, 2005.

[56] F. D'Souza, R. Chitta, S. Gadde, M. E Zandler, A L McCarty, A. S. D Sandanayaka, Y. Araki, and O. Ito. Effect of axial ligation or $\pi - \pi$-type interactions on photochemical charge stabilization in "two-point" bound supramolecular porphyrin-fullerene conjugates. *Chemistry – A European Journal*, 11(15):4416–4428, 2005.

[57] F. D'Souza, R. Chitta, S. Gadde, A. L McCarty, P. A Karr, M. E Zandler, A. S. D Sandanayaka, Y. Araki, and O. Ito. Design, syntheses, and studies of supramolecular porphyrin-fullerene conjugates, using bis-18-crown-6 appended porphyrins and pyridine or alkyl ammonium functionalized fullerenes. *Journal of Physical Chemistry B*, 110(12):5905–5913, 2006.

[58] F. D'Souza, E. Maligaspe, K. Ohkubo, M. E. Zandler, N. K. Subbaiyan, and S. Fukuzumi. Photosynthetic reaction center mimicry: Low reorganization energy driven charge stabilization in self-assembled cofacial zinc phthalocyanine dimer-fullerene conjugate. *Journal of the American Chemical Society*, 131(25):8787–8797, 2009.

[59] H.-J. Schneider. Binding mechanisms in supramolecular complexes. *Angewandte Chemie International Edition*, 48(22):3924–3977, 2009.

[60] J. W Steed, D. R Turner, and K. Wallace. *Core concepts in supramolecular chemistry and nanochemistry*. John Wiley & Sons, 2007.

[61] N. Solladie, M. E. Walther, M. Gross, T. M. Figueira D., C. Bourgogne, and J.-F. Nierengarten. A supramolecular cup-and-ball C_{60}-porphyrin conjugate system. *Chemical Communications*, 19:2412–2413, 2003.

[62] F. D'Souza, G. M Venukadasula, K. Yamanaka, M. E. Zandler N. K. Subbaiyan, and O. Ito. Through-bond photoinduced electron transfer in a porphyrin-fullerene conjugate held by a Hamilton type hydrogen bonding motif. *Organic & Biomolecular Chemistry*, 7(6):1076–1080, 2009.

[63] P. Atkins and J. De Paula. *Atkins' physical chemistry*. Oxford University Press, 2002.

[64] H. A. Benesi and J. H Hildebrand. A spectrophotometric investigation of the interaction of iodine with aromatic hydrocarbons. *Journal of the American Chemical Society*, 71(8):2703–2707, 1949.

[65] J. H. Yoe and A. L. Jones. Colorimetric determination of iron with disodium-1,2-dihydroxybenzene-3,5-disulfonate. *Industrial & Engineering Chemistry Analytical Edition*, 16(2):111–115, 1944.

[66] M. Grätzel. Recent advances in sensitized mesoscopic solar cells. *Accounts of Chemical Research*, 42(11):1788–1798, 2009.

[67] M. Wright and A. Uddin. Organic-inorganic hybrid solar cells: A comparative review. *Solar Energy Materials and Solar Cells*, 107:87–111, 2012.

[68] J. Gong, J. Liang, and K. Sumathy. Review on dye-sensitized solar cells (DSSCs): Fundamental concepts and novel materials. *Renewable & Sustainable Energy Reviews*, 16(8):5848–5860, 2012.

[69] J. Boucle and J. Ackermann. Solid-state dye-sensitized and bulk heterojunction solar cells using TiO_2 and ZnO nanostructures: recent progress and new concepts at the borderline. *Polymer International*, 61(3):355–373, 2012.

[70] T. J. Meyer, G. J. Meyer, B. W. Pfennig J. R., Schoonover C. J., Timpson, J. F. Wall, C. Kobusch, X. Chen, and B. M Peek and. Molecular-level electron transfer and excited state assemblies on surfaces of metal oxides and glass. *Inorganic Chemistry*, 33(18):3952–3964, 1994.

[71] Y.-X. Weng, L. Li, Y. Liu, L. Wang, and G.-Z. Yang. Surface-binding forms of carboxylic groups on nanoparticulate TiO_2 surface studied by the interface-sensitive transient triplet-state molecular probe. *The Journal of Physical Chemistry B*, 107(18):4356–4363, 2003.

[72] Q. Qu, H. Geng, R. Peng, Q. Cui, X. Gu, F. Li, and M. Wang. Chemically binding carboxylic acids onto TiO_2 nanoparticles with adjustable coverage by solvothermal strategy. *Langmuir*, 26(12):9539–9546, 2010.

[73] J. Rochford, D. Chu, A. Hagfeldt, and E. Galoppini. Tetrachelate porphyrin chromophores for metal oxide semiconductor sensitization: Effect of the spacer length and anchoring group position. *Journal of the American Chemical Society*, 129(15):4655–4665, 2007.

[74] J. Rochford and E. Galoppini. Zinc(II) tetraarylporphyrins anchored to TiO_2, ZnO, and ZrO_2 nanoparticle films through rigid-rod linkers. *Langmuir*, 24(10):5366–5374, 2008.

[75] S. Rangan, S. Katalinic, R. Thorpe, R. A. Bartynski, J. Rochford, and E. Galoppini. Energy level alignment of a Zinc(ii) tetraphenylporphyrin dye adsorbed onto TiO_2(110) and ZnO(1120) surfaces. *The Journal of Physical Chemistry C*, 114(2):1139–1147, 2010.

[76] A. S. Hart, C. B. KC, H. B. Gobeze, L. R. Sequeira, and F. D'Souza. Porphyrin-sensitized solar cells: Effect of carboxyl anchor group orientation on the cell performance. *ACS Applied Materials & Interfaces*, 5(11):5314–5323, 2013.

[77] R. Naaman. Molecular controlled nano-devices. *Physical Chemistry Chemical Physics*, 13:13153–13161, 2011.

[78] S. Ito, P. Chen, P. Comte, M. K Nazeeruddin, P. Liska, P. Péchy, and M. Grätzel. Fabrication of screen-printing pastes from TiO_2 powders for dye-sensitised solar cells. *Progress in Photovoltaics: Research and Applications*, 15(7):603–612, 2007.

[79] F. Wang, N. K. Subbaiyan, Q. Wang, C. Rochford, G. Xu, R. Lu, A. Elliot, F. D'Souza, R. Hui, and J.Wu. Development of nanopatterned fluorine-doped tin oxide electrodes for dye-sensitized solar cells with improved light trapping. *ACS Applied Materials & Interfaces*, 4(3):1565–1572, 2012.

[80] A. S. Hart, C. B. K. C., N. K Subbaiyan, P. A. Karr, and F. D'Souza. Phenothiazine-sensitized organic solar cells: Effect of dye anchor group positioning on the cell performance. *ACS Applied Materials & Interfaces*, 4(11):5813–5820, 2012.

[81] S. Ye, A. Kathiravan, H. Hayashi, Y. Tong, Y. Infahsaeng, P. Chabera, T. Pascher, A. P. Yartsev, S. Isoda, H. Imahori, and V. Sundström. Role of adsorption structures of Zn-porphyrin on TiO_2 in dye-sensitized solar cells studied by

sum frequency generation vibrational spectroscopy and ultrafast spectroscopy. *Journal of Physical Chemistry C*, 117(12):6066–6080, 2013.

[82] N. V Tkachenko. *Optical spectroscopy: methods and instrumentations*. Elsevier, 2006.

[83] H. Lehtivuori, A. Efimov, H. Lemmetyinen, and N. V. Tkachenko. Distributed decay kinetics of charge separated state in solid films. *Chemical Physics Letters*, 437:238–242, 2007.

[84] H. Lehtivuori, T. Kumpulainen, A. Efimov, H. Lemmetyinen, A. Kira, H. Imahori, and N. V. Tkachenko. Photoinduced electron transfer in langmuir–blodgett monolayers of double-linked phthalocyanine–fullerene dyads. *The Journal of Physical Chemistry C*, 112:9896–9902, 2008.

[85] M. E. El-Khouly, Y. Araki, M. Fujitsuka, A. Watanabe, and O. Ito. Photoinduced electron transfer between chlorophylls (a/b) and fullerenes (C_{60}/C_{70}) studied by laser flash photolysis. *Photochemistry and Photobiology*, 74(1):22–30, 2001.

[86] N. K. Subbaiyan, C. A. Wijesinghe, and F. D'Souza. Supramolecular solar cells: Surface modification of nanocrytalline TiO_2 with coordinating ligands to immobilize sensitizers and dyads via metal-ligand coordination for enhanced photocurrent generation. *Journal of the American Chemical Society*, 131(41):14646–14647, 2009.

[87] H. Imahori, S. Kang, H. Hayashi, M. Haruta, H. Kurata, S. Isoda, S. E. Canton, Y. Infahsaeng, A. Kathiravan, T. Pascher, P. Chabera, A. P. Yartsev, and V. Sundström. Photoinduced charge carrier dynamics of Zn-porphyrin-TiO_2 electrodes: The key role of charge recombination for solar cell performance. *The Journal of Physical Chemistry A*, 115(16):3679–3690, 2011.

[88] V. Chukharev, N. V. Tkachenko, A. Efimov, D. M. Guldi, A. Hirsch, M. Scheloske, and H. Lemmetyinen. Tuning the ground-state and excited-state interchromophore interactions in porphyrin-fullerene π-stacks. *The Journal of Physical Chemistry B*, 108:16377–16385, 2004.

PUBLICATION I

Excitation transfer in metal-ligand coordinated free-base porphyrin-magnesium phthalocyanine and free-base porphyrin-magnesium naphthalocyanine dyads

Kati Stranius, Rachel Jacobs, Eranda Maligaspe, Helge Lemmetyinen, Nikolai V. Tkachenko, Melvin E. Zandler and Francis D'Souza

Journal of Porphyrins and Phthalocyanines

Reprinted with permission from *Journal of Porphyrins and Phthalocyanines* **2010**, *14*, 948–961.

Excitation Transfer in Metal-Ligand Coordinated Free-Base Porphyrin-Magnesium Phthalocyanine and Free-base Porphyrin-Magnesium Naphthalocyanine Dyads

Kati Stranius,[a] Rachel Jacobs,[b] Eranda Maligaspe,[b] Helge Lemmetyinen,[a] Nikolai V. Tkachenko,[a,*] Melvin E. Zandler,[b] and Francis D'Souza[b,*]

[a]*Department of Chemistry and Bioengineering, Tampere University of Technology, P. O. Box 541, 33101 Tampere, Finland*

[b]*Department of Chemistry, Wichita State University, 1845 Fairmount, Wichita, KS 67260-0051, USA;*

Submitted 17 October 2010

Accepted 8 November 2010

ABSTRACT: Singlet excitation transfer in self-assembled dyads formed via axial coordination of imidazole appended free-base tetraphenylporphyrin, H_2PIm, to either a magnesium phthalocyanine, MgPc, or a magnesium naphthalocyanine, MgNc is investigated in non-coordinating solvents using spectroscopic (optical and mass), electrochemical, and time-resolved transient absorption techniques. The newly assembled dyads are fully characterized by spectroscopic, computational and electrochemical methods. The binding constants measured from optical absorption spectral data are found to be in the range of 10^3-10^4 M^{-1} for the 1:1 dyads suggesting fairly stable complex formation, however, the anticipated 2:1 complex for Mg coordination is not observed under the present solution conditions. Electrochemical and computational studies suggested that photoinduced electron transfer to be a thermodynamically unfavorable process when free-base porphyrin is excited in these dyads. However, selective excitation of H_2PIm entity in these dyads resulted in rapid excitation transfer and the position of the imidazole linkage on the H_2P entity seem to direct the overall efficiency of excited energy transfer. Kinetics of energy transfer is monitored by transient absorption measurements using pump-probe technique and is compared with the earlier reported H_2PIm:ZnPc and H_2PIm:ZnNc dyads. The time constants are in the order of 0.2-18 ps depending upon the type and relative orientation of the donor and acceptor entities of the dyad indicating ultrafast excitation transfer, and agree fairly well with theoretically estimated values assuming Förster energy transfer mechanism.

KEYWORDS: Excitation Transfer, magnesium phthalocyanine, axial coordination, Foster energy transfer

*Correspondence to: Nikolai V. Tkachenko, E-mail: *nikolai.tkachenko@tut.fi*, Francis D'Souza, E-mail: *Francis.DSouza@wichita.edu*, FAX: +316-978-3431

INTRODUCTION

Photosynthetic light harvesting complexes, often called as antenna pigments, play important role in the early events in photosynthesis, and have been studied by various spectroscopic methodologies during the last two decades.[1] The primary pigments of the antenna systems, chlorophylls and carotenoids, convert photon energy into an electron excitation. The supramolecular organization of these antenna molecules allows the unidirectional excitation energy transfer towards the reaction center, the final destination of the collected energy.[1,2] Inspired by this natural phenomenon, researchers have been attempting to mimic such light induced processes with the help of synthetic molecular architectures.[3-11] Research in this area hold promise in building devices for efficient light energy harvesting, molecular optoelectronics and photocatalysts capable of producing hydrogen.[12]

The different strategies developed to-date to mimic the natural excitation transfer process include, covalent linking the donor and acceptor chromophores,[13-16] arranging the chromophores on a polymer[17] or dendrimer[18] molecular framework, or self-assembly approaches.[19] In these model systems, as a result of well-matched energy levels, occurrence of successful excitation transfer from the donor to the acceptor entities has been demonstrated. A large number of studies have utilized porphyrins[20] and phthalocyanines[21] as energy donor/acceptor entities due to their close resemblance to the photosynthetic pigment, chlorophyll, and the established synthetic methodologies. Both macrocycles are ideal photoactive candidates with outstanding electronic properties, namely, strong absorption in the visible region and possibility of fine tuning the redox potentials. Further, their absorption can easily be extended into near-IR region by increasing macrocycle π-conjugation.[20-21]

Self-assembly via metal-ligand axial coordination is one of the simple yet successful approaches developed to study photoinduced electron transfer in donor-acceptor dyads.[11] Recently we utilized this approach to build dyads comprised of free-base porphyrin as donor and zinc phthalocyanine/naphthalocyanine as acceptor to mimic the natural excitation transfer process.[22,23] We were able to demonstrate excitation transfer from singlet excited porphyrin to zinc phthalocyanine and a near-IR emitting fluorophore, zinc naphthalocyanine.[23] However, such an approach has not been tested out for magnesium metallated fluorophores, although magnesium complexes (as chlorophylls) are the natural energy harvesting molecules. This has been investigated in the present study where the donor, free-base porphyrin has been coordinated to the acceptor, Mg phthalocyanine or Mg naphthalocyanine via metal-ligand coordination to form the dyads. Structures of the employed donor and acceptor molecules are shown in Chart 1. Substitution of the imidazole entity at the *ortho*, *meta* or *para* positions of one of the *meso*-aryl groups of porphyrin is expected to result in dyads of different orientations. Photochemical studies using both steady-state and time-resolved transient absorption techniques have been performed to probe efficiency and kinetics of excitation energy transfer, and the results have been compared to the recently reported dyads with ZnPc and ZnNc energy acceptors.[23]

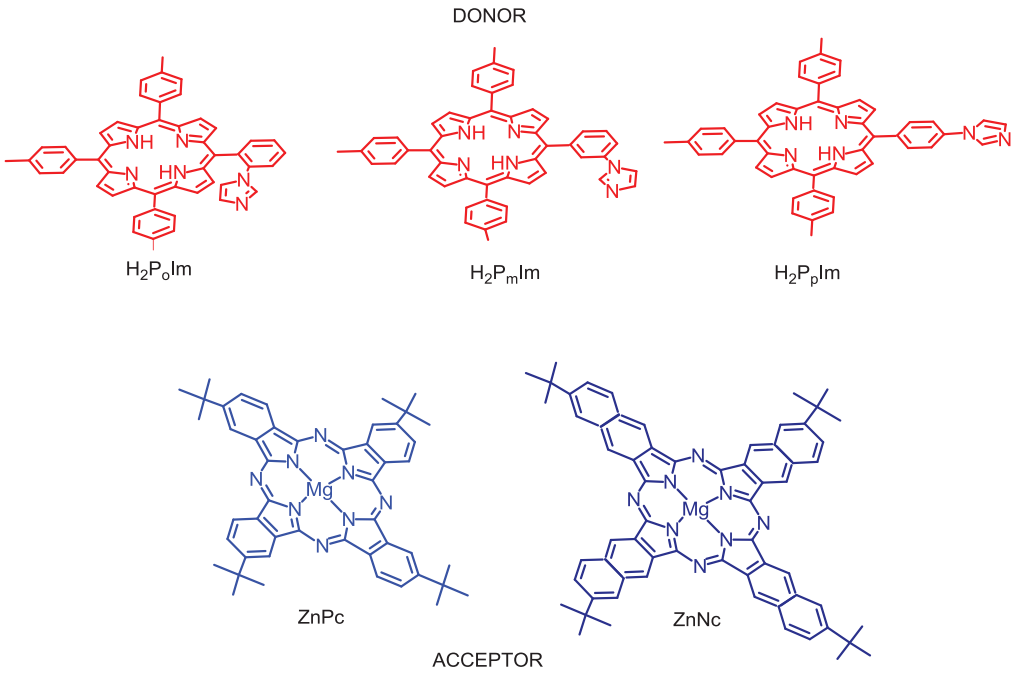

Chart 1. Structure of the free-base porphyrins employed as donor and Mg phthalocyanine/naphthalocyanine employed as acceptor in the present study to probe excitation energy transfer in dyads formed via axial coordination.

RESULTS AND DISCUSSION

Optical Absorption Studies of Dyad Formation

Figure 1 shows the optical absorption spectra of H_2P_oIm, MgPc and MgNc derivatives in *o*-dichlorobenzene (DCB), normalized to their most intense absorption bands. The absorption spectra of H_2P_mIm and H_2P_pIm were found to be similar to that of H_2P_oIm with an intense Soret at 424 and four visible bands at 518, 553, 594 and 652 nm. The spectral features of MgPc and MgNc were similar to their zinc analogs, that is, MgPc exhibited bands at 351, 618, and 681 nm while the spectrum of MgNc was stretched into the near-IR region with peaks at 332, 690, 734 and 770 nm, respectively. Importantly, the H_2PIm band at 518 nm had little or no overlap with the absorption bands of either MgPc or MgNc providing possibility for selective excitation of the donor, free-base porphyrin.

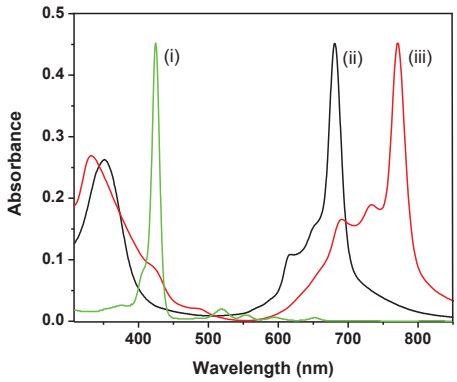

Figure 1. Absorption spectra of (i) H_2P_oIm, (ii) MgPc and (iii) MgNc in DCB, normalized to their most intense bands. The concentrations are in the range of 5-10 μM.

Figures 2a shows absorption spectral changes recorded during increasing addition of H_2P_pIm to the solution of MgPc. Similar spectral changes were observed for H_2P_oIm and H_2P_mIm binding to the acceptor magnesium macrocycles (see supporting information Figures S1 –S2 for additional figures). The binding of H_2PIm to MgPc or MgNc were characterized by diminished intensity of MgPc and MgNc Q-band with one or more isosbestic points indicating existence of only one equilibrium process in solution. Plots of mole ratio method confirmed 1:1 complex formation between the donor and acceptor entities (Figure 2c), although Mg macrocyclic complexes are known to form bis-ligated complexes.[24] This is perhaps higher concentrations of H_2PIm are needed to visualize 1:2 complex formation. The formation constants, *K*, for H_2PIm binding to MgPc and MgNc were obtained from the absorption spectral data using Benesi-Hildebrand method[25] (Figure 2b), and are listed in Table 1. The magnitudes of the *K* values are generally smaller than that of the corresponding Zn analogs,[23] especially for the H_2PIm:MgNc dyads and suggest moderately stable complex formation.

Attempts were also made to record the mass spectra of the dyads. The electrospray mass (ESI) spectrum of a mixture of H_2PpIm:MgPc and H_2PmIm:MgNc of molar ratio of 1:1 to 1:4 were recorded under mild temperature and ionization conditions in dry CH_2Cl_2. As shown in Figure S3, molecular ion peak corresponding to 1:1 complex was observed. Addition of higher amounts of MgPc or MgNc to the H_2PIm solution did not exhibit molecular ion peak corresponding to the anticipated 1:2 complex suggesting that the 1:1 complex is the major species present in solution and amount of 1:2 species, if any, is low in concentration.

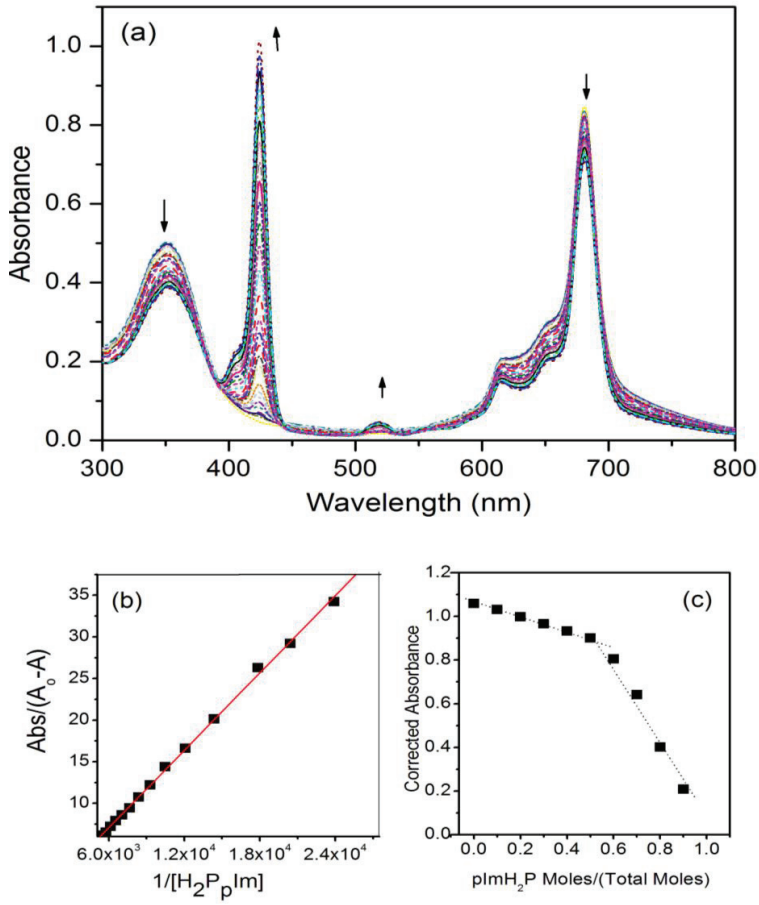

Figure 2. Spectral changes observed during increasing addition of H_2P_pIm (0.1 eq.) to a solution of (a) MgPc (0.11 mM) in DCB. Figures b and c show respectively, Benesi-Hildebrand plot constructed to obtain the binding constant and mole ratio plot to determine the supramolecular stoichiometry.

Table 1. Binding constants, *K* and B3LYP/3-21G(*) computed geometry parameters for the dyads formed by coordination of imidazole appended free-base porphyrin to magnesium phthalocyanine or magnesium naphthalocyanine.

Dyad[a]	*K* Mol^{-1}, [b]	Center-to-center distance, Å	Edge-to-edge distance, Å	Angle between rings
H_2P_oIm:MgPc	4.43 x 10^3	7.7	4.4	38
H_2P_mIm:MgPc	5.51 x 10^3	11.0	6.1	40
H_2P_pIm:MgPc	5.53 x 10^3	13.1	9.3	55
H_2P_oIm:MgNc	7.92 x 10^2	8.3	8.3	35
H_2P_mIm:MgNc	8.58x 10^2	12.1	9.2	55
H_2P_pIm:MgNc	9.22 x 10^2	13.1	8.7	55

[a] See Chart 1 for the structure of different donor and acceptor entities; in DCB at room temperature.

[b] Error = +10%

Electrochemical Studies

Differential pulse voltammetric studies (DPV) were performed to evaluate the oxidation and reduction potential of the compounds utilized to form the dyads. The first reversible oxidation and first two reversible reduction of H_2P_pIm were located at 0.49 V and -1.73 and -2.03 V vs. Fc/Fc^+, respectively. Similar voltammetric behavior was also observed for the H_2P_mIm and H_2P_oIm derivatives. The first oxidation of MgNc and MgPc were located at -0.32 V and 0.00 V vs. Fc/Fc^+, respectively, while the first reduction potential were located at -1.63 and -1.60 V vs. Fc/Fc^+, respectively. That is, these compounds revealed easier oxidations compared to the free-base porphyrins used in the present study. Additionally, the magnitude of the reduction potential of both MgNc and MgPc suggest these being poor electron acceptors. It may also be mentioned here that the redox behavior of MgNc and MgPc is close to the respective ZnNc and ZnPc compounds,[23] however, with slightly lower oxidation and reduction potentials for the Mg series of compounds.

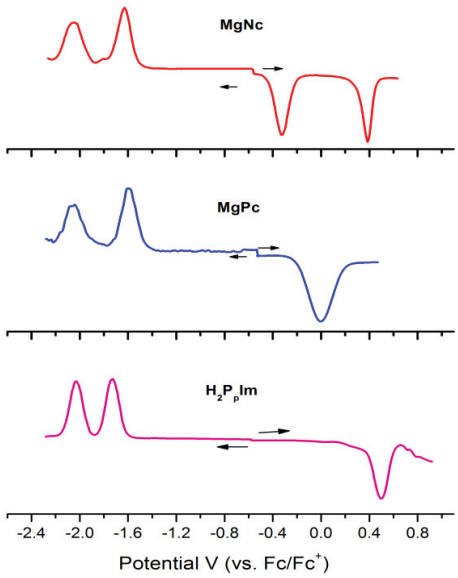

Figure 3. Differential pulse voltammograms of the MgNc, MgPc and H_2P_pIm (~0.5 mM) in DCB containing 0.1 M (TBAP)ClO_4. DPV conditions: scan rate = 20 mV/s, pulse width = 50 ms, step time = 100 ms and pulse height = 0.025 V.

Energy Optimization by B3LYP/3-21G(*) Method

The structure of the supramolecular dyads were visualized by performing computational studies at the B3LYP/3-21G(*) level.[26,27] Figure 4 shows the structures of the dyads energy optimized on a Born-Oppenheimer potential energy surface. In agreement with the earlier reported ZnPc and ZnNc analogs,[23] the two macrocyclic rings of the H_2P_oIm:MgPc and H_2P_oIm:MgNc dyads were found to be in a skipped coplanar arrangement while for the *meta* and *para* imidazole derivatized dyads, H_2P_mIm:MgPc and H_2P_pIm:MgNc, they were positioned at an angle less than a right angle. The edge-to-edge distances, center-to-center distances and angles between the two macrocycle planes of the donor acceptor entities are listed in Table 1. Generally, the distances varied as: *ortho* < *meta* < *para* imidazole substituted porphyrins. That is, closer distance and skipped coplanar configuration for the *ortho* derivatives, and relatively longer distance and higher angle between macrocycles for the *meta* and *para* substituted derivatives were observed. However, although fully energy optimized, other energetically stable geometries may exist due to the flexible nature of self-assembly protocol adopted in the present study. Nevertheless, such optimized structures are key in visualizing the possible geometries with respect to macrocycle orientations.

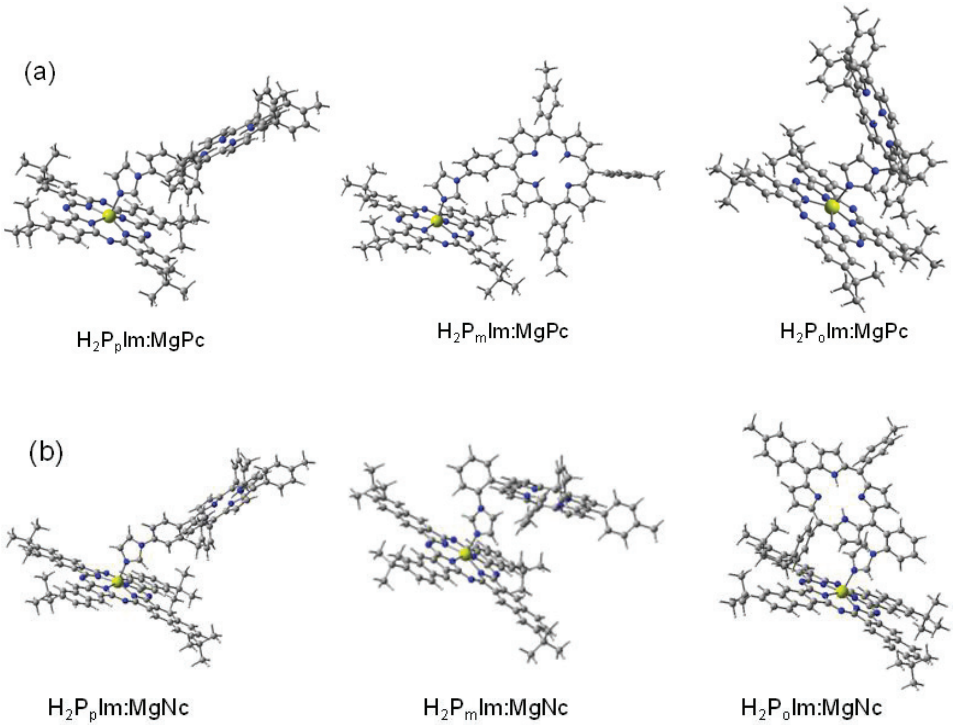

Figure 4. B3LYP/3-21G(*) optimized structures of the dyads formed via axial coordination of H_2PIm (*ortho*, *meta* or *para* derivatives) to (a) MgPc and (b) MgNc.

Using the electrochemical, computational, and excited energy data, the free-energies of charge-separation (ΔG_{CS}) were calculated using equations 1 by Weller's approach.[28]

$$-\Delta G_{CS} = \Delta E_{0\text{-}0} - e(E_{ox} - E_{red}) + \Delta G_S \quad (1)$$

where $\Delta E_{0\text{-}0}$ is the energy of the lowest excited state of H_2P (1.89 eV), E_{ox} and E_{red} are the oxidation and reduction potentials, respectively, $\Delta G_S = -e^2/(4\pi\varepsilon_0\varepsilon_R R)$ is the term accounting for Coulombic interaction between the cation and anion, R is the center-to-center distance between the donor and acceptor (Table 1), and ε_0 and ε_R refer to vacuum permittivity and dielectric constant of DCB.

The calculations revealed that the lowest energy of the charge separated state is achieved for phthalocyanine/naphthlocyanine cation and porphyrin anion. The ΔG_{CS} values is close to zero for the dyad with R = 13.1 Å, i.e. H_2P_pIm:MgPc, and slightly endothermic otherwise. This leaves open question on the possibility of the electron transfer in H_2P_pIm:MgPc but rules out the electron transfer as an efficient relaxation pathway.

Steady-State Emission Studies to Probe Excitation Transfer

An examination of absorption spectral features in Figure 1 points out that excitation of the donor, H_2PIm at its most intense Q-band located at 518 nm to a large extent selectively excites the free-base porphyrin thus allowing us to monitor energy transfer to the acceptor, MgPc or MgNc entities without them being directly getting excited. Figure 5a and b show the spectral changes observed for H_2P_pIm emission during increasing addition of MgPc and MgNc in DCB. The emission band of H_2P_pIm located at 655 nm revealed quenching with simultaneous appearance of new emission bands at 695 and 762 nm corresponding to MgPc (Figure 5a), and 783 and 822 nm corresponding to MgNc (Figure 5b). Similar results were obtained when H_2P_mIm and H_2P_oIm were titrated with either MgPc or MgNc (see supporting information for additional spectral data, Figures S4-S5). Further, the excitation spectra of the dyads were recorded by holding the emission wavelength at 762 nm for MgPc and 783 nm for MgNc. Such spectra revealed absorption bands corresponding to both donor and acceptor entities (see supporting information for the spectral data, Figures S6). In a control experiment, free-base *meso*-tetraphenylporphyrin, H_2TPP was also titrated with the acceptor molecules. Under these conditions, only a slight increase of the acceptor emission in the near-IR region was observed. These results confirm occurrence of singlet-singlet energy transfer in the self-assembled dyads and virtually no intermolecular events.

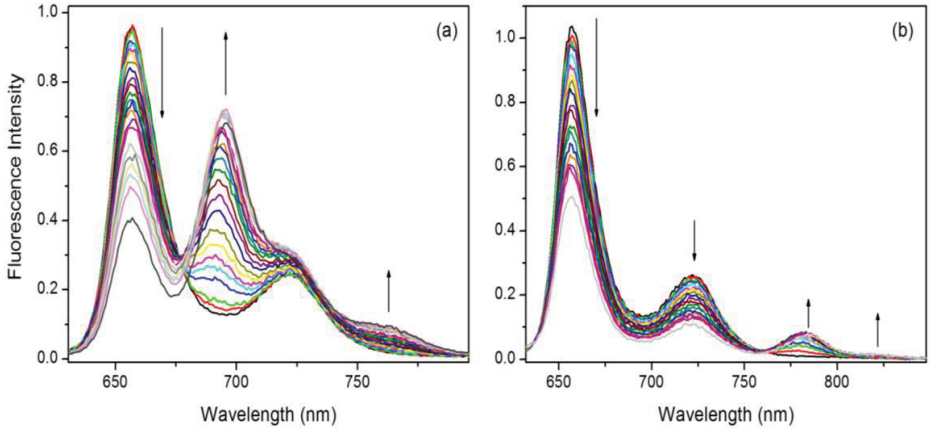

Figure 5. Steady state fluorescence spectra of H_2P_pIm (6.0×10^{-7} M) upon increasing addition of (a) MgPc and (b) MgNc, respectively in DCB, excited at 518 nm.

Theoretical Considerations of Excitation Transfer

The excitation transfer in donor-acceptor dyads could occur either via Dexter's exchange mechanism or Forster's dipole-dipole mechanism depending upon their structures.[29] The Dexter mechanism in the present series of dyads could be ruled out since no direct orbital overlap between the donor and acceptor entities was observed as revealed by the quantum mechanical calculations and the earlier discussed spectral studies. Hence, the results

have been analyzed and modeled according to Forster's mechanism; according to which the rate of excitation energy transfer, $k_{Forster}$, is given by the equation (2).

$$k_{Forster} = [8.8 \times 10^{-25} \kappa^2 \Phi_D J_{Forster}] / [n^4 \tau_D R^6] \quad (2)$$

where n is the solvent refractive index, Φ_D and τ_D are the fluorescence quantum yield (= 0.12) and the fluorescence lifetime of the isolated donor (H_2PIm), $J_{Forster}$ is the Forster's overlap integral representing the emission of the donor and absorption of the acceptor MgPc or MgNc, R is the donor-acceptor center-to-center distance (Table 1). The τ values measured using strobe technique were found to be 11.50, 9.95 and 9.45 ns, respectively, for the *ortho, meta* and *para*-imidazole derivatived free-base porphyrins.[11] In equation 2, κ^2 is the orientation factor as described in equation 3, often playing key role in determining the directionality of excitation energy transfer.

$$\kappa^2 = [\cos\nu - 3\cos\alpha \cos\beta]^2 \quad (3)$$

where α and β are the angles made by the transition dipoles of the donor and acceptor entities with the line joining the centers of the transitions and ν is the angle between the two transition dipoles. The transition dipoles of tetrapyrroles is known to lie along a line joining two opposing pyrrole nitrogens,[30] but owing to the fact that the donor and acceptor are free to rotate around the coordination bond the value of $\kappa^2 = 2/3$ was used which corresponds to random orientation of the two dipoles.

The $J_{Forster}$ spectral overlap integral representing the emission of the donor and absorption of the acceptor is given by equation 4.

$$J_{Forster} = \int F_D(\lambda)\, \varepsilon_A(\lambda)\, \lambda^4 d\lambda \quad (4)$$

$F_D(\lambda)$ is the fluorescence intensity of the donor with total intensity normalized to unity, $\varepsilon_A(\lambda)$ is the molar extinction coefficient of the acceptor expressed in units of $M^{-1}cm^{-1}$ and λ in nanometers. Figure 6 shows the spectral overlap of the donor and acceptor absorption and emission bands for both types of dyads. Analysis of the data according to equation (4) resulted in J values of 3.85×10^{-12} M^{-1} cm^3 and 5.02×10^{-12} M^{-1} cm^3, respectively, for the H_2PIm:MgPc and H_2PIm:MgNc series of dyads. These values are somewhat larger than those reported for Zn counterpart, 3.52×10^{-12} and 4.21×10^{-12} M^{-1} cm^3, for the H_2PIm:ZnPc and H_2PIm:ZnNc, respectively.[23] Therefore the energy transfer is expected to be slightly faster for MgPc and MgNc acceptors than for ZnPc and ZnNc ones.

Equation 1 can be further simplified in terms of Forster distance, R_o where half of the donor molecules decay by energy transfer and half decay by the usual radiative and non-radiative mechanisms.

$$k_{Forster} = 1/\tau_D\, (R_o/R)^6 \quad (5)$$

The rate constant of energy transfer can be calculated from the experimentally measured lifetimes of the energy donor, porphyrin, alone, τ_D, and in dyad, τ_{DA}, as

$$k_{ENT} = (\tau_{DA})^{-1} - (\tau_D)^{-1}. \quad (6)$$

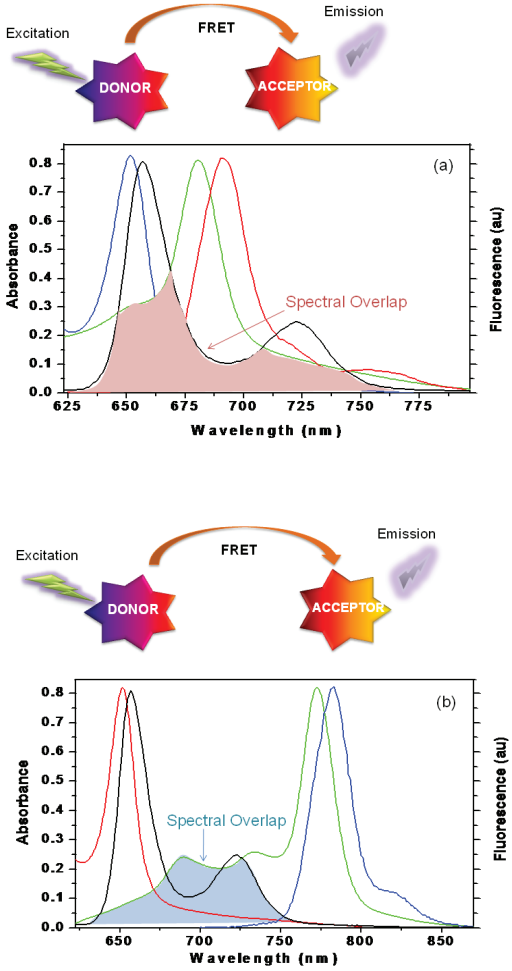

Figure 6. Spectral overlap (highlighted area) for (a) H_2PIm:MgPc and (b) H_2PIm:MgNc dyads. The donor absorption and emission, and the acceptor absorption and emission (all normalized) on an increasing wavelength scale are shown. The schematic above each figure shows the energy transfer path for each type of dyads.

As will be demonstrated later, for all dyads $\tau_D >> \tau_{DA}$, and a reasonably accurate estimation for the energy transfer rate is $k_{ENT} \approx (\tau_{DA})^{-1}$. The latter would also means that the steady state emission of the donor should efficiently quenched in case of homogeneous system, which was not the case of this study as seen from Figures 5a and 5b. In the concentration range used in this study some amount of non-bonded (free) donors exists in the solution, and the donor emission intensity reports on the number of non-bonded porphyrins rather than on the energy transfer rate.

Table 2. Estimated ($k_{Forster}$) and experimentally determined (k_{ENT}) rate constants of energy transfer for the dyads formed by coordination of imidazole appended free-base porphyrin to metal phthalocyanine or metal naphthalocyanine (metal = zinc or magnesium) in DCB.

Dyad[a]	$k_{Forster}$, s^{-1}, [b]	k_{ENT}, s^{-1}, [c]	Ref.
H_2P_oIm:MgPc	3.71×10^{11}	3.4×10^{11}	This work
H_2P_mIm:MgPc	2.30×10^{11}	0.9×10^{11}	This work
H_2P_pIm:MgPc	6.13×10^{11}	0.55×10^{11}	This work
H_2P_oIm:MgNc	4.17×10^{11}	5.0×10^{11}	This work
H_2P_mIm:MgNc	1.27×10^{11}	0.7×10^{11}	This work
H_2P_pIm:MgNc	2.71×10^{11}	0.7×10^{11}	This work
H_2P_oIm:ZnPc	3.94×10^{11}	1.4×10^{11}	23
H_2P_mIm:ZnPc	1.32×10^{11}	0.17×10^{11}	23
H_2P_pIm:ZnPc	2.30×10^{11}	0.33×10^{11}	23
H_2P_oIm:ZnNc	3.88×10^{11}	2.0×10^{11}	23
H_2P_mIm:ZnNc	1.41×10^{11}	0.9×10^{11}	23
H_2P_pIm:ZnNc	1.50×10^{11}	0.4×10^{11}	23

[a] See Chart 1 for the structure of different donor and acceptor entities.

[b] Estimated according to equations 1-5; Error = ± 10%.

[c] Determined from pump-probe technique.

The $k_{Forster}$ values were estimated by using the parameters described in equations 1 to 5 and found to be ~10^{11} s^{-1} revealing ultrafast energy transfer (Table 2). As explained in the subsequent paragraphs, the rate constant of energy transfer measured using pump-probe technique agrees reasonably well with the predictions of ultrafast energy transfer in the dyads.

Time-resolved Spectroscopy Studies

The energy transfer in the studied supramolecular dyads was found to occur in less than hundred picoseconds as will be shown later in this Section. In this time domain two methods are widely used to investigate dynamics of photoinduced processes, namely up-conversion and pump-probe. The former allows to measure evolution of emitting excited singlet states, and suits perfectly to study the energy transfer reactions. The latter makes possible to follow the transient absorption change of the samples thus allowing identifying both emitting and non-emitting transient state, which makes the data analysis and interpretation more complex than in the case of up-conversion measurements. Unfortunately, we found that under experimental conditions available, the degradation of MgPc

and MgNc during up-conversion was unacceptably high (from 50 to 90%). Therefore only pump-probe results will be discussed in this section, in which case the degradation during measurements was less than 10% for all reported data. The excitation wavelength was 420 nm which allows predominant excitation of the porphyrins even in samples with access of MgPc or MgNc.

The results of pump-probe measurements of H_2P_pIm, MgPc and MgNc are presented in Figure S7. The differential spectrum of H_2P_pIm (Fig. S7a) is typical for that of the excited singlet state of *meso*-tetraphenyl-porphyrins. For other porphyrin derivatives used in this study the spectra were essentially the same. The transient absorption responses of MgPc (Fig. S7b) and MgNc (Fig. S7c) were bi-exponential, however the longer-lived components, 1–2 ns, were dominating and can be attributed to the excited singlet states of the respective chromophores. The faster minor components, 4–8 ps, can be attributed to a presence of some amount aggregated phthalocyanines and/or solvent dynamics associated with relaxation of an access energy.

The pump-probe measurements were carried out in 1 mm cuvette where the optimum experimental conditions are achieved when the absorption maxima of the samples is in the range 0.5–2. This limits the range of possible concentrations of the porphyrins to 0.01–0.02 mM and of MgPc and MgNc to 0.02–0.04 mM, respectively. The samples were prepared at ratio roughly 1:2 of H_2PIm:MgPc and H_2PIm:MgNc, respectively. Accounting for the binding constants reported in Table 1 and concentrations of the samples as discussed above, the relative number of porphyrins forming a complex with phthalocyanines is expected to be from 5% (H_2P_oIm:MgPc) to 50% (H_2P_mIm:MgPc). Although the efficiency of complex formation was not high, it was possible to observe the energy transfer for all of the dyads; although for the samples with the lowest binding constant the energy transfer time constant have a larger error bar.

Figure 7 presents the results of the pump-probe measurements of porphyrin:phthalocyanine dyads. For H_2P_pIm:MgPc and H_2P_oIm:MgPc a three exponential fit model was used, and for H_2P_mIm:MgPc a bi-exponential fit was sufficient. For all samples the transient spectrum right after excitation (at 0 ps delay time, dashed line) is essentially the spectrum of the porphyrin excited singlet state with minor contribution of the phthalocyanine excited singlet state, which is seen as a weak negative absorption, i.e. bleaching of the phthalocyanine Q-band at 680 nm. This is reasonable as at the excitation wavelength, 420 nm, porphyrin is predominantly excited. A common feature of the samples is increasing bleaching of the phthalocyanine Q-band with time, though the time constants are different. The bleaching indicates increase in population of the excited singlet state of phthalocyanine as the consequence of the energy transfer from porphyrin entity. Comparing the shapes of the component spectra one can conclude that the time constants for the energy transfer are 18, 11 and 2.9 ps for *para, meta* and *ortho* derivatives of H_2PIm, respectively. The origin of the 85 ps component for H_2P_oIm:MgPc sample (Fig. 7c) is the relaxation of directly excited MgPc aggregates, since similar component was observed for pure MgPc sample. The fast component, 0.4 ps, observed for H_2P_pIm:MgPc dyad shows much broader band at 680 nm than that of MgPc monomers, and probably originates from the supramolecular structures more complex than porphyrin-phthlocyanine dyads. However the intensity of this component is the lowest and it was determined with a high degree of uncertainty, therefore it will not be discussed furthermore.

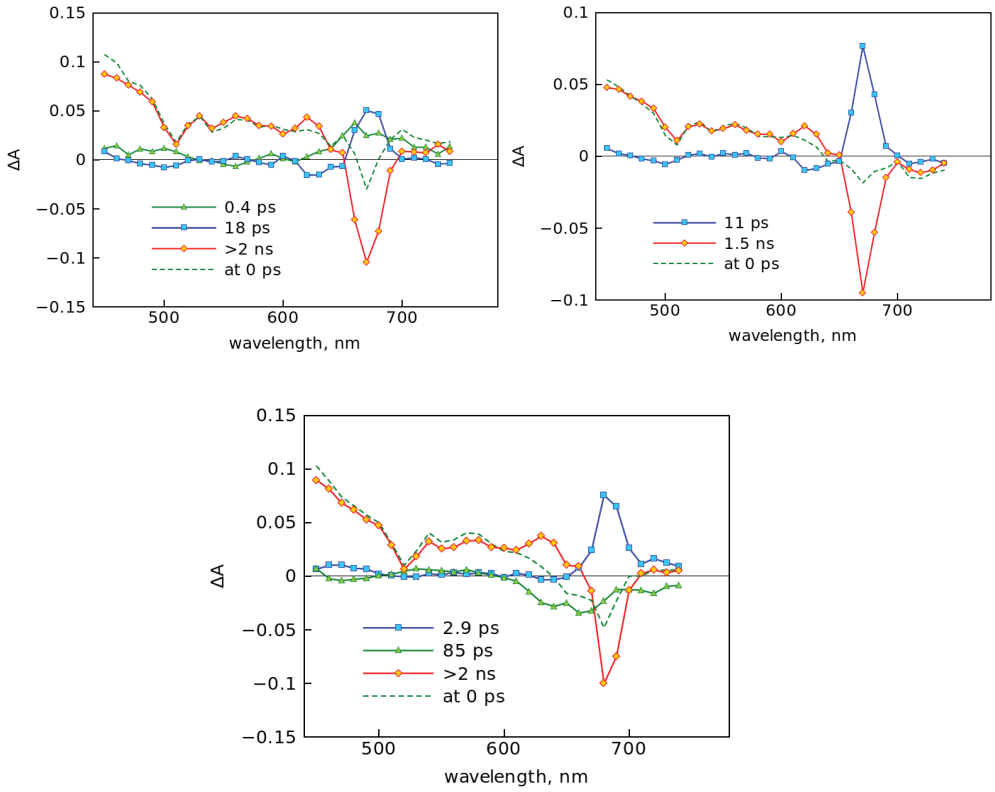

Figure 7. Transient absorption decay component spectra (symbols with solid lines) and time resolved transient absorption spectrum right after excitation (at 0 ps delay time, dashed line) of (a) H_2P_pIm:MgPc (b) H_2P_mIm:MgPc, and (c) H_2P_oIm:MgPc in toluene.

The transient absorption curves at 680 nm for different sample are presented in Figure 8 for comparison. At this wavelength the bleaching of the phthalocyanine Q bands is dominant, and the degree of bleaching can serve as an indicator of the excited singlet state population of MgPc. For all samples there is an instant bleaching of the Q-band resulting from the direct photoexcitation of the phthalocyanine, which is followed by a slower bleaching of the Q-band due to the energy transfer. The proportion between these two steps of bleaching is in agreement with the binding constant – the highest binding was observed for H_2P_mIm:MgPc and it shows the highest relative contribution of the slower bleaching. That is, the dyad has highest relative amount of phthalocyanines that receives excitation via the energy transfer process.

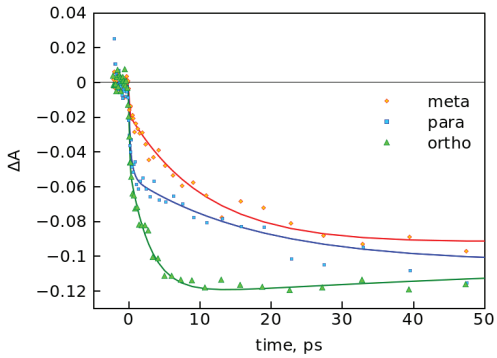

Figure 8. Transient absorption curves of supramolecular porphyrin-phthalocyanine dyads, H_2P_mIm:MgPc (*meta*), H_2P_pIm:MgPc (*para*) and H_2P_oIm:MgPc (*ortho*) at 680 nm.

For H_2PIm:MgPc dyads the slowest energy transfer is observed for H_2P_pIm (18 ps) and the fastest for H_2P_oIm (2.9 ps). The *para* position provides less steric restrictions for the complex formation but the distance between the energy donor, porphyrin, and energy acceptor, phthalocyanine, is the largest in the series. On the other hand, the *ortho* position allows the shortest donor-acceptor distance but this position of the binding group is sterically the least accessible for the dyad formation due to its close proximity to a bulky tetraphenylporphyrin chromophore.

Similar energy transfer properties were observed for H_2PIm:MgNc series of dyads. Since the absorption of MgNc at excitation wavelength, 420 nm, is higher than that of MgPc (see Fig. 1), the relative contribution of energy transfer to MgNc was smaller than that of MgPc. The results of the pump-probe measurements are presented in Fig. 9. The data were fitted using three-exponential model. The longest-lived component corresponds to a mixture of the singlet excited states of H_2PIm (with characteristic shape in 500-700 nm region) and that of MgNc (Q-band bleaching at 780 nm). There is a 1–2 ps component with similar shape for all samples (marked by the green triangles in Fig. 9). This component has no clear explanation but since it does not depend on the type of porphyrin compound it is probably due to the photodynamics of directly excited MgNc. The component which can be associated with the energy transfer is shown by the blue squares; it has roughly the same shape for different samples but different lifetimes: 13, 15 and 0.2 ps for *para*, *meta* and *ortho* porphyrins, respectively. The relative intensity of the energy transfer component is rather small for H_2P_mIm:MgNc sample, since the binding constant is smaller for H_2PIm:MgNc dyads than for H_2P_mIm:MgPc dyads, and the standard deviation for the calculated time constant, 15 ps, is compatible with the value itself. Therefore statistically the time constants for H_2P_mIm:MgNc and H_2P_pIm:MgNc are indistinguishable, which is in qualitative agreement with the results of computer modeling indicating much quite the same center-to-center distance for these two complexes.

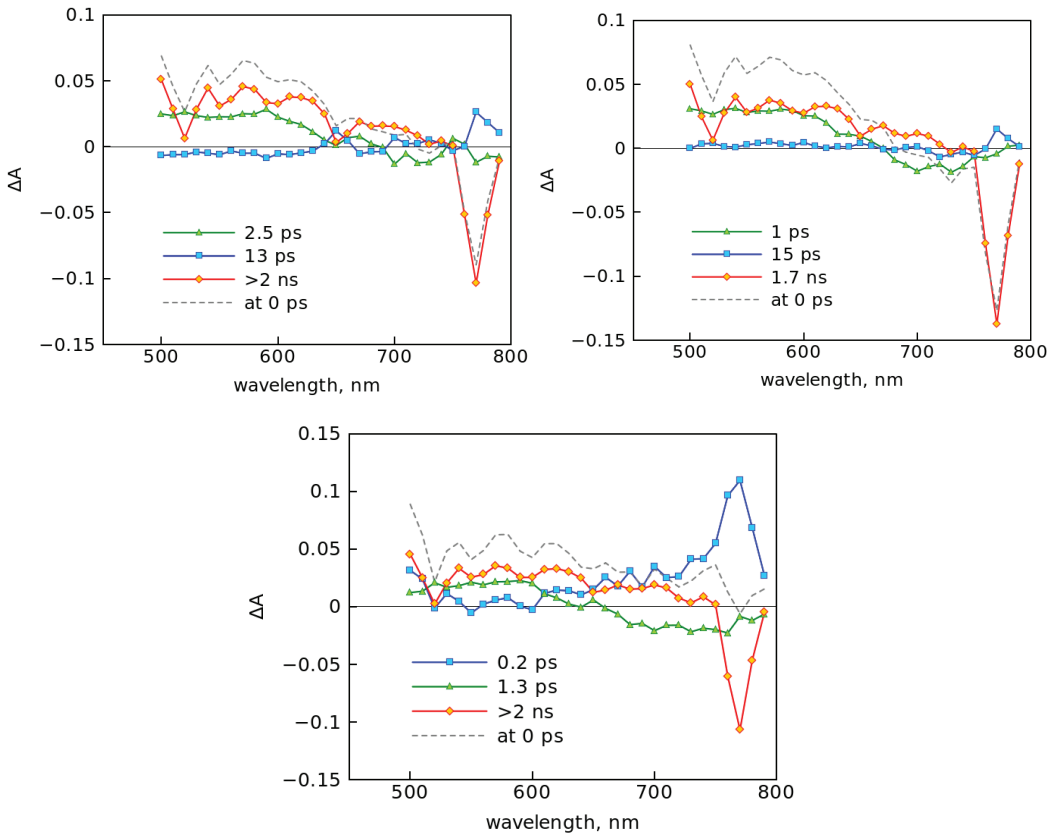

Figure 9. Transient absorption decay component spectra (symbols with solid lines) and time resolved transient absorption spectra (dashed line) at 0 ps delay time for (a) H_2P_pIm:MgNc, and (b) H_2P_mIm:MgNc, and (c) H_2P_oIm:MgNc in toluene.

Since the photoinduced electron transfer could not be ruled out base on electrochemical measurements (at least for H_2P_pIm:MgPc dyad) nanosecond flash-photolysis measurements were carried out with excitation at 420 nm. However, only triplet states were observed in time scale longer than 50 ns. The flash-photolysis measurements ruled out the photoinduced electron transfer in dyads with efficiency greater than 10%.

The obtained experimental results are in good qualitative agreement with the theoretical estimations based on the Förster energy transfer model, as summarized in Table 2. In particular the energy transfer was found to be somewhat faster for H_2PIm:MgNc complexes than for H_2P_oIm:MgPc ones. In addition the critical Förster energy transfer distance can be estimated to be in the range 25 – 35 Å, which is a reasonable value for this type of chromophores.

The calculated distances between the donor and acceptor decreases in proportion 1:0.84:0.59 for *para*:*meta*:*ortho* sequence, which should give increase in energy transfer rates in proportion 1:2.9:24, according to Equation (5) . The actual increase in the rates was in proportion 1:1.6:6.2. The trends are in good qualitative agreement, though the actual difference is not as big as predicted from theoretical modeling. The difference may

arise from a number of factors with most probable being: (i) restricted angular configurations for *meta* and *ortho* dyads which result in lower value of orientation factor, κ, and (ii) effect of solvent molecules which was not accounted in quantum mechanical calculations but expected to have a stronger influence on tighter conformers, i.e. *meta* and *ortho* dyads. The present results are complementary to the recently studied supramolecular dyads with zinc phthalocyanine acceptor.[23] The H_2P_pIm was the most favorable to the dyad formation, and the energy transfer time constants are very similar for ZnPc (30 ps) and MgPc (20 ps) acceptors. This is a reasonable result considering that the absorption spectra of ZnPc and MgPc are very similar to each other with somewhat better overlap for H_2P_pIm:MgPc dyad than that for H_2P_pIm:ZnPc dyad, which results in somewhat faster energy transfer.

CONCLUSIONS

Self-assembled via metal-ligand axial coordination free-base porphyrin-magnesium phthalocyanine and free-base porphyrin-magnesium naphthalocyanine dyads have been formed in non-coordinating solvents. The newly assembled dyads are fully characterized by spectroscopic, computational and electrochemical methods. The binding constants measured from optical absorption spectral data are found to be in the range of 10^2-10^3 M^{-1} for the 1:1 dyads suggesting fairly stable complex formation, however, the anticipated 2:1 complex is not observed under the present solution conditions. The geometry and electronic structures of the dyads, arrived from computational studies using B3LYP/3-21G(*) method, revealed flexible structures. The redox potential of the donor and acceptor entities were measured using differential pulse technique and free-energy calculations suggested electron transfer to be an inefficient process, also no experimental evidenced of the electron transfer were obtained. Excitation of H_2PIm entity in these dyads resulted in efficient excitation transfer and the position of the imidazole linkage on the H_2P entity seem to direct the overall efficiency of excited energy transfer. Kinetics of energy transfer, monitored by transient absorption measurements using pump-probe technique revealed time constants in the order of 1-20 ps depending upon the structure of the dyads and were close to the earlier reported H_2Im:ZnPc and H_2Im:ZnNc dyads. The experimentally determined rates agreed fairly well with those calculated based on Förster energy transfer mechanism.

EXPERIMENTAL SECTION

Chemicals

o-Dichlorobenzene (DCB) and toluene (in sure seal bottles under nitrogen) were from Aldrich Chemicals (Milwaukee, WI). Tetra-*n*-butylammonium perchlorate, (TBA)ClO_4 was from Fluka Chemicals. All the chromatographic materials and solvents were procured from Fisher Scientific and were used as received.

Synthesis of magnesium 2,9,16,23-tetra-*tert*-butyl-29*H*,31*H*-phthalocyanine

A mixture of 4-*tert*-butylphthalonitrile (72 mg, 0.39 mmol), $MgCl_2$ (74 mg, 0.78 mmol), and three drops of DBU in dry 1-pentanol (5 mL) was refluxed with stirring under an argon atmosphere for 7 hrs. After being cooled to room temperature, the green mixture was poured into methanol and the resulting precipitate was collected by

centrifugation. Then the dried precipitate was subjected to a silica gel column. The desired compound (yield: 55%) was obtained with hexane:chloroform (25:75 v/v). ^{1}H NMR in $CDCl_3$, δ (ppm) 9.60-9.41 (m, 8H), 8.28-8.15 (m, 4H), 1.90-1.84 (s, 36H, CH_3), (APCI mode in CH_2Cl_2): calcd, 760.95; found 762.01, λ_{max} = 352, 615, 649, 679 nm.

Synthesis of magnesium 2,11,20,29-tetra-*tert*-butyl-2,3-naphthalocyanine

6-*tert*-Butyl-2,3-naphthalenedicarbonitrile (80 mg, 0.34 mmol), $MgCl_2$ (65 mg, 0.68 mmol), and three drops of DBU were dissolved in 5 mL of dry 1-pentanol. Then the reaction mixture was refluxed with stirring under an argon atmosphere for 7 hrs. The mixture was cooled to room temperature, and poured into methanol. The resulting precipitate was collected by centrifugation. Then the dried precipitate was purified on silica gel column using hexane : chloroform (20:80 v/v). ^{1}H NMR in $CDCl_3$, δ (ppm) 9.69-9.50 (m, 8H), 9.40-9.35 (m, 8H), 8.25-8.12 (m, 4H), 1.91-1.86 (s, 36H, CH_3), (APCI mode in CH_2Cl_2): calcd, 961.23; found 962.80, λ_{max} = 332, 423, 489, 688, and 771 nm.

Instrumentation

The UV-visible spectral measurements were carried out with a Shimadzu Model 1600 UV-visible spectrophotometer. The fluorescence emission was monitored by using a Varian Eclipse spectrometer. A right angle detection method was used. The ^{1}H NMR studies were carried out on a Varian 400 MHz spectrometer. Tetramethylsilane (TMS) was used as an internal standard. Cyclic voltammograms were recorded on a EG&G model 263A Potentiostat/Galvanostat using a three electrode system. A platinum button electrode was used as the working electrode. A platinum wire served as the counter electrode and a Ag/AgCl electrode was used as the reference electrode. Ferrocene/ferrocenium redox couple was used as an internal standard. All the solutions were purged prior to electrochemical and spectral measurements using argon gas. The computational calculations were performed by DFT B3LYP/3-21G(*) methods with GAUSSIAN 03[25] software package on high speed PCs. The mass spectra of the newly synthesized compounds were recorded on a Varian 1200L Quadrupole MS using APCI mode in dry CH_2Cl_2 while the supramolecular complexes was monitored used Fennigan LCA-Deca mass spectrometer under mild temperature and voltage conditions. The dyads (about 1 mM concentration) were prepared in CH_2Cl_2, freshly distilled over calcium hydride.

Transient Absorption Measurements

Up-conversion instrument (FOG-100, CDP Corp.) for time-resolved fluorescence was used to detect the fast processes with a time resolution of ~200 fs. The primary Ti:sapphire generator (TiF-50, CDP Corp.) was pumped by Nd-YAG CW laser (Verdi-6, Coherent Inc.), and a second harmonic (~420 nm) was used to excite the sample solution in a rotating cuvette.[31] Emission from the sample was collected to a nonlinear crystal (NLC), where it was mixed with the so-called gate pulse, which was the laser fundamental. The signal was measured at a sum frequency of the gate pulse and the selected emission maximum of the sample. The gate pulses were passed through a delay line so that it arrived at NLC at a desired time after sample excitation. Scanning through the delay line the emission decay curve of the sample was detected.

Pump−probe and up-conversion techniques for time-resolved absorption and fluorescence, respectively, were used to detect the fast processes with a time resolution shorter than 0.2 ps. The instrument and the used data analysis procedure have been described earlier.[31] Samples for femtosecond transient absorption measurements

were prepared in 1 mm cuvette with absorbance of porphyrin adjusted to 1–1.5, and concentration or phthalocyanines was adjusted to provide molecular ratio of roughly 1:2 (ImP:MgPc). Molar absorption coefficients: ImP: 6.65 x 10^5 (@ 424 nm), MgPc: 1.76 x 10^5 (@ 680 nm), MgNc: 2.00x 10^5 (@773nm); this gives absorption ratios ImP:MgPc = 3.8 and ImP:MgNc = 3.3 were used.

Acknowledgments

This work was financially supported by the National Science Foundation (Grant Nos. 0804015 and EPS-0903806) and matching support from the State of Kansas through Kansas Technology Enterprise Corporation, and Academy of Finland.

Supporting Information Available

Absorption and fluorescence changes observed during the formation of dyads, Benesi-Hildebrand plots constructed to evaluate the binding constants, excitation spectra of the dyads, transient absorptions spectra of the donor and acceptor in DCB.

REFERENCES

1. (a) *Light-Harvsting Antennas in Photosynthesis* Green BR and Parson WW. (Eds) Kluwer: Dordrecht, Neth. 2003. (b) *Handbook of Photosynthesis*, 2nd Ed. Pessarakli M, (Ed.) CRC Press LLC: Boca Raton, Fla, 2005. (c) *Photosynthetic Protein Complexes; A Structural Approach,* Frome P. (Ed.) Wiley-VCH Verlag GmbH & Co.: Germany, 2008. (d) *Phtosynthetic Light Harvesting*, Cogdell R and Mullineaux C. (Eds.) Sprigner: Dordrecht, Neth. 2008.
2. (a) Deisenhofer J, Epp O, Miki K, Huber R and Michel H. *J. Mol. Biol.* 1984; **180**: 385. (b) *The Photosynthetic Reaction Center*, Deisenhofer J and Norris JR. (Eds.) Academic Press: San Diego, 2003. (c) Barber J and Anderson B. *Natur*e. 1994; **370**: 31. (d) Krauss N, Schubert WD, Klukas O, Fromme P, Witt HT and Saenger W. *Nature Struct. Biol*. 1996; **3**: 965.
3. (a) Wasielewski MR. *Chem. Rev*. 1992; **92**: 435. (b) Osuka A, Mataga N, Okada T. *Pure Appl. Chem*. 1997; **69**: 797. (c) *Molecular Level Artificial Photosynthetic Materials,* Meyer GJ. (Ed.) Wiley: New York, 1997. (d) Verhoeven JW. *Adv. Chem. Phys*. 1999; **106**: 603. (e) Flamigni L, Barigelletti F, Armaroli N, Collin J-P, Dixon IM, Sauvage J-P and Williams JAG. *Coord. Chem. Rev*. 1999; 190-192: 671. (f) Diederich F and Gomez-Lopez M. *Chem. Rev. Soc*. 1999; **28**: 263.
4. (a) Blanco M.-J, Consuelo Jimenez M, Chambron J-C, Heitz V, Linke M and Sauvage, J-P. *Chem. Rev. Soc*. 1999; **28**: 293. (b) Balzani V, Ceroni P, Juris A, Venturi M, Campagna S, Puntoriero F and Serroni S. *Coord. Chem. Rev*. 2001; **219**: 545. (c) Balzani V, Credi A and Venturi M. *ChemSusChem* 2008; **1**: 26.
5. Lewis FD, Letsinger RL and Wasielewski MR. *Acc. Chem. Res*. 2001; **34**: 159.

6. (a) Gust D, Moore TA and Moore AL. *Acc. Chem. Res*. 1993; **26**: 198. (b) Gust D and Moore TA. In *The Porphyrin Handbook*, Vol. 8, Kadish KM, Smith K and Guilard R (Eds.) Academic Press: San Diego, 2000; pp 153-190.

7. (a) Fukuzumi S. In *The Porphyrin Handbook*, Vol. 1, Kadish KM, Smith K and Guilard R (Eds.) Academic Press: San Diego, 2000, pp 115-151. (b) Fukuzumi S and Guldi DM. In *Electron Transfer in Chemistry*, Vol. 2, Balzani V (Ed.) Wiley-VCH: Weinheim, 2001, pp 270-337 (c) Fukuzumi S. *Phys. Chem. Chem. Phys*. 2008; **10**: 2283.

8. (a) Imahori H and Sakata Y. *Eur. J. Org. Chem*. 1999; 2445. (b) Imahori H, Tamaki K, Araki Y, Sekiguchi Y, Ito O, Sakata Y and Fukuzumi S. *J. Am. Chem. Soc*. 2002; **124**: 5165. (c) Umeyama T and Imahori H. *Energy & Environ. Sci*. 2008; **1**: 120.

9. (a) Guldi DM. *Chem. Commun*. 2000; 321. (b) Guldi DM. *Chem. Soc. Rev*. 2002; **31**: 22. (c) Sanchez L, Nazario M and Guldi DM. *Angew. Chem., Int. Ed.* 2005; **44**: 5374. (d) Sgobba V and Guldi DM. *Chem. Soc. Rev*. 2009; **38**: 165. (e) Mateo-Alonso A, Guldi DM, Paolucci F and Prato M. *Angew. Chem., Int. Ed*. 2007; **46**: 8120. (f) Guldi DM. *Phys. Chem. Chem. Phys*. 2007; **9**: 1400.

10. Sessler JS, Wang B, Springs SL and Brown CT. In *Comprehensive Supramolecular Chemistry*, Atwood JL, Davies JED, MacNicol DD and Vögtle F (Eds.) Pergamon, 1996; chapter 9.

11. El-Khouly ME, Ito O, Smith PM and D'Souza F. *Photochem. Photobiol. C*. 2004; **5**: 79. (b) D'Souza F and Ito O. *Coord. Chem. Rev*. 2005; **249**: 1410. (c) D'Souza F and Ito O. In *Handbook of Organic Electronics and Photonics*, Vol. 1, Nalwa HR (Ed.) American Scientific Publishers, 2008; chapter 13, 485-521. (d) Chitta R and D'Souza F. *J. Mater. Chem*. 2008; **18**: 1440. (e) D'Souza F and Ito O. *Chem. Commun*. 2009; 4913. (e) D'Souza F and Ito O. In *Handbook of Porphyrin Science.*Vol. 1, Kadish KM, Guilard R and Smith KM (Eds.) World Science Publishers: 2010; chapter 4, pp 307-437.

12. (a) *Introduction of Molecular Electronics*, Petty MC, Bryce MR, Bloor D. (Eds.) Oxford University Press, New York, 1995. (b) *Molecular Switches,* Feringa, BL. (Ed.) Wiley-VCH GmbH: Weinheim, 2001. (c) Tour JM. *Molecular Electronics; Commercial Insights, Chemistry, Devices*, *Architectures and Programming*, World Scientific: River Edge, NJ, 2003. (d) *Energy Harvesting Materials*, Andrews DL (Ed.) World Scientific: Singapore, 2005. (e) Gust D, Moore TA and Moore AL. *Chem. Commun*. 2006; 1169. (f) Balzani V, Credi A and Venturi M. In *Organic Nanostructures*, Atwood, JL and Steed JW (Ed.) 2008; 1-31.

13. (a) Luo C, Guldi DM, Imahori H, Tamaki, K and Sakata Y. *J. Am. Chem. Soc*. 2000; **122**: 6535. (b) Giribabu L, Kumar A, Neeraja V and Maiya BG. *Angew. Chem., Int. Ed. Engl*. 2001; **40**: 3621. (c) Choi M-S, Aida T, Yamazaki T and Yamazaki I. *Chem.-Eur. J*. 2002; **8**: 2667. (d) Aratani N, Cho HS, Ahn TK, Cho S, Kim D, Sumi H and Osuka A. *J. Am. Chem. Soc*. 2003; **125**: 9668. (e) Choi M-S. Aida T, Luo H, Araki Y and Ito O. *Angew. Chem., Int. Ed.* 2003; **42**: 4060. (f) Shinmori H, Ahn TK, Cho HS, Kim D, Yoshida N and Osuka A. *Angew. Chem., Int. Ed. Engl*. 2003; **42**: 2754. (g) Imahori H. *J. Phys. Chem. B* 2004; **108**, 6130. (h) Li X, Sinks LE, Rybtchinski B and Wasielewski MR. *J. Am. Chem. Soc*. 2004; **126**: 10810.

14. (a) Seth J, Palaniappan V, Johnson TE, Prathapan S, Lindsey JS and Bocian DF. *J. Am. Chem. Soc*. 1994; **116**: 10578. (b) Seth J, Palaniappna V, Wagner RW, Johnson TE, Lindsey JS, Holten D and Bocian DF. *J. Am. Chem. Soc*. 1996; **118**: 11194. (c) Hsiao J-S, Krueger BJ, Wagner RW, Johnson TE, Delaney JK, Mauzerall DC, Fleming GR, Lindsey JS, Bocian, DF, Donohoe RJ. *J. Am. Chem. Soc*. 1996; **118**: 11181.

(d) Bothner-By AA, Dodok J, Johnson TE, Delaney JK and Lindsey JS. *J. Phys. Chem*. 1996; **100**: 17551. (e) Wagner RW, Johnson TE, Lindsey JS. *J. Am. Chem. Soc*. 1996; **118**: 11166. (f) Strachan JP, Gentemann S, Seth J, Kalsback WA, Lindsey JS, Holten D and Bocian DF. *J. Am. Chem. Soc*. 1997; **119**: 11191. (g) Li F, Gentemann S, Kalsbeck WA, Seth J, Lindsey JS, Holten D and Bocian DF. *J. Mater. Chem*. 1997; **7**: 1245. (h) Li J, Ambroise A, Yang SI, Diers JR, Seth J, Wack CR, Bocian, DF, Holten D and Lindsey JS. *J. Am. Chem. Soc*. 1999; **121**: 8927.

15. (a) Sessler JL, Magda DJ and Harriman A. *J. Am Chem. Soc*. 1995; 117: 704. (b) Kral V, Springs SL and Sessler JL. *J. Am. Chem. Soc*. 1995; **117**: 8881. (c) Springs SL, Gosztola D, Wasielewski MR, Kral V, Andrievsky A and Sessler JL. *J. Am. Chem. Soc.* 1999; **121**: 2281.

16. (a) D'Souza F, Smith PM, Zandler ME, McCarty AL, Itou M, Araki Y and Ito O. *J. Am. Chem. Soc*. 2004; **126**: 7898. (b) D'Souza F, Gadde S, Islam DJS, Wijesinghe CA, Schumacher AL, Zandler ME, Araki Y and Ito O. *J. Phys. Chem. A* 2007; **111**: 8552. (c) Maligaspe E, Tkachenko, NV, Subbaiyan NK, Chitta R, Zandler ME, Lemmetyinen H and D'Souza F. *J. Phys. Chem. A* 2009; **113**: 8478.

17. Webber SE. *Chem. Rev*. 1990; **90**: 1469.

18. Frechet JM. *J. Polym. Sci., Part A: Polym. Chem.* 2003; **41**: 3713.

19. (a) Haycock RA, Hunter CA, James DA, Michelsen U and Sutton LR. *Org. Lett*. 2000; **2**: 2435. (b) van der Boom T, Hayes RT, Zhao Y, Bushard PJ, Weiss EA and Wasielewski MR. *J. Am. Chem. Soc*. 2002; **124**: 9582. (c) Takahashi R and Kobuke Y. *J. Am. Chem. Soc.* 2003; **125**: 2372. (d) Chen X and Drain CM. *Encycl. Nanosci. Nanotechnol.* 2004; **9**: 593. (e) Kuramochi Y, Satake A, Itou M, Ogawa K, Araki Y, Ito O and Kobuke Y. *Chem.–Eur. J.* 2008; **14**: 2827. (f) Uyar Z, Satake A, Kobuke Y and Hirota S. *Tet. Lett*. 2008; **49**: 5484. (g) Kuramochi Y, Sandanayaka ASD, Satake A, Araki Y, Ogawa K, Ito O and Kobuke Y. *Chem.–Eur. J*. 2009; **15**: 2317.

20. (a) Smith KM. *Porphyrins and Metalloporphyrins*, Elsevier: Amsterdam, 1972. (b) *The Porphyrin Handbook*; Vols. 1-20, Kadish KM, Smith KM and Guilard R. (Eds.) Academic Press: San Diego, CA, 2000.

21. (a) *Phthalocyanine: Properties and Applications*; Leznoff CC, Lever ABP. (Eds.) VCH: New York, 1993. (b) Howe L and Zhang JZ. *J. Phys. Chem. A*, 1997; **101**: 3207-3213. (c) *Phthalocyanine Materials: Structure, Synthesis and Function*, McKeown NB. (Ed.) Cambridge University Press: Cambridge, 1998. (d) Claessens CG, González-Rodríguez D and Torres T. *Chem. Rev.* 2002; **102**: 835. (e) Gunaratne TC, Gusev AV, Peng X, Rosa A, Ricciardi G, Baerends EJ, Rizzoli C, Kenney ME and Rodgers MAJ. *J. Phys. Chem. A*, 2005; **109**: 2078-2089. (f) Bottari G, de la Torre G, Guldi DM and Torres T. *Chem. Rev*. 2010; ASAP article.

22. For related studies on porphyrin-phthalocyanine dyads see: (a) Kobayashi N, Nishiyama Y, Ohya T, Sato M. *J. Chem. Soc., Chem. Commun.* 1987; 390. (b) Tian H-J, Zhou Q-F, Shen S-Y and Xu H-J. *J. Photochem. Photobiol. A* 1993; **72**: 163. (c) Li J and Lindsey JS. *J. Org. Chem*. 1999; **64**: 9101. (d) Yang SI, Li J, Cho HS, Kim D, Bocian DF, Holten D and Lindsey JS. *J. Mater. Chem.* 2000, **10**, 283. (e) Miller MA, Lammi RK, Prathapan S, Holten D and Lindsey JS. *J. Org. Chem.* 2000; **65**: 6634. (f) Ambroise A, Wagner RW, Rao PD, Riggs JA, Hascoat P, Diers JR, Seth J, Lammi RK, Bocian DF, Holten D and Lindsey JS. *Chem. Mater.* 2001; **13**: 1023. (g) Sutton JM and Boyle RW. *Chem. Commun.* 2001; 2014. (h) Kameyama K, Satake A and Kobuke Y. *Tetrahedron Lett.* 2004; **45**: 7617. (i) Zhao Z, Nyokong T and Maree MD. *Dalton Trans*. 2005; 3732. (j) Tome JPC, Pereira AMVM, Alonso CMA, Neves MGPMS, Tome AC, Silva AMS,

Cavaleiro JAS, Martinez-Diaz MV, Torres T, Rahman GMA, Ramey J and Guldi DM. *Eur. J. Org. Chem*. 2006; 257. (k) Ito F, Ishibashi Y, Khan SR, Miyasaka H, Kameyama K, Morisue M, Satake A, Ogawa K and Kobuke Y. *J. Phys. Chem. A* 2006; **110**: 12734. (j) Giribabu L, Kumar CV, Reddy PD. *Chem. Asian J*. 2007; **2**: 1574. (l) Tannert S, Ermilov EA, Vogel JO, Choi MTM, Ng DKP and Röder B. *J. Phys. Chem. B* 2007; **111**: 8053. (m) Soares ARM, Martinez-Diaz MV, Bruckner A, Pereira AMVM, Tome JPC, Alonso CMA, Faustino MAF, Neves MGPMS, Tome AC, Silva AMS, Cavaleiro JAS, Torres T and Guldi DM. *Org. Lett*. 2007; **9**: 1557. (n) Ali H and va Lier J. E. *Tet. Letts*. 2009; **50**: 1113. (o) Kojima T, Honda T, Ohkubo K, Shiro M, Kusukawa T, Fukuda T, Kobayashi N and Fukuzumi S. *Angew. Chem., Int. Ed*. 2008; **47**: 6712.

23. Maligaspe E, Kumpulainen T, Lemmetyinen H, Tkachenko NV, Subbaiyan NK, Zandler ME and D'Souza F. *J. Phys. Chem. A* 2010; **114**: 268.
24. Ough E, Nyokong T, Creber KAM and Stillman MJ. *Inorg. Chem*. 1998; **27**: 2724.
25. Benesi HA, Hildebrand JH. *J. Am. Chem. Soc*. 1949; **71**: 2703.
26. *Gaussian 03*, Frisch MJ, Trucks GW, Schlegel HB, Scuseria GE, Robb MA, Cheeseman JR, Zakrzewski VG, Montgomery JA, Stratmann RE, Burant JC, Dapprich S, Millam JM, Daniels AD, Kudin KN, Strain MC, Farkas O, Tomasi J, Barone V, Cossi M, Cammi R, Mennucci B, Pomelli C, Adamo C, Clifford S, Ochterski J, Petersson GA, Ayala PY, Cui Q, Morokuma K, Malick DK, Rabuck AD, Raghavachari K, Foresman JB, Cioslowski J, Ortiz JV, Stefanov BB, Liu G, Liashenko A, Piskorz P, Komaromi I, Gomperts R, Martin RL, Fox DJ, Keith, T, Al-Laham MA, Peng CY, Nanayakkara A, Gonzalez C, Challacombe M, Gill PMW, Johnson BG, Chen W, Wong MW, Andres JL, Head-Gordon M, Replogle ES, Pople JA. Gaussian, Inc., Pittsburgh PA, 2003.
27. For applications of B3LYP on supramolecualr systems see: Zandler ME, D'Souza F. *C. R. Chemie*. 2006; **9**: 960.
28. Weller AZ. *Phys. Chem.* 1982; **132**: 93.
29. *Principles of Fluorescence Spectroscopy*, 3rd ed. By Lakowicz JR. 2006; Springer: Singapore.
30. Gouterman M. *J. Mol. Spectrosc*. 1961; **6**: 138.
31. Tkachenko NV, Rantala L, Tauber AY, Helaja J, Hynninen PH and Lemmetyinen H. *J. Am. Chem. Soc*. 1999; **121**: 9378. (b) Vehmanen V, Tkachenko NV, Imahori H, Fukuzumi S, Lemmetyinen H. *Spectrochim. Acta*. A 2001; **57**: 2229. (c) Isosomppi M, Tkachenko NV, Efimov A, Lemmetyinen H. *J. Phys. Chem. A* 2005; **109**: 4881.

PUBLICATION II

Syntheses and Excitation Transfer Studies of Near-Orthogonal Free-Base Porphyrin-Ruthenium Phthalocyanine Dyads and Pentad

Rachel Jacobs, Kati Stranius, Eranda Maligaspe, Helge Lemmetyinen, Nikolai V. Tkachenko, Melvin E. Zandler and Francis D'Souza

Inorganic chemistry

Inorganic Chemistry

Article

pubs.acs.org/IC

Syntheses and Excitation Transfer Studies of Near-Orthogonal Free-Base Porphyrin–Ruthenium Phthalocyanine Dyads and Pentad

Rachel Jacobs,[†] Kati Stranius,[‡] Eranda Maligaspe,[†] Helge Lemmetyinen,[‡] Nikolai V. Tkachenko,*[,‡] Melvin E. Zandler,[†] and Francis D'Souza*[,†,§]

[†]Department of Chemistry, Wichita State University, 1845 Fairmount, Wichita, Kansas 67260-0051, United States

[‡]Department of Chemistry and Bioengineering, Tampere University of Technology, P.O. Box 541, 33101 Tampere, Finland

[§]Department of Chemistry, University of North Texas, 1155 Union Circle, 305070, Denton, Texas 76203-5017, United States

Supporting Information

ABSTRACT: A new series of molecular dyads and pentad featuring free-base porphyrin and ruthenium phthalocyanine have been synthesized and characterized. The synthetic strategy involved reacting free-base porphyrin functionalized with one or four entities of phenylimidazole at the meso position of the porphyrin ring with ruthenium carbonyl phthalocyanine followed by chromatographic separation and purification of the products. Excitation transfer in these donor–acceptor polyads (dyad and pentad) is investigated in nonpolar toluene and polar benzonitrile solvents using both steady-state and time-resolved emission techniques. Electrochemical and computational studies suggested that the photoinduced electron transfer is a thermodynamically unfavorable process in nonpolar media but may take place in a polar environment. Selective excitation of the donor, free-base porphyrin entity, resulted in efficient excitation transfer to the acceptor, ruthenium phthalocyanine, and the position of imidazole linkage on the free-base porphyrin could be used to tune the rates of excitation transfer. The singlet excited Ru phthalocyanine thus formed instantly relaxed to the triplet state via intersystem crossing prior to returning to the ground state. Kinetics of energy transfer (k_{ENT}) was monitored by performing transient absorption and emission measurements using pump–probe and up-conversion techniques in toluene, respectively, and modeled using a Förster-type energy transfer mechanism. Such studies revealed the experimental k_{ENT} values on the order of 10^{10}–10^{11} s^{-1}, which readily agreed with the theoretically estimated values. Interestingly, in polar benzonitrile solvent, additional charge transfer interactions in the case of dyads but not in the case of pentad, presumably due to the geometry/orientation consideration, were observed.

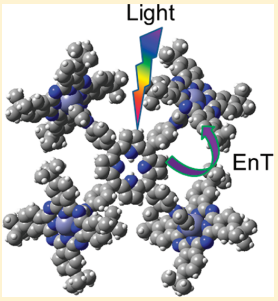

INTRODUCTION

Solar energy technologies are the most promising solution for sustainable energy production. Sunlight constitutes the primary energy source for almost all of the interdependent biological events in nature, thus making life possible.[1,2] For developing efficient and affordable light energy harvesting systems, molecular systems capable of collecting, translating, and accumulating sunlight are desirable toward clean energy production. However, design of such multifaceted devices requires building multicomponent arrays of units by a modular approach such that they perform key functions of photosynthesis, viz., energy capture and funneling, and electron transfer, ultimately creating the energetic oxidizing and reducing equivalents of sufficient lifetimes (milliseconds to seconds).[3−11]

This approach is for not only useful building artificial photosynthetic devices but also photovoltaics and optoelectronic applications.[12]

In natural photosynthesis, energy capture and funneling (converting the energy of an absorbed photon into an electron excitation) has efficiently been done by chlorophylls and carotenoids that are supramolecularly organized for unidirectional excitation transfer toward a reaction center.[1,2] Researchers have been attempting to mimic this process with the help of molecular donor–acceptor systems combining two or more chromophores.[3−11] These chromophores are covalently linked,[13−16] form part of a polymer system,[17] associated with a dendrimeric structure,[18] or self-assembled systems by intermolecular forces.[19] Due to their structural similarity to the natural light harvesting chlorophyll material and the established synthetic methodologies and their outstanding electronic properties, in a majority of these studies porphyrins[20] and phthalocyanines[21] have been used as common chromophores. Evidently, several dyads featuring these two chromophores have been reported.[22]

Recently, we reported on free-base porphyrin–Zn (or Mg) phthalocyanine (or naphthalocyanine) dyads via metal–ligand axial coordination and reported ultrafast singlet–singlet excitation transfer.[23] Although phenylimidazole-functionalized porphyrin was used to achieve a higher stability of the complexes instead of more the traditional pyridine-functionalized porphyrin, it was not possible to isolate the complexes due

Received: November 29, 2011
Published: March 5, 2012

Chart 1. Structure of the Dyads and Pentad Developed in the Present Study To Probe Excitation Energy Transfer

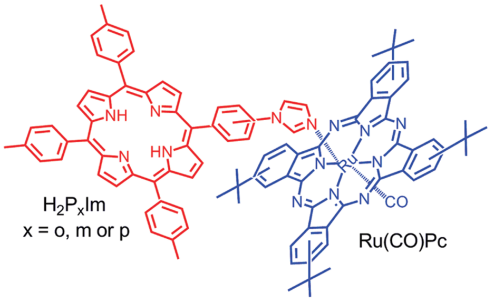

Dimer H_2P_xIm:Ru(CO)Pc

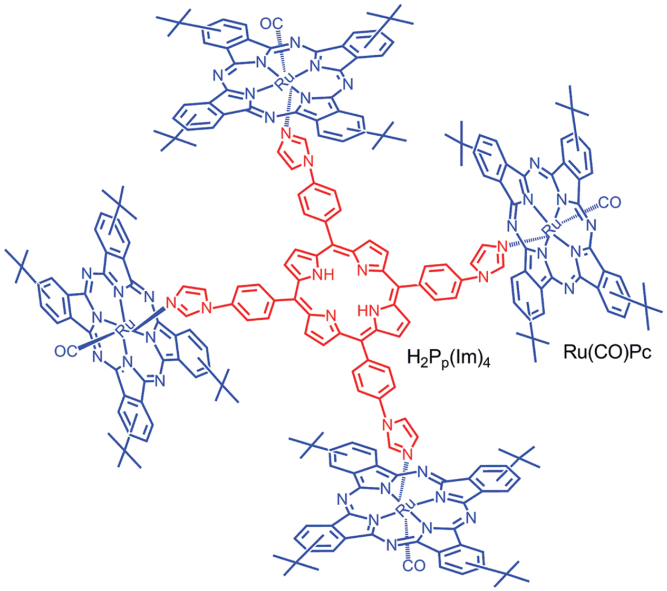

Pentamer H_2P_x(Im:Ru(CO)Pc)$_4$

to the labile nature of the metal−ligand coordinate bond. Hence, the synthetic protocol could not be extended to create a higher version of the polyads (triads, tetrads, pentads, etc.) as biomimetic multicomponent energy funneling antenna models. To overcome this issue, in the present study we employed ruthenium carbonyl phthalocyanine, Ru(CO)*Pc*, instead of their Zn or Mg phthalocyanines and synthesized dyads using 2-, 3-, or 4-imidozylphenyl-substituted free-base porphyrins. Further, this strategy has been extended to form a pentad using a porphyrin functionalized with four entities of 4-imidozylphenyl substituents at the porphyrin periphery (Chart 1). Different substitution resulted in dyads of different orientations. Photochemical studies using both steady-state and time-resolved emission techniques have been performed to probe the efficiency and kinetics of excitation transfer in the newly formed dyads and pentad.

RESULTS AND DISCUSSION

Synthesis of the Dyads and Pentad. Porphyrins bearing an imidazole group at one of its meso phenyl positions have been synthesized by reaction of stoichiometric amounts of pyrrole, tolualdehyde, and 4-imidazolylbenzaldehyde using the standard procedure.[20] The imidazole entity on the phenyl group was functionalized at the ortho, meta, or para positions to visualize the relative orientation of the donor−acceptor entities on their photochemical properties. For formation of pentad, all of the meso positions have been substituted with 4′-imidazolyl benzene groups. The employed phthalocyanine had four *tert*-butyl substituents at the periphery to improve its solubility and reduce aggregation without significantly perturbing the electronic structure in organic solvents. Ru(CO)*Pc* was synthesized in good yields by reaction of free-base phthalocyanine with trisruthenium dodecacarbonyl in phenol following the literature procedure.[24] The choice of the CO group on Ru(CO)*Pc* provided stronger ligation due to the π-acceptor

dx.doi.org/10.1021/ic202574q | *Inorg. Chem.* 2012, 51, 3656−3665

carbonyl ligand at one of the two axial Ru(II) coordination sites. Syntheses of the dyads and pentad involved reacting stoichiometric amounts of imidazole-functionalized porphyrin with Ru(CO)*Pc* followed by chromatographic separation. This approach has earlier been used to form molecular architectures using various pyridine-derivatized molecular components.[25] The present method differs from the earlier method where imidazole–ruthenium binding instead of pyridine–ruthenium was successfully used.[24] As shown here, due to the better ligating behavior of imidazole, the synthetic methodology has been facile, resulting in higher yields of products. The newly synthesized compounds were purified over a silica gel column prior to performing spectral measurements and characterized by mass spectrometry, NMR spectroscopy, and other methods. Additionally, thin-layer chromatography (TLC) on all of the newly synthesized compounds was performed to ensure the absence of impurities.

Optical Absorption Spectral Studies. Figure 1 shows the optical absorption spectra of the newly synthesized compounds

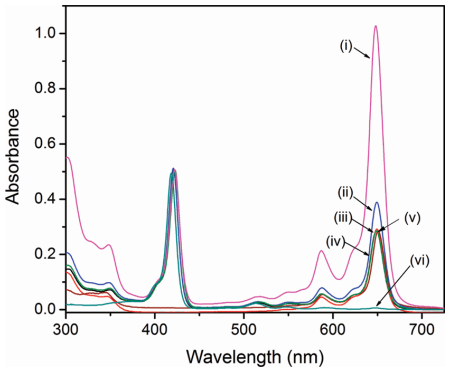

Figure 1. Normalized to the porphyrin Soret band absorption spectra of (i) $H_2P_p(Im:Ru(CO)Pc)_4$ pentad, (ii) $H_2P_mIm:Ru(CO)Pc$ dyad, (iii) $H_2P_pIm:Ru(CO)Pc$ dyad, (iv) $H_2P_oIm:Ru(CO)Pc$ dyad, (iv) PhIm:Ru(CO)*Pc*, (v) Ru(CO)*Pc*, and (vi) H_2TPP in toluene.

along with the control compounds normalized to the porphyrin Soret band. The free-base porphyrin, H_2TPP (or H_2P_xIm derivatives in Chart 1), has a Soret band at 418 nm and four less intense visible bands. Both Ru(CO)*Pc* and PhIm:Ru(CO)*Pc*, the control compound synthesized by reacting phenyl imidazole and Ru(CO)*Pc* (the colon symbol represents the metal–ligand axial bond), revealed a strong absorption band at 650 nm accompanied by weaker absorption bands at 587 and 346 nm. For the dyads, the spectral features were similar to the 1:1 mixture of H_2TPP and PhIm:Ru(CO)*Pc* with less than a 1 nm red shift of the porphyrin Soret and less than 2 nm blue shift of the phthalocyanine absorption band positions. For the pentad, the phthalocyanine peak intensity was nearly four times that of the dyads with less than a 2 nm change in spectral peak positions, providing proof for the structural integrity of the pentad. It is important to note that the 516 nm peak of H_2P had no significant spectral overlap with Ru(CO)*Pc* absorption bands, suggesting this wavelength is suitable for selective excitation of the porphyrin in the dyads and pentad.

Steady-state fluorescence spectra of the compounds are shown in Figure 2. Pristine H_2TPP (or H_2P_xIm derivatives in

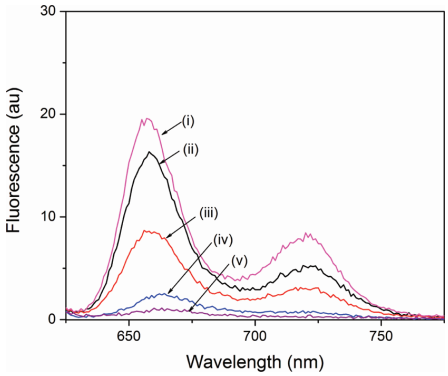

Figure 2. Fluorescence emission spectra of (i) $H_2P_oIm:Ru(CO)Pc$ dyad, (ii) $H_2P_pIm:Ru(CO)Pc$ dyad, (iii) $H_2P_mIm:Ru(CO)Pc$ dyad, (iv) $H_2P_p(Im:Ru(CO)Pc)_4$ pentad, and (v) Ru(CO)*Pc* in toluene. λ_{ex} = 518 nm. Concentrations were held at 10 μM.

Chart 1) revealed emission bands at 650 and 720 nm. For all of the dyads and pentad, the porphyrin emission bands were found to be quenched over 95% of their initial intensity, more so for the pentad (97%), accompanied by red shifts of ~6 nm for the dyads and 12 nm for the pentad (see Supporting Information Figure S1 for comparative emission spectra with respect to H_2TPP emission). Interestingly, under the experimental conditions used, Ru(CO)*Pc* revealed a very weak emission at 670 nm. Direct excitation of Ru(CO)*Pc* at any of its absorption peak maxima also revealed weak emission at 670 nm, indicating very low emission quantum yields. This property has earlier been attributed to the gradually quenched emission of the phthalocyanine singlet excited state which undergoes rapid intersystem crossing populating the triplet state due to the presence of a heavy atom in the phthalocyanine cavity.[24a] The small red shift in H_2P emission could be ascribed to axial coordination and/or overlap of Ru(CO)*Pc* emission as a result of energy transfer.

To unravel the quenching mechanism of the porphyrin fluorescence as to energy or electron transfer, further electrochemical and computational studies were performed, as summarized below.

Electrochemical and Computational Studies. Figure 3 shows the cyclic voltammograms of Ru(CO)*Pc* and

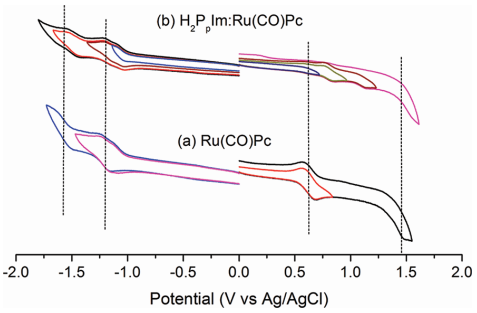

Figure 3. Cyclic voltammograms of (a) Ru(CO)*Pc* and (b) $H_2P_pIm:Ru(CO)Pc$ dyad (~0.5 mM) in *o*-dichlorobenzene containing 0.1 M $(TBA)ClO_4$. Scan rate = 100 mV/s.

dx.doi.org/10.1021/ic202574q | *Inorg. Chem.* 2012, 51, 3656–3665

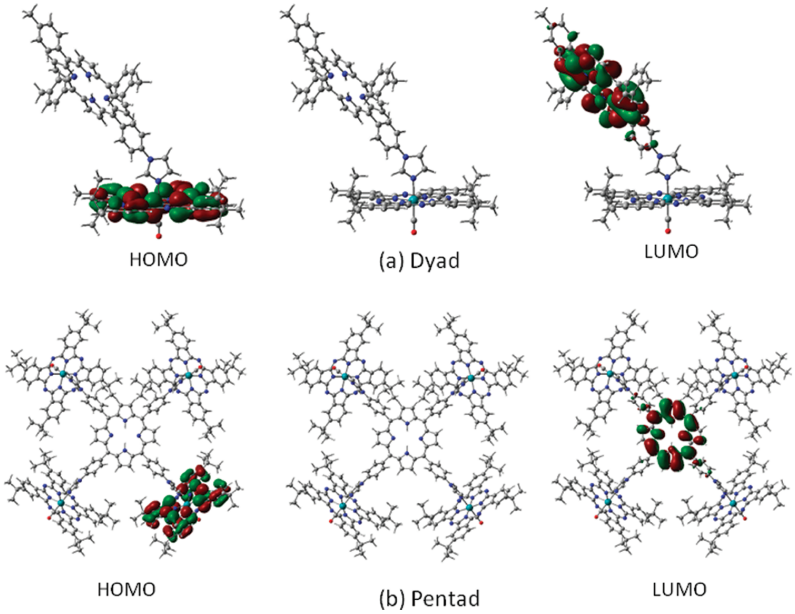

Figure 4. B3LYP/3-21G(*)-optimized structures of the (a) H_2P_pIm:Ru(CO)*Pc* dyad and (b) H_2P_p(Im:Ru(CO)*Pc*)$_4$ pentad. HOMO and LUMO of the respective compounds are shown in the left and right side of each optimized structure.

H_2P_pIm:Ru(CO)*Pc* in *o*-dichlorobenzene containing 0.1 M (TBA)ClO_4. For electrochemical measurements we used *o*-dichlorobenzene instead of toluene due to insolubility of the supporting electrolyte in the latter solvent. The precursor, Ru(CO)*Pc* revealed the first reversible oxidation at 0.61 V and a second one at 1.43 V vs Ag/AgCl. The first two reversible reductions of Ru(CO)*Pc* were located at −1.20 and −1.57 V vs Ag/AgCl. In agreement with earlier reports,[24] these electrode processes were all macrocycle based and had no metal center involved. The first reversible oxidation and first two reversible reductions of H_2P_oIm were located at 0.55 and −1.67 and −2.02 V vs Fc/Fc$^+$ in 0.1 (TBA)ClO_4, respectively.[23a] For H_2P_mIm and H_2P_pIm, the first reduction was shifted in the negative direction by 50−60 mV while the first oxidation was anodically shifted by 40 mV.[23a] The dyad, H_2P_pIm:Ru(CO)*Pc*, revealed four oxidations located at 0.62, 0.80, 1.09, and 1.45 V vs Ag/AgCl and four reductions located at −1.12, −1.20, −1.49, and −1.58 V vs Ag/AgCl. By comparing the redox potential values with those of Ru(CO)*Pc* and H_2TPP (or H_2P_xIm derivatives), the first and fourth oxidation and second and fourth reductions of the dyad were ascribed to the Ru(CO)*Pc* entity while the second and third oxidation and the first and third reduction processes were ascribed to the porphyrin entity. Consequently, the lowest energy required for the charge transfer reaction to occur is 1.74 eV, in which case electron transfer would take place from Ru(CO)*Pc* donor to H_2P_xIm acceptor. Very similar redox chemistry was observed for the other two dyads, while for the pentad the four equivalents of Ru(CO)*Pc* overpowered the currents of the redox waves in which case the redox processes of H_2P appeared as shoulder waves at almost the same potential values.

Figure 4 shows the structures of the H_2P_pIm:Ru(CO)*Pc* dyad and the H_2P_p(Im:Ru(CO)*Pc*)$_4$ pentad, energy optimized on a Born−Oppenheimer potential energy surface using the B3LYP/3-21G(*) method.[26,27] Similar structures were obtained for the other two dyads. In agreement with the results of earlier reported ZnPc- and MgPc-based dyads, the two macrocyclic porphyrin and phthalocyanine rings were found to be in a skipped coplanar arrangement with an angle less than a right angle between the two planes. The center-to-center distance between the two macrocycles ranged between 8 to 12 Å, while the edge-to-edge distances were between 5.7 and 8.8 Å, depending upon the position of substitution of the imidazole ring on the porphyrin macrocycle. Generally, the distances varied as ortho < meta < para imidazole-substituted porphyrins.

In the case of the H_2P_p(Im:Ru(CO)*Pc*)$_4$ pentad, the peripheral imidazole-coordinated Ru(CO)*Pc* entities were positioned about 50° to the plane of the porphyrin ring. In addition, two of the four Ru(CO)*Pc* macrocycles positioned at opposite side of the porphyrin macrocycle had the same orientation while the other two Ru(CO)*Pc* macrocycles had an opposite orientation (roughly a C_2 rotation axis). As a result, the four Ru centers created a dihedral angle of about 25°. The Ru−Ru distance from the neighboring macrocycles were in the range of 18.6−19.9 Å, while the distance between Ru and the center of free-base porphyrin was ∼13.2 Å. The Ru−Ru distance between the oppositely positioned Ru(CO)*Pc* rings were 23.6 and 25.9 Å.

The frontier orbitals, HOMO and LUMO, were also evaluated for both dyads and the pentad, and the representative orbitals are shown in Figure 4. The HOMO for all of the studied polyads was fully localized on the Ru(CO)*Pc*, while the LUMO was located on the free-base porphyrin macrocycle. In agreement with the electrochemical results, these results point out that the lowest energy charge transfer state is $H_2P_pIm^{-\bullet}$:Ru(CO)*Pc*$^+$. The gas-phase HOMO−LUMO gap for the dyads was ∼2.06 eV, which was slightly larger than that of the pentad, 1.90 eV.

dx.doi.org/10.1021/ic202574q | *Inorg. Chem.* 2012, 51, 3656−3665

Using the electrochemical, computational, and emission data, the free energies of charge separation (ΔG_{CS}) were calculated using eq 1 by Weller's approach[28]

$$-\Delta G_{CS} = \Delta E_{0-0} - e(E_{ox} - E_{red}) + \Delta G_S \quad (1)$$

where ΔE_{0-0} is the energy of the lowest excited state of the fluorophore (1.90 eV for H_2P and 1.85 eV for Ru(CO)*Pc*), E_{ox} and E_{red} represent, respectively, the first oxidation of the donor and first reduction of the acceptor, $\Delta G_S = -e^2/(4\pi\varepsilon_0\varepsilon_R R_{Ct\text{-}Ct})$, and ε_0 and ε_R refer to the vacuum permittivity and dielectric constant of the solvent. The lowest energy charge-separated state, $H_2P_pIm^{-\bullet}$:Ru(CO)$Pc^{+\bullet}$, is only 0.13 eV lower than the lowest singlet excited state Ru(CO)Pc^{S1} if the Coulombic term, ΔG_S, is neglected. Accounting for the Coulombic interaction makes photoinduced electron transfer an endothermic reaction in nonpolar and moderately polar solvents but slightly exothermic in polar media.

Excited Energy Transfer: Theoretical and Experimental Considerations. Since photoinduced electron transfer is not a likely mechanism based on energetic considerations, photoinduced energy transfer as a quenching mechanism was considered. Such an energy transfer between excited donor to an acceptor could be explained via either Dexter's exchange mechanism or Förster's dipole−dipole mechanism.[29] The former mechanism is based on double-electron exchange involving one electron from the LUMO of the excited donor to the empty LUMO of the acceptor with a simultaneous transfer of another electron from the HOMO of the acceptor to the half-filled HOMO of the donor.[29c] The rate constant is given by eq 2

$$k_D = 4\pi^2 H^2 J_D/h \quad (2)$$

where h is Plank's constant, H is the electronic exchange parameter, and J_D is the Dexter spectral overlap integral.[29c] The frontier orbitals from the B3LYP studies and the large separation between the donor and the acceptor entities (Figure 4) in conjunction with the spectroscopic studies reveal that such electronic interactions are almost nonexistent. Therefore, Förster's-type energy transfer mechanism is considered.

According to the Förster mechanism,[29b] the rate of excitation transfer, $k_{Förster}$, is given by eq 3

$$k_{Förster} = [8.8 \times 10^{-25}\kappa^2\Phi_D J_{Förster}]/[\eta^4\tau_D R^6] \quad (3)$$

where η is the solvent refractive index, Φ_D and τ_D are the fluorescence quantum yield (= 0.12) and fluorescence lifetime of the isolated donor (free-base porphyrin), $J_{Förster}$ is Forster's overlap integral representing the emission of the donor and absorption of the acceptor Ru(CO)*Pc*, and R is the donor−acceptor center-to-center distance. The τ_D values measured using the strobe technique were found to be 11.50, 9.95, and 9.45 ns, respectively, for the *o*-, *m*-, and *p*-imidazole-derivatived free-base porphyrins. In eq 3, κ^2 is the orientation factor as described in eq 4, often playing a key role in determining the efficiency of excitation energy transfer

$$\kappa^2 = [\cos\nu - 3\cos\alpha\cos\beta]^2 \quad (4)$$

where α and β are the angles made by the transition dipoles of the donor and acceptor entities with the line joining the centers of the transitions and ν is the angle between the two transition dipoles. The transition dipoles of tetrapyrroles is known to lie along a line joining two opposing pyrrole nitrogens.[30] The values of κ^2 evaluated based on computed optimum geometries of compounds are given in Table 1. It worth mentioning here that although the donor−acceptor are linked, there is enough flexibility in the dyads to deviate significantly from the low-energy-optimized structure. Under the condition of random dipole orientations one could assign a value of 2/3 for κ^2. Therefore, one can expect the actual values of κ^2 to be between the calculated ones and 2/3. The κ^2 value estimated for the meta derivative is close to this value. The κ^2 value estimated for the ortho derivative is much larger than 2/3 and is expected to be overestimated, whereas for the para derivative it is much lower than 2/3 and is expected to be underestimated.

Table 1. Förster Distance and Estimated ($k_{Förster}$) and Experimentally Determined (k_{ENT}) Rates of Energy Transfer for the Dyads and Pentad Formed by Coordination of Imidazole Appended Free-Base Porphyrin to Ru(CO) Phthalocyanine in Toluene

polyads[a]	κ^2	R_o (Å)	$k_{Förster}$ (s^{-1})[b]	k_{ENT} (s^{-1})[c]
H_2P_oIm:Ru(CO)*Pc*	3.25	26.20	5.18×10^{11}	1.25×10^{11}
H_2P_mIm:Ru(CO)*Pc*	0.82	26.19	1.24×10^{11}	7.14×10^{10}
H_2P_pIm:Ru(CO)*Pc*	0.12	26.18	1.56×10^{10}	3.22×10^{10}
H_2P_p(Im:Ru(CO)*Pc*)$_4$	0.14	26.43	1.82×10^{10}	3.71×10^{10}

[a]See Chart 1 for structures of different donor and acceptor entities. [b]Estimated according to eqs 3−5. Error = ±10%. [c]Determined from the pump−probe technique.

The spectral overlap integral, $J_{Förster}$, representing the emission of the donor and absorption of the acceptor is given by eq 5

$$J_{Förster} = F_D(\lambda)\varepsilon_A(\lambda)\lambda^4\,d\lambda \quad (5)$$

where $F_D(\lambda)$ is the fluorescence intensity of the donor with total intensity normalized to unity and $\varepsilon_A(\lambda)$ is the molar extinction coefficient of the acceptor expressed in units of M^{-1} cm^{-1} and λ in nanometers. Figure 5 shows the spectral overlap of the H_2PIm emission (donor) and Ru(CO)*Pc* absorption (acceptor) for the dyads. The $J_{Förster}$ values calculated based on eq 5 were in the range of $2.6-3.98 \times 10^{-14}$ M^{-1} cm^3 for the investigated compounds. However, care must be exercised while using such results since the currently used donor and acceptor entities are known to have degenerate dipole

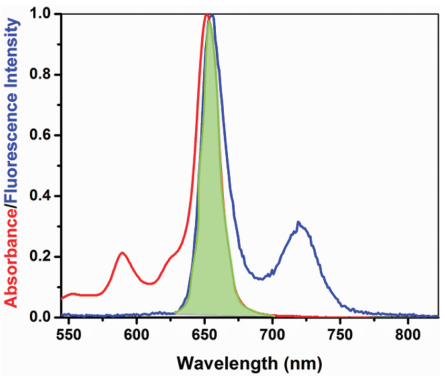

Figure 5. Spectral overlap (shaded area) for H_2PIm emission (donor) and Ru(CO)*Pc* absorption (acceptor) in toluene.

dx.doi.org/10.1021/ic202574q | *Inorg. Chem.* 2012, 51, 3656−3665

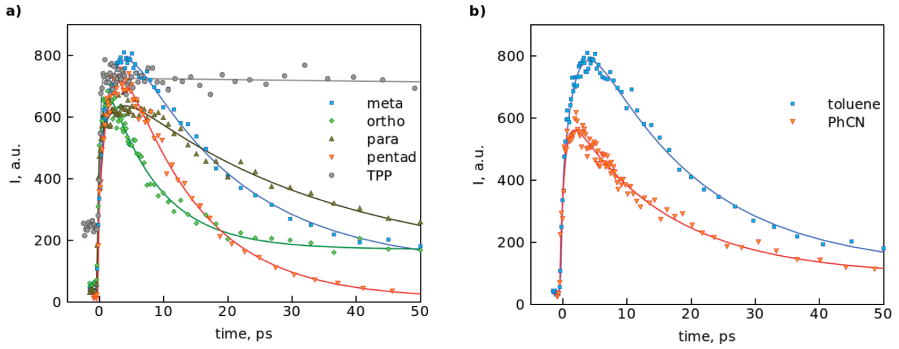

Figure 6. Emission decay curves for all compounds in toluene (a) and for H_2P_mIm:Ru(CO)*Pc* in toluene and PhCN (b).

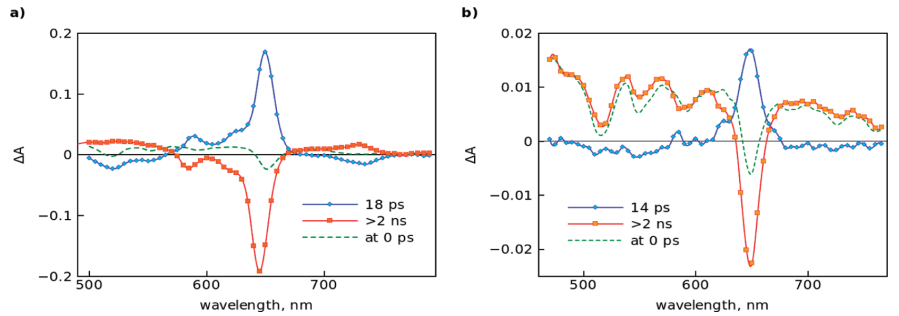

Figure 7. Transient absorption component and time-resolved (at zero delay) spectra (pump probe) of H_2P_mIm:Ru(CO)*Pc* in (a) toluene and (b) benzonitrile.

moments,[30] creating additional complications in estimating orientation-dependent rates, although such calculations serve as a very good tool to predict the experimental rate parameters (vide infra).

Equation 3 can be further simplified in terms of Förster distance, R_o, where one-half the donor molecules decay by energy transfer and one-half decay by the usual radiative and nonradiative mechanisms.[29a]

$$k_{\text{Förster}} = 1/\tau_D(R_o/R)^6 \quad (6)$$

The R_o and $k_{\text{Förster}}$ values estimated using the parameters described in eqs 2–6 were found to be about 26 Å and 10^{10}–10^{11} s^{-1}, predicting ultrafast energy transfer (Table 1). As explained in subsequent paragraphs, the rate of energy transfer measured using pump–probe and up-conversion techniques agrees well with predictions.

Up-Conversion and Pump–Probe Spectral Studies. Up-conversion measurements were carried out in a 1 mm rotating cuvette in both toluene and benzonitrile (PhCN) solvents. The excitation wavelength was set to 420 nm, while fluorescence decay was monitored at 720 nm, corresponding to porphyrin absorption and emission, respectively. Decays were measured in the time range of 200 ps, and the typical time resolution of the instrument was ~0.2 ps. Decay curves for the samples in toluene are shown in Figure 6a. The decay time constants are approximately the same in both solvents as presented by the example of the H_2P_mIm:Ru(CO)*Pc* dyad in Figure 6b (emission decays for all dyads and pentad in benzonitrile can be found in Supporting Information Figure S2). This suggests energy transfer as the main porphyrin fluorescence quenching mechanism.

The pump–probe measurements were also carried out in a 1 mm rotating cuvette. The excitation wavelength was 420 nm, and measurements were carried out in the wavelength range of 520–790 nm. The time resolution of the instrument was ~0.2 ps. Excitation was reduced to 20% of the maximum to ensure that no more than one chromophore in the dyads is excited at a time.

The results of the biexponential fit of pump–probe measurements of the H_2P_mIm:Ru(CO)*Pc* dyad in toluene are presented in Figure 7a. The time-resolved transient absorption spectrum right after excitation (at 0 ps) is essentially the spectrum of the porphyrin singlet excited state with characteristic holes at 515, 550, and 585 nm due to the Q-bands bleaching. This is expected since porphyrin absorption is much higher than that of phthalocyanine at the excitation wavelength, 420 nm. On the contrary, the spectrum of the longest lived component (>2 ns) is characteristic of the phthalocyanine excited state with clear bleaching of the phthalocyanine Q-bands at 585 and 645 nm and no signs of the porphyrin intermediates. Therefore, the component with a time constant of ~18 ps had straightforward interpretation, that is, quenching of the porphyrin singlet excited state by energy transfer to Ru(CO)*Pc*, the process in which the singlet excited state of porphyrin disappears and Ru(CO)*Pc* becomes involved into the excitation relaxation (bleaching of the Ru(CO)*Pc* Q-band). This is also in agreement with fluorescence decay measurements showing relaxation of the porphyrin singlet excited state with essentially the same time constant. However, the band at

dx.doi.org/10.1021/ic202574q | *Inorg. Chem.* 2012, 51, 3656–3665

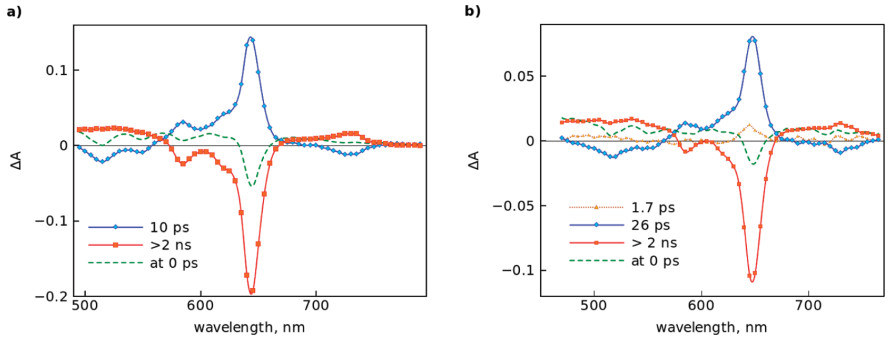

Figure 8. Transient absorption component and time-resolved (at zero delay) spectra (pump probe) of $H_2P_p(Im:Ru(CO)Pc)_4$ pentad in toluene (a) and benzonitrile (b).

720−730 nm is a characteristic feature of the Ru(CO)*Pc* triplet state, and it is formed with virtually the same time constant as the porphyrin singlet state decays. As stated earlier, although the energy transfer should take place between singlet states of H_2P_mIm and Ru(CO)*Pc*, $*H_2P_mIm^{1S}$:Ru(CO)*Pc* → H_2P_mIm:$*Ru(CO)Pc^{1S}$, the intersystem crossing is rather fast for Ru(CO)*Pc*, in the range of 3−5 ps, i.e., faster than the energy transfer; thus, the singlet excited state of Ru(CO)*Pc* is not observed as it is converted almost instantly to the triplet state. This observation is fully in agreement with the steady-state fluorescence observations.

The results of the biexponential fit of pump−probe measurements of the H_2P_mIm:Ru(CO)*Pc* dyad in benzonitrile are presented in Figure 7b. Right after excitation (at 0 ps) the transient absorption spectrum revealed a clear feature of the H_2P_mIm singlet excited state, as can be expected, although some bleaching of the Ru(CO)*Pc* Q-band was seen at 650 nm. The following process with a time constant of 14 ps resulted in gradual enhancement of the Ru(CO)*Pc* Q-band bleaching and formation of the transient state with a differential spectrum presented by the longest lived component. The spectrum had clear features of ground state bleaching of both chromophores, H_2P_mIm and Ru(CO)*Pc*, indicating that H_2P_mIm does not return to the ground state on completion of the 14 ps process, which is in sharp contrast to the excitation relaxation in toluene. There is another clear difference between the long-lived states in toluene and benzonitrile in the red part of the spectrum, 670−780 nm. In toluene a relatively narrow band is seen around 720−730 nm, whereas in benzonitrile there was a strong broad absorption in the whole range 690−780 nm, which is indicative for Ru(CO)*Pc* cation radical.[24] At the same time, the 14 ps component indicates an increase in transient absorption around 570 nm, which is typical for a porphyrin transition from the singlet excited state to an anion radical.[11e] As suggested by the free-energy calculations, the electron transfer from $*Ru(CO)Pc^1$ to H_2P_mIm is possible in polar benzonitrile and may compete with the intersystem crossing process.

The other two dyads, H_2P_pIm:Ru(CO)*Pc* and H_2P_oIm:Ru(CO)*Pc*, revealed spectral features similar to the H_2P_mIm:Ru(CO)*Pc* dyad (see Supporting Information Figures S3 and S4 for spectral details). For the H_2P_pIm:Ru(CO)*Pc* dyad, a biexponential fit was sufficient for toluene, but for benzonitrile data, a three-exponential fit was needed. The emission decay measurements at 720 nm suggested that $*H_2P_pIm^1$ decayed with a time constant of 30 ps in toluene and 28 ps in benzonitrile, respectively. For the H_2P_oIm:Ru(CO)*Pc* dyad, a two-exponential fit was sufficient for both solvents. The time constants for the reaction were 6 and 9 ps in toluene and benzonitrile, respectively.

Transient absorption spectra of the $H_2P_p(Im:Ru(CO)Pc)_4$ pentad in toluene and PhCN are presented in Figure 8. A biexponential fit was sufficient for toluene data, but for benzonitrile data three-exponential fit gave the best sigma value. The time constants of the reaction in toluene were 10 and 12 ps from transient absorption and emission decay fits, respectively. The results in PhCN differed from those of the H_2P_pIm:Ru(CO)*Pc* dyad in that the long-lived state (longer than a few hundreds of picoseconds) had almost no features of porphyrin transients (Figures 6b and 8b). It had characteristic triplet state spectral features of RuPc at 730 nm. In this case, a simple model of energy transfer from porphyrin to phthalocyanine with a time constant of 26 ps and following fast intersystem crossing, $*Ru(CO)Pc^S$ → $*Ru(CO)Pc^T$, with a time constant of a few picoseconds was satisfactory. Unlike the dyads, there was relatively a discrepancy between the time constant obtained from transient absorption and emission decay measurements in PhCN, 26 and 11 ps, respectively.

The kinetic parameters of excitation transfer calculated from the up-conversion and pump−probe techniques are listed in Table 1 along with the theoretically estimated values assuming Förster-type energy transfer. It has to be noted that the theoretical estimations were carried out for fixed conformer geometries obtained from the computational modeling. Accounting for the dyad flexibility, the κ^2 values could be overestimated for the ortho dyad and underestimated for the para dyad and pentad. With this in mind, theoretical estimations are in good agreement with the measured rate constant of energy transfer. The results show that the energy transfer rate can be effectively tuned by changing the attachment position of the linker but keeping the overall design of the donor and acceptor units untouched.

The charge transfer was observed only for the dyads in polar solvent, benzonitrile. Unfortunately the time constant for this process cannot be determined from the presented results, since the time limiting step in all cases is the energy transfer, which occurs in the 10−30 ps range depending on the dyad. Further, charge transfer is competing with intersystem crossing, $*Ru(CO)Pc^S$ → $*Ru(CO)Pc^T$; thus, the time constant for this process has to be 1 ps or less in order to give a detectable

dx.doi.org/10.1021/ic202574q | Inorg. Chem. 2012, 51, 3656−3665

population. Alternatively, the charge transfer rate can be obtained by direct excitation of the phthalocyanine chromophore at 655 nm; however, it was not possible with the instrument used. It is also important to note that there was no detectable charge transfer in the pentad. Although this discrepancy is not completely understood, it could be due to some conformational differences in the arrangements of the donor and acceptor in dyad and pentad structures resulting in either a decrease of the rate of the charge transfer or an increase of the rate of intersystem crossing, thus shifting the competition between the two processes in favor of the latter.

The following points emerge from this investigation. (i) There is very good agreement between the theoretically predicted and experimentally determined k_{ENT} values of the dyads with different relative orientations. (ii) The magnitude of k_{ENT} values reveals ultrafast excitation transfer in agreement with the earlier reported H_2P_xIm:MPc (M = Zn or Mg, *x* = ortho, meta, or para) dyads.[23] (iii) The k_{ENT} values are generally high for the H_2P_oIm:Ru(CO)*Pc* that can be easily ascribed to geometry consideration of the close proximity and favorable orientation of the two macrocycles. (iv) The k_{ENT} value for the H_2P_m(Im:Ru(CO)*Pc*)$_4$ pentad was slightly better than that of the H_2P_pIm:Ru(CO)*Pc* dyad, indicating a higher number of acceptor entities increases the rate of energy transfer in these near-orthogonally positioned donor−acceptor systems. (v) In polar solvent, benzonitrile, the energy transfer in dyads is followed by electron transfer from Ru(CO)*Pc* to H_2P_xIm, which is not observed in nonpolar solvent, toluene, because of the slightly higher energy of the charge-separated state in nonpolar media.

CONCLUSIONS

Using the metal−ligand binding approach, stable molecular dyads and pentad featuring free-base porphyrin and ruthenium carbonyl phthalocyanine were synthesized and spectrally characterized. Unlike previous studies involving ZnPc and MgPc,[23] the current Ru(CO)*Pc* yield stable complexes those could be easily isolated and purified by column chromatography. The molecular structure and electronic states were deduced from computational, spectral, and electrochemical studies. Using steady-state and time-resolved transient absorption techniques, photochemical events taking place in these molecular polyads upon excitation of the free-base entity were systematically investigated. Steady-state emission predicted excitation transfer in which the position of imidazole linkage on the free-base porphyrin entity and the number of Ru(CO)*Pc* entities influenced the efficiency of excitation transfer. The kinetics of energy transfer (k_{ENT}), monitored by performing transient absorption measurements using both upconversion and pump−probe techniques and modeled using the Förster-type energy transfer mechanism, revealed a good match between the theoretically estimated and the experimentally measured kinetic results. The excitation transfer product *Ru(CO)Pc^S instantaneously underwent intersystem crossing to populate *Ru(CO)Pc^T prior to returning to the ground state. Interestingly, the dyads in polar benzonitrile revealed subsequent charge transfer from the excited Ru(CO)*Pc* (product of initial energy transfer) to H_2P, resulting in formation of Ru(CO)$Pc^{+\bullet}$−$H_2P^{-\cdot}$. However, such charge transfer interactions were absent in the case of the pentad in benzonitrile, which could be due to different orientation factors promoting the competing (intersystem crossing) photochemical process.

EXPERIMENTAL SECTION

Chemicals. Free-base 2,11,20,29-tetra-*tert*-butyl-phthalocyanine, *o*-dichlorobenzene, and toluene (in sure seal bottles under nitrogen) were from Aldrich Chemicals (Milwaukee, WI). Tetra-*n*-butylammonium perchlorate, $(TBA)ClO_4$, was from Fluka Chemicals. All chromatographic materials and solvents were procured from Fisher Scientific and used as received. Syntheses of 5-[1*H*-Imidazol-1-yl)phenyl]-10,15,20-tritolylporphyrin derivatives, H_2P_xIm (*x* = ortho, meta, or para positions), is given elsewhere.[23]

Synthesis of Carbonyl-2(3),9(10),16(17),23(24)-tetrakis-*tert*-butylphthalocyaninato]Ru(II), Ru(CO)*Pc*.[24] A mixture of tetra-*tert*-butylphthalocyanine (200 mg, 0.26 mmol), $Ru_3(CO)_{12}$ (346 mg, 0.54 mmol), and phenol (13 g) was refluxed at 180−185 °C under argon for 12 h. The reaction mixture was cooled to room temperature, and then it was dissolved 50 mL of ethanol. The resulting solution was dissolved in 200 mL of water and allowed to precipitate. The resulting blue precipitate was filtered, washed with a 4:1 mixture of water and methanol, and dried. The crude was purified by silica gel column chromatography using chloroform as eluent. ^{1}H NMR (400 MHz, $CDCl_3$): 1.90, 1.70, 1.20, (3 s, 36H, $C(CH_3)_3$);), 8.40−7.89, (br m, aromatic 4H), 9.60−8.85, (br m, aromatic 8H). ESI mass in CH_2Cl_2: *m*/*z* calcd, 866.03; found, 866.30 (100) $[M]^+$.

5,10,15,20-Tetrakis-4-(1*H*-imidazol-1-yl)phenylporphyrin, $H_2P_p(Im)_4$. To 200 mL of propionic acid, 5.8 mmol (1.0 g) of 4-(1*H*-imidazol-1-yl)benzaldehyde and 5.8 mmol of pyrrole (452 mL) were added. The solution was refluxed for 6 h, and solvent was removed under reduced pressure. The crude was purified on a basic alumina column chromatography with $CHCl_3$:MeOH (92:8 v/v) as eluent. ^{1}H NMR (400 MHz, $CDCl_3$) (in ppm): δ −2.79 (s, 2H), 7.25 (s, 4H, imidazole *H*), 7.58 (s, 4H, imidazole *H*), 7.78 (d, 8H, phenyl *H*), 8.16 (s, 4H, imidazole *H*), 8.28 (d, 8H, phenyl *H*), 8.82 (br s, 8H, β pyrrole). Mass (APCI mode in CH_2Cl_2): calcd, 879.5; found, 880.4

Synthesis of H_2P_xIm:Ru(CO)*Pc* Dyads. A solution of Ru(CO)*Pc* (20 mg, 0.027 mmol) and H_2P_xIm (26 mg, 0.03 mmol) in chloroform (8 mL) was stirred under inert conditions (Ar) at room temperature and protected from light for 18 h. Solvent was evaporated, and the residue was subjected to a silica gel column using hexane:$CHCl_3$ (40:60 v/v) as eluent. **H_2P_oIm:Ru(CO)*Pc*.** ^{1}H NMR (300 MHz, $CDCl_3$): −2.96 (s, 2H), 1.90, 1.73, 1.22, (3 s, 36H, $C(CH_3)_3$) 2.76 (s, 9H), 5.37 (s, 1H, imidazolium H), 6.21 (br s, 2H, imidazole *H*), 6.75−6.83 (m, 4H, phenyl *Hs* next to imidazole moiety) 7.59−9.58 (br m for porphyrin and phthalocyanine aromatic 32H). ESI mass in CH_2Cl_2: *m*/*z* calcd, 1588.91; found, 1588.60 (100%) $[M]^+$, 1589.21 (81%). **H_2P_mIm:Ru(CO)*Pc*.** ^{1}H NMR (300 MHz, $CDCl_3$): −2.95 (s, 2H), 1.92, 1.73, 1.22, (3 s, 36H, $C(CH_3)_3$) 2.79 (s, 9H), 5.32 (s, 1H, imidazole H), 5.37 (s, 1H, phenyl H next to imidazole ring), 6.18 (br s, 2H, imidazole *H*), 6.76 (m, 3H, phenyl *Hs* next to imidazole ring) 7.54−9.58 (br m for porphyrin and phthalocyanine aromatic 32H). ESI mass in CH_2Cl_2: *m*/*z* calcd, 1588.91; found, 1588.60 (100%) $[M]^+$, 1589.21 (85%). **H_2P_pIm:Ru(CO)*Pc*.** ^{1}H NMR (300 MHz, $CDCl_3$): −2.96 (s, 2H), 1.91, 1.73, 1.21, (3 s, 36H, $C(CH_3)_3$), 2.75 (s, 9H), 5.35 (s, 1H, imidazolium H), 6.18 (br s, 2H, imidazole *H*), 6.80 (dd, 4H, phenyl *Hs* next to imidazole moiety) 7.56−9.58 (br m for porphyrin and phthalocyanine aromatic 32H). ESI mass in CH_2Cl_2: *m*/*z* calcd, 1588.91; found, 1588.60 (100%) $[M]^+$, 1589.21 (85%). Yields were in the order of 50−60%,

H_2P_pIm:(Ru(CO)*Pc*)$_4$ Pentad. A solution of Ru(CO)*Pc* (20 mg, 0.027 mmol) and $H_2P_p(Im)_4$ (5.8 mg, 0.03 mmol) in a mixture of chloroform (7 mL) and MeOH (1 mL) was stirred under inert conditions (Ar) at room temperature and protected from light for 24 h. Solvent was evaporated, and the residue was subjected to a silica gel column using hexane:$CHCl_3$ (20:80 v/v) as eluent. ^{1}H NMR (300 MHz, $CDCl_3$): δ −2.79 (s, 2H), 1.25−1.85, (144H, $C(CH_3)_3$) 5.31 (s, 4H, imidazole *H*), 6.05 (br s, 8H, imidazole *H*), 6.91 (dd, 16H, phenyl *H*), 8.01(br s, 8H, β pyrrole *H*), 9.21−9.58 (br multiplet, 48H, *Pc* aromatic *H*). Yield = 45%. ESI mass revealed fragments of dyad, triad, etc., suggesting lower stability of the molecular ion peak under the experimental conditions.

Instrumentation. The optical absorbance measurements were carried out with a Shimadzu model 2550 double-monochromator

dx.doi.org/10.1021/ic202574q | *Inorg. Chem.* 2012, 51, 3656−3665

UV−vis spectrophotometer. The fluorescence emission was monitored using a Varian Eclipse spectrometer. A right angle detection method was used. ^{1}H NMR studies were carried out on Varian 300 MHz and Varian 400 MHz spectrometers. Tetramethylsilane ($Si(CH_3)_4$) was used as an internal standard. Cyclic voltammograms were recorded on a EG&G PARSTAT electrochemical analyzer using a three-electrode system. A platinum button electrode was used as the working electrode. A platinum wire served as the counter electrode, and a Ag/AgCl electrode was used as the reference electrode. Ferrocene/ferrocenium redox couple was used as an internal standard. All solutions were purged prior to electrochemical and spectral measurements using argon gas. Computational calculations were performed by DFT B3LYP/3-21G(*) methods with the GAUSSIAN 03[26] software package on high-speed PCs. Mass spectra were recorded on a Varian 1200 L Quadrupole MS using APCI mode in dry CH_2Cl_2.

Transient Absorption Measurements.[31] An up-conversion instrument (FOG-100, CDP Corp.) for time-resolved fluorescence was used to detect the fast processes with a time resolution of ∼200 fs. The primary Ti:sapphire generator (TiF-50, CDP Corp.) was pumped by a Nd CW laser (Verdi-6, Coherent Inc.), and a second harmonic (∼420 nm) was used to excite the sample solution in a rotating cuvette. Emission from the sample was collected to a nonlinear crystal (NLC), where it was mixed with the so-called gate pulse, which was the laser fundamental. The signal was measured at a sum frequency of the gate pulse and the selected emission maximum of the sample. The gate pulses were passed through a delay line so that it arrived at NLC at a desired time after sample excitation. On scanning through the delay line the emission decay curve of the sample was detected.

Pump−probe and up-conversion techniques for time-resolved absorption and fluorescence, respectively, were used to detect fast processes with a time resolution shorter than 0.2 ps. The instrument and used data analysis procedure have been described earlier.[31]

■ ASSOCIATED CONTENT

Ⓢ Supporting Information

Comparative emission spectra of the investigated compounds with respect to H_2TPP, emission decays, transient absorption component spectra (pump probe) of H_2P_oIm:Ru(CO)*Pc* and H_2P_pIm:Ru(CO)*Pc* dyads in toluene and benzonitrile, and Cartesian coordinates of the optimized geometries of the dyads and pentad. This material is available free of charge via the Internet at http://pubs.acs.org.

■ AUTHOR INFORMATION

Corresponding Author

*E-mail: nikolai.tkachenko@tut.fi (N.V.T.); Francis.DSouza@unt.edu (F.D.).

Notes

The authors declare no competing financial interest.

■ ACKNOWLEDGMENTS

This work was financially supported by the National Science Foundation (grant nos. 1110942 and EPS-0903806) and matching support from the State of Kansas through Kansas Technology Enterprise Corp. and the Academy of Finland. R.J. is thankful to the McNair Scholar Program and the K-INBRI Scholar Program for support.

■ REFERENCES

(1) (a) In *Photosynthetic Protein Complexes; A Structural Approach*; Frome, P., Ed.; Wiley-VCH Verlag GmbH & Co.: Germany, 2008. (b) In *Photosynthetic Light Harvesting*; Cogdell, R., Mullineaux, C., Eds.; Sprigner: Dordrecht, The Netherlands, 2008. (c) In *Handbook of Photosynthesis*, 2nd ed.; Pessarakli, M., Ed.; CRC Press LLC: Boca Raton, FL, 2005. (d) In *Light-Harvsting Antennas in Photosynthesis*; Green, B. R., Parson, W. W., Eds.; Kluwer: Dordrecht, The Netherlands, 2003.

(2) (a) In *The Photosynthetic Reaction Center*; Deisenhofer, J., Norris, J. R., Eds.; Academic Press: San Diego, 1993. (b) Deisenhofer, J.; Epp, O.; Miki, K.; Huber, R.; Michel, H. *J. Mol. Biol.* **1984**, *180*, 385.

(3) (a) In *Photochemical Conversion and Storage of Solar Energy*; Connolly, J. S., Ed.; Academic: New York, 1981. (b) In *Molecular Level Artificial Photosynthetic Materials*; Meyer, G. J., Ed.; Wiley: New York, 1997. (c) Wasielewski, M. R. *Chem. Rev.* **1992**, *92*, 435. (d) Osuka, A.; Mataga, N.; Okada, T. *Pure Appl. Chem.* **1997**, *69*, 797. (e) Flamigni, L.; Barigelletti, F.; Armaroli, N.; Collin, J.-P.; Dixon, I. M.; Sauvage, J.-P.; Williams, J. A. G. *Coord. Chem. Rev.* **1999**, *190−192*, 671. (f) Diederich, F.; Gomez-Lopez, M. *Chem. Rev. Soc.* **1999**, *28*, 263.

(4) (a) Blanco, M.-J.; Consuelo Jimenez, M.; Chambron, J.-C.; Heitz, V.; Linke, M.; Sauvage, J.-P. *Chem. Rev. Soc.* **1999**, *28*, 293. (b) Balzani, V.; Credi, A.; Venturi, M. *ChemSusChem* **2008**, *1*, 26.

(5) (a) Bixon, M.; Fajer, J.; Feher, G.; Freed, J. H.; Gamliel, D.; Hoff, A. J.; Levanon, H.; Möbius, K.; Nechushtai, R.; Norris, J. R.; Scherz, A.; Sessler, J. L.; Stehlik, D. *Isr. J. Chem.* **1992**, *32*, 449. (b) Lewis, F. D.; Letsinger, R. L.; Wasielewski, M. R. *Acc. Chem. Res.* **2001**, *34*, 159.

(6) (a) Gust, D.; Moore, T. A.; Moore, A. L. *Acc. Chem. Res.* **1993**, *26*, 198. (b) Gust, D.; Moore, T. A. In *The Porphyrin Handbook*; Kadish, K. M., Smith, K., Guilard, R., Eds.; Academic Press: San Diego, 2000; Vol. *8*, pp 153−190.

(7) (a) Fukuzumi, S.; Guldi, D. M. In *Electron Transfer in Chemistry*; Balzani, V., Ed.; Wiley-VCH: Weinheim, 2001; Vol. *2*, pp 270−337. (b) Fukuzumi, S. In *The Porphyrin Handbook*; Kadish, K. M., Smith, K., Guilard, R., Eds.; Academic Press: San Diego, 2000; Vol. *8*, pp 115−151. (c) Fukuzumi, S. *Phys. Chem. Chem. Phys.* **2008**, *10*, 2283.

(8) (a) Sakata, Y.; Imahori, H.; Tsue, H.; Higashida, S.; Akiyama, T.; Yoshizawa, E.; Aoki, M.; Yamada, K.; Hagiwara, K.; Taniguchi, S.; Okada, T. *Pure Appl. Chem.* **1997**, *69*, 1951. (b) Imahori, H.; Sakata, Y. *Eur. J. Org. Chem.* **1999**, 2445. (c) Imahori, H.; Tamaki, K.; Araki, Y.; Sekiguchi, Y.; Ito, O.; Sakata, Y.; Fukuzumi, S. *J. Am. Chem. Soc.* **2002**, *124*, 5165. (d) Umeyama, T.; Imahori, H. *Energy Environ. Sci.* **2008**, *1*, 120.

(9) (a) Guldi, D. M. *Chem. Commun.* **2000**, 321. (b) Guldi, D. M. *Chem. Soc. Rev.* **2002**, *31*, 22. (c) Sgobba, V.; Guldi, D. M. *Chem. Soc. Rev.* **2009**, *38*, 165. (d) Mateo-Alonso, A.; Guldi, D. M.; Paolucci, F.; Prato, M. *Angew. Chem., Int. Ed.* **2007**, *46*, 8120. (e) Guldi, D. M. *Phys. Chem. Chem. Phys.* **2007**, *9*, 1400. (f) Sanchez, L.; Nazario, M.; Guldi, D. M. *Angew. Chem., Int. Ed.* **2005**, *44*, 5374.

(10) Sessler, J. S.; Wang, B.; Springs, S. L.; Brown, C. T. In *Comprehensive Supramolecular Chemistry*; Atwood, J. L., Davies, J. E. D., MacNicol, D. D., Vögtle, F., Eds.; Pergamon: New York, 1996; Chapter 9.

(11) (a) El-Khouly, M. E.; Ito, O.; Smith, P. M.; D'Souza., F. *Photochem. Photobiol. C* **2004**, *5*, 79. (b) Chitta, R.; D'Souza, F. *J. Mater. Chem.* **2008**, *18*, 1440. (c) D'Souza, F.; Ito, O. *Chem. Commun.* **2009**, 4913. (d) D'Souza, F.; Ito, O *Chem. Soc. Rev.* **2012**, *41*, 86.

(12) (a) In *Introduction of Molecular Electronics*; Petty, M. C., Bryce, M. R., Bloor, D., Eds.; Oxford University Press: New York, 1995. (b) Molecular Electronics: Science and Technology *Ann. N.Y. Acad. Sci.* **1998**, 852. (c) In *Molecular Switches*; Feringa, B. L., Ed.; Wiley-VCH GmbH: Weinheim, 2001. (d) Gust, D.; Moore, T. A.; Moore, A. L. *Chem. Commun.* **2006**, 1169. (e) Balzani, V.; Credi, A.; Venturi, M. In *Organic Nanostructures*; Atwood, J. L., Steed, J. W., Eds.; 2008, pp 1−31. (f) Tour, J. M. *Molecular Electronics; Commercial Insights, Chemistry, Devices, Architectures and Programming*; World Scientific: River Edge, NJ, 2003.

(13) (a) Imahori, H. *J. Phys. Chem. B* **2004**, *108*, 6130. (b) Li, X.; Sinks, L. E.; Rybtchinski, B.; Wasielewski, M. R. *J. Am. Chem. Soc.* **2004**, *126*, 10810. (c) Giribabu, L.; Kumar, A.; Neeraja, V.; Maiya, B. G. *Angew. Chem., Int. Ed. Engl.* **2001**, *40*, 3621. (d) Aratani, N.; Cho, H. S.; Ahn, T. K.; Cho, S.; Kim, D.; Sumi, H.; Osuka, A. *J. Am. Chem. Soc.* **2003**, *125*, 9668. (e) Shinmori, H.; Ahn, T. K.; Cho, H. S.; Kim, D.; Yoshida, N.; Osuka, A. *Angew. Chem., Int. Ed. Engl.* **2003**, *42*, 2754. (f) Choi, M.-S.; Aida, T.; Yamazaki, T.; Yamazaki, I. *Chem.—Eur. J.* **2002**, *8*, 2667. (g) Choi, M.-S.; Aida, T.; Luo, H.; Araki, Y.; Ito, O.

Angew. Chem., Int. Ed. **2003**, *42*, 4060. (h) Luo, C.; Guldi, D. M.; Imahori, H.; Tamaki, K.; Sakata, Y. *J. Am. Chem. Soc.* **2000**, *122*, 6535. (i) Lazarides, T.; Charalambidis, G.; Vuillamy, A.; Reglier, M.; Klontzas, E.; Froudakis, G.; Kuhri, S.; Guldi, D. M.; Coutsolelos, A. *Inorg. Chem.* **2011**, *50*, 8926.

(14) (a) Seth, J.; Palaniappna, V.; Wagner, R. W.; Johnson, T. E.; Lindsey, J. S.; Holten, D.; Bocian, D. F. *J. Am. Chem. Soc.* **1996**, *118*, 11194. (b) Hsiao, J.-S.; Krueger, B. J.; Wagner, R. W.; Johnson, T. E.; Delaney, J. K.; Mauzerall, D. C.; Fleming, G. R.; Lindsey, J. S.; Bocian, D. F.; Donohoe, R. J. *J. Am. Chem. Soc.* **1996**, *118*, 11181. (c) Seth, J.; Palaniappan, V.; Johnson, T. E.; Prathapan, S.; Lindsey, J. S.; Bocian, D. F. *J. Am. Chem. Soc.* **1994**, *116*, 10578. (d) Bothner-By, A. A.; Dodok, J.; Johnson, T. E.; Delaney, J. K.; Lindsey, J. S. *J. Phys. Chem.* **1996**, *100*, 17551. (e) Wagner, R. W.; Johnson, T. E.; Lindsey, J. S. *J. Am. Chem. Soc.* **1996**, *118*, 11166. (f) Strachan, J. P.; Gentemann, S.; Seth, J.; Kalsback, W. A.; Lindsey, J. S.; Holten, D.; Bocian, D. F. *J. Am. Chem. Soc.* **1997**, *119*, 11191. (g) Li, F.; Gentemann, S.; Kalsbeck, W. A; Seth, J.; Lindsey, J. S.; Holten, D.; Bocian, D. F. *J. Mater. Chem.* **1997**, *7*, 1245. (h) Li, J.; Ambroise, A.; Yang, S. I.; Diers, J. R.; Seth, J.; Wack, C. R.; Bocian, D. F.; Holten, D.; Lindsey, J. S. *J. Am. Chem. Soc.* **1999**, *121*, 8927.

(15) (a) Sessler, J. L.; Magda, D. J.; Harriman, A. *J. Am. Chem. Soc.* **1995**, *117*, 704. (b) Kral, V.; Springs, S. L.; Sessler, J. L. *J. Am. Chem. Soc.* **1995**, *117*, 8881. (c) Springs, S. L.; Gosztola, D.; Wasielewski, M. R.; Kral, V.; Andrievsky, A.; Sessler, J. L. *J. Am. Chem. Soc.* **1999**, *121*, 2281.

(16) (a) D'Souza, F.; Smith, P. M.; Zandler, M. E.; McCarty, A. L.; Itou, M.; Araki, Y.; Ito, O. *J. Am. Chem. Soc.* **2004**, *126*, 7898. (b) D'Souza, F.; Gadde, S.; Islam, D. J. S.; Wijesinghe, C. A.; Schumacher, A. L.; Zandler, M. E.; Araki, Y.; Ito, O. *J. Phys. Chem. A* **2007**, *111*, 8552. (c) Maligaspe, E.; Tkachenko, N. V.; Subbaiyan, N. K.; Chitta, R.; Zandler, M. E.; Lemmetyinen, H.; D'Souza, F. *J. Phys. Chem. A* **2009**, *113*, 8478.

(17) Webber, S. E. *Chem. Rev.* **1990**, *90*, 1469.

(18) Frechet, J. M. *J. Polym. Sci., Part A: Polym. Chem.* **2003**, *41*, 3713.

(19) (a) Takahashi, R.; Kobuke, Y. *J. Am. Chem. Soc.* **2003**, *125*, 2372. (b) Haycock, R. A.; Hunter, C. A.; James, D. A.; Michelsen, U.; Sutton, L. R. *Org. Lett.* **2000**, *2*, 2435. (c) van der Boom, T.; Hayes, R. T.; Zhao, Y.; Bushard, P. J.; Weiss, E. A.; Wasielewski, M. R. *J. Am. Chem. Soc.* **2002**, *124*, 9582. (d) Chen, X.; Drain, C. M. *Encycl. Nanosci. Nanotechnol* **2004**, *9*, 593. (e) Kuramochi, Y.; Satake, A.; Itou, M.; Ogawa, K.; Araki, Y.; Ito, O.; Kobuke, Y. *Chem.—Eur. J.* **2008**, *14*, 2827. (f) Uyar, Z.; Satake, A.; Kobuke, Y.; Hirota, S. *Tetrahedron Lett.* **2008**, *49*, 5484. (g) Kuramochi, Y.; Sandanayaka, A. S. D.; Satake, A.; Araki, Y.; Ogawa, K.; Ito, O.; Kobuke, Y. *Chem.—Eur. J.* **2009**, *15*, 2317.

(20) (a) Smith, K. M. *Porphyrins and Metalloporphyrins*; Elsevier: Amsterdam, 1972. (b) In *The Porphyrin Handbook*; Kadish, K. M., Smith, K. M., Guilard, R., Eds.; Academic Press: San Diego, CA, 2000; Vol. *1*–*20*.

(21) (a) In *Phthalocyanine Materials: Structure, Synthesis and Function*; McKeown, N. B., Ed.; Cambridge University Press: Cambridge, 1998. (b) In *Phthalocyanine: Properties and Applications*; Leznoff, C. C., Lever, A. B. P., Eds.; VCH: New York, 1993. (c) Claessens, C. G.; González-Rodríguez, D.; Torres, T. *Chem. Rev.* **2002**, *102*, 835. (d) Howe, L.; Zhang, J. Z. *J. Phys. Chem. A* **1997**, *101*, 3207–3213. (e) Gunaratne, T. C.; Gusev, A. V.; Peng, X.; Rosa, A.; Ricciardi, G.; Baerends, E. J.; Rizzoli, C.; Kenney, M. E.; Rodgers, M. A. J. *J. Phys. Chem. A* **2005**, *109*, 2078.

(22) (a) Kobayashi, N.; Nishiyama, Y.; Ohya, T.; Sato, M. *J. Chem. Soc., Chem. Commun.* **1987**, 390. (b) Tian, H.-J.; Zhou, Q.-F.; Shen, S.-Y.; Xu, H.-J. *J. Photochem. Photobiol. A* **1993**, *72*, 163. (c) Li, J.; Lindsey, J. S. *J. Org. Chem.* **1999**, *64*, 9101. (d) Yang, S. I.; Li, J.; Cho, H. S.; Kim, D.; Bocian, D. F.; Holten, D.; Lindsey, J. S. *J. Mater. Chem.* **2000**, *10*, 283. (e) Ambroise, A.; Wagner, R. W.; Rao, P. D.; Riggs, J. A.; Hascoat, P.; Diers, J. R.; Seth, J.; Lammi, R. K.; Bocian, D. F.; Holten, D.; Lindsey, J. S. *Chem. Mater.* **2001**, *13*, 1023. (f) Miller, M. A.; Lammi, R. K.; Prathapan, S.; Holten, D.; Lindsey, J. S. *J. Org. Chem.* **2000**, *65*, 6634. (g) Sutton, J. M.; Boyle, R. W. *Chem. Commun.* **2001**, 2014. (h) Kameyama, K.; Satake, A.; Kobuke, Y. *Tetrahedron Lett.* **2004**, *45*, 7617. (i) Zhao, Z.; Nyokong., T.; Maree, M. D. *Dalton Trans.* **2005**, 3732. (j) Tome, J. P. C; Pereira, A. M. V. M; Alonso, C. M. A.; Neves, M. G. P. M. S.; Tome, A. C.; Silva, A. M. S.; Cavaleiro, J. A. S.; Martinez-Diaz, M. V.; Torres, T.; Rahman, G. M. A.; Ramey, J.; Guldi, D. M. *Eur. J. Org. Chem.* **2006**, 257. (k) Ito, F.; Ishibashi, Y.; Khan, S. R.; Miyasaka, H.; Kameyama, K.; Morisue, M.; Satake, A.; Ogawa, K.; Kobuke, Y. *J. Phys. Chem. A* **2006**, *110*, 12734. (l) Giribabu, L.; Kumar, C. V.; Reddy, P. D. *Chem. Asian J.* **2007**, *2*, 1574. (m) Tannert, S.; Ermilov, E. A.; Vogel, J. O.; Choi, M. T. M.; Ng, D. K. P.; Röder, B. *J. Phys. Chem. B* **2007**, *111*, 8053. (n) Soares, A. R. M.; Martinez-Diaz, M. V.; Bruckner, A.; Pereira, A. M. V. M; Tome, J. P. C; Alonso, C. M. A.; Faustino, M. A. F.; Neves, M. G. P. M. S.; Tome, A. C.; Silva, A. M. S.; Cavaleiro, J. A. S.; Torres, T.; Guldi, D. M. *Org. Lett.* **2007**, *9*, 1557. (o) Ali, H.; va Lier, J. E. *Tetrahedron Lett.* **2009**, *50*, 1113. (p) Kojima, T.; Honda, T.; Ohkubo, K.; Shiro, M.; Kusukawa, T.; Fukuda, T.; Kobayashi, N.; Fukuzumi, S. *Angew. Chem., Int. Ed.* **2008**, *47*, 6712.

(23) (a) Maligaspe, E.; Kumpulainen, T.; Lemmetyinen, H.; Tkachenko, N. V.; Subbaiyan, N. K.; Zandler, M. E.; D'Souza, F. *J. Phys. Chem. A* **2010**, *114*, 268. (b) Stranius, K.; Jacobs, R.; Maligaspe, E.; Lemmetyinen, H.; Tkachenko, N. V.; Zandler, M. E.; D'Souza, F. *J. Porphyrins Phthalocyanines* **2010**, *14*, 948.

(24) (a) Rodriguez-Morgade, M. S.; Plonska-Brzezinska, M. E.; Athans, A. J.; Carbonell, E.; de Miguel, G.; Guldi, D. M.; Echegoyen, L.; Torres, T. *J. Am. Chem. Soc.* **2009**, *131*, 10484. (b) Jiménez, A. J.; Grimm, B.; Gunderson, V. L.; Vagnini, M. T.; Calderon, S. K.; Rodríguez-Morgade, M. S.; Wasielewski, M R.; Guldi, D. M.; Torres, T. *Chem.—Eur. J.* **2011**, *17*, 5024.

(25) (a) D'Souza, F.; Ito, O. *Coord. Chem. Rev.* **2005**, *249*, 1410. (b) D'Souza, F.; Ito, O. In *Handbook of Organic Electronics and Photonics*; Nalwa, H. R., Ed.; American Scientific Publishers: New York, 2008; Vol. *1*, Chapter 13, pp 485–521. (c) D'Souza, F.; Ito, O In *Multiporphyrin Array: Fundamentals and Applications*; Kim, D., Ed.; Pan Stanford Publishing: Singapore, 2012; Chapter 8, pp 389–437.

(26) Frisch, M. J.; Trucks, G. W.; Schlegel, H. B.; Scuseria, G. E.; Robb, M. A.; Cheeseman, J. R.; Zakrzewski, V. G.; Montgomery, J. A.; Stratmann, R. E.; Burant, J. C.; Dapprich, S.; Millam, J. M.; Daniels, A. D.; Kudin, K. N.; Strain, M. C.; Farkas, O.; Tomasi, J.; Barone, V.; Cossi, M.; Cammi, R.; Mennucci, B.; Pomelli, C.; Adamo, C.; Clifford, S.; Ochterski, J.; Petersson, G. A.; Ayala, P. Y.; Cui, Q.; Morokuma, K.; Malick, D. K.; Rabuck, A. D.; Raghavachari, K.; Foresman, J. B.; Cioslowski, J.; Ortiz, J. V.; Stefanov, B. B.; Liu, G.; Liashenko, A.; Piskorz, P.; Komaromi, I.; Gomperts, R.; Martin, R. L.; Fox, D. J.; Keith, T.; Al-Laham, M. A.; Peng, C. Y.; Nanayakkara, A.; Gonzalez, C.; Challacombe, M.; Gill, P. M. W.; Johnson, B. G.; Chen, W.; Wong, M. W.; Andres, J. L.; Head-Gordon, M.; Replogle, E. S.; Pople, J. A. *Gaussian 03*; Gaussian, Inc.: Pittsburgh, PA, 2003.

(27) Zandler, M. E.; D'Souza, F. *C. R. Chem.* **2006**, *9*, 960.

(28) (a) Rehm, D.; Weller, A. *Isr. J. Chem.* **1970**, *8*, 259. (b) Mataga, N.; Miyasaka, H. In *Electron Transfer*; Jortner, J., Bixon, M., Eds.; John Wiley & Sons: New York, 1999; Part 2, pp 431–496.

(29) (a) In *Principles of Fluorescence Spectroscopy*, 3rd ed.; Lakowicz, J. R., Ed.; Springer: Singapore, 2006. (b) Förster, T. *Ann. Phys.* **1948**, *437*, 55. (c) Dexter, D. L. *J. Chem. Phys.* **1953**, *21*, 836.

(30) (a) Gouterman, M. *J. Mol. Spectrosc.* **1961**, *6*, 138. (b) Gouterman, M. In *Porphyrins*; Dolphin, D., Ed.; Academic Press: New York, 1978; Vol. *3*, Part A, pp 1–165.

(31) (a) Tkachenko, N. V.; Rantala, L.; Tauber, A. Y.; Helaja, J.; Hynninen, P. H.; Lemmetyinen, H. *J. Am. Chem. Soc.* **1999**, *121*, 9378. (b) Vehmanen, V.; Tkachenko, N. V.; Imahori, H.; Fukuzumi, S.; Lemmetyinen, H. *Spectrochim. Acta. A* **2001**, *57*, 2229. (c) Isosomppi, M.; Tkachenko, N. V.; Efimov, A.; Lemmetyinen, H. *J. Phys. Chem. A* **2005**, *109*, 4881.

PUBLICATION III

Sequential Photoinduced Energy and Electron Transfer Directed Improved Performance of the Supramolecular Solar Cell of a Zinc Porphyrin-Zinc Phthalocyanine Conjugate Modified TiO_2 Surface

Chandra B. KC, Kati Stranius, Preston D'Souza, Navaneetha K. Subbaiyan, Helge Lemmetyinen, Nikolai V. Tkachenko and Francis D'Souza

The Journal of Physical Chemistry C

THE JOURNAL OF PHYSICAL CHEMISTRY C

Article

pubs.acs.org/JPCC

Sequential Photoinduced Energy and Electron Transfer Directed Improved Performance of the Supramolecular Solar Cell of a Zinc Porphyrin–Zinc Phthalocyanine Conjugate Modified TiO_2 Surface

Chandra B. KC,[†] Kati Stranius,[‡] Preston D'Souza,[†] Navaneetha K. Subbaiyan,[†] Helge Lemmetyinen,[‡] Nikolai V. Tkachenko,*[,‡] and Francis D'Souza*[,†]

[†]Department of Chemistry, University of North Texas, 1155 Union Circle, #305070, Denton, Texas 76203-5017, United States

[‡]Department of Chemistry and Bioengineering, Tampere University of Technology, P.O. Box 541, 33101 Tampere, Finland

Supporting Information

ABSTRACT: Improved performance of a photosynthetic antenna–reaction center mimicking supramolecular solar cell is demonstrated. Toward this, porphyrin–phthalocyanine conjugates connected by amide linkers, as wide-band capturing solar energy harvesting materials, have been newly synthesized and characterized. Efficient singlet–singlet energy transfer from the zinc or free-base porphyrin to phthalocyanine is evidenced from steady-state emission and transient absorption studies in nonpolar and polar solvents. Further, the dyad was immobilized via axial coordination of zinc porphyrin of the dyad on semiconducting TiO_2 surface modified with axial coordinating ligand functionality, phenylimidazole. Photoelectrochemical studies revealed improved performance of this cell compared to either zinc porphyrin or zinc phthalocyanine only modified electrodes under similar experimental conditions. Transient absorption studies performed on the dyad immobilized on glass/TiO_2 surface suggested that upon excitation of the axially coordinated zinc porphyrin of the dyad singlet–singlet energy transfer to zinc phthalocyanine occurs within 0.2 ps instead of a competing charge injection reaction from the singlet excited zinc porphyrin to TiO_2. Further, sequential photoinduced electron transfer from the newly formed singlet excited zinc phthalocyanine to zinc porphyrin producing $ZnP^{\bullet-}$–$ZnPc^{\bullet+}$ with a 2 ps time constant and followed by electron injection from the $ZnP^{\bullet-}$ to TiO_2 within 30 ps has been proposed as a mechanism of photocurrent generation in the biomimetic supramolecular photocell.

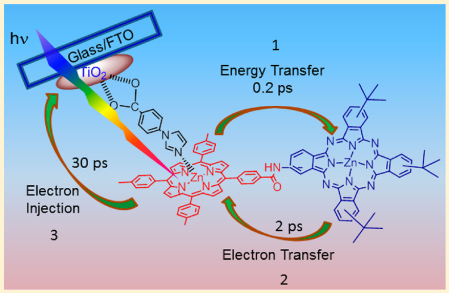

INTRODUCTION

Photoinduced energy and electron transfer are key processes of photosynthesis[1,2] and have attracted significant scientific attention in order to prepare artificial photosynthetic systems, molecular logic switches and gates, wires for photonic systems, and energy harvesting photovoltaic devices, to name a few of their diverse applications.[3−14] The presence of porphyrins in natural photosynthetic systems has assured their dominance as electron donors in model compounds.[15] However, phthalocyanines are increasing their presence in such systems due to the special features they display, e.g., enhanced absorptive cross section at wavelengths corresponding to maxima of solar spectrum including near-IR, relatively easier oxidation, higher fluorescence quantum yield (6–10 times larger), and higher rigidity and photostability compared to porphyrins.[16] Consequently, they have been often used in developing electrocatalysts, infrared sensors, nonlinear optical materials, and photodynamic therapy agents.[14,16]

A combination of porphyrin and phthalocyanine macrocycles offers interesting conjugate structures for various reasons.[17] A noteworthy observation is that these molecules have complementary absorptions in the visible region, and the emission spectra of phthalocyanines do not significantly overlap with those of porphyrins. Consequently, such molecular dyads and polyads (triads, tetrads, pentads, etc.) with good spectral coverage in the blue and red wavelengths are ideal for building light energy harvesting architectures. A literature survey shows that both covalent and noncovalent strategies including host–guest ion-pairing and axial coordination have been effectively used to build such architectures.[17−21] Different types of rigid and flexible spacers have been used to covalently connect the chromophores.[18−20] Ultrafast photoinduced energy transfer from singlet excited porphyrin to phthalocyanine with efficiency depending on the relative orientation and distance between the chromophores have been reported.[17−21] However, usage of such porphyrin–phthalocyanine conjugates to build organic solar cells to exploit their combined spectral features and probe any new mechanism of photocurrent generation that they may offer are limited to only one study involving ion-paired porphyrin–phthalocyanine dimers.[22] In the present study, we

Received: September 7, 2012
Revised: December 11, 2012
Published: December 20, 2012

Scheme 1. Structure of the Newly Synthesized Porphyrin−Phthalocyanine Conjugates in the Present Study To Build Supramolecular Solar Cells

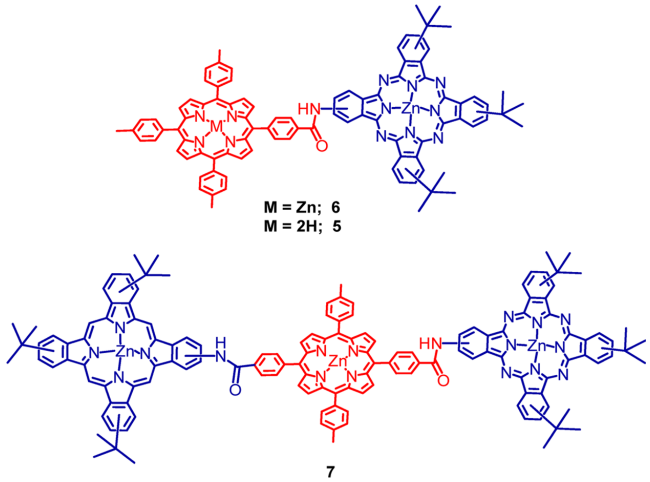

Scheme 2. Synthetic Procedure Adapted for the Porphyrin−Phthalocyanine Dyads and Triad in the Present Study

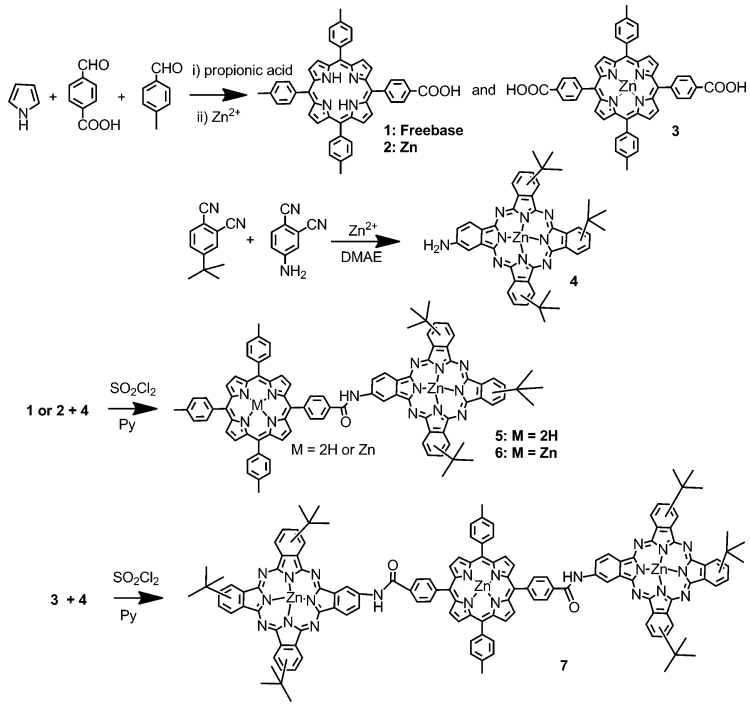

have undertaken a task of building solar cells using covalently linked porphyrin−phthalocyanine conjugates with the help of self-assembled supramolecular methodology for device construction.

Scheme 1 shows the structure of the newly synthesized porphyrin−phthalocyanine dyads and triad conjugates. To ensure solubility of the compounds, tolyl groups on porphyrin and *tert*-butyl groups on the phthalocyanine macrocycle periphery are introduced. We have intentionally used semi-flexible amide bond to connect the two macrocycles. The presence of two phthalocyanine macrocycles in the triad was to envision the effect of increased phthalocyanine rings on the

dx.doi.org/10.1021/jp308923e | *J. Phys. Chem. C* 2013, 117, 763−773

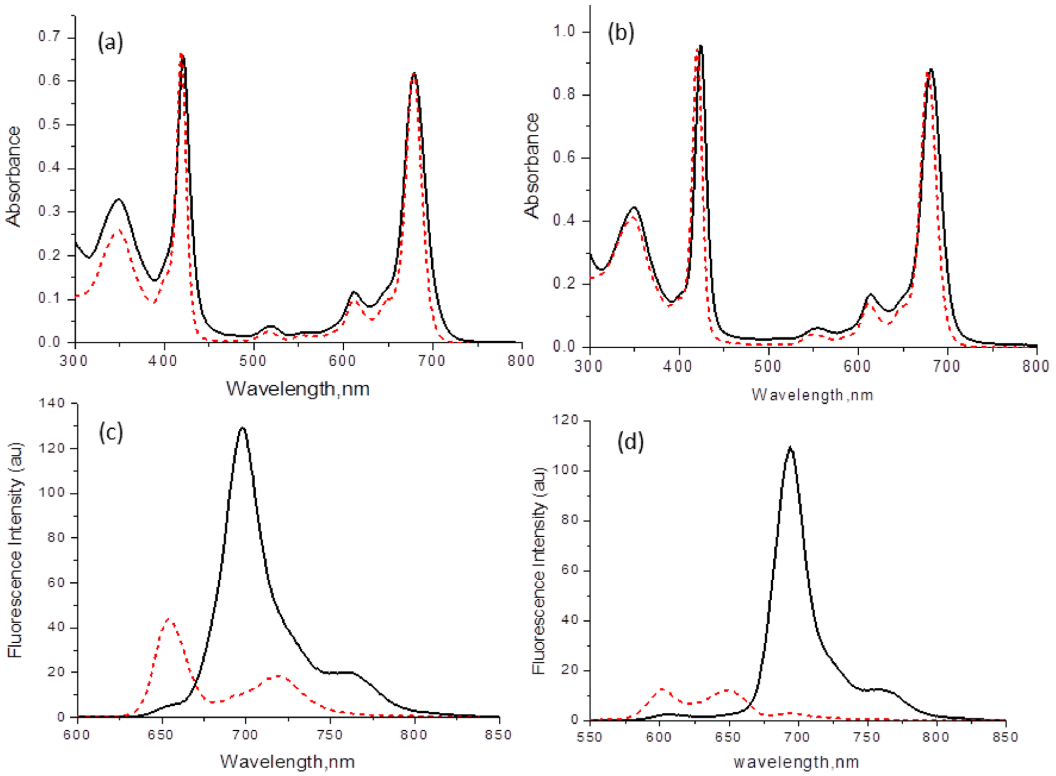

Figure 1. Absorption (a, b) and fluorescence (c, d) of **5** (a, c) and **6** (b, d) (solid lines) and equimolar mixture of free base porphyrin (a, c) or zinc porphyrin (b, d) and ZnPc (dashed line) in DCB at the Soret band excitation of the porphyrin.

efficiency of energy transfer from singlet excited porphyrin to phthalocyanines. As part of the study, first, photoinduced processes originating in these conjugates, relevant to solar cells, were investigated in solution. Next, solar cells were built by using semiconducting TiO_2 nanoparticle surface functionalized with 4-carboxyphenylimidazole. The imidazole entity here served as a coordinating ligand to zinc porphyrin of the conjugates. It has been possible to demonstrate improved performance for the dyad modified electrode compared to either zinc porphyrin or zinc phthalocyanine monomer modified electrodes as a result of the occurrence of sequential photoinduced energy and electron transfer processes.

RESULTS AND DISCUSSION

Syntheses of Porphyrin–Phthalocyanine Conjugates. The synthetic procedure adopted for amide linked dyads and triad is shown in Scheme 2 while details are summarized in the Experimental Section. Briefly, mono- and biscarboxyphenyl meso-substituted porphyrins (**1** and **3**) were synthesized by reacting stoichiometric amounts of 4-formylbenzoic acid, tolualdehyde, and pyrrole in propionic acid followed by chromatographic separation of desired isomers over flash silica gel column. Porphyrin **1** was subsequently converted to its respective zinc derivative **2**. In a separate reaction, *tert*-butylphthalonitrile and 4-aminophthalonitrile were reacted in *N*,*N*-dimethylaminoethanol (DMAE) to obtain amino-functionalized phthalocyanine, **4**. To obtain the porphyrin–phthalocyanine dyads, **5** and **6**, the acid chloride of **1** or **2** was treated with **4** in the presence of pyridine base, followed by chromatographic purification. Similarly, the triad **7** was obtained by the reaction of the acid chloride form of **3** and aminophthalocyanine **4** in the presence of pyridine followed by chromatographic purification. The newly synthesized compounds were fully characterized by ^{1}H NMR, ESI-mass, and spectroscopic methods.

Steady-State Absorption and Emission Studies. Photoinduced energy transfer from singlet excited porphyrin (free base or zinc) to phthalocyanine in both the covalently linked or self-assembled conjugates is a well-known phenomenon.[17−21] Using time-resolved emission and transient techniques, the kinetics of this photochemical process in different solution conditions is well documented. As discussed below, such excitation transfer has also been observed in the newly synthesized porphyrin–phthalocyanine conjugates in both nonpolar and polar solvents.

Figures 1a and 1b show the absorption spectra of the dyads **5** and **6** in *o*-dichlorobenzene (DCB). The presence of porphyrin (Soret band around 420 nm and visible bands in the 500–600 nm range) and phthalocyanine (Soret band around 347 nm and visible bands in the 600–700 nm range) entities was clear from the position and relative intensity of the absorption bands. In order to visualize any intramolecular interactions between these

dx.doi.org/10.1021/jp308923e | J. Phys. Chem. C 2013, 117, 763−773

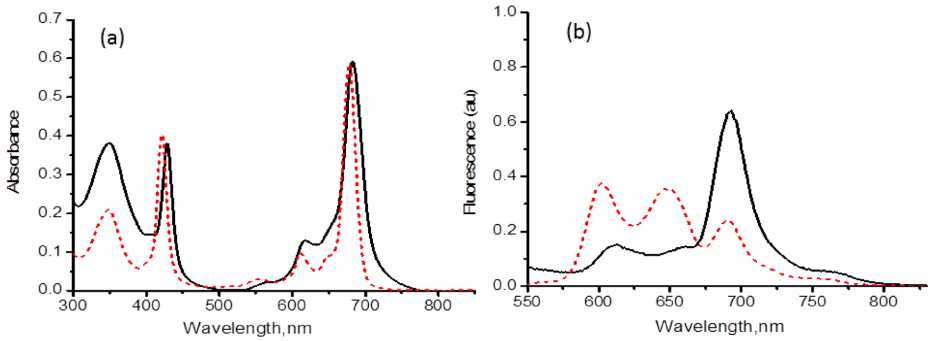

Figure 2. Absorption (a) and fluorescence (b) of **7** (solid lines) and 1:2 mixture of ZnTTP and ZnPc (dashed line) in DCB at the Soret band excitation of the porphyrin.

two chromophores, absorption spectra of an equimolar mixture of tetratolylporphyrin (H_2TTP or ZnTTP) and *tert*-butyl phthalocyaninatozinc (ZnPc) were also recorded. Such spectral revealed a 2−3 nm blue shift of the bands compared to that observed for the covalently linked dyads, suggesting occurrence of weak intramolecular interactions between the two chromophores in **5** and **6**.

Figures 1c and 1d show fluorescence spectra of the dyads and equimolar mixture of the individual components when excited at the Soret band region of porphyrins in DCB. In separate control experiments, the emissions of H_2TTP at 650 and 720 nm, ZnTTP at 600 and 650 nm, and ZnPc at 690 and 755 (sh) nm were confirmed when excited at their respective Soret or one of the visible bands. For the free-base porphyrin−zinc phthalocyanine dyad, **5**, the emission band of free-base porphyrin was found to be quenched over 85% of its original intensity accompanied by a new band at 690 nm corresponding to zinc phthalocyanine. In a control experiment, when a 1:1 mixture of H_2TTP and ZnPc was excited at the Soret band of porphyrin, no emission of ZnPc was observed, indicating occurrence of photoinduced energy transfer in the dyad.[23] Similarly, for zinc porphyrin−zinc phthalocyanine dyad, **6**, excitation of zinc porphyrin revealed diminished intensity accompanied by the ZnPc band at 690 nm. Control experiment using the 1:1 mixture of ZnTTP and ZnPc revealed no such quenching of ZnTTP and occurrence of ZnPc emission (<3% due to direct excitation). The excitation spectrum of these dyads was also recorded by holding the emission monochromator at 690 nm corresponding to emission of ZnPc (see Supporting Information Figure S1). Such measurements revealed peaks corresponding not only to ZnPc but also to H_2TTP or ZnTTP, confirming the occurrence of photoinduced energy transfer in these dyads.[24] Energy transfer efficiency of **6** was also estimated in tetrahydrofuran (THF) using the peak intensity ratio of the porphyrin Soret and the phthalocyanine intense visible band from the optical absorption and excitation data (Figure S8).[24] For dyad **6**, this efficiency was close to that of the ZnTTP quenching efficiency (~80%) in the dyad, suggesting occurrence of efficient energy transfer as the main quenching mechanism.

The spectral behavior of triad **7** is shown in Figure 2. The Soret and visible bands of both chromophores of **7** were found to be red-shifted by 5−8 nm compared to the spectrum obtained by 1:2 mixture of ZnTTP and ZnPc, suggesting stronger intramolecular interactions compared to the earlier discussed dyad, **6**. In addition, broadening of the ZnPc Soret band was also seen. Interestingly, the fluorescence spectrum of **7** revealed quenching of ZnTTP emission at 600 and 650 nm accompanied by rise of ZnPc band at 695 nm due to excitation transfer. The excitation spectrum recorded by holding the emission monochromator to ZnPc emission revealed excitation peaks of both ZnPc and ZnTTP, offering additional evidence for excitation energy transfer (see Figure S2 in the Supporting Information).

Further time-resolved emission and transient spectra using pump−probe techniques were performed to monitor the kinetics and secure additional evidence of excitation transfer in these conjugates.

Time-Resolved Fluorescence Studies. Fluorescence decays of the samples were measured using a time-correlated single photon counting (TCSPC) method in a 1 cm cuvette. The excitation wavelength was 405 nm for all samples, and the time resolution was approximately 60−70 ps. Decay curves for **6** in DCM are shown in Figure 3. The decays were virtually

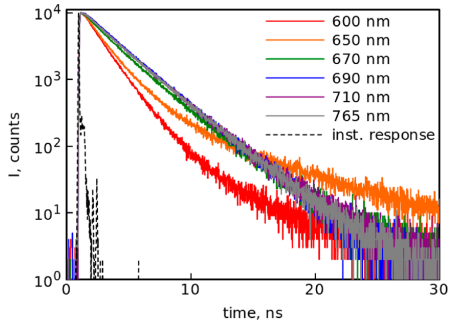

Figure 3. Emission decay curves for the dyad **6** in DCM measured by TCSPC method (60 ps time resolution).

monoexponential with lifetimes of roughly 3 ns at wavelengths specific for the phthalocyanine emission (>700 nm) and somewhat faster at the porphyrin fluorescence region (600−670 nm). Importantly, no fast decay was observed at emission wavelengths of the porphyrin chromophores, which indicates that the energy transfer is faster than the time resolution of the TCSPC instrument, ~70 ps. The latter was confirmed by femtosecond pump−probe studies as discussed below. It has

dx.doi.org/10.1021/jp308923e | J. Phys. Chem. C 2013, 117, 763−773

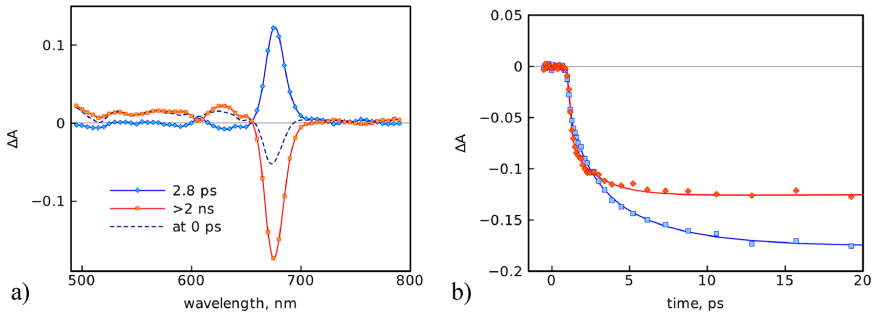

Figure 4. (a) Transient absorption decay component spectra (solid lines with symbols) and time-resolved spectrum at zero delay time (dashed line) of H_2P–ZnPc in THF and (b) transient absorption time profiles at 675 nm of H_2P–ZnPc (blue squares) and ZnP–ZnPc (blue rhombs) in THF and biexponential fits of the bleaching rise (the time constants are 1.3 ± 0.7 and 4.7 ± 2 ps for H_2P–ZnPc and 0.2 ± 0.1 and 1.8 ± 0.8 ps for ZnP–ZnPc).

also to be noted that the excitation at 405 nm is not optimal for energy transfer studies, since it is relatively far from the Soret band maximum, and in most cases the relative amount of directly excited phthalocyanine chromophores can be comparable to that of porphyrins.

Pump–Probe Measurements. All of the pump–probe measurements were carried out in 1 mm rotating cuvette. For this, the samples have to be prepared at relatively high concentration giving absorption close to 1, and it was recognized that in both DCM and benzonitrile the samples were aggregated as witnessed from the ratio of intensities of absorption of porphyrin at Soret band and phthalocyanine at Q-band, which was 0.5 or less. Gradual broadening of the phthalocyanine Q-band and a sharp change in absorption to its "normal" shape by adding a small portion of pyridine (e.g., 1/100 by volume) was observed. Though the pump–probe measurements were carried out in DCM and benzonitrile, the results are not shown here as transient absorption responses were strongly affected by aggregation. To avoid aggregation, a few other solvents were tested, and it was found that at least for the dyad there was no detectable aggregation in tetrahydrofuran (THF). Absorption spectra of the samples in THF prepared for pump–probe measurements are presented in Figure S3 in the Supporting Information. The excitation wavelength was around 420 nm, and the measurements were carried out in the wavelength range 490–790 nm. The time resolution of the instrument was 150–200 ps. Essentially, no change in absorption spectrum of the samples was observed after the measurements, indicating higher photostability.

A reasonable global fit of the transient absorption data was obtained with biexponential model. An example of resulting decay component spectra and the time-resolved spectrum right after excitation (at $t = 0$) is presented in Figure 4a for the H_2TTP–ZnPc dyad. The longest lifetime in pump–probe measurements goes beyond the longest time scale of the measurements, and the spectrum corresponding to this time constant can be identified as the transient absorption spectrum of ZnPc chromophore due to strong bleaching at the phthalocyanine Q-band, ca. 675 nm, and minor spectral features around 600 nm. However, the excitation wavelength of 420 nm should predominantly populate the singlet excited state of the porphyrin chromophore, which is indeed the case since the time-resolved spectrum at zero delay time shows much weaker bleaching in the phthalocyanine Q-band region and distinguishable bleaching at Q-band region of the porphyrin chromophore at 515 nm. Therefore, 2.8 ps component can be attributed to the energy transfer from the primary excited porphyrin to phthalocyanine chromophore.[21] A close examination of the transient absorption decay profiles at the Pc Q-band region reveals some deviation of the bleaching rise from the monoexponential law. The biexponential fit gave much better approximation of the experimental data (presented in Figure 4b) but only 5% improvement in global standard deviation value. Two picoseconds time constant obtained from biexponential fit were 1.3 ± 0.7 and 4.7 ± 2 ps. The non-monoexponential dynamics of the energy transfer can be attributed to coexistence of few conformers of the dyad due to rotational degree of freedom permitted by the linker, which may give rather essential difference in orientations of the dipole moments of the donor and acceptor and also somewhat difference in distance between them.

For the ZnP–ZnPc dyad, the results of the pump–probe study were essentially the same, but the energy transfer was faster. The monoexponential decay gave a time constant associated with the energy transfer of 1.5 ± 0.5 ps while a biexponential decay gave time constants of 0.2 ± 0.1 and 1.8 ± 0.8 ps, respectively. The faster energy transfer can be attributed to the better overlap of porphyrin emission and phthalocyanine absorption spectra in case of ZnP–ZnPc dyad as compared to the H_2P–ZnPc one. It is interesting to note that no charge transfer was observed in solution, though energetically one can expect the photoinduced charge separation to take place at least in ZnP–ZnPc dyad.

Photoelectrochemical Studies. The newly synthesized dyads and triad were used to build photoelectrochemical cells by supramolecular self-assembly method. Here, the semiconducting TiO_2 surface was modified with a ligand capable of axially binding of coordinatively unsaturated metal tetrapyrroles. Although the overall performance of the cells is relatively low compared to some of the well-engineered photocells, this method has given us a unique opportunity to test multimodular solar dyes and their ability to improve the performance of the photocell by adapting photosynthetic light energy harvesting mechanism involving both energy and electron transfer. The low performance is due to the less polar solvent (DCB) used here, needed to hold the self-assembled dye components of the photo cell. Earlier, using this approach, we have been able to demonstrate improved photocurrent generation when the

dx.doi.org/10.1021/jp308923e | J. Phys. Chem. C 2013, 117, 763–773

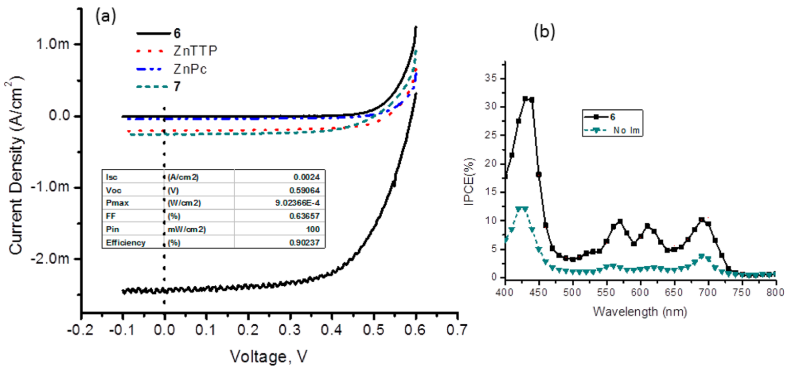

Figure 5. (a) $I-V$ characteristics showing the effect of different sensitizers bound to 4-carboxyphenylimidazole modified TiO_2 electrode surface. The inset table provides the performance of dyad modified photocell. (b) IPCE curves for **6** axially coordinated to 4-carboxyphenylimidazole modified TiO_2 (solid line) and **6** directly adsorbed on TiO_2 surface (dashed line) revealing the effect of axial coordination. The $I-V$ curves were generated in DCB containing I_3^-/I^- (0.5 M/0.03 M) redox mediator using an AM 1.5 simulated light source with a 340 nm UV cutoff filter.

surface was modified with donor$_1$–donor$_2$ (zinc porphyrin covalently linked to ferrocene) type dye as compared with only donor$_1$ dye (zinc porphyrin).[25] In another study, the effect of anion binding to zinc porphyrin–oxoporphyrinogen dyad was demonstrated. That is, upon anion binding to oxoporphyrinogen imino protons of the dyad, improved photocurrent was observed due to redox modulation of the oxoporphyrinogen macrocycle.[26] The present zinc porphyrin–zinc phthalocyanine conjugate has provided us an opportunity to unravel the excitation transfer effect on the overall performance of the solar cell. In the present study, nanocrystalline TiO_2 surface is modified with 4-carboxyphenylimidozole. Here, the carboxyl entity binds to the TiO_2 surface, leaving the imidazole entity to axially coordinate the metal center of the conjugate.[25]

Figure 5a shows the $I-V$ curves[27] for the porphyrin–phthalocyanine conjugate bound to 4-carboxyphenylimidazole modified TiO_2 electrode surface. In agreement with previous report,[25] the performance of the monomeric ZnTPP or ZnPc modified electrodes was minimal; that is, the short circuit currents, I_{SC}, were 0.2 mA/cm^2 for ZnTPP and 0.04 mA/cm^2 for the ZnPc modified electrodes with the open circuit potential, V_{OC}, of around 0.5 V. Notably, although less photocurrent is generated, the performance of ZnTTP was better than that of ZnPc. Interestingly, the performance of the dyad **6** modified electrode was significantly higher; that is, I_{SC} and V_{OC} of 2.45 mA/cm^2 and 0.59 V, respectively, were observed; the I_{SC} was an order of magnitude higher than either ZnTTP or ZnPc modified electrodes with substantial increase in V_{OC}. When the free-base porphyrin–ZnPc dyad **5** was used, both I_{SC} and V_{OC} values were similar to that of ZnPc, indicating that the axial coordination is through ZnPc. However, to explain the difference between the two dyads, one can suggest that ZnP–ZnPc dyad is coordinated predominantly through porphyrin side, which can also be predicted based on slightly higher binding constant of ZnTTP to 1-phenylimidazole compared to ZnPc,[28] in addition to any steric effects caused by bulkier ZnPc. To establish this effect, the following control experiments were performed. First, ZnPc was coordinated to 4-carboxyphenylimidazole modified TiO_2 electrode surface in DCB. After recording the absorption spectrum of the electrode, the electrode was dipped into a solution of ZnTTP in DCB for about 20 min; during this process, it was found that all of the adsorbed ZnPc was replaced by ZnTTP as revealed by the absorption spectrum of the electrode and solution independently. In another control experiment, first, ZnTTP was coordinated to 4-carboxyphenylimidazole modified TiO_2 electrode surface in DCB. When this electrode was dipped into a solution of ZnPc in DCB, no replacement of ZnTPP by ZnPc was observed. These control experiments confirm that the coordination through ZnTTP is stronger than ZnPc of the dyad. Apparently, both the binding constant and steric factors control the mode of binding of the ZnP–ZnPc dyad **6** to 4-carboxyphenylimidazole modified TiO_2 electrode surface. Interestingly, when the triad **7** was used, due to less dye intake (perhaps the oppositely positioned ZnPc rings on ZnP macrocycle hindered strong binding), the performance of the cell was not significant (the photocurrents were an order of magnitude smaller than that of the ZnP–ZnPc modified photocell). Figure 5a inset shows the overall performance of the dyad **6** modified solar cell. An overall light conversion efficiency (η) of 0.9 has been achieved for this cell.

Figure 5b shows the incident photon-to-current conversion (IPCE%)[29] curve for the dyad **6** modified electrode. For comparison purposes, the performance of the dyad directly adsorbed on TiO_2 (without 4-carboxyphenylimidazole connector) is shown. The low performance of this cell signifies the importance of the imidazole ligand as a connector of TiO_2 and the dyad. Importantly, the IPCE curve covered a spectral range of 400–740 nm revealing bands corresponding to both ZnP and ZnPc of the dyad with an IPCE value of 32% at the Soret band position of ZnP. The photocurrent efficiency of the ZnPc region was somewhat less than that of the ZnTTP region, a trend similar to the earlier discussed monomer alone modified electrodes.

In order to further understand the mechanistic details of the photochemical events leading to enhanced photocurrents in the case of ZnTTP–ZnPc dyad modified electrode, additional transient spectral studies on modified surface were performed. For this, dyad **6** was immobilized on 4-carboxyphenylimidazole modified TiO_2 on a glass surface instead of FTO used in photoelectrochemical studies. Figure S4 in the Supporting Information shows the picture of such dyad modified TiO_2 surface along with its absorption spectrum. The peak

dx.doi.org/10.1021/jp308923e | J. Phys. Chem. C 2013, 117, 763–773

absorbance values were well above 2.0, sufficient to perform the photochemical measurements.

The dyad modified TiO_2 surface was excited at 420 nm in a nitrogen atmosphere corresponding to ZnTTP absorption, and the spectra were collected at two wavelength ranges and were fitted globally using the four-exponential model. Figure 6 shows

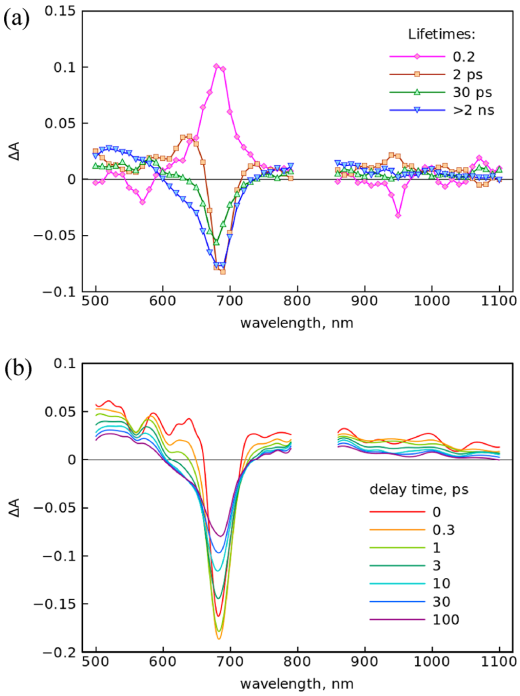

Figure 6. Transient absorption component spectra obtained from global four-exponential fit (a) and time-resolved transient absorption spectra (b) of dyad **6** modified TiO_2 surface film. The lifetimes of the components and delay times for the time-resolved spectra are indicated in the plots.

the transient absorption component spectra as obtained from the fit and time-resolved transient absorption spectra at a few delay times. Within 1 ps after excitation, the bleaching of phthalocyanine Q-band increased, which can result from two reactions, via the energy transfer and charge transfer from the singlet excited porphyrin. In the case of energy transfer one would expect recovery of the porphyrin Q-band at 540 nm, which was not observed. At the same time there were other spectral changes, namely reshaping of the absorption in the near-infrared part (>710 nm) so that a broad band around 850 nm becomes apparent, and decrease in absorption in the 600–660 nm range and formation of a broad band around 500 nm were also visible. All these changes were characteristic for the formation of phthalocyanine cation radical, and they were completed by 3 ps delay time. At this delay the porphyrin was not in the ground state since the Q-band (540 nm) was still bleached. This can be interpreted in favor of charge separation between phthalocyanine and porphyrin to form the $ZnP^{\bullet-}$–$ZnPc^{\bullet+}$ charge separated state. At later delay times of >10 ps, the porphyrin Q-band recovered completely without appreciable changes in the phthalocyanine cation radical spectrum, indicating that $ZnP^{\bullet-}$ donates an electron quickly to TiO_2.

Three lifetimes were obtained from global data fitting, 0.2, 2, and 30 ps, and relaxation was extended to the nanosecond time domain with the spectrum almost identical to that at 100 ps delay time. Thus, a rough attribution of the time constants are: (i) porphyrin–phthalocyanine energy transfer ~0.2 ps, (ii) phthalocyanine–porphyrin electron transfer ~2 ps, and (iii) porphyrin–TiO_2 electron transfer ~30 ps, though the numbers are indications of the time scale of the phenomena but not exact time constants. For ZnP–ZnPc dyad in solution the average time constant for the intramolecular energy transfer was ca. 1.5 ps. The energy transfer is much faster for the same dyads assembled on TiO_2 surface. Apparently intermolecular interactions are dominating in the latter case which means that the distance between the neighboring molecules is short enough for intermolecular energy transfer prevailing over the intramolecular. Another important consequence of the intermolecular interactions is the formation of the charge-separated state. As was mentioned above, the charge separation was not observed in solutions but clearly takes place in films. A rational explanation for this observation is in films the average distance between the phthalocyanines (the electron donors) and porphyrins (the electron acceptors) is much shorter than in solution, which means that the primary charge separation takes place between the donor and acceptor belonging to different dyads, i.e., intermolecularly.

As pointed out earlier, the ZnPc of ZnP–ZnPc dyad has the ability to bind the TiO_2 modified surface and direct donation of the electron by excited phthalocyanine to TiO_2 although coordination through ZnP of the dimer is well-established from the previous discussions. In order to further verify the effect of ZnPc of the dimer coordination on the overall photoelectrochemical response, the H_2P–ZnPc dyad was studied in the same arrangement, in which case only ZnPc has ability to bind to the semiconductor surface. The time-resolved transient absorption spectra for this sample are presented in Figure S5 of the Supporting Information. Right after excitation, the bleached Q-bands can be seen for both porphyrin (at 520 nm) and phthalocyanine (at 690 nm). However, for this sample the porphyrin Q-band recovered synchronously with enhanced bleaching of the Q-band and reshaping of all over the spectrum of the phthalocyanine chromophore. Also, the reshaping was not as drastic as that observed for the ZnP–ZnPc dyad. It seems that in this case porphyrin participates in the reaction by energy transfer only. Furthermore, the electron transfer takes place from the singlet excited state of phthalocyanine but it is spread widely in time, and already at zero delay time (with is measured with time resolution of 200 fs) some phthalocyanine molecules are in cationic form. Three lifetimes in the picosecond time domain obtained from global fit are 0.8, 5, and 90 ps. The fast time constant, 0.8 ps, is attributed tentatively to the porphyrin–phthalocyanine energy transfer; the 5 ps time constant corresponds to "slow" part of electron transfer from phthalocyanine to TiO_2; and the relatively weak 90 ps component is most likely the "fast" charge recombination, although for most of phthalocyanine cation radicals the lifetime is extended to nanosecond time domain.

As shown in Figure S6 of the Supporting Information, time-resolved transient absorption spectra of reference ZnPc modified TiO_2 were also recorded. Unlike for dyad layers, the spectra revealed very weak, if any, degree of electron transfer from phthalocyanine to the semiconductor as the intensities of

dx.doi.org/10.1021/jp308923e | J. Phys. Chem. C 2013, 117, 763–773

the 500 and 850 nm cation radical bands were minimal. In addition, the transient absorption decay almost completed within 300 ps, i.e., much faster than in the case of the dyad. These results are consistent with the low photoelectrochemical response of ZnPc modified solar cell.

As a final remark, one can speculate on the importance of primary charge separation in the organic layer. Predominant order of chromophores for the dyad **6** is TiO_2|ZnP−ZnPc, whereas for dyad **5** is TiO_2|ZnPc−H_2P. In the latter case, although the performance of the cell is not better than the ZnPc along modified electrode, it is likely that the primary electron transfer (less efficient) takes place between ZnPc and TiO_2.[30] In the former case the primary charge separation takes place in the organic layer, and the formed porphyrin anion donates the electron quickly to the semiconductor. In both cases the "final" charge separation takes place between the phthalocyanine and titanium dioxide; in the former case phthalocyanine and titanium dioxide are separated by the layer of porphyrins, which makes the charge recombination much slower and overall the photocurrent generation efficiency much higher.

SUMMARY

The photochemical events responsible for enhanced photocurrent generation and alignment of the ZnP−ZnPc dyad bound by axial coordination onto the TiO_2 surface are shown in Figure 7. The synthesized porphyrin−phthalocyanine conjugates are found to be useful to unravel the mechanism of photocurrent generation in the supramolecular solar cells as a consequence of photoinduced energy and electron transfer events occurring in succession. As predicted from the binding constants,[28] the preferential binding of ZnP over ZnPc of the dyad to the imidazole entity of the TiO_2 surface was clear from the control experiments. As revealed by the transient absorption studies, upon excitation of the ZnP entity of the dyad, energy transfer to ZnPc takes place within 0.2 ps (process 1 in Figure 7) and is clearly preferred over electron injection to the conduction band of TiO_2. Most likely, the covalent connectivity and distance between the donor and acceptor entities of the dyad, in addition to a slow charge injection process from excited ZnP to TiO_2, could be considered responsible factors. The product of energy transfer from reaction 1, singlet excited ZnPc, undergoes photoinduced electron transfer (process 2) within 2 ps, producing $ZnP^{\bullet-}$−$ZnPc^{\bullet+}$ radical ion pair; energy calculations according to Weller approach show that such a process is energetically favorable by about 0.12 eV.[31,32] The final step involves charge injection from $ZnP^{\bullet-}$ to semiconducting TiO_2 (process 3) which is estimated to take place within 30 ps. A direct consequence of these multiphotochemical events is the ultimate slowing down the charge recombination process that would occur in the cell with only ZnP or ZnPc sensitizer modified TiO_2 instead of the dyad modified TiO_2 surface. That is, in the final step a reduced TiO_2 and ZnPc cation radical separated by ZnP as distant charge-separated species are formed. The multistep photochemical events discussed here mimic the photochemical events of natural photosynthesis resulting into better performance of the solar device as a result of sequential energy transfer/charge separation processes.

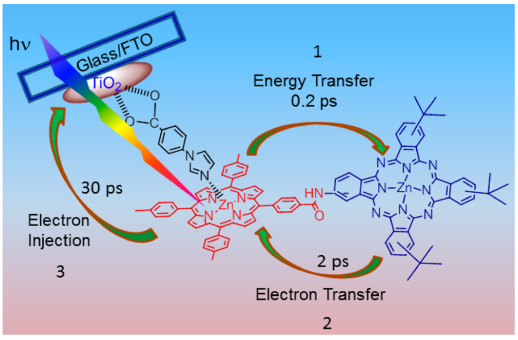

Figure 7. Photochemical events of ZnP−ZnPc dyad (**6**) modified TiO_2 electrode resulting in better performance of the solar cell. The sequence of photochemical events are numbered 1, 2, etc., along with the time constant of each process estimated by time-resolved studies.

EXPERIMENTAL SECTION

Chemicals. All of the reagents were from Aldrich Chemicals (Milwaukee, WI) while the bulk solvents utilized in the syntheses were from Fischer Chemicals.

Synthetic Procedure of Dyads and Triad. *5-(4-Carboxyphenyl)-10,15,20-tris(tolualyl)porphyrin (**1**).* *p*-Tolualdehyde (1.17 mL, 9.99 mmol), 4-formylbenzoic acid (500 mg, 3.33 mmol), and pyrrole (0.924 mL, 13.32 mmol) were added in a 500 mL RB flask containing 250 mL of propionic acid, and whole mixture was refluxed for 4 h. After removing the solvent by distillation, the black crude compound was purified by silica column. The desired compound was obtained as a second fraction eluted by chloroform:methanol (90:10 v/v). Yield 300 mg (12.8%). ^{1}H NMR ($CDCl_3$: 400 MHz), δ ppm: −2.45 (s, 2H, −NH), 2.75 (s, 9H, $-CH_3$), 7.55 (d, 6H, phenyl H), 8.10 (dd, 6H, phenyl H), 8.30 (d, 2H, phenyl H), 8.45 (d, 2H, phenyl H), 8.82 (d, 2H, pyrrole), 8.92 (m, 6H, pyrrole H). Mass-ESI $[M + H]^+$: obtained, 701.5; calculated, 700.83.

*[5-(4-Carboxyphenyl)-10,15,20-tris(tolualyl)porphyrinato]-zinc(II) (**2**).* Compound **1** (200 mg, 0.28 mmol) was dissolved in chloroform (30 mL) and methanol (20 mL) in a 100 mL RB flask, and then zinc acetate (185 mg, 0.90 mmol) was added and whole mixture was refluxed until free base porphyrin was metalated which was checked by the UV−vis spectrum which showed disappearance of the 512 nm band of free-base porphyrin. After evaporation of solvent, the crude compound was purified by silica column, and the desired compound was eluted by chloroform:methanol (95:5 v/v). Yield: 180 mg (84%). ^{1}H NMR ($CDCl_3$: 400 MHz), δ ppm: 2.70 (s, 9H, $-CH_3$), 7.60 (d, 6H, phenyl H), 8.15 (dd, 6H, phenyl H), 8.25 (d, 2H, phenyl H), 8.45 (d, 2H, phenyl H), 8.85 (d, 2H, pyrrole), 8.95 (m, 6H, pyrrole H). Mass-ESI $[M + H]^+$: obtained, 765.60; calculated, 764.22.

*5,15-Bis(4-carboxyphenyl)-10,20-bis(tolualyl)porphyrin (**3a**).* *p*-Tolualdehyde (0.785 mL), 4-formylbenzoic acid (1 g, 6.66 mmol), and pyrrole (1.84 mL, 26.64 mmol) were added in a 500 mL RB flask containing 200 mL of propionic acid, and the whole mixture was refluxed for 4 h. After removing the solvent by distillation, the black crude compound was purified by flash column of alumina. The desired compound was eluted by chloroform:methanol (70:30 v/v). Yield: 280 mg (6%). ^{1}H NMR (DMSO-*d*, 400 MHz), δ ppm: −2.40 to −2.95 (s, broad, 2H, −NH), 2.60 (s, 6H, $-CH_3$), 7.55−7.65 (d, 4H, phenyl H),

dx.doi.org/10.1021/jp308923e | J. Phys. Chem. C 2013, 117, 763−773

8.10−8.20 (d, 4H, phenyl H), 8.40 (d, 8H, phenyl H), 8.85 (dd, 8H, pyrrole H). Mass-ESI: obtained, 731.45; calculated, 730.81.

[5,15-Bis(4-carboxyphenyl)-10,20-bis(tolualyl)-porphyrinato]zinc(II) (**3**). Compound **3** (250 mg, 0.34 mmol) was dissolved in chloroform (30 mL) and methanol (20 mL) in a 100 mL RB flask, and then Zn acetate (225 mg, 1.02 mmol) was added and whole mixture was refluxed until free base porphyrin was metalated which was checked by the UV−vis spectrum, which showed disappearance of the 512 nm band of free-base porphyrin. After evaporation of solvent, the crude compound was purified by alumina column, and the desired compound was eluted by chloroform:methanol (80:20 v/v). Yield: 150 mg (55%). ^{1}H NMR (DMSO-*d*, 400 MHz), δ ppm: 2.60 (s, 6H, $-CH_3$), 7.55−7.65 (d, 4H, phenyl H), 8.10−8.20 (d, 4H, phenyl H), 8.40 (d, 8H, phenyl H), 8.90 (dd, 8H, pyrrole H). Mass-ESI: obtained, 795.65; calculated, 794.20.

2-Amino-9,16,23-tri-tert-butylphthalocyaninatozinc(II) (**4**). 4-*tert*-Butylphthalonitrile (695 mg, 3.77 mmol), 4-aminophthalonitrile (90 mg, 0.62 mmol), and $ZnCl_2$ (257 mg, 1.90 mmol) were kept in a 100 mL RB flask under N_2 for 20 min. Then DMAE (4 mL) was added, and whole mixture was heated at 150 °C for 18 h. After cooling the mixture at room temperature, the solution was dissolved with methanol and centrifuged for 1.5 h. The obtained green residue was dissolved in minimum of chloroform and purified by silica column. The desired compound was obtained as a second fraction eluted by chloroform. Yield: 120 mg (25%). ^{1}H NMR ($CDCl_3$-*d*, 400 MHz), δ ppm: 1.50 (m, 27H, $-CH_3$), 7.20 (m, 4H, Ar−H), 7.70 (m, 4H, Ar−H), 7.90 (m, 4H, Ar−H). Mass-ESI. $[M + H]^+$: obtained, 762.50; calculated, 761.27.

5-[2-Amido-9,16,23-tri-tert-butylphthalocyaninatozinc-(II)]-10,15,20-tris(tolualyl)porphyrin (**5**). Compound **1** (120 mg, 0.17 mmol) was dissolved in 20 mL of toluene in a 100 mL RB flask under N_2. Then thionyl chloride (0.24 mL, 3.40 mmol) and pyridine (0.27 mL, 3.4 mmol) were added into the RB flask and refluxed for 3 h. After cooling the mixture at room temperature, the solvent was evaporated to get the green H_2P-acyl compound. Without further purification, H_2P-acyl compound was dissolved in 20 mL of toluene under N_2. Then pyridine (0.886 mL, 10.96 mmol) and **4** (130.34 mg, 0.17 mmol) were added and stirred for 18 h at room temperature. After evaporation of solvent, the crude compound was purified by silica column. The desired compound was eluted by $CHCl_3$:MeOH (95:5 v/v). Yield: 30 mg (12.2%). ^{1}H NMR ($CDCl_3$: 400 MHz), δ ppm: −2.43 (s, 2H, −NH), 1.20−1.85 (m, 27H, *tert*-butyl *Pc*−H), 2.90 (s, 9H, tolualyl P−H), 7.5 (m, 6H, Por−H), 7.95 (m, 3H, *Pc*−H), 8.10 (m, 4H, Por−H), 8.25 (m, 6H, Por−H), 8.70−8.90 (broad, 8H, pyrrole H), 9.40−9.60 (broad, 9H, *Pc*−H). Mass-ESI $[M + CH_3OH]^+$: obtained, 1476.95; calculated, 1444.10.

{5-[2-Amido-9,16,23-tri-tert-butylphthalocyaninatozinc-(II)]-10,15,20-tris(tolualylporphyrinato}zinc(II) (**6**). Compound **2** (120 mg, 0.15 mmol) was dissolved in 20 mL of toluene in a 100 mL RB flask under N_2. Then thionyl chloride (0.21 mL, 3.0 mmol) and pyridine (0.24 mL, 3.0 mmol) were added into the RB flask and refluxed for 3 h. After cooling the mixture at room temperature, the solvent was evaporated to get the green ZnP-acyl compound. Without further purification, the ZnP-acyl compound was dissolved in 20 mL of toluene under N_2. Then pyridine (0.78 mL, 9.67 mmol) and **4** (119 mg, 0.15 mmol) were added and stirred for 18 h at room temperature. After evaporation of solvent, the crude compound was purified by silica column. The desired compound was eluted by $CHCl_3$:MeOH (95:5 v/v). Yield: 25 mg (11%). ^{1}H NMR ($CDCl_3$: 400 MHz), δ ppm: 1.20−1.85 (m, 27H, *tert*-butyl *Pc*−H), 2.85 (s, 9H, tolualyl Por−H), 7.55 (m, 6H, Por−H), 7.75 (m, 3H, *Pc*−H), 8.10 (m, 6H, Por−H), 8.30 (m, 4H, Por−H), 8.90 (m, 8H, pyrrole−H), 9.40−9.60 (broad, 9H, *Pc*−H). Mass-ESI, $[M + H]^+$: obtained, 1508.6; calculated, 1507.47.

{5,15-Bis[2-amido-9,16,23-tri-tert-butylphthalocyaninatozinc(II)]-10,20-bis(tolualyl)-porphyrinato}zinc(II) (**7**). Compound **8** (90 mg, 0.11 mmol) was dissolved in 20 mL of toluene in a 100 mL RB flask under N_2. Then thionyl chloride (0.39 mL, 5.5 mmol) and pyridine (0.44 mL, 5.5 mmol) were added into the RB flask and refluxed for 3 h. After cooling the mixture at room temperature, the solvent was evaporated to get the green ZnP-$(acyl)_2$ compound. Without further purification, ZnP-$(acyl)_2$ compound was dissolved in 20 mL of toluene under N_2. Then pyridine (1.44 mL, 17.73 mmol) and **4** (209 mg, 0.27 mmol) were added and stirred for 18 h at room temperature. After evaporation of solvent, the crude compound was purified by silica column. The desired compound was eluted by $CHCl_3$:MeOH (90:10 v/v). Yield: 15 mg (6%). ^{1}H NMR ($CDCl_3$: 400 MHz), δ ppm: 1.10−1.95 (m, 54H, *tert*-butyl *Pc*−H), 2.75 (s, 6H, $-CH_3$), 7.56−7.80 (m, 8H, Por−H), 7.90−8.10 (m, 6H, *Pc*−H), 8.18−8.40 (m, 8H, Por−H), 8.75−8.95 (m, 8H, pyrrole H), 9.30−9.60 (broad, 18H, *Pc*−H). Mass-ESI, $[M + H]^+$: obtained, 2282.40; calculated, 2280.70.

Instrumentation. The UV−vis spectral measurements were carried out either on a Shimadzu Model 2550 double monochromator UV−vis spectrophotometer or a Jasco V-670 spectrophotometer. The steady-state fluorescence spectra were measured by using a HORIBA Jobin Yvon Nanolog UV−vis−NIR spectrofluorometer equipped with a PMT (for UV−vis) and InGaAs (for NIR) detectors. A right angle detection method was used. The ^{1}H NMR studies were carried out on a Varian 400 MHz spectrometer. Tetramethylsilane (TMS) was used as an internal standard. The compounds were freshly purified over TLC prior spectral measurements.

Photoelectrochemical Measurements. Photocurrent−photovoltage characteristics of the solar cells were measured using a Keithly Instruments Inc. (Cleveland, OH) Model 2400 Current/Voltage Source Meter under illumination with an AM 1.5 simulated light source (Newport Corporation (Irvine, CA) Solar Simulator Model 9600 of 150 W). A 340 nm filter was introduced in the light path to eliminate UV radiation. Light intensity was monitored by using an Optical Model 1916-C Power Meter of Newport. The solar simulator was calibrated according to a literature method.[33] Incident photon-to-current efficiency (IPCE) of conversion measurements were performed under conditions of ∼2.5 mW cm^{-2} monochromatic light illumination using a setup comprising a 450 W Xe lamp and monochromator. Thin films of TiO_2 on FTO were prepared using the doctor blade technique according to a literature procedure.[34] Photoelectrochemical cells were constructed using platinized ITO as counter electrode in noncoordinating DCB containing 0.5 M $(n\text{-}Bu)_4NI$ and 0.03 M I_2 as redox mediator.

For the photoelectrochemical cell construction, a thin noncrystalline TiO_2 film coated fluorine doped indium tin oxide (FTO) electrode (∼10−12 μm, tec7 grade from Pilkington) was surface modified by placing the electrode in an ethanolic solution of 4-carboxyphenylimidazole (0.20 M) overnight, according to our earlier published method.[25] After removal of unbound material (2−3 ethanol washings), the TiO_2 electrode was immersed in DCB solution containing dye for

dx.doi.org/10.1021/jp308923e | J. Phys. Chem. C 2013, 117, 763−773

about 30 min. After this, the electrode was rinsed with DCB to remove excess of uncoordinated dye. Photoelectrochemical cell assembly was completed using platinized FTO as counter electrode in noncoordinating DCB containing 0.50 M $(n\text{-}Bu)_4NI$ and 0.030 M I_2 as redox mediator.

Transient Absorption Measurements. The pump−probe method was used to detect the fast processes with a time resolution of ∼200 fs, as described elsewhere.[35] In brief, femtosecond light pulses were obtained from Ti:sapphire generator coupled with Ti:sapphire multipass amplifier. The pulses at fundamental wavelength, 840 nm, were split in two beams: to generate second harmonic used as the pump pulse at 420 nm and white continuum used as the probe pulse. The time-resolved spectra were recorded after the same using CCD detector coupled with monochromator, and the measurements were repeated at a number of delay times to reconstruct time dependence of the signal. Solutions were measured in rotating 1 mm cuvette. For solid sample measurements the cuvette holder was replaced with the assembly consisting of two plates: one is the sample with the sensitized TiO_2 film, and another is quartz window. The inner volume was sealed and filled with nitrogen, and the sample surface was inside the sealed volume to conduct the measurements in an oxygen-free atmosphere. The thickness of the TiO_2 films was about 10 μm, and the plate orientation was orthogonal with respect to the pump and probe beams.

■ ASSOCIATED CONTENT

Ⓢ Supporting Information

Excitation spectrum of dyads **5**, **6** and triad **7** in chloroform and THF, absorption spectra of the dyad and triad in THF, absorption spectrum and picture of the dyad **6** modified TiO_2, transient absorption spectrum of dyad **5** modified TiO_2, transient absorption spectrum of ZnPc modified TiO_2 and binding constant plots. This material is available free of charge via the Internet at http://pubs.acs.org.

■ AUTHOR INFORMATION

Corresponding Author

*E-mail: Francis.DSouza@unt.edu (F.D.); nikolai.tkachenko@tut.fi (N.V.T.).

Notes

The authors declare no competing financial interest.

■ ACKNOWLEDGMENTS

The authors are thankful to the National Science Foundation (Grant No. 1110942 to F.D.) and the Academy of Finland for support of this work.

■ REFERENCES

(1) (a) *Photosynthetic Protein Complexes; A Structural Approach*; Frome, P., Ed.; Wiley-VCH Verlag GmbH & Co.: Germany, 2008. (b) *Photosynthetic Light Harvesting*; Cogdell, R., Mullineaux, C., Eds.; Springer: Dordrecht, Netherlands, 2008. (c) *Handbook of Photosynthesis*, 2nd ed.; Pessarakli, M., Ed.; CRC Press LLC: Boca Raton, FL, 2005. (d) *Light-Harvsting Antennas in Photosynthesis*; Green, B. R., Parson, W. W., Eds.; Kluwer: Dordrecht, Netherlands, 2003.

(2) (a) *The Photosynthetic Reaction Center*; Deisenhofer, J., Norris, J. R., Eds.; Academic Press: San Diego, 1993. (b) Deisenhofer, J.; Epp, O.; Miki, K.; Huber, R.; Michel, H. *J. Mol. Biol.* **1984**, *180*, 385−398.

(3) (a) Connolly, J. S., Ed.; *Photochemical Conversion and Storage of Solar Energy*; Academic: New York, 1981. (b) *Molecular Level Artificial Photosynthetic Materials*; Meyer, G. J., Ed.; Wiley: New York, 1997. (c) Wasielewski, M. R. *Chem. Rev.* **1992**, *92*, 435−461. (d) Verhoeven, J. W. *Adv. Chem. Phys.* **1999**, *106*, 603−644. (e) Osuka, A.; Mataga, N.; Okada, T. *Pure Appl. Chem.* **1997**, *69*, 797−802. (f) Flamigni, L.; Barigelletti, F.; Armaroli, N.; Collin, J.-P.; Dixon, I. M.; Sauvage, J.-P.; Williams, J. A. G. *Coord. Chem. Rev.* **1999**, *190−192*, 671−682. (g) Diederich, F.; Gomez-Lopez, M. *Chem. Rev. Soc.* **1999**, *28*, 263−277.

(4) (a) Blanco, M.-J.; Consuelo Jimenez, M.; Chambron, J.-C.; Heitz, V.; Linke, M.; Sauvage, J.-P. *Chem. Rev. Soc.* **1999**, *28*, 293−305. (b) Balzani, V.; Ceroni, P.; Juris, A.; Venturi, M.; Campagna, S.; Puntoriero, F.; Serroni, S. *Coord. Chem. Rev.* **2001**, *219*, 545−572. (c) Balzani, V.; Credi, A.; Venturi, M. *ChemSusChem* **2008**, *1*, 26−58.

(5) (a) Bixon, M.; Fajer, J.; Feher, G.; Freed, J. H.; Gamliel, D.; Hoff, A. J.; Levanon, H.; Möbius, K.; Nechushtai, R.; Norris, J. R.; et al. *Isr. J. Chem.* **1992**, *32*, 449. (b) Lewis, F. D.; Letsinger, R. L.; Wasielewski, M. R. *Acc. Chem. Res.* **2001**, *34*, 159−170.

(6) (a) Gust, D.; Moore, T. A.; Moore, A. L. *Acc. Chem. Res.* **1993**, *26*, 198−205. (b) Gust, D.; Moore, T. A. In *The Porphyrin Handbook*; Kadish, K. M., Smith, K., Guilard, R.; Eds.; Academic Press: San Diego, 2000; Vol. *8*, pp 153−190.

(7) (a) Fukuzumi, S.; Guldi, D. M. In *Electron Transfer in Chemistry*; Balzani, V., Ed.; Wiley-VCH: Weinheim, 2001; Vol. *2*, pp 270−337. (b) Fukuzumi, S. In *The Porphyrin Handbook*; Kadish, K. M., Smith, K., Guilard, R., Eds.; Academic Press: San Diego, 2000; Vol. *8*, pp 115−151. (c) Fukuzumi, S. *Phys. Chem. Chem. Phys.* **2008**, *10*, 2283−2297.

(8) (a) El-Khouly, M. E.; Ito, O.; Smith, P. M.; D'Souza, F. *J. Photochem. Photobiol., C* **2004**, *5*, 79−104. (b) D'Souza, F.; Ito, O. *Coord. Chem. Rev.* **2005**, *249*, 1410−1422. (c) D'Souza, F.; Ito, O. In *Handbook of Organic Electronics and Photonics*; Nalwa, H. R., Ed.; American Scientific Publishers: London, 2008; Vol. *1*, Chapter 13, pp 485−521. (d) Chitta, R.; D'Souza, F. *J. Mater. Chem.* **2008**, *18*, 1440−1471. (e) D'Souza, F.; Ito, O. *Chem. Commun.* **2009**, 4913−4928. (f) D'Souza, F.; Ito, O. *Chem. Soc. Rev.* **2012**, *41*, 86−96. (g) D'Souza, F.; Ito, O. In *Handbook of Porphyrin Science*; Kadish, K. M., Guilard, R., Smith, K. M., Eds.; World Science Publishers: Singapore, 2010; Vol. *1*, Chapter 4, pp 307−437. (h) D'Souza, F.; Ito, O. *Molecules* **2012**, *17*, 5816−5835.

(9) (a) Guldi, D. M. *Chem. Commun.* **2000**, 321−327. (b) Guldi, D. M. *Chem. Soc. Rev.* **2002**, *31*, 22−36. (c) Sgobba, V.; Guldi, D. M. *Chem. Soc. Rev.* **2009**, *38*, 165−184. (d) Mateo-Alonso, A.; Guldi, D. M.; Paolucci, F.; Prato, M. *Angew. Chem., Int. Ed.* **2007**, *46*, 8120−8126. (e) Guldi, D. M. *Phys. Chem. Chem. Phys.* **2007**, *9*, 1400−1420. (f) Sanchez, L.; Nazario, M.; Guldi, D. M. *Angew. Chem., Int. Ed.* **2005**, *44*, 5374−5382. (g) Delgado, J. L.; Herranz, M. Á.; Martín, N. *J. Mater. Chem.* **2008**, *18*, 1417−1426. (h) Tasis, D.; Tagmatarchis, N.; Bianco, A.; Prato, M. *Chem. Rev.* **2006**, *106*, 1105−1136. (i) Sgobba, V.; Rahman, G. M. A.; Ehli, C.; Guldi, D. M. In *Fullerenes—Principles and Applications*; Langa, F., Nierengarten, N. J., Eds.; Royal Society of Chemistry: Cambridge, UK, 2007.

(10) (a) Sessler, J. S.; Wang, B.; Springs, S. L.; Brown, C. T. In *Comprehensive Supramolecular Chemistry*; Atwood, J. L., Davies, J. E. D., MacNicol, D. D., Vögtle, F., Eds.; Pergamon: Oxford, 1996; Chapter 9. (b) Sessler, J. L.; Lawrence, C. M.; Jayawickramarajah, J. *Chem. Soc. Rev.* **2007**, *36*, 314−325.

(11) (a) Kamat, P. V. *J. Phys. Chem. C* **2007**, *111*, 2834−2860. (b) Umeyama, T.; Imahori, H. *Energy Environ. Sci.* **2008**, *1*, 120−133. (c) Hasobe, T. *Phys. Chem. Chem. Phys.* **2010**, *12*, 44−57. (d) Imahori, H.; Umeyama, T.; Kei, K.; Yuta, T. *Chem. Commun.* **2012**, *48*, 4032−4045. (e) Kamat, P. V.; Schatz, G. C. *J. Phys. Chem. C* **2009**, *113*, 15473−15475. (f) Dang, X.; Hupp, J. T. *J. Photochem. Photobiol., A* **2001**, *143*, 251−256.

(12) (a) Schuster, D. I.; Li, K.; Guldi, D. M. *C. R. Chim.* **2006**, *9*, 892−908. (b) Ziessel, R.; Harriman, A. *Chem. Commun.* **2011**, *47*, 611−631. (c) Benniston, A. C.; Harriman, A. *Coord. Chem. Rev.* **2008**, *252*, 2528−2539.

(13) (a) de la Torre, G.; Vazquez, P.; Agullo-Lopez, F.; Torres, T. *Chem. Rev.* **2004**, *104*, 3723−3750. (b) Bottari, G.; de la Torre, G.; Guldi, D. M.; Torres, T. *Chem. Rev.* **2010**, *110*, 6768−6816.

(14) (a) *Introduction of Molecular Electronics*; Petty, M. C., Bryce, M. R., Bloor, D., Eds.; Oxford University Press: New York, 1995. (b) *Molecular Electronics: Science and Technology*; Aviram, A., Ratner, M., Eds.; Ann. N. Y. Acad. Sci., 1998; p 852. (c) *Molecular Switches*; Feringa, B. L., Ed.; Wiley-VCH GmbH: Weinheim, 2001. (d) Gust, D.; Moore, T. A.; Moore, A. L. *Chem. Commun.* **2006**, 1169−1178. (e) Balzani, V.; Credi, A.; Venturi, M. In *Organic Nanostructures*; Atwood, J. L., Steed, J. W., Eds.; 2008; pp 1−31. (f) *Energy Harvesting Materials*; Andrews, D. L., Ed.; World Scientific: Singapore, 2005. (g) Tour, J. M. *Molecular Electronics; Commercial Insights, Chemistry, Devices, Architectures and Programming*; World Scientific: River Edge, NJ, 2003.

(15) (a) Smith, K. M. *Porphyrins and Metalloporphyrins*; Elsevier: Amsterdam, 1972. (b) *The Porphyrin Handbook*; Kadish, K. M., Smith, K. M., Guilard, R., Eds.; Academic Press: San Diego, CA, 2000; Vols. *1*−*20*.

(16) (a) *Phthalocyanine Materials: Structure, Synthesis and Function*; McKeown, N. B., Ed.; Cambridge University Press: Cambridge, 1998. (b) *Phthalocyanine: Properties and Applications*; Leznoff, C. C., Lever, A. B. P., Eds.; VCH: New York, 1993. (c) Claessens, C. G.; González-Rodríguez, D.; Torres, T. *Chem. Rev.* **2002**, *102*, 835−854.

(17) Lo, P.-C.; Leng, X.; Ng, D. K. P. *Coord. Chem. Rev.* **2007**, *251*, 2334−2353.

(18) (a) Kobayashi, N.; Nishiyama, Y.; Ohya, T.; Sato, M. *J. Chem. Soc., Chem. Commun.* **1987**, 390−392. (b) Tian, H.-J.; Zhou, Q.-F.; Shen, S.-Y.; Xu, H.-J. *J. Photochem. Photobiol., A* **1993**, *72*, 163−168. (c) Tian, H.-J.; Zhou, Q.-F.; Shen, S.-Y.; Xu, H.-J. *Chin. J. Chem.* **1996**, *14*, 412−420. (d) Tian, H.-J.; Zhou, Q.-F.; Shen, S.-Y.; Xu, H.-J. *Chin. J. Chem.* **1998**, *16*, 97−108. (e) Yang, S. I.; Li, J.; Cho, H. S.; Kim, D.; Bocian, D. F.; Holten, D.; Lindsey, J. S. *J. Mater. Chem.* **2000**, *10*, 283−296. (f) Ambroise, A.; Wagner, R. W.; Rao, P. D.; Riggs, J. A.; Hascoat, P.; Diers, J. R.; Seth, J.; Lammi, R. K.; Bocian, D. F.; Holten, D.; et al. *Chem. Mater.* **2001**, *13*, 1023−1034. (g) Miller, M. A.; Lammi, R. K.; Prathapan, S.; Holten, D.; Lindsey, J. S. *J. Org. Chem.* **2000**, *65*, 6634−6649. (h) Sutton, J. M.; Boyle, R. W. *Chem. Commun.* **2001**, 2014−2015. (i) Zhao, Z.; Nyokong, T.; Maree, M. D. *Dalton Trans.* **2005**, 3732−3737.

(19) (a) Kameyama, K.; Satake, A.; Kobuke, Y. *Tetrahedron Lett.* **2004**, *45*, 7617−7620. (b) Tomé, J. P. C.; Pereira, A. M. V. M.; Alonso, C. M. A.; Neves, M. G. P. M. S.; Tomé, A. C.; Silva, A. M. S.; Cavaleiro, J. A. S.; Martínez-Díaz, M. V.; Torres, T.; Rahman, G. M. A.; et al. *Eur. J. Org. Chem.* **2006**, 257−267. (c) Ito, F.; Ishibashi, Y.; Khan, S. R.; Miyasaka, H.; Kameyama, K.; Morisue, M.; Satake, A.; Ogawa, K.; Kobuke, Y. *J. Phys. Chem. A* **2006**, *110*, 12734−12742.

(20) (a) Giribabu, L.; Kumar, C. V.; Reddy, P. D. *Chem.—Asian J.* **2007**, *2*, 1574−1580. (b) Tannert, S.; Ermilov, E. A.; Vogel, J. O.; Choi, M. T. M.; Ng, D. K. P.; Röder, B. *J. Phys. Chem. B* **2007**, *111*, 8053−8062. (c) Soares, A. R. M.; Martinez-Diaz, M. V.; Bruckner, A.; Pereira, A. M. V. M.; Tome, J. P. C; Alonso, C. M. A.; Faustino, M. A. F.; Neves, M. G. P. M. S.; Tome, A. C.; Silva, A. M. S.; et al. *Org. Lett.* **2007**, *9*, 1557−1560. (d) Ali, H.; va Lier, J. E. *Tetrahedron Lett.* **2009**, *50*, 1113−1116. (e) Kojima, T.; Honda, T.; Ohkubo, K.; Shiro, M.; Kusukawa, T.; Fukuda, T.; Kobayashi, N.; Fukuzumi, S. *Angew. Chem., Int. Ed.* **2008**, *47*, 6712−6716.

(21) (a) Maligaspe, E.; Tkachenko, N. V.; Subbaiyan, N. K.; Chitta, R.; Zandler, M. E.; Lemmetyinen, H.; D'Souza, F. *J. Phys. Chem. A* **2009**, *113*, 8478−8489. (b) Stranius, K.; Jacobs, R.; Maligaspe, E.; Lemmetyinen, H.; Tkachenko, N. V.; Zandler, M. E.; D'Souza, F. *J. Porphrins Phthalocyanines* **2010**, *14*, 948−961. (c) KC, C. B.; Subbaiyan, N. K.; D'Souza, F. *J. Phys. Chem. C* **2012**, *116*, 11964−11972. (d) Jacobs, R.; Stranius, K.; Maligaspe, E.; Lemmetyinen, H.; Tkachenko, N. V.; Zandler, M. E.; D'Souza, F. *Inorg. Chem.* **2012**, *51*, 3656−3665.

(22) Subbaiyan, N. K.; D'Souza, F. *Chem. Commun.* **2012**, *48*, 3641−3643.

(23) *Principles of Fluorescence Spectroscopy*, 3rd ed.; Lakowicz, J. R., Ed.; Springer: Singapore, 2006.

(24) (a) Maligaspe, E.; Kumpulainen, T.; Subbaiyan, N. K.; Zandler, M. E.; Lemmetyinen, H.; Tkachenko, N. V.; D'Souza, F. *Phys. Chem. Chem. Phys.* **2010**, *12*, 7434−7444. (b) D'Souza, F.; Wijesinghe, C. A.; El-Khouly, M. E.; Hudson, J.; Niemi, M.; Lemmetyinen, H.; Tkachenko, N. V.; Zandler, M. E.; Fukuzumi, S. *Phys. Chem. Chem. Phys.* **2011**, *13*, 18168−18178. (b) El-Khouly, M. E.; Wijesinghe, C. A.; Nesterov, V. N.; Zandler, M. E.; Fukuzumi, S.; D'Souza, F. *Chem.—Eur. J.* **2012**, *18*, 13844−13853.

(25) Subbaiyan, N. K.; Wijesinghe, C. A.; D'Souza, F. *J. Am. Chem. Soc.* **2009**, *131*, 14646−14647.

(26) (a) Subbaiyan, N. K.; Hill, J. P.; Ariga, K.; Fukuzumi, S.; D'Souza, F. *Chem. Commun.* **2011**, *47*, 6003−6005. (b) Fukuzumi, S.; Ohkubo, K.; D'Souza, F.; Sessler, J. L. *Chem. Commun.* **2012**, *48*, 9801−9815.

(27) *Dye-Sensitized Solar Cells*; Kalyanasundaram, K., Ed.; EPFL Press: Lausanne, 2010.

(28) The binding constant evaluated for ZnTTP binding to 1-phenylimidazole in DCB using optical absorbance data and Benesi−Hildebrand method (see refs 8a and 8b for details) was found to be 4.26×10^4 M^{-1} while that for ZnPc binding, this value was 2.55×10^4 M^{-1} (see Figures S9 and S10 in the Supporting Information).

(29) The monochromatic incident photon-to-current conversion efficiency (IPCE), defined as the number of electrons generated by light in the outer circuit divided by the number of incident photons, was determined according to the equation IPCE (%) = $100 \times 1240 \times I_{SC}$ (mA cm^{-2})/[λ (nm) × P_{in} (mW cm^{-2})], where I_{SC} is the short-circuit photocurrent generated by the incident monochromatic light and λ is the wavelength of this light with intensity P_{in}.

(30) For both TiO_2|ZnPc−ref and TiO_2|ZnPc−H_2P samples the phthalocyanine chromophores are at the TiO_2 surface. However, the molecular organizations on the surface are quite difference for these two samples as evidenced by the absorption spectra (Figure S8). The Q-band area indicates rather heavy aggregation of ZnPc-ref but not of the ZnPc−H_2P dyad. The aggregation leads to fast nonradiative decay of the singlet excited state in the TiO_2|ZnPc−ref samples, which reduces the electron transfer from ZnPc to TiO_2 to virtually undetectable level, as compared to that of the TiO_2|ZnPc−H_2P sample.

(31) Using the electrochemical, computational, and excited energy data, the free energies of charge separation (ΔG_{CS}) were calculated using Weller's approach:[32] $-\Delta G_{CS} = \Delta E_{0-0} - e(E_{ox} - E_{red}) + \Delta G_S$, where ΔE_{0-0} is the energy of the lowest excited state of ZnPc (1.92 eV), E_{ox} the first oxidation potential of ZnPc (= −0.08 V vs Fc/Fc^+), E_{red} the first reduction potential of ZnTTP (−1.94 V vs Fc/Fc^+) = $\Delta G_S = -e^2/(4\pi\varepsilon_0\varepsilon_R R_{Ct-Ct})$, and ε_0 and ε_R refer to vacuum permittivity and dielectric constant of DCB.

(32) Weller, A. *Z. Phys. Chem. (Munich)* **1982**, *133*, 93−98.

(33) Ito, S.; Matsui, H.; Okada, K.; Kusano, S.; Kitamura, T.; Wada, Y.; Yanagida, S. *Sol. Energy Mater. Sol. Cells* **2004**, *82*, 421−429.

(34) (a) Ito, S.; Chen, P.; Comte, P.; Nazeeruddin, M. K.; Liska, P.; Péchy, P.; Grätzel, M. *Prog. Photovoltaics: Res. Appl.* **2007**, *15*, 603−612. (b) Wang, F.; Subbaiyan, N. K.; Wang, Q.; Rochford, C.; Xu, G.; Lu, R.; Elliot, A.; D'Souza, F.; Hut, R.; Wu, J. *ACS Appl. Mater. Interfaces* **2012**, *4*, 1565−1572. (c) Hart, A. S.; KC, C. B.; Subbaiyan, N. K.; Karr, P. A.; D'Souza, F. *ACS Appl. Mater. Interfaces* **2012**, *4*, 5813−5820.

(35) (a) Tkachenko, N. V.; Rantala, L.; Tauber, A. Y.; Helaja, J.; Hynninen, P. H.; Lemmetyinen, H. *J. Am. Chem. Soc.* **1999**, *121*, 9378−9387. (b) Vehmanen, V.; Tkachenko, N. V.; Imahori, H.; Fukuzumi, S.; Lemmetyinen, H. *Spectrochim. Acta, Part A* **2001**, *57*, 2229−2244. (c) Isosomppi, M.; Tkachenko, N. V.; Efimov, A.; Lemmetyinen, H. *J. Phys. Chem. A* **2005**, *109*, 4881−4890.

PUBLICATION IV

Effect of Mutual Position of Electron Donor and Acceptor on Photoinduced Electron Transfer in Supramolecular Chlorophyll-Fullerene Dyads

Kati Stranius, Vladimir Iashin, Taru Nikkonen, Mikko Muuronen, Juho Helaja and Nikolai Tkachenko

The Journal of Physical Chemistry A

THE JOURNAL OF PHYSICAL CHEMISTRY A

Article

pubs.acs.org/JPCA

Effect of Mutual Position of Electron Donor and Acceptor on Photoinduced Electron Transfer in Supramolecular Chlorophyll–Fullerene Dyads

Kati Stranius,[†] Vladimir Iashin,[‡] Taru Nikkonen,[‡] Mikko Muuronen,[‡] Juho Helaja,*[,‡] and Nikolai Tkachenko*[,†]

[†]Department of Chemistry and Bioengineering, Tampere University of Technology, 33720 Tampere, Finland

[‡]Department of Chemistry, University of Helsinki, 00100 Helsinki, Finland

Supporting Information

ABSTRACT: In this study we have explored the influence of mutual position of chlorin electron donor and fullerene C_{60} electron acceptor on photoinduced electron transfer. Two zinc-chlorin-aza-[18]crown-6 compounds and three pyrrolidino[60]fullerenes with alkyl aminium and varying coordinative moieties were synthesized and used for self-assembling of a set of complexes via two-point binding. The aza[18]crown6 moieties were connected to chlorins via amide linker either at 13^4 or 17^4 position, hence, being attached on different sides of the chlorin plane. Furthermore, in the former case, the linker holds the crown closely spaced, whereas, in the latter, the linker gives more space and conformational freedom for the crown with respect to the chlorin macrocycle. The coordinative moieties at fullerene site, 3-pyridine, 4-pyridine, and 3-furan, were built by utilizing the Prato reaction. The two-point binding drove the molecules into specific complex formation by self-assembling; aminium ion was chelated by crown ether, while zinc moiety of chlorin was coordinated by pyridine and furan. Such pairing resulted in distinct supramolecular chlorin-fullerene dyads with defined distance and orientation. The performed computational studies at DFT level in solution, with TPSS-D3/def2-TZVP//def2-SVP, indicated different geometries and binding energies for the self-assembling complexes. Notably, the computations pointed out that for all the studied complexes, the donor–acceptor distances and binding energies were dictated by chirality of pyrrolidino ring at C_{60}. The selective excitation of chlorin chromophore revealed efficient emission quenching in all dyads. The ultrafast spectroscopy studies suggested a fast and efficient photoinduced charge transfer in the dyads. The lifetimes of the charge separated states range from 55 to 187 ps in *o*-dichlorobenzene and from 14 to 60 ps in benzonitrile. Expectedly, the electron transfer rate was found to be critically dependent on the donor–acceptor distance; additionally, the mutual orientation of these entities was found to have significant contribution on the rate.

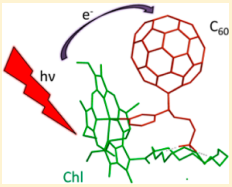

INTRODUCTION

Chlorophylls play key roles in primary photosynthetic events, i.e., in light harvesting, energy transfer, and charge separation, occurring in natural photosystems.[1,2] Elucidation of mechanistic details of these individual actions paves the way for development of artificial biomimetic devices such as solar light harvesting systems and photoactive molecular devices such as sensors, switches, and memories.

Chlorophyll analogues, porphyrins, and phtalocyanines have been widely studied as electron donors.[1,3−8] All these highly conjugated macrocycles absorb light over wide wavelength range in the visible and UV regions also possessing high electron–donor abilities. The central atom substitution and modification of the peripheral substituents of macrocycles can be used to change these properties for improving chromophore activity in donor–acceptor (DA) systems. Although nature has evolved chlorophyll to show excellence in the multitasking roles, the complicated purification of chlorophylls, instability of unmodified chlorophyll being exposure to light and limited amount of synthetic modification methods have limited its use in artificial systems.[2,9−15] However, in comparison to the semisynthetic chlorophyll analogues, the asymmetry of chlorophyll has its advantages over easily accessible symmetric synthetic porphyrines and phtalocyanines. It has been recently shown that the asymmetry enables precise supramolecular assemblies, e.g., derivation of chlorins for face-selective ligation[16] and high order helix formation.[17]

One practical advantage of the supramolecular DA dyad self-assembling over much wider explored covalent dyad linking strategy is the possibility to prepare a series of donors and acceptors with the same interlocking groups and generate a large number of DA dyads solely by mixing different combinations of donor and acceptor molecules. Self-assembled systems are typically formed via metal–ligand or crown-ether coordination or ion pairing, hydrogen bonding or $\pi-\pi$ stacking interactions.[1,8,18−20] Self-assembling methods based on multiple modes of binding instead of one-point were also proposed and allowed to form complexes with higher binding strength and

Received: December 19, 2013
Revised: February 3, 2014

   dx.doi.org/10.1021/jp412442t | J. Phys. Chem. A XXXX, XXX, XXX–XXX

better defined distances and orientation between the donor and acceptor.[8] This is an important advantage of the multipoint binding, since the mutual orientation and distance of the functional units in DA dyads affect the electron transfer rate. In flexibly linked dyads, the distance and orientation vary and cannot be controlled.[1,12,21−23]

Fullerene C_{60} has high electron affinity, and electron transfer reactions involving fullerene are characterized by relatively small reorganization energy. Therefore, it is one of most commonly used acceptors in the DA design.[24,25] The fullerene has low absorption in the visible region, which requires utilization of donor compounds with sufficient absorption in the visible range. Therefore chlorin−fullerene combination is an appropriate choice for supramolecular design. In this case the donor, chlorin, can be excited selectively, and the unique anion absorption band of the fullerene in the near-IR makes detection of the electron transfer dynamics reliable and reasonably accurate.[22,26]

In the present study, the supramolecular dyads were formed by specially designed Zn−chlorin and fullerene derivatives which implements two-point interaction to increase the binding efficiency and to achieve well determined mutual orientation between the donor and acceptor. Crown-ether moiety was attached to Zn−chlorin and alkyl aminium ion and pyridine entities to fullerene. The DA dyad was formed via axial coordination of pyridine entity to the zinc center of chlorin and complexation of the aminium ion with crown-ether. The photoinduced electron transfer in these dyads has been studied with steady-state and time-resolved spectroscopy.

EXPERIMENTAL METHODS

General. All the solvents used in synthesis and measurements were obtained as HPLC quality and used as received. ^{1}H, ^{13}C, and COSY spectra were recorded at 27 °C using Varian Mercury 300 MHz or Varian Inova 500 MHz Spectrometer. ^{1}H and ^{13}C NMR spectra were referenced to the solvent signals (in $CDCl_3$ 7.26 and 77 ppm, respectively). High-resolution mass spectra were obtained on HR-ESI MS with Bruker micrOTOF instrument.

Compounds. The structures of the electron donating chlorins (**Chl-1** and **Chl-2**) and the electron accepting pyrrolidino-[60]fullerenes (**C60-1**, **C60-2**, **C60-3**) are presented in Scheme 1. **Chl-1** was synthesized by EDCI-assisted coupling of pyropheophorbide *a* with 1-aza-18-crown-6 followed by insertion of zinc (see Supporting Information (SI)). **Chl-2** was prepared via selective aminolysis of 13^4-position, which has been recently developed in our laboratory,[27] and subsequent zinc insertion (see SI).

Fullerenes **C60-1**, **C60-2**, and **C60-3** were synthesized via Prato reaction[27] and further one-pot deprotection of amine moiety and aminium salt formation (see SI).

It should be noted that each synthesized pyrrolidino-[60]fullerene was obtained as a 1:1 mixture of two enantiomers (*R* and *S*). The asymmetry is invisible in a symmetrical environment for instance when similar mixtures of enantiomers have been complexed with symmetric porphyrin derivatives.[22,23] However, in case of chiral chlorophyll derivatized host molecules each enantiomer results in different DA distances and geometries. This will be discussed in detail later.

Steady State Spectroscopy. The UV−vis spectral measurements were carried out with a Shimadzu UV-3600 UV−vis−NIR spectrophotometer. The fluorescence spectra were recorded with an ISA-Jobin Yvon-SPEX-Horiba Fluorolog-2-111 fluorometer and corrected using the instrument response function supplied by the manufacturer. Solutions were prepared from solid compounds. Approximately 1 mg of each solid sample was dissolved in 1 mL of *o*-dichlorobenzene (ODCB) or benzonitrile (PhCN), and these solutions were used as stock solutions to prepare the samples for further measurements. Concentration of chlorophyll was maintained at ∼0.08−0.1 mM in all spectroscopic measurements. Due to low solubility of **C60-2** at concentrations above 0.1 mM, special procedure was developed for preparing of **C60-2** solution. One milligram of solid compound was first dissolved in 10 μL of dimethylformamide (DMF) and then 1 mL of ODCB was added to the solution.

Scheme 1. Chlorin-Derived Electron Donors (Chl-1 and -2) and C_{60}-Derived Electron Acceptors (C60-1, -2, and -3)

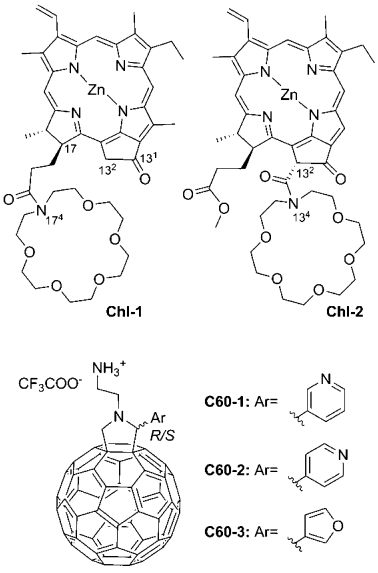

Time-Resolved Spectroscopy. Pump−probe and up-conversion techniques were used to detect the fast photo-induced processes in solutions with a time resolution of 0.2 ps. The instruments and data analysis procedure have been described earlier.[9,10,28] All measurements were carried out in 1 mm rotating cuvette. Absorbance of chlorophyll was around 0.8 (0.1 mM) at Soret band maximum and concentration of fullerene was adjusted to provide molecular ratio of roughly 1:1−5 (Chl@C60) depending on the emission quenching efficiency by the fullerenes. The excitation wavelength was around 420 nm, and the measurements were carried out in wavelength ranges 510−800 nm and 870−1100 nm. The excitation intensity was adjusted to provide 10−50% excitation efficiency.

Differential Pulse Voltammetry. Differential pulse voltammetry (DPV) was used to measure the oxidation and reduction potentials of chlorins and fullerenes separately. Measurements were done at room temperature under nitrogen flow and recorded with a Iviumstat Compactstat IEC 61326 Standard potentiostat controlled by the Iviumsoft software. A platinum wire sealed in glass was used as working electrode and was polished with 0.05 μm alumina suspension before each

dx.doi.org/10.1021/jp412442t | J. Phys. Chem. A XXXX, XXX, XXX−XXX

measurement. Ag/AgCl wire was used as reference electrode and platinum wire as a counter electrode. Measurements were done in 0.1 M $TBAClO_4$ in ODCB (dried and stored under molecular sieves) as supporting electrolyte and ferrocene was used as an internal reference redox system. Concentration of all measured samples was 0.46 mM. Scanning rate was 0.05 V/s, the pulse time 20 ms, the pulse amplitude 20 mV, and the equilibration time 5s. The potential cycling was performed between −1 and 1 V and vice versa.

Computational Methods. Computational study was performed at DFT level in solution for all the self-assembling pairs including the both *R*- and *S*-enantiomers of fullerene. All computations were performed using the Turbomole 6.4 program package.[29] Solvation effects were taken into account using COSMO solvation model in all computations with dielectric constant of *o*-dichlorobenzene (ε = 10).[30] A keyword "use_contcav" was used to assure that no COSMO cavity was built inside fullerene ring. The TPSS-D3[31,32] functional was chosen with double ζ quality basis set, def2-SVP, for optimizations, and single point properties were calculated using triple ζ quality basis set, def2-TZVP.[33] The empirical dispersion correction D3 was used with zero-damping. The MARI-J approximation was used in all computations with suitable auxiliary basis set.[34−37] To discover the effect of the functional and basis set, **Chl-1@*S*-C60-3** complex was also optimized using TPSS-D3/def2-TZVP and B97-D3.[32,38] Change of the functional did not lead to any notable changes in the structure and upgrade of the basis set did not change nature of the result. Therefore, all optimizations were performed using def2-SVP basis set. Grid m4 was used throughout all computations. Pictures were generated using TmoleX, and orbitals were plotted using isovalue of 0.01.

RESULTS

Steady State Spectroscopy. The normalized absorption spectra of the both chlorins, **Chl-1** and **Chl-2**, and 3-pyridine derivatized pyrrolidino[60]fullerene, **C60-1**, in ODCB are presented in Figure 1. The absorption spectra of **Chl-2** show intense Soret band at 430 nm and Q_y band at 662 nm. There is a minor (less than 2 nm) difference in positions of the bands for **Chl-1** compared to **Chl-2**. The ratio of Soret and Q-band intensities is also somewhat different in the studied chlorins as can be expected considering different substituents at position 13[4].

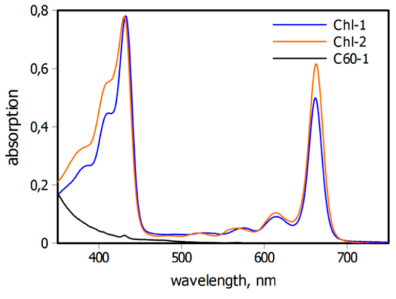

Figure 1. Absorption spectra of **Chl-1**, **Chl-2**, and **C60-1** in ODCB. Concentrations of **Chl-2** and **C60-1** are 0.1 mM, while absorption spectrum of **Chl-1** is normalized to match that of **Chl-2** at the Soret band.

The aim of this work was time-resolved study of the photoinduced electron transfer in supramolecular dyads, which was carried out in 1 mm thick cuvettes and sample absorption close to 1 at the Soret band. Therefore, titration experiments were done in conditions close to those used in pump−probe measurements, i.e., in 1 mm cuvettes and chlorin concentrations roughly 0.1 mM. Figure 2 shows changes in absorption

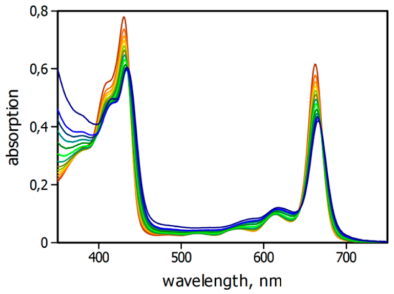

Figure 2. Corrected titration absorption spectra of increasing concentration of **C60-1** in the solution of **Chl-2** (0.1 mM) in ODCB. The red-brown line represents the starting point with no **C60-1** present.

spectrum of **Chl-2** upon addition of **C60-1** in ODCB. Titration was done by adding the fullerene solution to chlorin solution so that the sample volume was increased by 15% at the end of titration. The absorption spectra presented in Figure 2 were corrected by taking the changes in chlorin concentration into account. The concentration of fullerene increases during the titration to the level at which fullerene absorption cannot be ignored, and therefore no clear isosbestic points can be seen in the figure. Observed diminished intensities and red shifts of the Soret and first Q bands along with increasing intensities of other Q_y-bands indicate the binding of **C60-1**. Absorption spectra of the **Chl-2@C60-1**, **-2**, and **-3** supramolecular dyads (Figure 1 and Figure S16 in SI) show 1−3 nm red shifts and decrease in intensities of the bands compared to the free **Chl-2**, which is typical for ligand coordination to zinc atom in the chlorin macrocycle.[3] The chlorin band shift upon formation of **Chl-1@C60-1**, **-2**, and **-3** dyads is less pronounced being less than 1 nm, though the decrease in intensity is also well observed.

To get better insight to the complex formation, we studied the fluorescence quenching of the both chlorins, **Chl-1** and **Chl-2**, in the presence of **C60-1**, **-2**, and **-3**. The best wavelength for selective excitation of chlorin chromophore in the dyad was found to be 615 nm which corresponds to the second intense Q_y-band. Fluorescence spectra of **Chl-2** mixtures with **C60-1**, **-2**, and **-3** in ODCB are shown in Figure 3. The fluorescence intensity decreases upon addition of fullerene, but the shape of the emission spectrum remains intact. This is typical behavior for emission quenching via energy or electron transfer mechanism in dyads. The most efficient quenching (80%) was observed for **Chl-2@C60-1** complex already at 1:1 ratio. For other complexes (Table 1, Figure S17 in the SI) the emission quenching was less than 50% for 1:1 ratios and therefore higher amounts of fullerenes were needed for achieving higher quenching at concentrations suitable for pump−probe measurements. With an excess of C_{60} weakest quenching (less than 60%) was recorded for both

dx.doi.org/10.1021/jp412442t | J. Phys. Chem. A XXXX, XXX, XXX−XXX

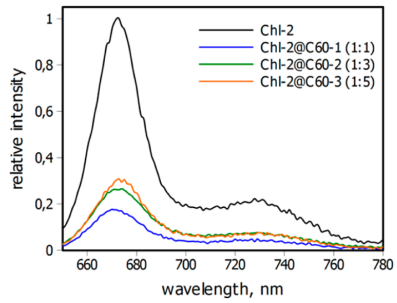

Figure 3. Relative emission spectra **Chl-2@C60** mixtures in ODCB with ratios used for time-resolved measurements. Concentration of **Chl-2** is 0.1 mM in all samples.

Table 1. Chl@C60 Concentration Ratios (Chlorin Concentration 0.1 mM), Measured Emission Quenching Values $(I_0 - I)/I_0$ and Binding Constants (K) for Samples Used for Time-Resolved Measurements in ODCB

chlorin	fullerene	ratio	$(I_0 - I)/I_0$	K, M^{-1}
Chl-1	**C60-1**	1:3	0.70	1.6×10^4
Chl-1	**C60-2**	1:3	0.80	7.8×10^4
Chl-1	**C60-3**	1:5	0.55	4.4×10^3
Chl-2	**C60-1**	1:1	0.80	4.6×10^5
Chl-2	**C60-2**	1:3	0.70	6.8×10^4
Chl-2	**C60-3**	1:5	0.55	4.7×10^3

chlorin−**C60-3** complexes (1:5). While for **Chl-2@C60-2** and both **Chl-1@C60-1** and **Chl-1@C60-2** over 70% quenching was achieved at 1:3 ratio. The limiting factor in these cases was relatively poor solubility of **C60-2** and **C60-3**, which reduces accuracy and reliability of the measurements. Also absorption of the fullerene chromophores at the excitation wavelength, 615 nm, could not be neglected anymore, and it was accounted for in evaluation of the quenching efficiency in Table 1 and Figure S16 in the SI. To improve the solubility of **C60-2**, a small amount of DMF (10 μL) was added to ODCB for dissolving fullerene at higher concentrations. There was no notable difference in solubility of **C60-3** with such amount of DMF, which did not affect the properties of the dyads otherwise. Accounting for the fullerene absorption at the excitation wavelength gives estimation for actual quenching lower than 60% even at 1:5 ratios for **C60-3** complexes, and thus one can expect that not more than half of chlorin molecules form the dyads in the best case.

A usual method to determine binding constants, K, is to present the emission quenching data in Stern−Volmer plot, and calculate the constant from the slope of data linear approximation. However, the linear dependence is only observed when the concentration of the emitting compound, chlorin, is much smaller compared to that of the quencher, fullerene, which is not the case of this study, since the binding constants have to be determined at concentrations close to those used in transient absorption measurements. Therefore, an exact model for the complex formation (see SI) was used to fit the dependence of the fluorescence intensity on the concentration of the compounds to obtain the binding constants (Figure S17 in the SI). It was noted that for **Chl-2@C60-1** at low concentration of **C60-1** (when the concentration of chlorin is higher than that of fullerene) the calculated complex concentration is lower than that determined from the fluorescence quenching. This can be due to possible formation of complexes when fullerene is bound to two chlorin units by pyridine and crown sites respectively. However, Job's method measurements carried out at concentration 0.1 mM indicated formation of 1:1 complexes (Figure S18 in the SI), which confirms that in conditions used in time-resolved measurements, the dominating complex stoichiometry is 1:1.

The values of K for each dyad are listed in Table 1. The magnitude of the K value for **Chl-1** and **Chl-2** are in agreement with that previously measured for a similar dyad,[12] suggesting enhanced binding efficiency due to two-point binding. The combination **Chl-2@C60-1** has even 1 order of magnitude larger equilibrium constant than others. In general, **C60-1** and **C60-2** form strong supramolecular dyads with both chlorins. Binding constants for furan functionalized **C60-3** were found to be lower compared to pyridine derivatives **C60-1** and **C60-2**.

Emission quenching was also studied in PhCN. Figure 4 shows the emission spectra for **Chl-2** and its 1:3 mixture with

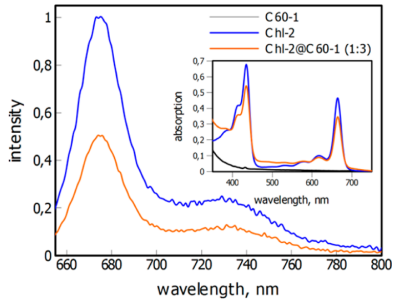

Figure 4. Emission spectra of **Chl-2** and its 1:3 mixture with **C60-1** in PhCN. Excitation wavelength was 615 nm. Inset in plot shows absorption spectra of measured samples. Concentration of **Chl-2** is 0.1 mM in all samples.

C60-1. The emission quenching at ratio 1:1 was 26%, and the 1:3 ratio was needed for both chlorins to achieve 50% quenching (Figure S19 in the SI). Thus the emission quenching in PhCN was found to be less efficient compared to that in ODCB.

Electrochemical Studies. Differential pulse voltammetry (DPV) measurements were carried out to estimate the oxidation and reduction potentials of the compounds (Figure 5). The first oxidation potentials of **Chl-1** and **Chl-2** were located at 0.08 and 0.10 V vs Fc/Fc^+, respectively. The oxidation was reversible only for the latter compound. The second oxidation potentials were located at 0.33 and 0.45 V vs Fc/Fc^+, for **Chl-1** and **Chl-2**, respectively, but were not reversible for either of the chlorins. The first reduction of the fullerene derivatives was located at −1.17 V vs Fc/Fc^+. The difference between chlorin first oxidation and fullerene first reduction potentials gives a rough estimation of the energy of the charge separate state. The energies are 1.25 and 1.27 eV for **Chl-1** and **Chl-2** based dyads, respectively, without accounting for the Coulombic interaction.

Measured oxidation potentials for **Chl-2** correspond well to that of a similar Zn-Chlorin.[39] The oxidation potential of **Chl-1** is slightly shifted by 20 mV, which is likely a consequence of the crown ether orientation over the aromatic chlorin ring.

dx.doi.org/10.1021/jp412442t | J. Phys. Chem. A XXXX, XXX, XXX−XXX

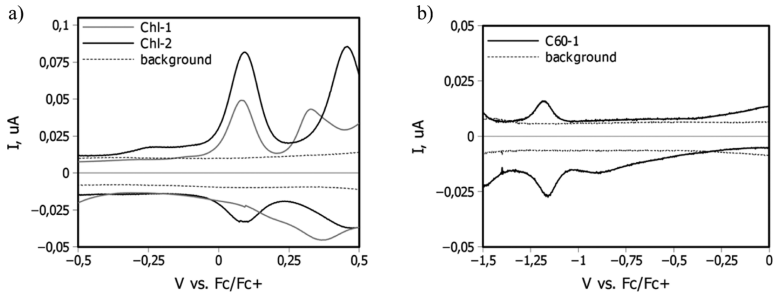

Figure 5. Differential pulse voltammograms of (a) **Chl-1** and **Chl-2** (0.45 mM) and (b) **C60-1** (0.45 mM) in 0.1 M $TBAClO_4$/ODCB.

Time-Resolved Measurements. The fluorescence decay measurements were done for all the self-assembling pairs with the fluorescence up-conversion technique. The decays were recorded at 670 nm, which is roughly the maximum of the steady-state fluorescence of chlorin chromophore. The samples, 1:1−5 mixtures of chlorin and fullerene derivatives, were excited at 420 nm. At this wavelength, chlorin absorption is higher than that of fullerene even for 1:5 mixtures (Figure S20 in the SI). Furthermore, since the emission quantum yield of fullerene is much lower than that of chlorin, the contribution of the fullerene fluorescence at the monitoring wavelength can be neglected and the measured emission decays can be attributed to chlorin solely. Figure 6 shows the fluorescence decays for

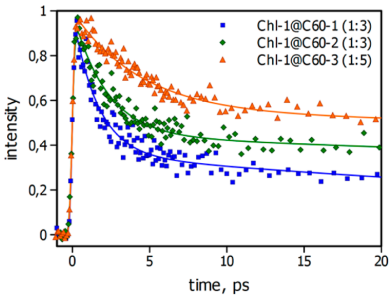

Figure 6. The fluorescence decays of **Chl-1** with **C60-1**, **C60-2**, and **C60-3** monitored at 670 nm in ODCB. Concentration of **Chl-1** is 0.1 mM in all samples, and **Chl-1@C60** concentration ratios are indicated in the plot.

Chl-1 dyads in ODCB. The emission decays consist of two clear components. The fast components in the picoseconds time domain were attributed to the emission decays in supramolecular dyads, and the calculated lifetimes are summarized in Table 2. The longer components have lifetimes in nanosecond time domain, and attributed to free chlorin molecules. The lifetime of the singlet excited state in supramolecular dyads increases in order **C60-1** < **C60-2** < **C60-3** for both chlorin derivatives. The proportion of the fast to slow components is in agreement with emission quenching efficiency. The highest quenching was observed with **C60-1**, which also shows highest proportion of the fast to slow components.

The transient absorption measurements (pump−probe) were carried out with excitation at the same wavelength as for emission decays, 420 nm. The data were collected in a wide

Table 2. Time Constants Obtained from Up-Conversion and Pump−Probe Measurements for the Chl@C60 Dyads in ODCB and PhCN

chlorin	fullerene	τ^a, ps	τ_{CS}, ps	τ_{CR}, ps
measured in ODCB:				
Chl-1	**C60-1**	2.0	1.7	63
Chl-1	**C60-2**	2.5	0.3	76
Chl-1	**C60-3**	3.1		
Chl-2	**C60-1**	1.6	5	55
Chl-2	**C60-2**	2.2	7	187
Chl-2	**C60-3**	4.4		
measured in PhCN:				
Chl-1	**C60-1**		n.a.	14
Chl-2	**C60-1**		2.6	15
Chl-2	**C60-2**		7	60

[a]Fluorescence lifetime obtained from up-conversion measurements.

spectrum range from 500 to 1100 nm, and fitted globally. At least a three-exponential decay model has to be used to achieve a reasonable goodness of the global fit of the pump−probe data. Transient absorption decay component spectra and time-resolved spectrum right after excitation (t = 0 ps) obtained from three-exponential global fit of pump−probe data of **Chl-2@C60-1** (1:1) are presented in Figure 7a. The long-lived component (lifetime >2 ns) arises from nonbonded chlorins (Figure S21 in the SI), and its relative intensity depends on the efficiency of the DA complex formation. The shorter-lived components were observed for all DA combinations. They originate from the interaction between the chlorin and fullerene counterparts, and, they are the subject of further analysis. The 55 ps component in Figure 7a has spectrum typical for the CS state with bleaching of the ground-state absorption of chlorin, new band around 750 nm, and also broad absorption in the NIR region with a band at 1040 nm. It is known that the fullerene anion has a transient absorption band around 1000 nm and chlorin cation near 750 nm.[15,40−42] Therefore this state was attributed to the charge separated (CS) state with lifetime of 55 ps.

The fastest component (5 ps) shows formation of the CS state $Chl^+-C_{60}^-$ as indicated by the band formation at 1040 nm (negative intensity of the component) which is typical for the fullerene anion. At the same time in the Q-band region the component shows an increase in the bleaching of the ground state of chlorin. This behavior resembles that of covalently linked phytochlorin-fullerene dyads,[9] in which the formation of charge separated state was mediated by an exciplex state and appeared in two competing pathways. The first includes

dx.doi.org/10.1021/jp412442t | J. Phys. Chem. A XXXX, XXX, XXX−XXX

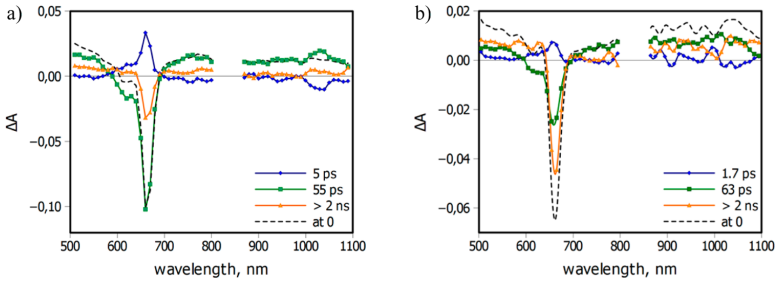

Figure 7. Transient absorption decay component spectra of the (a) **Chl-2@C60-1** (1:1) and (b) **Chl-1@C60−1** (1:3) in ODCB. Concentration of chlorins is 0.1 mM.

formation of the exciplex from the singlet excited state of chlorin chromophore and the exciplex relaxation to the CS state. The second starts from the energy transfer from the primary excited chlorin to the fullerene and follows by the exciplex formation and its relaxation to the complete charge separated state. The latter route results in the recovery of the ground state bleaching of the chlorin upon the energy transfer and following bleaching as the exciplex and CS states are formed. The spectrum of the 5 ps component can be interpreted in a similar manner. For part of the complexes, the primary reaction is the energy transfer from chlorin to fullerene, and when the CS takes place starting from the fullerene singlet excited state the reinvolvement of the chlorin in the relaxation pathway is observed as an increase of bleaching at the Q-band. The degree of recovery of the Q-band bleaching can serve as a rough measure of the relative part of dyads, which pass through the fullerene singlet excited state, and for this dyad it was found to be ≤25%.

There is a noticeable difference in the time constants of the fast component obtained for **Chl-2@C60-1** from the transient absorption and emission decay measurements, 5 and 1.7 ps, respectively (Table 2). Apparently, the excited singlet state does not decay directly to the CS state, and many other processes contribute to that what is observed as a 5 ps component in transient absorption measurements. These are energy transfer, electron transfer starting from both the chlorin and fullerene excited state, and possibly exciplex intermediate prior to formation of the complete CS state. In fluorescence decay measurements, only the chlorin singlet excited state is observed, which is the initial state for all of the following reactions. Attempts to resolve more intermediates in transient absorption measurements were not successful: four-exponential fit gave only 5% improvement in the sigma value and a relatively short-lived component (~0.3 ps) with the spectrum indicating some changes in the Q-band region and around 1000 nm but not allowing unambiguous assignment of the component. The accuracy of the transient absorption measurements was insufficient to identify all processes preceding the formation of the CS state. One reason for this is the limited yield of complexes under experimental conditions favorable for the transient absorption measurements, which was found to be 80% in the best case. Therefore we will limit our following discussion by the analysis of the lifetime of the CS state of different combinations of the donors and acceptors, which was determined with reasonable accuracy.

For samples other than **Chl2@C60-1** higher amount of fullerene was needed to achieve sufficient yield of supramolecular complexes (Table 1). Similar spectral features were also seen for other dyads (Figure 7b and S22 in SI). The lifetimes for CS states are listed in Table 2. However, due to low binding constant of **C60-3** with both **Chl-1** and **Chl-2**, it was not possible to resolve the CS state lifetime from pump−probe measurements, and for that reason only lifetimes of the first singlet state (from up-conversion measurements) are provided in Table 2.

In PhCN solution, a weaker complex formation was observed for all the self-assembling pairs. Accordingly, the lower relative dyad population was concomitant with detection of less intense CS signal. Nonetheless, the spectral main features of the studied samples were fundamentally similar in both ODCB and PhCN. The transient absorption decay component spectra obtained from four-exponential global fit of pump−probe data of **Chl-2@C60-1** (1:3) in PhCN are presented in Figure 8. The

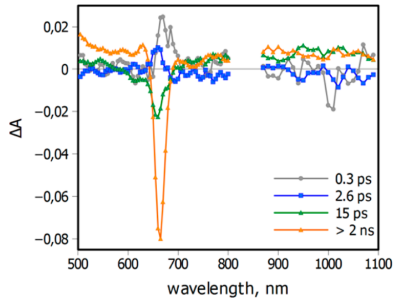

Figure 8. Transient absorption decay component spectra of the **Chl-2@C60-1** (1:3) in PhCN. Concentration of **Chl-2** is 0.1 mM.

components with time constants 2.6 and 15 ps can be identified as those corresponding to charge separation and recombination, respectively. Compared to the same dyad in ODCB, the lifetime of CS state is 4 times shorter in PhCN, as can be expected since higher solvent polarity lowers the energy of the charge separate state and higher reorganization energy, which cumulatively results in shorter lifetime of the CS state in the case of chlorin−fullerene dyads.[9] Similar spectral features were also observed for **Chl-2@C60-2**. However, in the case of **Chl-1@C60-1**, the signal was weak and only component corresponding to the charge recombination was obtained (Figure S23 in the SI). The lifetimes for CS states in PhCN are presented in Table 2. The order of CS state lifetimes is the

dx.doi.org/10.1021/jp412442t | J. Phys. Chem. A XXXX, XXX, XXX−XXX

same both in ODCB and PhCN. Lifetimes of complexes with **C60-2** were found to be higher compared to those with **C60-1**.

DFT Calculations. In order to acquire some theoretical insight about complex formations DFT calculations were performed with DFT TPSS-D3/def2-TZVP//def2-SVP method for all the complexes (Figure 9). Photophysically critical

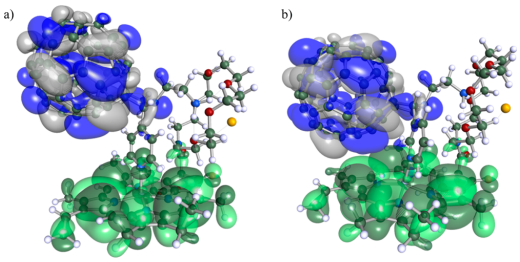

Figure 9. Geometry-optimized structures with depicted empty and filled frontier orbitals for (a) **Chl-2**@*R*-**C60−2** and (b) **Chl-2**@*S*-**C60−1** (LUMO = blue-gray and HOMO = dark-light green) with isosurface value 0.01. In calculations, CF_3COO^- counterion is replaced by Cl^- ion (yellow sphere).

distance parameters, i.e., chlorin−fullerene center-to-center and edge-to-edge spacing, and energy differences between the fullerene derivative enantiomers are listed in Table 3.

Table 3. Computed Geometry Parameters for the Chl@C60 Dyads

chlorin	fullerene	R_{E-E}, Å	R_{C-C}, Å	E_{rel}, kcal/mol
Chl-1	*R*-**C60-1**	3.2	8.9	0.00[a]
	S-**C60-1**	3.4	8.9	2.56
Chl-1	*R*-**C60-2**	6.5	8.9	0.00
	S-**C60-2**	3.4	10.9	−1.97[a]
Chl-1	*R*-**C60-3**	3.3	8.9	0.00[a]
	S-**C60-3**	3.3	9.2	5.15
Chl-2	*R*-**C60-1**	4.2	9.6	0.00
	S-**C60-1**	3.5	8.6	−3.49[a]
Chl-2	*R*-**C60-2**	6.3	9.6	0.00[a]
	S-**C60-2**	4.0	10.7	7.07
Chl-2	*R*-**C60-3**	4.2	9.6	0.00
	S-**C60-3**	3.7	8.8	−3.94[a]

[a]Complex formation is more favorable.

Expectedly, diastereomeric chlorin derivatives showed enantiospesific binding and energetics for the fullerene enantiomers. The calculated energies of complexes for both *R*- and *S*-fullerene enantiomers show that the relative energy of **Chl-2**@*S*-**C60-1** is lower than that of **Chl-2**@*R*-**C60-1** (Table 3). Thus, it is apparent that in excess of racemic **C60-1** formation of **Chl-2**@*S*-**C60-1** complex dominates over that of **Chl-2**@*R*-**C60-1**. Additionally, the calculations also insist that in case of **Chl-2**@**C60-2** complex *R*-enantiomer of **C60-2** is more favorable toward binding, whereas for **Chl-2**@**C60-3** *S*-enantiomer is expected to be bound stronger. However, in case of **Chl-1** the trend is opposite: *R*-**C60-1**, *S*-**C60-2**, and *R*-**C60-3** are clearly favored in the analogous complex formations. Overall, the computational studies suggest that both **Chl-1** and **Chl-2** have an ability to discriminate between different enantiomers of studied fullerene derivatives, although racemic mixtures of **C60-1**, **C60-2**, and **C60-3** were used for all the measurements.

DISCUSSION

Some important remarks can be drawn from the absorption spectra upon titration. The most pronounced differences in the absorption spectra can be seen in **Chl-2** upon formation of complexes with **C60-1** and **C60-2**. Titration of **Chl-2** with furan derivative **C60-3** does not show remarkable changes in absorption, due to the fact that the oxygen electron pair donating ability is lower compared to that of nitrogen, which makes it a looser ligand for Zn compared to pyridine coordinating group. In the case of **Chl-1**, relatively small changes are observed while titrating it with **C60-1**, **-2**, or **-3**. Structurally, the crown moiety of **Chl-1** is hanging in the terminal position of long flexible propionic amide side arm (17^4), meanwhile in **Chl-2**, it is attached into a close proximity of chlorin macrocycle at the 13^2-position. The latter seems to fit better to the geometry of the fullerene counterparts.

Considering two enantiomers of fullerene, a simple equilibrium model may be insufficient to explain the observed results, and the latter may differ at different concentrations. At low concentration of chlorin and sufficiently high concentration of fullerene, one can expect that most of complexes will be formed by enantiomer providing lower energy of the complex, and the logarithm of the complex concentration ratio to be proportional to the energy difference divided by the thermal energy, kT. This is the limit of low chlorin concentration and high excess of fullerenes, and obviously it is not suitable for the time-resolved spectroscopy studies. At higher chlorin concentration and chlorin:fullerene ratio close to 1:1, the outcome depends on the equilibrium constants for each pair that each chlorin forms either with *S*- or *R*-**C60** enantiomer. If products of the binding constants and chlorin (or fullerene) concentrations for both enantiomers are greater than one, both enantiomers will form the complexes, leaving almost no free chlorins or fullerenes. In this case, we expect to see high fluorescence quenching efficiency as is the case of **Chl-2**@**C60-1** in conditions used in this study (80%, Table 1). If the product is greater than one only for a lower energy complex, only the lower energy complex will be formed predominantly, and fluorescence quenching will be roughly 50%, assuming that enantiomers present in solution in equal amounts. This is the case of **Chl-1**@**C60-1** and **Chl-2**@**C60-2**, and, to a lesser degree, of **Chl-1**@**C60-2**. To increase the yield of complexes, we increased the concentration of fullerene, and under this condition, again, the lower energy complex will be formed predominantly since it has higher binding constant, and the enantiomers are competing in the complex formation again. The latter is the case of the pump−probe measurements for all samples except **Chl-2**@**C60-1**. It should be noted that the equilibrium constants were determined using standard methods, which do not account for presence of enantiomers, and thus the determined constants are not accurate and correspond to the lower energy complexes.

On the basis of the above discussion, we can presume that in three cases of time-resolved spectroscopy measurements, we studied monoenantiomer complexes, namely, **Chl-1**@*R*-**C60-1**, **Chl-1**@*S*-**C60-2** and **Chl-2**@*R*-**C60-2**. In the case of **Chl-2**@**C60-1**, we probably have minor domination of **Chl-2**@*S*-**C60-1**, but the properties of **Chl-2**@*S*-**C60-1** and **Chl-2**@*R*-**C60-1** seem to be rather close to each other, and we cannot distinguish between them within experimental accuracy.

The combination **Chl-2**@**C60-1** has 1 order of magnitude larger equilibrium constant compared to those of other studied

dx.doi.org/10.1021/jp412442t | J. Phys. Chem. A XXXX, XXX, XXX−XXX

complexes. Thus it is the best matching pair for ditopic binding. Another advantage of ditopic binding is the complex formation in both relatively nonpolar ODCB and polar PhCN. Since the proportion of the charge recombination time constants is the same in these two solvents, we can presume that the complex geometries are rather similar in two solvents.[22]

The differences in the lifetimes of CS state for different combination of donors and acceptors in supramolecular dyad can be attributed to different geometries of the dyads and can be discussed further based on the results of the dyad modeling. In a simplified case the lifetime distance dependence is given by an exponential law, $\tau_{CR} \sim \exp(-\beta r)$, where r is the distance and β is a damping factor, and it arises from the exponential decay of the electronic coupling with the distance.[43] An open question here is how to measure the distance r. Two usual approaches are to look at the center-to-center distance, R_{C-C}, and edge-to-edge distance, R_{E-E}. From Table 2 one can pick up two pairs of dyads that have photophysically similar features, namely **Chl-2**@*S*-**C60-1** and **Chl-2**@*R*-**C60-2**, and **Chl-1**@*R*-**C60-1** and **Chl-1**@*S*-**C60-2**, to examine whether these complexes have also some structural relations. For the first pair, the lifetimes differ 3.4 times, and for the latter by 1.2 times only. For the first pair, the difference in R_{C-C} is 1 Å, and for the second it is 2 Å, which does not agree with the lifetime differences. However, for the former pair, the difference in R_{E-E} is 2.8 Å, and for the latter pair it is 0.2 Å, which supports very well the observed difference in the charge recombination time constants and suggests the damping factor to be 0.44 $Å^{-1}$. The damping factors reported for through-space electron transfer for a number of porphyrin-based DA systems are in the range 0.3−0.6 $Å^{-1}$.[44−46] Therefore, one may conclude that the edge-to-edge distance is the key parameter for the distance dependence. On the other hand, the CS state lifetime for covalently linked Zn phytochlorin-fullerene dyad was reported to be 21 ps in benzonitrile,[9] which is longer than that of **Chl-1**@*R*-**C60-1** and **Chl-2**@*S*-**C60-1** dyads (14 and 15 ps, respectively), despite the edge-to-edge distance being shorter. In this case, center-to-center distance correlates better with the lifetimes. Striking difference in geometries between the mentioned covalent-linked dyad and the supramolecular dyads in this study is that in covalently linked dyad the fullerene is located closer to the peripheral part of the chlorin macrocycle, whereas for the supramolecular dyads, the fullerenes are on top of the macrocycle. One explanation is that in the latter case, the electronic coupling is stronger at the same edge-to-edge distance, and the center-to-center distance appears to be better value to compare the lifetimes.

In both cases dyads with **C60-1** (3-pyridine linker) had shorter CS state lifetime than that with **C60-2** (4-pyridine linker). This is the expected result based on the calculated distances between donor and acceptor, which showed that the DA distance is shorter for dyads with **C60-1** acceptor than that with **C60-2** acceptor.

CONCLUSIONS

Two zinc chlorins equipped with aza-[18]crown-6 ether moiety at 13^4 or 17^4 positions (**Chl-2** and **Chl-1**, respectively) and three pyrrolidine functionalized fullerenes armed with alkyl aminium and 3-furan, 3- or 4-pyridine linkers (**C60-3**, **C60-1**, and **C60-2**, respectively) were synthesized to study self-assembled DA dyads and characterized by computational and spectroscopic methods. The computational studies revealed that the complex formation was energetically clearly more favorable for each chlorin diastereomer with particular fullerene enantiomer. Thus, in solution of a racemic mixture of fullerene derivatives, enantioselective complexes **Chl-2**@*S*-**C60-1**, **Chl-2**@*R*-**C60-2**, **Chl-2**@*S*-**C60-3**, **Chl-1**@*R*-**C60-1**, **Chl-1**@*S*-**C60-2** and **Chl-1**@*S*-**C60-3** were most likely formed, which is also supported by the experimentally observed behavior of studied systems.

The time-resolved absorption spectroscopy studies demonstrated fast charge separation with time constants less than 10 ps in supramolecular dyads. The lifetimes of the charge separated states are in 55−190 ps range in nonpolar ODCB and 15−60 ps in polar PhCN depending on the DA distance in the dyads and giving the damping factor β = 0.44 $Å^{-1}$ for the distance dependence. Compared to previously measured covalently bonded chlorin-fullerene dyads, the results showed that mutual orientation of donor and acceptor in dyads also influences the electron transfer rates. Namely, at the same edge-to-edge distance, the electronic coupling is stronger for fullerene located on top of macrocycle than at the macrocycle periphery.

ASSOCIATED CONTENT

Supporting Information

Synthesis of molecules, UV/vis and emission titration spectra, equations and fittings for binding constant determination, time-resolved transient absorption spectra and detailed information about computational methods. This material is available free of charge via the Internet at http://pubs.acs.org

AUTHOR INFORMATION

Corresponding Authors

*E-mail: juho.helaja@helsinki.fi (J.H.).
*E-mail: nikolai.tkachenko@tut.fi (N.T.).

Notes

The authors declare no competing financial interest.

ACKNOWLEDGMENTS

This work has been supported by Academy of Finland [No. 135113 and 135058]. Dr. Petri Heinonen is accredited for the HRMS measurements. The National Centre for Scientific Computing (CSC) is acknowledged for computational resources. V.I. and T.N. acknowledge the Graduate School of Organic Chemistry and Chemical Biology (GSOCCB). V.I. is also grateful to Magnus Ehnrooth and University of Helsinki foundations for financial support.

REFERENCES

(1) Wróbel, D.; Graja, A. Photoinduced Electron Transfer Processes in Fullerene−Organic Chromophore Systems. *Coord. Chem. Rev.* **2011**, *255*, 2555−2577.
(2) Grimm, B.; Porra, R. J.; Rüdiger, W.; Scheer, H. *Chlorophylls and Bacteriochlorophylls: Biochemistry, Biophysics, Functions and Applications*; Springer: Dordrecht, The Netherlands, 2006.
(3) D'Souza, F.; Ito, O. Photoinduced Electron Transfer in Supramolecular Systems of Fullerenes Functionalized with Ligands Capable of Binding to Zinc Porphyrins and Zinc Phthalocyanines. *Coord. Chem. Rev.* **2005**, *249*, 1410−1422.
(4) Araki, Y.; Ito, O. Factors Controlling Lifetimes of Photoinduced Charge-Separated States of Fullerene-Donor Molecular Systems. *J. Photochem. Photobiol., C* **2008**, *9*, 93−110.
(5) El-Khouly, M. E.; Ito, O.; Smith, P. M.; D'Souza, F. Intermolecular and Supramolecular Photoinduced Electron Transfer Processes of Fullerene−Porphyrin/Phthalocyanine Systems. *J. Photochem. Photobiol., C* **2004**, *5*, 79−104.

(6) Guldi, D. M.; Zilbermann, I.; Gouloumis, A.; Vázquez, P.; Torres, T. Metallophthalocyanines: Versatile Electron-Donating Building Blocks for Fullerene Dyads. *J. Phys. Chem., B.* **2004**, *108*, 18485−18494.
(7) Schuster, D. I.; Li, K.; Guldi, D. M.; Palkar, A.; Echegoyen, L.; Stanisky, C.; Cross, R. J.; Niemi, M.; Tkachenko, N. V.; Lemmetyinen, H. Azobenzene-Linked Porphyrin−Fullerene Dyads. *J. Am. Chem. Soc.* **2007**, *129*, 15973−15982.
(8) Bottari, G.; Trukhina, O.; Ince, M.; Torres, T. Towards Artificial Photosynthesis: Supramolecular, Donor−Acceptor, Porphyrin- and Phthalocyanine/Carbon Nanostructure Ensembles. *Coord. Chem. Rev.* **2012**, *256*, 2453−2477.
(9) Tkachenko, N. V.; Rantala, L.; Tauber, A. Y.; Helaja, J.; Hynninen, P. H.; Lemmetyinen, H. Photoinduced Electron Transfer in Phytochlorin-[60]Fullerene Dyads. *J. Am. Chem. Soc.* **1999**, *121*, 9378−9387.
(10) Vehmanen, V.; Tkachenko, N. V.; Imahori, H.; Fukuzumi, S.; Lemmetyinen, H. Charge-Transfer Emission of Compact Porphyrin−Fullerene Dyad Analyzed by Marcus Theory of Electron-Transfer. *Spectrochim. Acta, Part A* **2001**, *57*, 2229−2244.
(11) Vehmanen, V.; Tkachenko, N. V.; Efimov, A.; Damlin, P.; Ivaska, A.; Lemmetyinen, H. The Role of the Exciplex State in Photoinduced Electron Transfer of Phytochlorin-[60]Fullerene Dyads. *J. Phys. Chem., A* **2002**, *106*, 8029−8038.
(12) Kavakka, J. S.; Heikkinen, S.; Kilpelainen, I.; Tkachenko, N. V.; Helaja, J. Zn Pyro-Pheophorbide a-Fulleronicotine Dyad; Supramolecular Self Assembled Donor-Acceptor System for Photoinduced Charge Separation. *Chem. Commun.* **2009**, *7*, 758−760.
(13) Zheng, G.; J. Dougherty, T.; K. Pandey, R.; K. Pandey, R. Novel Chlorin-Diene Building Block by Enyne Metathesis: Synthesis of Chlorin−Fullerene Dyads. *Chem. Commun.* **1999**, *24*, 2469−2470.
(14) Montforts, F.; Kutzki, O. Simple Synthesis of a Chlorin−Fullerene Dyad with a Novel Ring-Closure Reaction. *Angew. Chem., Int. Ed.* **2000**, *39*, 599−601.
(15) Fukuzumi, S.; Ohkubo, K.; Imahori, H.; Shao, J.; Ou, Z.; Zheng, G.; Chen, Y.; Pandey, R. K.; Fujitsuka, M.; Ito, O.; Kadish, K. M. Photochemical and Electrochemical Properties of Zinc Chlorin-C60 Dyad as Compared to Corresponding Free-Base Chlorin-C60, Free-Base Porphyrin-C60, and Zinc Porphyrin-C60 Dyads. *J. Am. Chem. Soc.* **2001**, *123*, 10676−10683.
(16) Kavakka, J. S.; Heikkinen, S.; Helaja, J. Zn Pyropheophorbide *a*: A *β*-Face Selective Nicotine Receptor. *Eur. J. Org. Chem.* **2008**, *2008*, 4932−4937.
(17) Shinozaki, Y.; Richards, G.; Ogawa, K.; Yamano, A.; Ohara, K.; Yamaguchi, K.; Kawano, S.; Tanaka, K.; Araki, Y.; Wada, T.; Otsuki, J. Double Helices of a Pyridine-Appended Zinc Chlorophyll Derivative. *J. Am. Chem. Soc.* **2013**, *135*, 5262−5265.
(18) D'Souza, F.; Maligaspe, E.; Sandanayaka, A. S. D.; Subbaiyan, N. K.; Karr, P. A.; Hasobe, T.; Ito, O. Photochemical Charge Separation in Supramolecular Phthalocyanine−Multifullerene Conjugates Assembled by Crown Ether-Alkyl Ammonium Cation Interactions. *J. Phys. Chem. A* **2010**, *114*, 10951−10959.
(19) El-Khouly, M. E.; Kay, K.; D'Souza, F.; Fukuzumi, S. Supramolecular Tetrad of Subphthalocyanine−Triphenylamine−Zinc Porphyrin Coordinated to Fullerene as an "Antenna-Reaction-Center" Mimic: Formation of a Long-Lived Charge-Separated State in Nonpolar Solvent. *Chem.—Eur. J.* **2010**, *16*, 6193−6202.
(20) Rodríguez-Morgade, M. S.; Plonska-Brzezinska, M.; Athans, A. J.; Carbonell, E.; de Miguel, G.; Guldi, D. M.; Echegoyen, L.; Torres, T. Synthesis, Characterization, and Photoinduced Electron Transfer Processes of Orthogonal Ruthenium Phthalocyanine−Fullerene Assemblies. *J. Am. Chem. Soc.* **2009**, *131*, 10484−10496.
(21) D'Souza, F.; Deviprasad, G.; Zandler, M.; El-Khouly, M.; Fujitsuka, M.; Ito, O. Photoinduced Electron Transfer in "Two-Point" Bound Supramolecular Triads Composed of *N*,*N*-Dimethylaminophenyl−Fullerene−Pyridine Coordinated to Zinc Porphyrin. *J. Phys. Chem., A* **2003**, *107*, 4801−4807.
(22) D'Souza, F.; Chitta, R.; Gadde, S.; Zandler, M.; McCarty, A.; Sandanayaka, A.; Araki, Y.; Ito, O. Effect of Axial Ligation Or *π*−*π*-Type Interactions on Photochemical Charge Stabilization in "Two-Point" Bound Supramolecular Porphyrin−Fullerene Conjugates. *Chem.—Eur. J.* **2005**, *11*, 4416−4428.
(23) D'Souza, F.; Chitta, R.; Gadde, S.; McCarty, A.; Karr, P.; Zandler, M.; Sandanayaka, A.; Araki, Y.; Ito, O. Design, Syntheses, and Studies of Supramolecular Porphyrin−Fullerene Conjugates, Using Bis-18-Crown-6 Appended Porphyrins and Pyridine or Alkyl Ammonium Functionalized Fullerenes. *J. Phys. Chem., B* **2006**, *110*, 5905−5913.
(24) Ito, O.; D'Souza, F. Recent Advances in Photoinduced Electron Transfer Processes of Fullerene-Based Molecular Assemblies and Nanocomposites. *Molecules* **2012**, *17*, 5816−5835.
(25) Imahori, H.; Sakata, Y. Fullerenes as Novel Acceptors in Photosynthetic Electron Transfer. *Eur. J. Org. Chem.* **1999**, *1999*, 2445−2457.
(26) Guldi, D. M.; Prato, M. Excited-State Properties of C60 Fullerene Derivatives. *Acc. Chem. Res.* **2000**, *33*, 695−703.
(27) Maggini, M.; Scorrano, G.; Prato, M. Addition of Azomethine Ylides to C60: Synthesis, Characterization, and Functionalization of Fullerene Pyrrolidines. *J. Am. Chem. Soc.* **1993**, *115*, 9798−9799.
(28) Isosomppi, M.; Tkachenko, N.; Efimov, A.; Lemmetyinen, H. Photoinduced Electron Transfer in Double-Bridged Porphyrin−Fullerene Triads. *J. Phys. Chem., A.* **2005**, *109*, 4881−4890.
(29) *TURBOMOLE V6. 4*; University of Karlsruhe and Forschungszentrum Karlsruhe GmbH, 1989−2007; TURBOMOLE GmbH, s. 2., 2012.
(30) Schafer, A.; Klamt, A.; Sattel, D.; Lohrenz, J. C. W.; Eckert, F. COSMO Implementation in TURBOMOLE: Extension of an Efficient Quantum Chemical Code Towards Liquid Systems. *Phys. Chem. Chem. Phys.* **2000**, *2*, 2187−2193.
(31) Tao, J.; Perdew, J. P.; Staroverov, V. N.; Scuseria, G. E. Climbing the Density Functional Ladder: Nonempirical Meta-Generalized Gradient Approximation Designed for Molecules and Solids. *Phys. Rev. Lett.* **2003**, *91*, 146401.
(32) Grimme, S.; Antony, J.; Ehrlich, S.; Krieg, H. A Consistent and Accurate Ab Initio Parametrization of Density Functional Dispersion Correction (DFT-D) for the 94 Elements H-Pu. *J. Chem. Phys.* **2010**, *132*, 154104.
(33) Weigend, F.; Ahlrichs, R. Balanced Basis Sets of Split Valence, Triple Zeta Valence and Quadruple Zeta Valence Quality for H to Rn: Design and Assessment of Accuracy. *Phys. Chem. Chem. Phys.* **2005**, *7*, 3297−3305.
(34) Sierka, M.; Hogekamp, A.; Ahlrichs, R. Fast Evaluation of the Coulomb Potential for Electron Densities Using Multipole Accelerated Resolution of Identity Approximation. *J. Chem. Phys.* **2003**, *118*, 9136−9148.
(35) Eichkorn, K.; Weigend, F.; Treutler, O.; Ahlrichs, R. Auxiliary Basis Sets for Main Row Atoms and Transition Metals and Their Use to Approximate Coulomb Potentials. *Theor. Chem. Acc.* **1997**, *97*, 119−124.
(36) Weigend, F. Accurate Coulomb-Fitting Basis Sets for H to Rn. *Phys. Chem. Chem. Phys.* **2006**, *8*, 1057−1065.
(37) Hellweg, A.; Hättig, C.; Höfener, S.; Klopper, W. Optimized Accurate Auxiliary Basis Sets for RI-MP2 and RI-CC2 Calculations for the Atoms Rb to Rn. *Theor. Chem. Acc.* **2007**, *117*, 587−597.
(38) Grimme, S. Semiempirical GGA-Type Density Functional Constructed with a Long-Range Dispersion Correction. *J. Comput. Chem.* **2006**, *27*, 1787−1799.
(39) Nonomura, Y.; Igarashi, S.; Yoshioka, N.; Inoue, H. Spectroscopic Properties of Chlorophylls and their Derivatives. Influence of Molecular Structure on the Electronic State. *Chem. Phys.* **1997**, *220*, 155−166.
(40) Tkachenko, N. V.; Rantala, L.; Tauber, A. Y.; Helaja, J.; Hynninen, P. H.; Lemmetyinen, H. Photoinduced Electron Transfer in Phytochlorin-[60] Fullerene Dyads. *J. Am. Chem. Soc.* **1999**, *121*, 9378−9387.
(41) El-Khouly, M. E.; Araki, Y.; Fujitsuka, M.; Watanabe, A.; Ito, O. Photoinduced Electron Transfer between Chlorophylls (a/b) and

Fullerenes (C60/C70) Studied by Laser Flash Photolysis. *Photochem. Photobiol.* **2001**, *74*, 22−30.
(42) Kesti, T. J.; Tkachenko, N. V.; Vehmanen, V.; Yamada, H.; Imahori, H.; Fukuzumi, S.; Lemmetyinen, H. Exciplex Intermediates in Photoinduced Electron Transfer of Porphyrin−Fullerene Dyads. *J. Am. Chem. Soc.* **2002**, *124*, 8067−8077.
(43) Wasielewski, M. R. Photoinduced Electron Transfer in Supramolecular Systems for Artificial Photosynthesis. *Chem. Rev.* **1992**, *92*, 435−461.
(44) Imahori, H.; Tamaki, K.; Guldi, D. M.; Luo, C.; Fujitsuka, M.; Ito, O.; Sakata, Y.; Fukuzumi, S. Modulating Charge Separation and Charge Recombination Dynamics in Porphyrin−Fullerene Linked Dyads and Triads: Marcus-Normal Versus Inverted Region. *J. Am. Chem. Soc.* **2001**, *123*, 2607−2617.
(45) Kang, Y. K.; Rubtsov, I. V.; Iovine, P. M.; Chen, J.; Therien, M. J. Distance Dependence of Electron Transfer in Rigid, Cofacially Compressed, π-Stacked Porphyrin-Bridge-Quinone Systems. *J. Am. Chem. Soc.* **2002**, *124*, 8275−8279.
(46) Wiberg, J.; Guo, L.; Pettersson, K.; Nilsson, D.; Ljungdahl, T.; Mårtensson, J.; Albinsson, B. Charge Recombination Versus Charge Separation in Donor−Bridge−Acceptor Systems. *J. Am. Chem. Soc.* **2007**, *129*, 155−163.

PUBLICATION V

Self-assembled donor-acceptor two-layer film on TiO_2

Kati Stranius, Lijo George, Alexander Efimov, Tero-Petri Ruoko, Juuso Pohjola and Nikolai V. Tkachenko

Langmuir (Submitted)

Tampereen teknillinen yliopisto
PL 527
33101 Tampere

Tampere University of Technology
P.O.B. 527
FI-33101 Tampere, Finland

ISBN 978-952-15-3412-6
ISSN 1459-2045